QUIET CLEAN STOL EXPERIMENTAL ENGINE STUDY PROGRAM TASK II-PRELIMINARY DESIGN STUDIES

NOV 1972

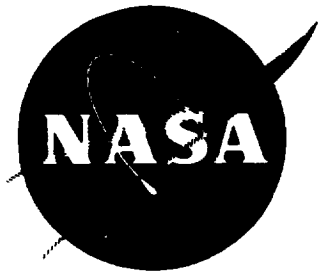

QUIET CLEAN STOL EXPERIMENTAL ENGINE STUDY PROGRAM

Task II—Preliminary Design Studies

by H. E. Helms

EDR 7610

Part A

DETROIT DIESEL ALLISON, DIVISION OF GENERAL MOTORS

prepared for

NATIONAL AERONAUTICS AND SPACE ADMINISTRATION

NASA Lewis Research Center

Contract NAS3-16727

1. Report No.	2. Government Accession No.	3. Recipient's Catalog No.

4. Title and Subtitle	5. Report Date
QUIET CLEAN STOL EXPERIMENTAL ENGINE STUDY PROGRAM (TASK II—PRELIMINARY DESIGN STUDIES)	November 1972
	6. Performing Organization Code
7. Author(s)	8. Performing Organization Report No.
H. E. Helms	EDR 7610
	10. Work Unit No.
9. Performing Organization Name and Address	11. Contract or Grant No.
Detroit Diesel Allison Division of General Motors Indianapolis, Indiana 46206	NAS3-16727
	13. Type of Report and Period Covered
12. Sponsoring Agency Name and Address	
National Aeronautics and Space Administration Washington, D. C. 20546	14. Sponsoring Agency Code

15. Supplementary Notes

Project Manager, Robert Denington, and Technical Director, Robert Koenig, of the V/STOL and Noise Division, NASA Lewis Research Center, Cleveland, Ohio

16. Abstract

Preliminary design studies were conducted on five propulsion systems designed to meet a 95-EPNdB noise level at 41-m/s (80-kt) forward velocity at 30-m (100-ft) altitude and at take-off power and to meet NASA defined pollution standards. Performance data, component definition, and layouts of engines and flight type nacelles were produced. These designs included provisions for thrust reversing, variable fan nozzles, STOL control system requirements, response rates for engine-out conditions, inlet distortions (stability), growth capabilities, and two noise levels (95 and 100 PNdB). Installations were based on studies conducted by NASA STOL Aircraft System Studies contractors (McDonnell-Douglas and Lockheed Aircraft) and NASA inputs. Four externally blown flap propulsion systems were designed—two for under-the-wing and two for over-the-wing aircraft. The fifth propulsion system is for an augmentor wing aircraft. An existing ATEGG core engine was used and new low-pressure systems were designed with matching nacelles. These propulsion systems establish a credible base for the NASA Quiet Clean STOL Experimental Engine program.

17. Key Words (Suggested by Author(s))		18. Distribution Statement
STOL	Pollution	Unclassified
Noise	Thrust Reversing	
EBF	Performance	
AW	Propulsion systems	
Variable-pitch fans	Fixed-pitch fans	

19. Security Classif. (of this report)	20. Security Classif. (of this page)	21. No. of Pages	22. Price*
Unclassified	Unclassified		

* For sale by the National Technical Information Service, Springfield, Virginia 22151

FOREWORD

The propulsion system study described herein was performed under the direction of the NASA Lewis Research Center—Mr. Robert J. Denington, Program Manager, and Mr. Robert W. Koenig, Technical Coordinator.

This report was prepared under the direction of H. E. Helms, Detroit Diesel Allison (DDA) Program Manager, with contributions from the following DDA and subcontractor personnel:

- Detroit Diesel Allison
  - H. E. Shaner
  - J. C. Gill
  - T. A. Lyon
  - M. J. Orelup
  - R. A. Sulkoske

- Hamilton Standard Division of United Aircraft (Variable Pitch Fan Data)
  - R. Levintan
  - M. Seery

- Rohr Industries, Inc. (Nacelle Installation)
  - F. Hom
  - R. Preece

- Wyle Laboratories (Noise Consultants)
  - E. Grande
  - L. Sutherlin

DDA also wishes to acknowledge the cooperation and support of the following STOL Aircraft System Studies contractors who performed companion aircraft studies (under the direction of the NASA Ames Research Center) in parallel with this study:

- Lockheed Aircraft Corporation
  - T. P. Higgins, Jr, Program Manager

- McDonnell Douglas Corporation
  - L. F. Rochte, Program Manager

TABLE OF CONTENTS

LIST OF ILLUSTRATIONS

LIST OF TABLES

I. SUMMARY

Results of the Task I parametric studies and inputs from the STOL Aircraft System Studies provided guidance for recommending propulsion systems for the Task II Preliminary Design Studies. A target noise level of 95 PNdB at 41-m/s (80-kt) forward velocity and 30-m (100-ft) altitude after takeoff, target pollution values at takeoff and idle, and minimum direct operating costs were criteria used in defining the propulsion systems on which to base the forthcoming QCSEE program. Based on recommendations, criteria and other supporting data, NASA Lewis Research Center designated four Task II propulsion systems using the GMA100 core engine with cycle parameters as follows:

- Externally blown flap propulsion systems:
  - PD287-5
    - Fan pressure ratio = 1.25 (variable pitch)
    - Turbine inlet temperature = 1589°K (2400°F)
    - Primary exhaust velocity = 213 m/s (700 ft/sec)
  - PD287-6
    - Fan pressure ratio = 1.325 (variable pitch)
    - Turbine inlet temperature = 1589°K (2400°F)
    - Primary exhaust velocity = 213 m/s (700 ft/sec)
  - PD287-7 (scaled GMA100 core)
    - Fan pressure ratio = 1.25 (variable pitch)
    - Turbine inlet temperature = 1589°K (2400°F)
    - Overall pressure ratio = 20-22
    - Primary exhaust velocity = 213 m/s (700 ft/sec)
- Augmented wing propulsion system:
  - PD287-51
    - Fan pressure ratio = 3.0 (fixed pitch)
    - Turbine inlet temperature = 1534°K (2300°F)
    - Overall pressure ratio = 20-22
    - Primary exhaust velocity = 213 m/s (700 ft/sec)

It was recommended by DDA that a fifth propulsion system be carried through preliminary design. This fifth propulsion system was an externally blown flap type with the following cycle parameters:

- PD287-11
  - Fan pressure ratio = 1.35 (fixed pitch)
  - Turbine inlet temperature = 1589°K (2400°F)
  - Overall pressure ratio = 20
  - Primary exhaust velocity = 213 m/s (700 ft/sec)

These five propulsion systems were carried through preliminary design with Hamilton Standard design activity on variable pitch fans, Rohr Industries Inc. design of nacelles, and DDA overall propulsion system integration and engine design.

The preliminary design procedure used was to establish flight weight propulsion systems which minimized noise, met pollution standards, and had performance compatible with STOL aircraft. The definition of STOL aircraft geometry is still evolving from NASA and industry studies and tests. The nacelle geometry and noise treatment, therefore, is subject to change because of this evolving STOL aircraft technology. Performance analysis for each of the five propulsion systems was accomplished and provided to each of the NASA Aircraft System Study contractors and NASA Lewis for use in STOL aircraft studies. Schematic diagrams for propulsion system control were established and identify with the aircraft automatic control systems. Thrust reversing was achieved by using either variable-pitch fans or conventional thrust reversers. Emphasis was placed on acoustic and aerodynamic performance. Table 1-I presents a summary of the characteristics of the Task II propulsion systems.

Preliminary design layouts are presented (Figures 1-1 and 1-2 show one set of typical engine and nacelle layouts) for each integrated propulsion system. Design analysis is presented which establishes the feasibility of the propulsion systems.

The technology that should be demonstrated in the NASA QCSEE program as revealed in this preliminary design activity falls into the following three categories:

- Propulsion system
- Component evaluations
- Advanced technology demonstrations

A breakdown of each of these item follows:

- Propulsion system characteristics
  - 95 EPNdB
  - Aerodynamic losses of acoustic materials (performance penalties)
  - Acoustic material geometry variation effects on acoustic and aerodynamic performance
- Propulsion systems operation
  - Thrust and sfc (over a defined power spectrum)
  - Secondary nozzle performance
  - Thrust reversing capability
  - Response rates for rapid thrust changes
  - Pollution for complete installation (compared to either gas generator or combustor data)

Table 1-I.

QCSEE Task II propulsion systems.

	PD287-5	PD287-6	PD287-7	PD287-11	PD287-51
Engine—General					
Bypass ratio	17.6	13.8	17.3	12.7	2.53
Turbine inlet temperature, °K (°F)	1589 (2400)	1589 (2400)	1589 (2400)	1589 (2400)	1533 (2300)
Weight, kg (lbm)	2055 (4531)	1880 (4144)	1686 (3716)	2083 (4593)	1358 (2993)
Gear ratio	3.89	2.96	3.62	3.40	---
Fan					
Type	VP (geared)	VP (geared)	VP (geared)	FP (geared)	FP (non-geared)
Pressure ratio (bypass)	1.25	1.325	1.25	1.35	3.0
Nacelle—General					
Type	EBF-UW	EBF-OW	EBF-UW	EBF-OW	AW-UW
Nozzle types	Separate flow	Separate flow	Separate flow	Separate flow	2-stream
Fan nozzle	Variable	Variable	Variable	Variable	---
Primary nozzle velocity, m/s (ft/sec)	213 (700)	213 (700)	213 (700)	213 (700)	213 (700)
Fan reverser	None	Blow-in doors	None	Cascade	Cascade
Primary reverser	None	None	None	None	Target spoiler
Nacelle weight, kg (lbm)	1514 (3338)	2203 (4857)	1280 (2822)	2182 (4010)	1071 (2361)
Acoustic treatment					
Inlet cowl splitters		2	1	2	0 (sonic IGV)
Fan exhaust splitters	1	0 (wall only)	1	0 (wall only)	0
Primary exhaust	Wall only	Wall only	Wall only	Wall only	Wall only
Propulsion System—General					
Noise, EPNdB	95	95	95	95	95
Total weight, kg (lbm)	3569 (7869)	4083 (9001)	2966 (6538)	4265 (9403)	2429 (5354)
Pollution level (staged combustor)					
Takeoff					
Oxides of nitrogen*	3.8	4.2	5.1	4.7	5.1
Smoke (SAE No.)	<15	<15	<15	<15	<15
Idle**					
Carbon monoxide*	7.7	6.1	12.9	7.3	4.9
Unburned hydrocarbons*	0.5	0.4	0.3	0.4	0.3

*Gm of pollutant per 1000 lbm of fuel.

**CO and HC_X values decrease with increasing bleed.

- Lightweight component integration into the propulsion system (especially nacelle parts)
- Control system operation (interfacing with the aircraft control)

- Component evaluations
  - Variable-pitch fan performance and acoustics
  - Augmentor wing sonic inlet performance and acoustics
  - Combustor pollution demonstrations
  - Variable secondary nozzle performance
  - Mechanical integrity of composite materials (both engine and nacelle components)
  - Thrust reversing effectiveness
  - Combined fan-compressor stability with distorted inlets

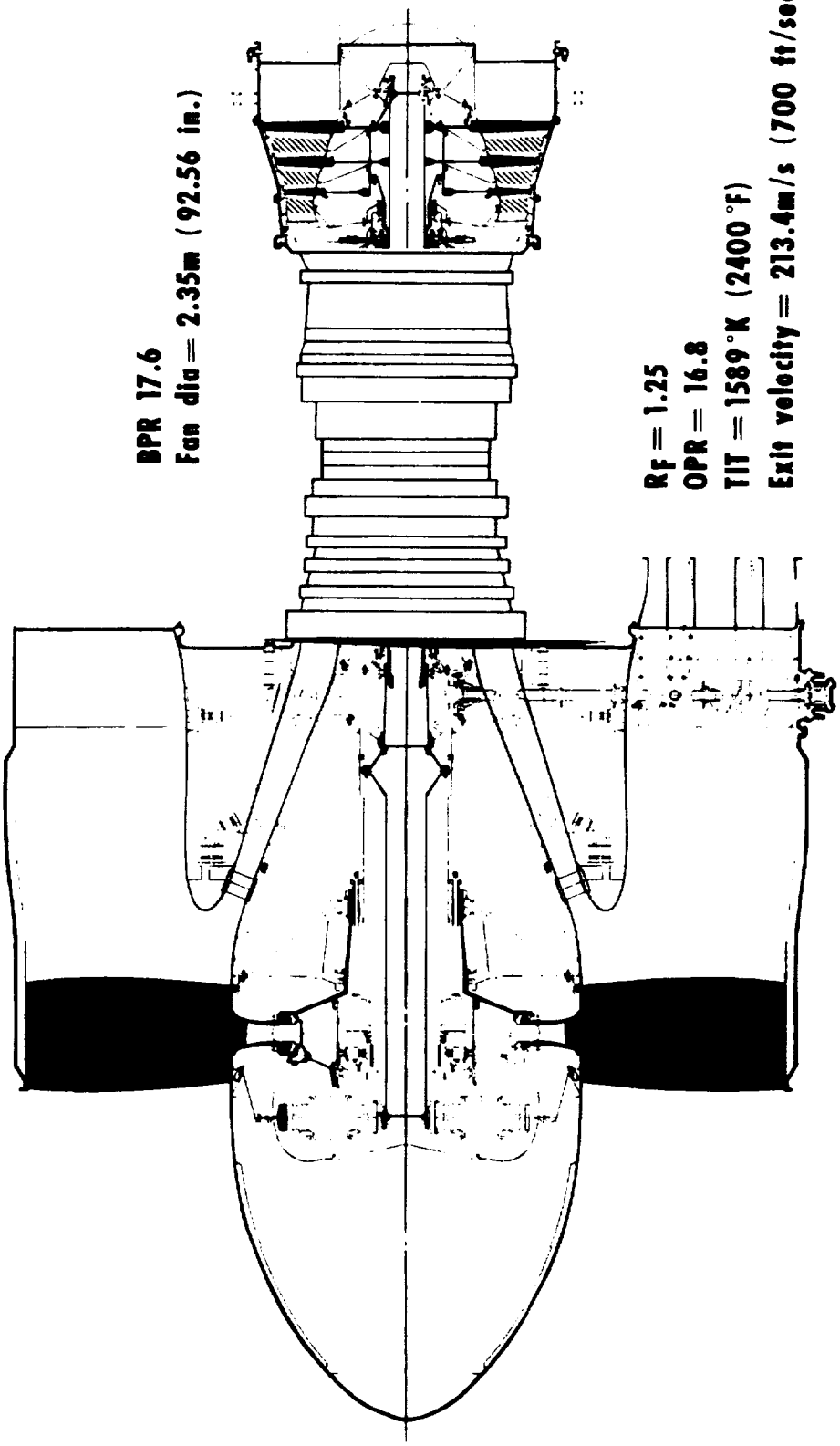

Figure 1-1. PD287-5 variable-pitch fan engine.

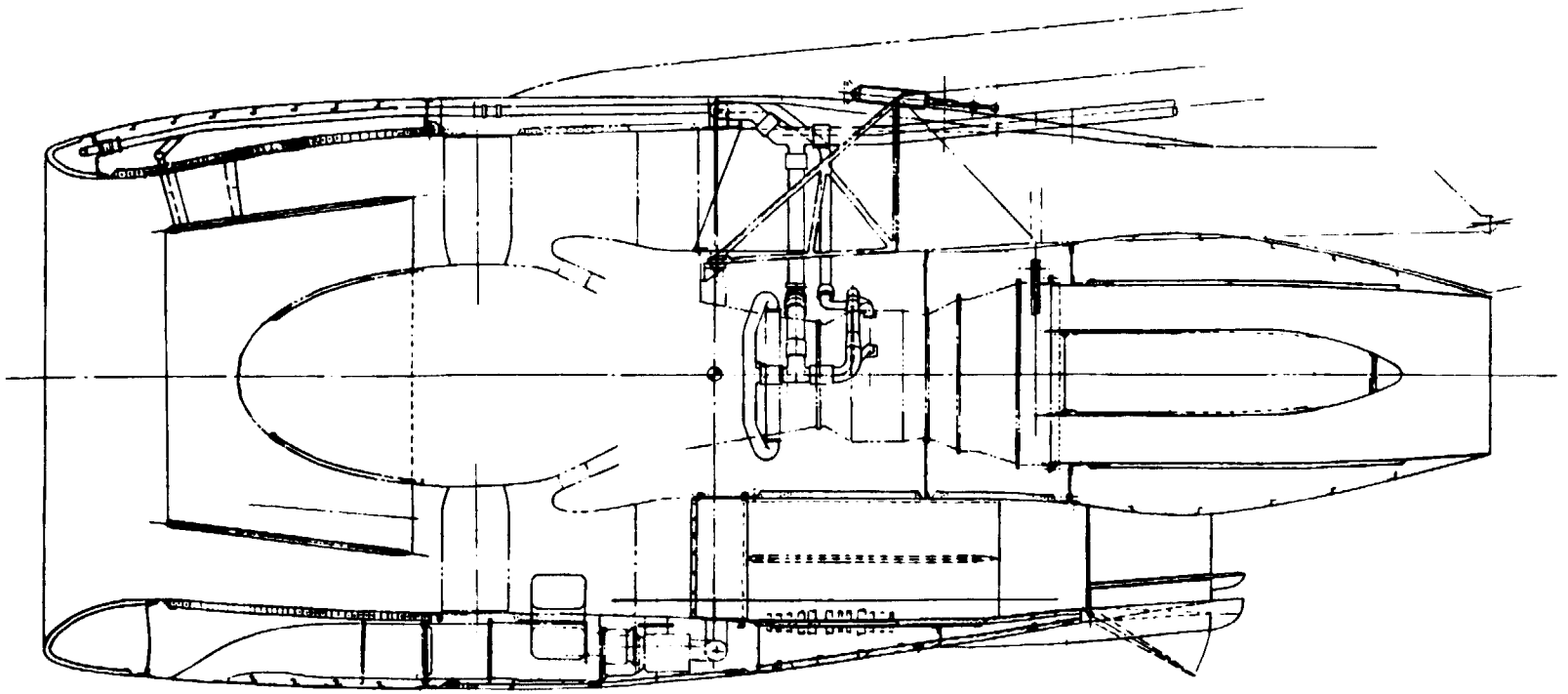

Figure 1-2. PD287-5 (95 EPNdB) engine nacelle for EBF under-the-wing system.

- Advanced technology demonstrations
  - Boron-epoxy fan blades, composite nacelle structure
  - Digital control systems
  - Advanced fan blade configurations—acoustic reduction
  - Advanced noise suppressor designs—variable-impedance balancing

II. INTRODUCTION

ENGINE SELECTION—PRELIMINARY DESIGN

Two objectives were established for the preliminary design studies.

1. The propulsion systems designed must meet STOL Aircraft System Study contractors' requirements for aircraft to be used in the 1978-80 time period. This required flight weight propulsion systems.

2. The propulsion systems should form a basis for the NASA QCSEE program. Flight weight nacelles are not necessary to demonstrate the noise, pollution, and performance technology.

The propulsion system designs and performance analysis generated in Task II meet the first objective. The second objective will be met as deviations from the flight weight propulsion systems are established by NASA and individual contractors in determining how required noise, pollution, and performance technology will best be demonstrated.

Task II Propulsion System Cycle parameters were defined by NASA from results of Task I studies, STOL Aircraft System Studies, and from other STOL aircraft system data. The most controlling of the propulsion system constraints was the 95-EPNdB noise requirement. Because of flap noise, this requirement places the externally blown flap (EBF) fan pressure ratio into two ranges: one for propulsion systems under-the-wing (UTW) and a second range for propulsion systems mounted over-the-wing (OTW). These ranges are:

- 1.25 to 1.28 for UTW
- 1.32 to 1.35 for OTW

The variation in fan pressure ratio level between UTW and OTW configurations is derived from benefits derived from OTW lower flap impingement noise and wing noise shielding. The exact OTW benefit is a function of the installation and optimum aircraft geometries are being established by extensive test programs. Similarly, the AW propulsion system cycle parameters were constrained by geometry limitations in the aircraft wing. The Task I studies revealed an AW fan pressure ratio of 2.6 to 2.8 to be near optimum. However, the practical limit on ducts which can be installed in a wing dictated a fan pressure ratio of 3.0 as a lower limit for the propulsion system. A second constraint found was the inlet noise for the 3.0 fan pressure ratio. Noise generated by a fan of this pressure ratio requires noise suppression sufficiently high so that either a partial sonic block with acoustic suppression rings or a full sonic block must be used on the engine inlet to meet the 95-EPNdB goal.

Propulsion system characteristics established in Task I and by analysis in Task II defined several nacelle and engine component characteristics. Fan-generated noise suggested blade-vane spacing of approximately two axial fan blade chords; fan tip speeds as low as possible (less than 1000 ft/sec for EBF engines) along with minimum number of blades were maintained. Fan-generated frequencies were kept as low as possible to satisfy minimum annoyance for noise summation in establishing effective perceived noise in decibels (EPNdB). Minimum numbers of inlet and exhaust noise suppression splitter rings were an objective to keep aerodynamic losses to a minimum and retain reasonable cruise performance characteristics. Fan tip speed and blade aspect ratios were monitored carefully to achieve proper stability for inlet flow distortion angles of as high as 36 deg . The exhaust systems were designed with separate flow because of the extreme sensitivity of low-pressure fans to performance losses from mixed flow engines. Composite fan blades were used on variable-pitch fans with lightweight fan casings. Composite nacelle parts were used in selected components. The primary nozzles were shown as straight concentric units even though canted nozzles were recommended separately (because the canting required is determined by the aircraft installation and varies with flap system geometry selection). The inlet cowl shape was selected to prevent separation of flow in the worst inlet distortion case. Optimum packaging of accessory gearboxes (fan case lower quadrant), engine buildup units, engine bleed lines (including anti-icing), and thrust reversers were carefully selected to ensure practical operation. Nacelle inspection and maintenance doors were drawn to reflect good accessibility for borescope inspections, minor component replacement, and other fast maintenance. Vertical propulsion system lowering from the aircraft was incorporated. Thrust reversing was established to satisfy the deceleration required (0.35 g) for wet and icy runways. Variable fan exhaust nozzles were employed on EBF engines to maximize engine performance at cruise, takeoff, and reverse thrust.

APPROACH TO OVERALL PROPULSION SYSTEM DESIGN

Integration of the nacelle and engine design to minimize weight and specific fuel consumption while maintaining maximum propulsion system thrust required a coordinated team effort by engine and nacelle experts. A three member team consisting of DDA (prime contractor), Rohr Industries (subcontractor), and Hamilton Standard (subcontractor) was selected to accomplish the preliminary design of the Task II propulsion systems. DDA has extensive aircraft gas turbine experience. Rohr Industries has installed nacelles on engines for many years and currently is the nacelle manufacturer for nacelles on commercial aircraft such as the DC-10, DC-9, 747, and other commercial aircraft. Thus, the engine and nacelle are assured of the experience and know-how for packaging to provide maximum credibility. The requirement for low-noise and minimum direct operating cost make the variable-pitch fan the best contender for future quiet engines. Hamilton Standard was selected as a subcontractor who has the variable pitch fan experience to give maximum credibility in this area. With this three member team, every detailed propulsion system item was covered by experienced personnel and the preliminary design activity was conducted.

The technical approach to the preliminary design was to select advanced propulsion system components by analysis, make detailed layouts to show compatibility of components, and to conduct performance analyses which could be provided to airframe companies and to NASA. The depth of the analyses was that required to show feasibility of design while meeting target noise, pollution, and performance goals. This required identification of critical components which needed thorough analysis and knowing what parts did not need an in-depth analysis. For example, four of the five propulsion systems used an existing core engine. Analysis on this core engine had been accomplished in prior programs and only integration of this engine into each propulsion system was necessary. Further, the primary technology required for a "quiet, clean" propulsion system is that involving aerodynamics (mostly in the low-pressure side of the turbofan engine except for the pollution) and acoustics which are a joint nacelle-engine design team activity. Emphasis was thus placed in the aerodynamics and acoustics areas with adequate structural activity to ensure credible mechanical design.

COORDINATION WITH NASA STOL AIRCRAFT SYSTEM STUDY CONTRACTORS

The immediate applicability of the five propulsion systems designed in Task II is with the NASA STOL Aircraft System Study contractors. Propulsion system computer decks or data were provided these contractors for use in their Phase II aircraft studies (similar computerized performance decks were provided to NASA). It was established that the propulsion systems in Task II should reflect installed nacelle geometry which was as compatible as possible with the two NASA STOL Aircraft System Study contractors Phase I aircraft while reflecting NASA test data where applicable. Visits to NASA Lewis, Lockheed Aircraft, and McDonnel-Douglas Aircraft were made and several scheduled reports by NASA, and the two NASA STOL Aircraft System Study contractors established the basic nacelle overall configurations reported herein. This coordination was a scheduled part of the program. Figures 2-1 through 2-3 show the reference aircraft geometrics used for the EBF-UTW, EBF-OTW, and AW propulsion systems. Figures 2-4 through 2-6 are the corresponding Douglas and Lockheed propulsion system installations. These installations were selected as starting geometries to initiate preliminary design. Detailed analysis, layouts and design trade-offs then established nearly optimum propulsion system designs for the five Task II propulsion systems. New and improving EBF and AW technologies from NASA and industry will almost certainly suggest improvements beyond the selected geometries. Coordination which occurred with NASA and aircraft companies was constructive and further integrated propulsion system-aircraft studies will promote improved STOL aircraft designs.

UNIQUE STOL PROPULSION SYSTEM PRELIMINARY DESIGN PROBLEMS

STOL aircraft are evolving with basic parameters such as final noise levels, runway length, design mission, aircraft size, and numbers of engines determined. For this task, 95-EPNdB, 610-m (2000-ft) runways, 926-km (500-nmi) design mission, 100 to 200 passenger size, and four engine aircraft were assumed. Unique design problems encountered with propulsion systems for STOL aircraft are:

- Acoustically treated nacelles

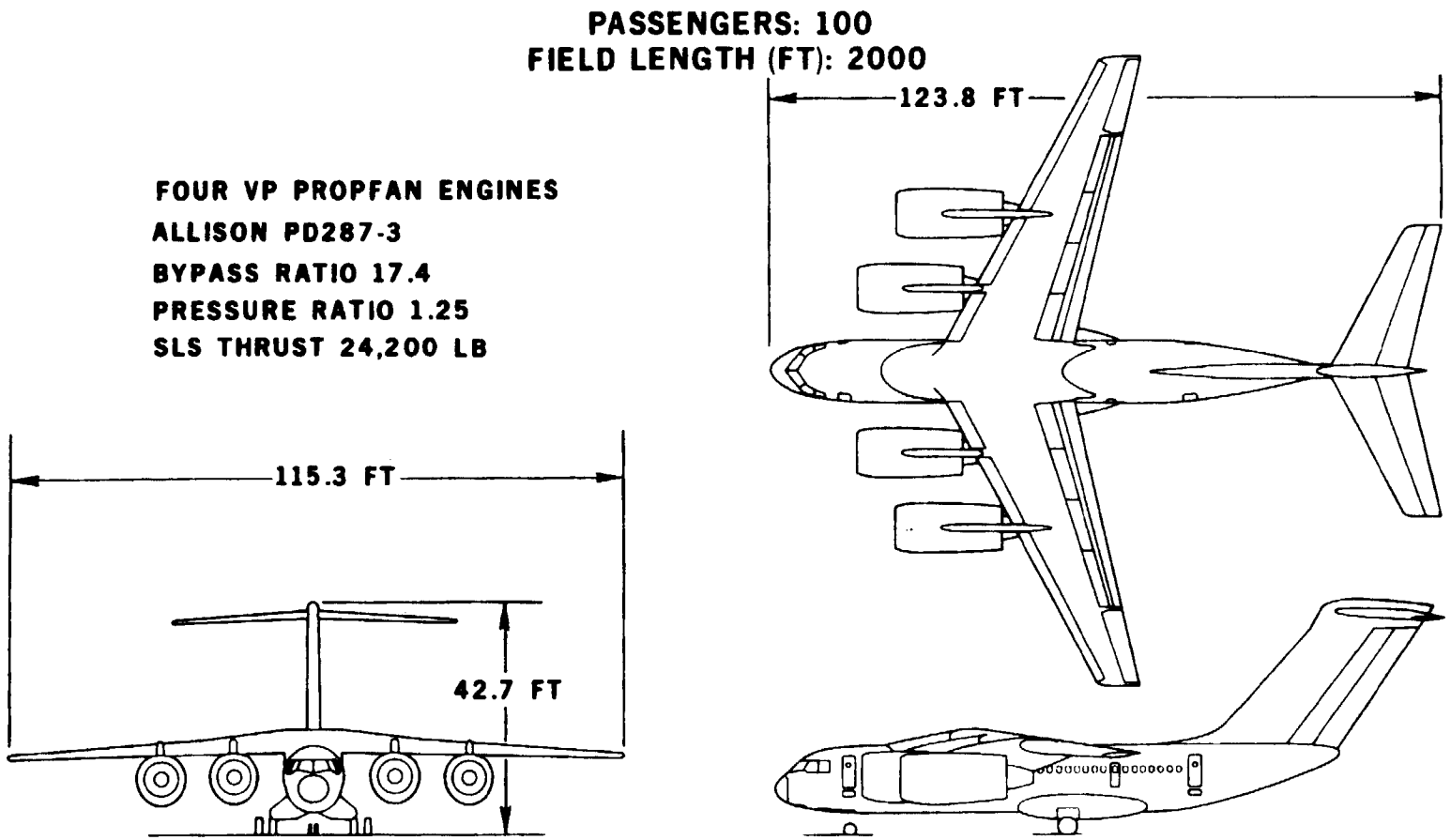

Figure 2-1. EBF-UTW aircraft (Reference 1).

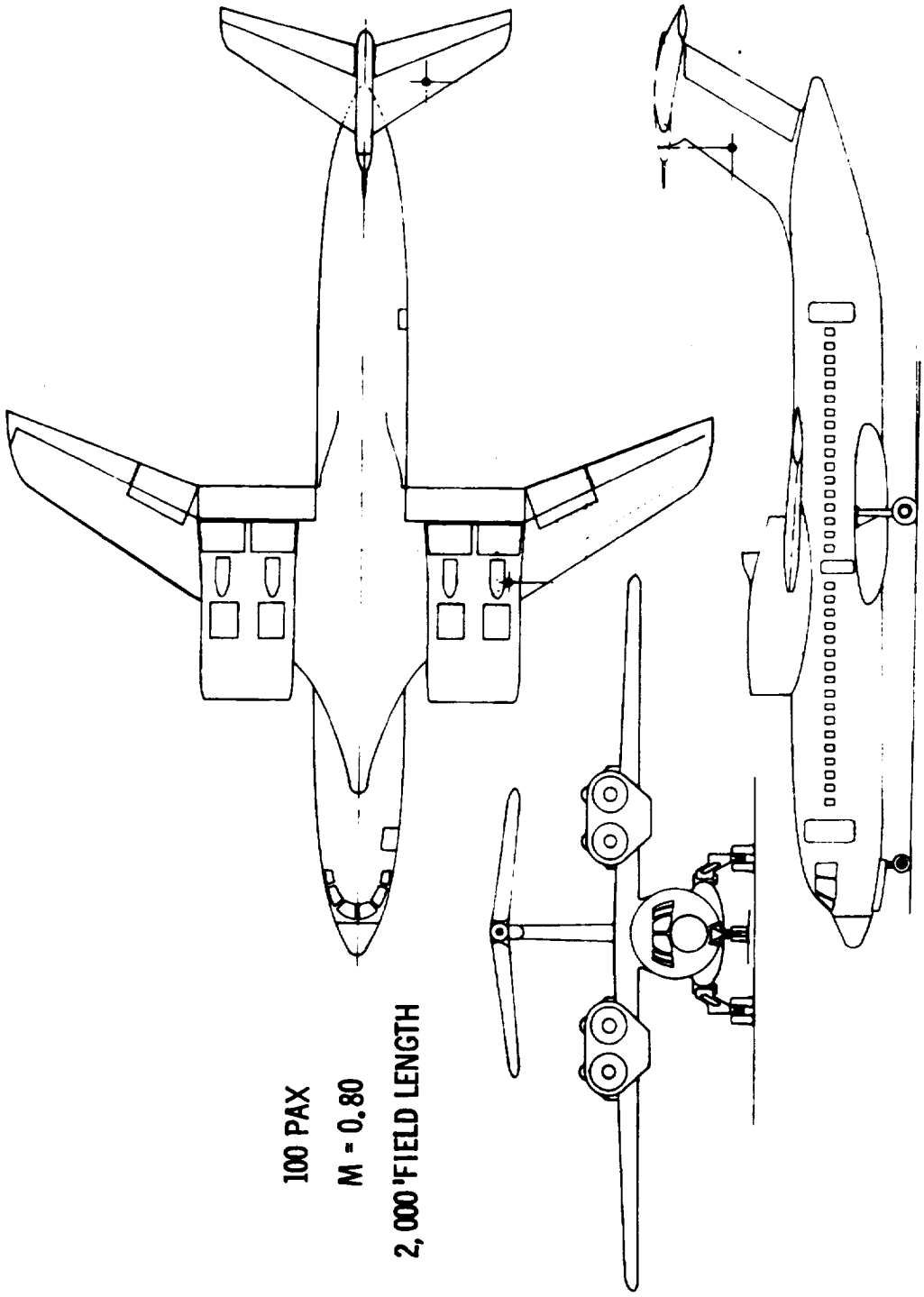

Figure 2-2. EBF-OTW aircraft (Reference 2).

PASSENGERS: 100 FIELD LENGTH (FT): 2000

FOUR TURBOFAN ENGINES
ALLISON PD287-43
BYPASS RATIO 2.8
PRESSURE RATIO 3.0
SLS THRUST 17,400 LB

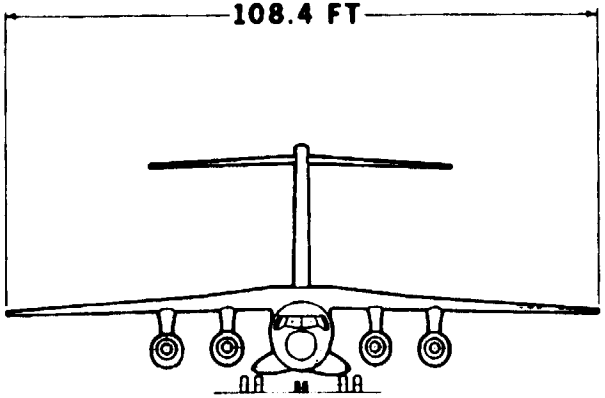

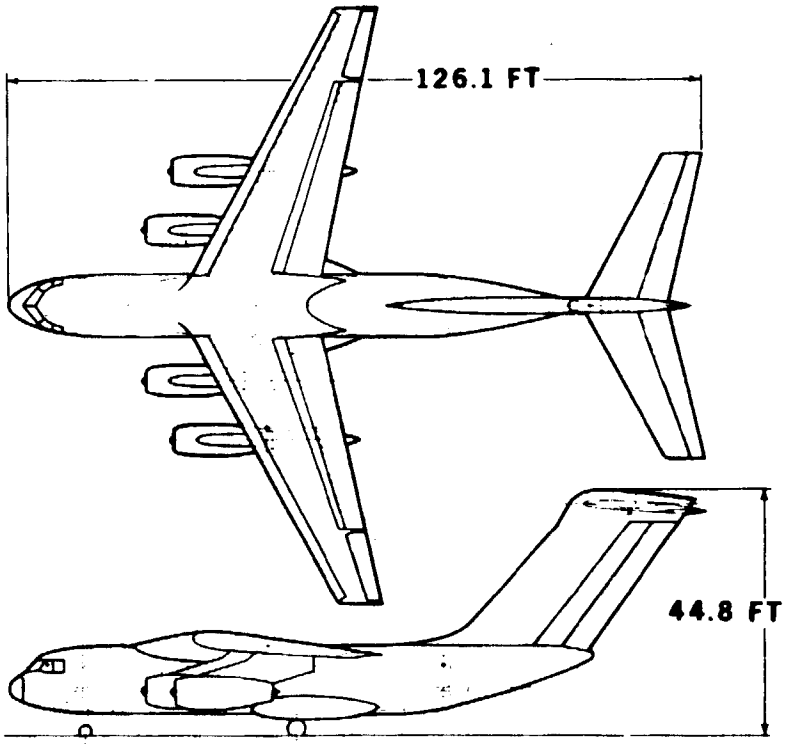

Figure 2-3. AW aircraft (Reference 1).

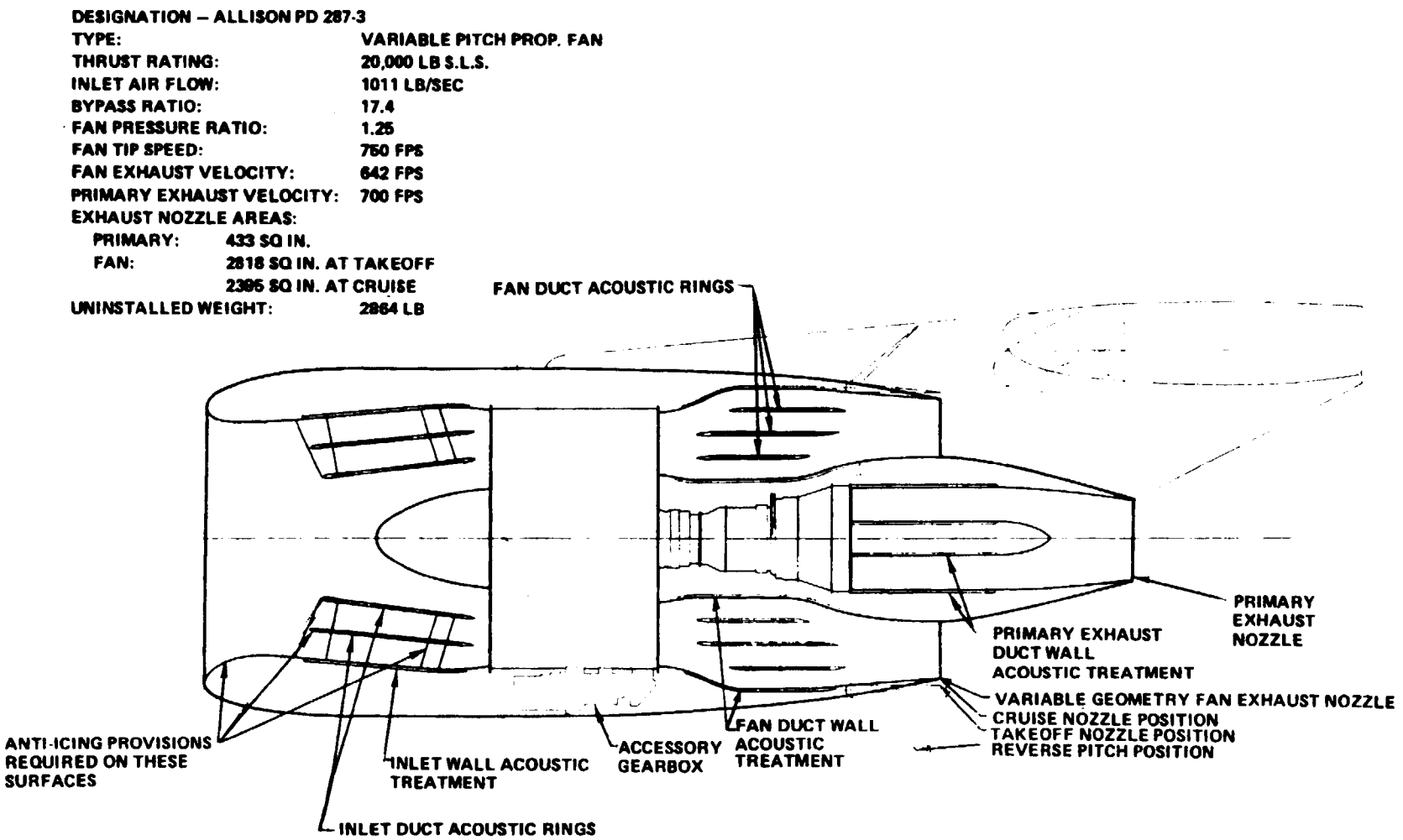

Figure 2-4. EBF-UTW propulsion system installation (Reference 1).

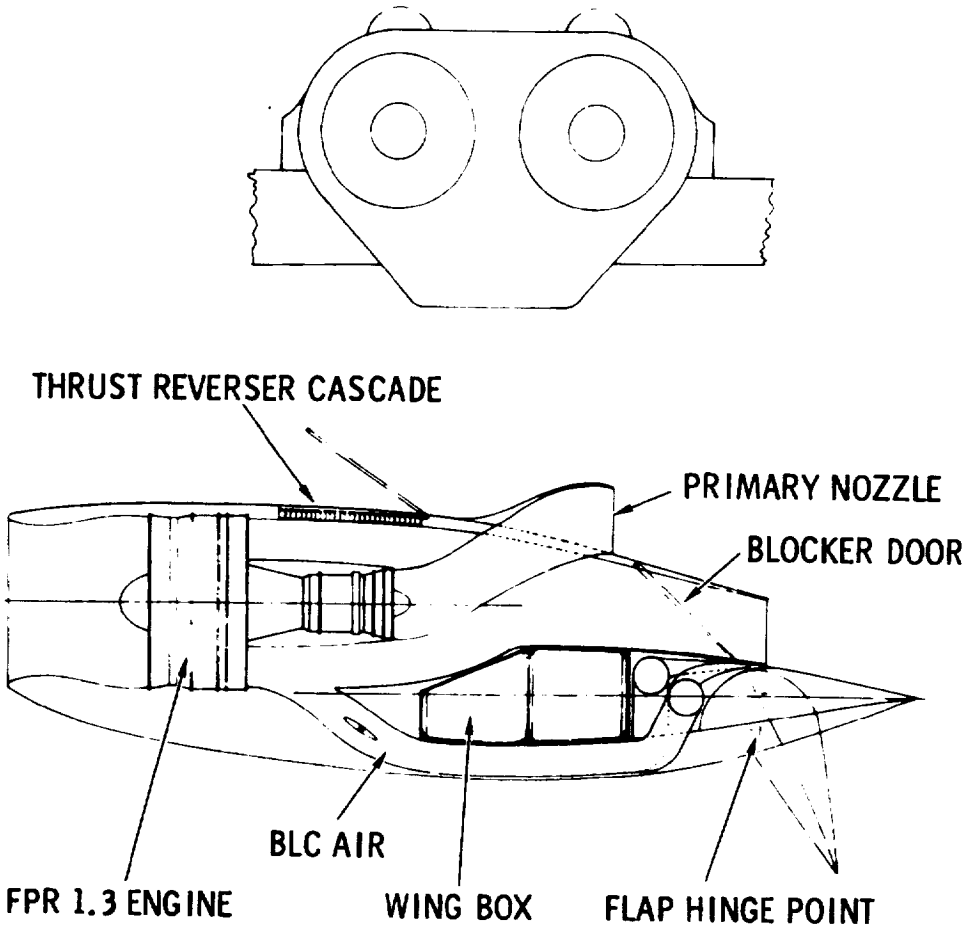

Figure 2-5. EBF-OTW propulsion system installation (Reference 2).

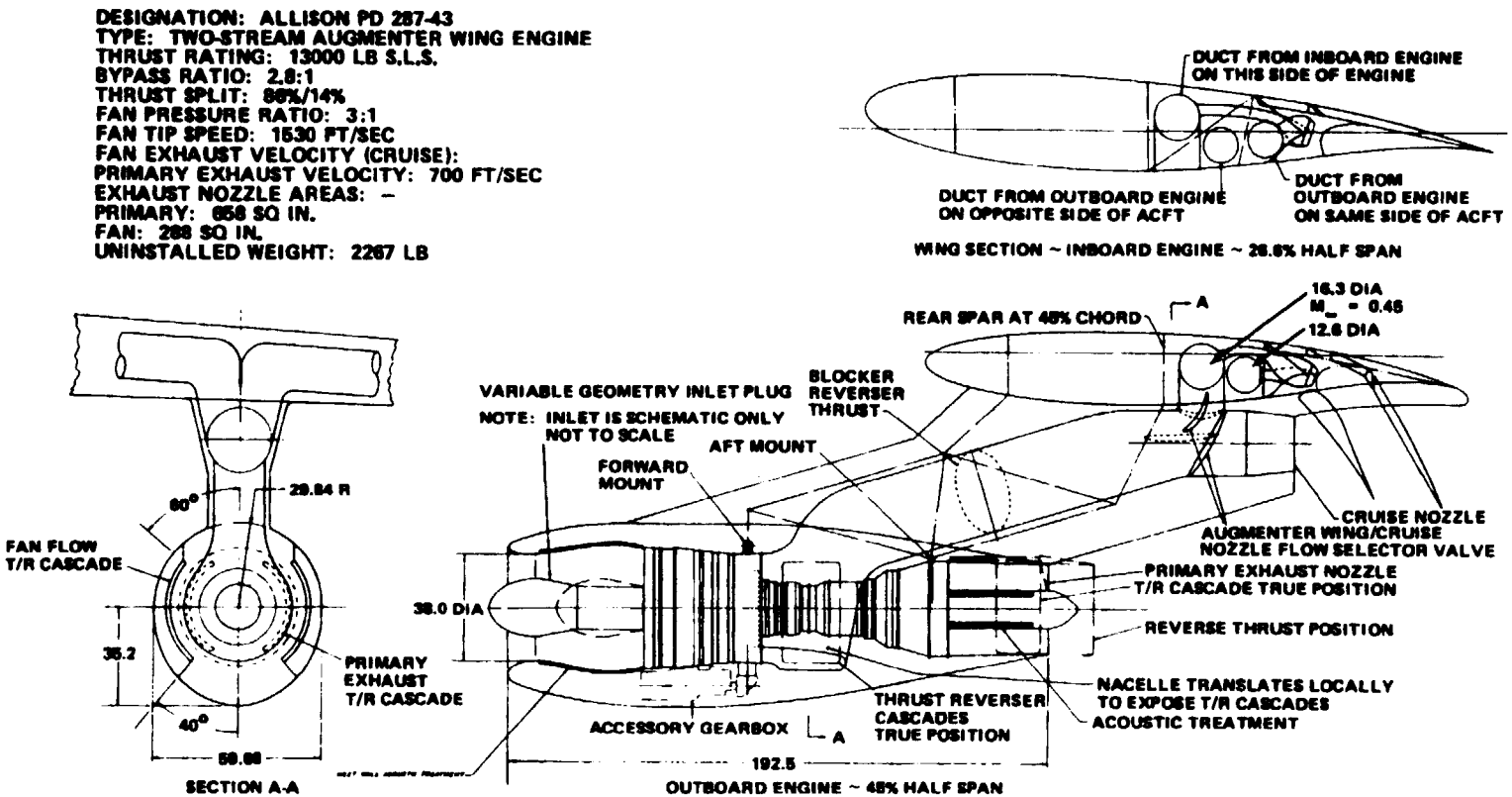

Figure 2-6. AW propulsion system installation (Reference 1).

- High-bypass ratio turbofan engines
- Low-primary engine exhaust velocities
- Variable-pitch fans
- Variable-fan exhaust nozzles
- Unique thrust reversers (variable-pitch fan and stationary reversers which deflect the thrust up to prevent F. O. D. and recirculation problems)
- High-inlet distortion because of high angle of attack in STOL aircraft transient operating conditions
- Fast engine thrust change for engine-out on takeoff or approach
- Rigorous pollution standards
- Aircraft-propulsion system integrated noise design
- Potentially high engine bleed
- Emergence of composite material usage in engines and nacelles
- Automatic control systems with propulsion system interlock to aircraft control surfaces

Each of these problem areas have been studied in sufficient depth to establish that each Task II propulsion system will either satisfy the new problem area or show that propulsion system design accommodates the unique requirement.

PRESENTATION OF STUDY RESULTS

The preliminary design activity presented is placed in the following order:

- Design requirements—Specific design requirements are discussed for STOL propulsion systems.
- Propulsion system descriptions—Each propulsion system is described in detail.
- Noise characteristics—Detailed noise data for 95- and 100-EPNdB propulsion system configurations are presented and acoustic methods are shown.
- Component definitions—Each important propulsion system component area is defined in detail and analysis shown where required.
- Conclusions and recommendations of the Task II effort are presented.

This order of presentation helps the reader to first understand each of the five propulsion systems and then to examine the details of the preliminary designs.

REFERENCES

1. Study of Quiet Turbofan STOL Aircraft for Short-Haul Transportation, Phase I Review. NASA Contract NAS2-6994. McDonnell Douglas Corporation. 18 September 1972.

2. Quiet Turbofan STOL Aircraft for Short Haul Transportation, Phase I Oral Review. NASA Contract NAS2-6995. Lockheed Aircraft Corporation. 19 September 1972.

III. PRELIMINARY DESIGN STUDY RESULTS

3a. Design Requirements

The development of a viable, commercial STOL mass transportation system will, to a large extent, depend on the successful development of a quiet, clean STOL propulsion system. The design of such a system must integrate a multitude of requirements, some of which are unique to STOL aircraft operation. Any STOL mass transportation system must be as unobstrusive as possible during operation to gain and maintain public acceptance and must be demonstrated to be safe to operate and economically viable before commercial operators will consider its use.

Noise and air pollution are receiving ever-increasing attention from the public, and this increased awareness is being manifested by legislative action imposing strict requirements on both types of pollution. Commercial aircraft noise is already subject to federal legislation administered through stringent FAA certification requirements (FAR 36). The requirements for further reduction in aircraft noise, particularly for STOL aircraft, suggests that maximum noise levels of 95 EPNdB may become a standard for future commercial aircraft. Combustion emission levels for automotive and heavy duty vehicles are already subject to requirements specified by the 1967 Clean Air Act administered by the EPA and an FAA set of requirements to cover aircraft pollutant emissions is imminent.

The development of STOL propulsion systems capable of meeting these requirements is a necessity to maintain a healthy and expanding air transportation industry. The design of all Task II QCSEE propulsion systems has addressed to these requirements. The proposed propulsion systems meet the noise goal of 95 EPNdB at 152 m (500 ft). This has been accomplished by judicious selection of engine operating parameters (fan tip speed, jet efflux velocity, turbine configuration, etc) in combination with optimum noise attenuation components. In the case of the AW propulsion system, forward propagation of fan noise is blocked by a sonic noise inlet formed in the throat area of the inlet vanes. In the EBF installations, low noise operation is obtained by design configurations which assure low noise generation and efficient attenuation of the noise generated.

The exhaust emission levels specified by NASA made necessary the selection of a staged fuel combustor in each propulsion system. The design pollutant emission levels are summarized in Table 3a-I.

The proposed combustor meets or exceeds the specified pollutant limits. The system utilized a combustion geometry featuring high efficiency combustion at idle to reduce the formation of carbon monoxide and unburned hydrocarbons and a premix-prevaporization system at high powers to obtain uniform combustion free of "hot spots" (which produce high levels of oxides of nitrogen).

Table 3a-I.
QCSEE pollutant limits.

Pollutant	Critical condition	Limits
Smoke	Takeoff	SAE No. = 15
Carbon monoxide	Idle	$0.040 \frac{\text{mass of pollutant}}{\text{mass of fuel}}$
Unburned hydrocarbons	Idle	$0.008 \frac{\text{mass of pollutant}}{\text{mass of fuel}}$
Oxides of nitrogen	Takeoff	$[R_o = 18.0]$ $0.006 \frac{\text{mass of pollutant}}{\text{mass of fuel}}$
		$[R_o = 30.0]$ $0.012 \frac{\text{mass of pollutant}}{\text{mass of fuel}}$

The operational safety of a STOL transport aircraft will, to a large extent, depend on the dynamic thrust response of the engines and the successful integration of the aircraft and propulsion system controls. DDA has addressed to these requirements through the use of variable gas path geometry and an integrated control system which allow the maintenance of high rotor speeds over a wide range of engine operation. This approach has resulted in engine configurations capable of meeting the dynamic thrust response characteristics show in Figure 3a-1. Consideration has been given to the eventual integration of the propulsion system control with the aircraft's automatic flight control system and components that are compatible with a digital control system have been utilized.

Control of a STOL aircraft will require that engine bleed air be available to blow various aircraft control surfaces and (to ensure safe operation during icing conditions) that aerodynamic surfaces be kept ice-free. For these reasons, ample engine bleed ports are provided to supply the required air.

In order to assure safe operation on short runways, most STOL aircraft will require a thrust reversal system capable of safe operation down to ground speeds as low as 10 m/s (20 kt). The Task II propulsion systems have been designed to address to the problem areas that limit the usefulness of conventional thrust reversing device (i.e., exhaust gas reingestion, undesirable exhaust gas impingement, buoyancy effects, drag interference, and engine stability problems). The use of a reversible, variable pitch fan configuration minimizes these problems. On the fixed pitch fan engines, care has been taken to select configurations and geometry to deflect reverse gas upward and away from the engine inlet cowl.

To preclude the necessity for attempting a landing approach with one engine inoperable because of engine shutdown during flight, the combustion systems have been designed with the capabilty for relight up to 9.144-m (30,000-ft) altitude.

The initial cost, size, and operational costs associated with a STOL aircraft are heavily dependent on propulsion system thrust-to-weight ratio. This requirement was met by utilizing advanced technology design concepts and materials consistent with the expected date of service introduction (i.e., late 1970's to early 1980's). This approach is manifested in the use of composite materials, an advanced technology high performance core gas generator, careful integration of the engine and nacelle, and component design using advanced turbine engine materials.

The growth potential of the propulsion system has been given careful consideration. The incorporation of the GMA 100 gas generator ensures the flexibility required to increase operating

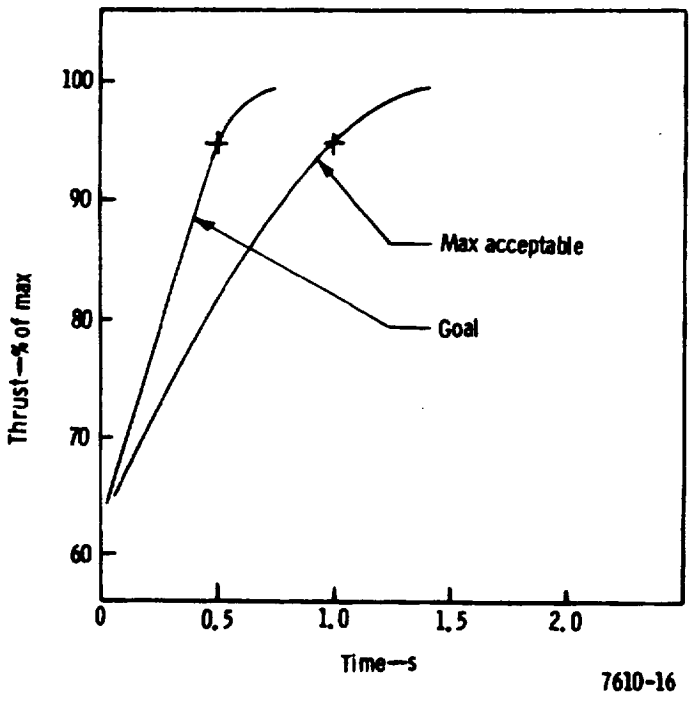

Figure 3a-1. Dynamic thrust response characteristics. *

*Note: Curve labeled "goal" from contract work statement; curve labeled. "Max acceptable" from McDonnel-Douglas Phase I comments on propulsion systems for STOL aircraft.

parameters such as airflow, cycle pressure ratio, and turbine temperatures without significantly impacting size or weight. The propulsion system inlet cowls have been designed to accept a 5% increase in airflow.

Operational costs are an important part of the economic success of any system. DDA has addressed to this design requirement by designing the propulsion systems to be highly maintainable. The nacelles are designed to open readily for rapid access to any area of the engine. All engine accessories are mounted on the outer fan case and a separate cowl is provided to allow access without disturbing other engine or nacelle components. The propulsion systems are designed to allow easy removal of the engine which can be dropped straight down for safety considerations. The engine design features simple, rugged construction in modular components to allow engine disassembly and component replacement with minimum elapsed time. Borescope ports are provided to allow inspection of all gas path components.

System reliability has been an important design requirement. The reliability oriented design approach utilized is evident in the GMA100 gas generator. This gas generator utilizes simple construction designed specifically for STOL applications. The high performance compressor uses approximately 30% fewer blades than contemporary compressors operating at the same pressure ratio. Labyrinth seals are used throughout the engine to provide reliable operation. The rotor construction minimizes the number of main rotor bearings. All components have been designed for long life when operating under conditions peculiar to STOL operation (e.g., high number of start-stop cycles). Allowable design stresses have been established based on a historically determined reliability apportionment for each engine component and desired engine reliability. These design criteria also include consideration of a typical 926-km (500-nmi) duty mission cycle. The specific engine design life and operating duty cycle characteristics used are summarized in Table 3a-II.

Table 3a-II.
Engine design life and duty cycle characteristics.

Design life	
Cold section parts, 72 Ms (20,000 hr)	18,000 cycles
Hot section parts, 29 Ms (8,000 hr)	7,100 cycles
Engine duty cycle	
Maximum power	2.3% of total time
Climb power	6.5% of total time
Cruise power	91.2% of total time
Environmental temperature distribution	
Ambient temperature, 305°K (90°F) or higher—17.5% of total time	
Ambient temperature, 289°K (60°F) or higher—82.5% of total time	

System components have been designed to operate satisfactorily within the flight envelope shown in Figure 3a-2 under the flight maneuver loading conditions specified in Figure 3a-3. The flight maneuver load envelope has been developed by DDA for STOL transport operation to recognize the more stringent requirements imposed by STOL takeoffs and landings.

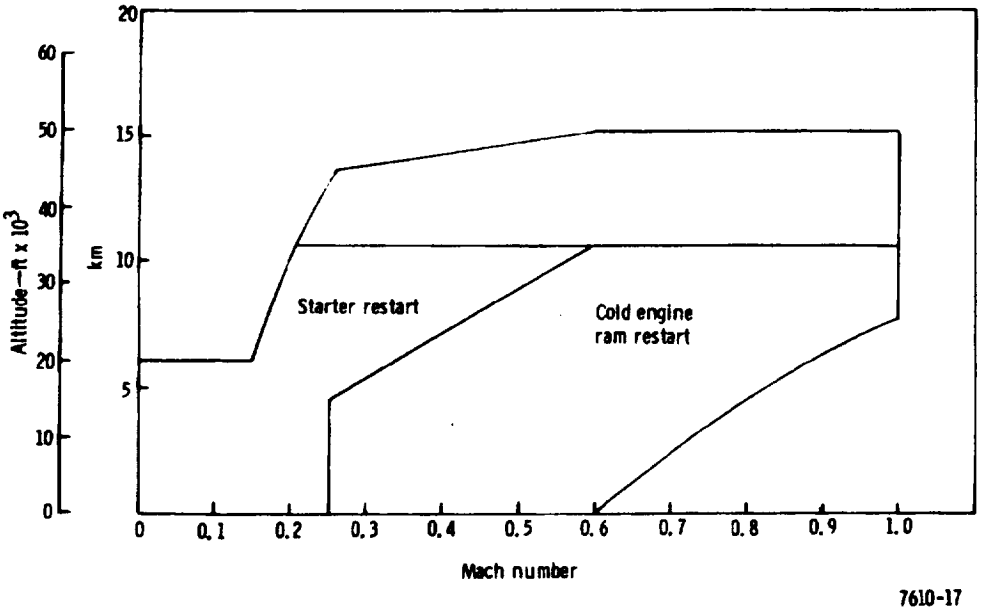

Figure 3a-2. Flight envelope.

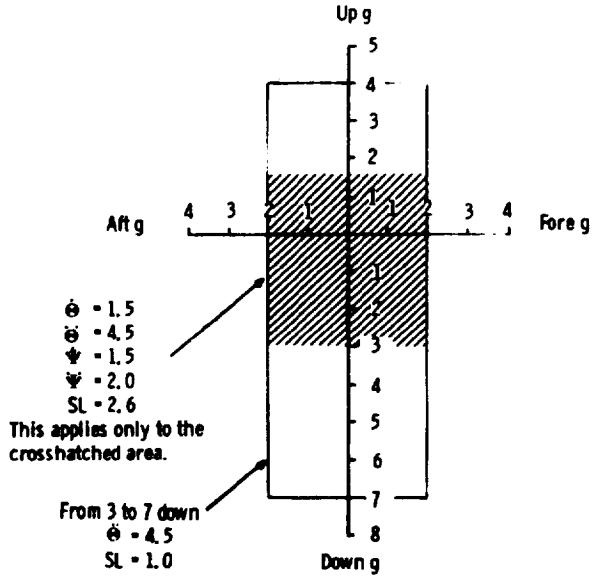

1. $\dot{\theta}$ and $\ddot{\theta}$ are pitching velocity and acceleration—rad/s and rad/s^2.
2. $\dot{\psi}$ and $\ddot{\psi}$ are yawing velocity and acceleration—rad/s and rad/s^2.
3. SL is the side load to either side, g.
4. Load factors, angular velocities, and accelerations should be taken at or about the center of gravity of the engine.

7610-18

Figure 3a-3. Maneuver loads.

3b. Description of Propulsion Systems

The five propulsion systems selected for Task II preliminary design are applicable to STOL aircraft that use both EBF and AW high lift systems. The five engines, all of which are configured around the GMA100 advanced technology core gas generator, cover a bypass ratio range from approximately 2 (AW) to 18 (EBF). They encompass both direct and gear-driven fans featuring fixed and variable pitch fan blading. Common hardware has been used wherever possible. For example, three of the EBF QCSEE engines use common gas generator and fan turbine hardware with the exception of reset turbine airfoils.

The resulting propulsion systems—engine, nacelle, and ancillary systems—have been configured for both major EBF concepts (i.e., UTW and OTW engine placement) as well as a UTW augmentor wing installation. Detailed nacelle designs are shown in Subsection 3d1 of this report.

The pertinent features and estimated weight summaries for each propulsion system are summarized in Tables 3b-I through 3b-III of the Supplement to this report.

GMA100 GAS GENERATOR

The design description and performance of the GMA100 advanced technology core used in the five Task II engines is presented in Subsection 3b1 of the Supplement to this report.

PD287-5 PROPULSION SYSTEM (R_F = 1.25—Variable Pitch)

PD287-5 is a high bypass ratio, geared turbofan engine. The engine consists of a Q-Fan, variable pitch fan system driven through a 3.89:1 ratio star-type planetary gear arrangement by a three-stage, high-speed fan turbine. The advanced technology GMA100 gas generator, comprising an axial flow compressor, an annular combustor, and an air-cooled, two-stage turbine forms the core of the PD287-5 engine. An engine general arrangement highlighting the fan system is shown in Figure 3b-1, and Figure 3b-2 shows the UTW installation. A complete general arrangement drawing of the engine showing core gas generator detail is contained in the Supplement to this report (Ref: Figure 3b2-1).

The PD287-5 Q-Fan system consists of 17 fan blades retained in a fan rotor supported on two main shaft bearings in the fan rotor/gear case. The fan rotor/gear case also contains two main components of the Q-Fan system (i.e., the pitch change mechanism and the reduction gear assembly). The fan is aerodynamically designed to produce a pressure ratio of 1.25 at the sea level static design point and operate at 31 s^{-1} (1857 rpm) which yields a fan tip speed of 229 m/s (750 ft/sec). The fan blades are retained in the hub by a single-row ball bearing which allow variable pitch operation. The variable pitch system consists of a hydraulic motor

drive mounted on the engine fan case driving a differential gear arrangement through a "no-back" device located in the fan rotor/gear case. Rotation of the hydraulic motor causes a differential speed relationship in the differential gear. This differential movement is transmitted through a harmonic drive gear to a synchronizing bevel gear meshing with bevel gear segments attached to the base of each blade. Each blade is thus rotated to the desired pitch which is controlled by the engine main fuel control. The reduction gear assembly is a star-type, planetary spur gear arrangement consisting of an input sun gear driven by the fan turbine, four planet gears mounted on a stationary carrier assembly, and an output ring gear attached to the fan rotor hub.

The Q-Fan assembly is integrated with and supported by the fan forward frame which forms the main structural element of the engine. This frame is an aluminum casting and supports the following propulsion system elements:

- Q-Fan assembly
- Inlet cowl
- Fan cowl
- Fan duct and variable nozzle assembly
- Core engine forward support bearing

The fan forward frame also contains the engine forward mount.

The core engine is the GMA100 advanced technology gas generator. This core consists of an axial flow compressor featuring an integral welded rotor drum and variable geometry vane stages, a high heat release annular combustor, and a two-stage, air-cooled turbine. The entire rotor system is cradled and simply supported. It is mounted on a ball bearing located in the fan forward frame below the first-stage wheel and a roller bearing in the interturbine transition duct structure aft of the second-stage turbine wheel. This arrangement leaves the diffuser/combustor inlet area free of nonaerodynamic structure and reduces the number of engine bearing sumps.

The short length, high heat release annular combustor has been designed to produce low emissions and an acceptable temperature pattern factor to ensure adequate turbine component life. The low pollution, staged combustor designed to meet NASA pollution standards will fit within this combustor envelope.

The two-stage, air-cooled turbine uses airfoils incorporating advanced technology cooling techniques to allow long service life at minimum performance penalty. These cooling techniques have been demonstrated at temperatures considerably in excess of the maximum rating temperatures selected for PD287-5.

Figure 3b-1. PD287-5 general arrangement—fan system. (Sheet 1 of 2) 7610-39

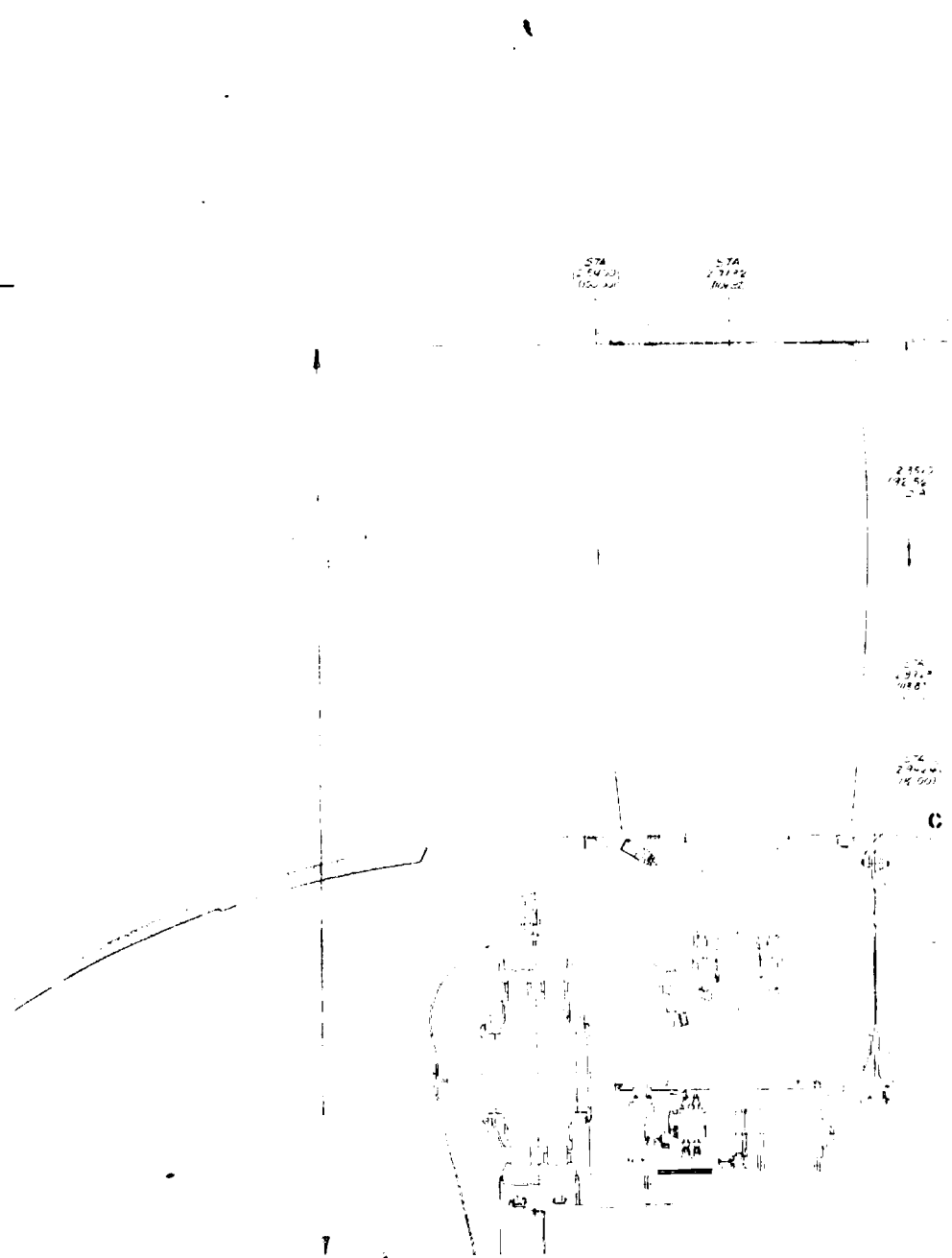

3b-3 A

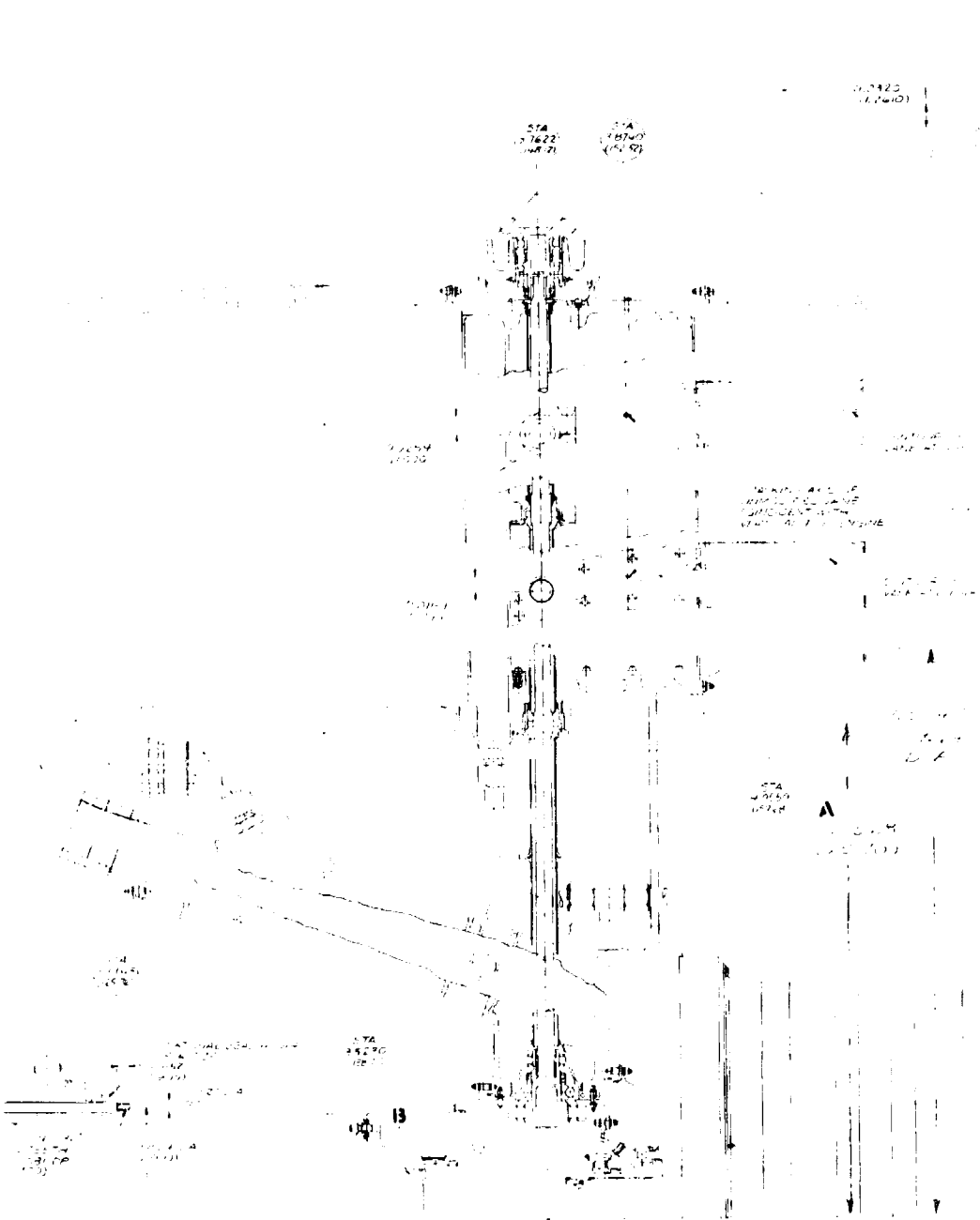

3b-3 B

Figure 3b-1. PD287-5 general arrang ment

Nacelle assembly	Material (alloy)
Inlet nose cowl	
Outer barrel	Aluminum
Inner barrel	Aluminum
Nose lip	Aluminum
Lip liner	Titanium
Bulkheads	Titanium
Attachment ring	Aluminum
Suppression ring	Aluminum
Fan cowl	Aluminum
Fan duct	
Inner wall	Aluminum
Outer wall	Aluminum
Bulkheads	Aluminum
Fan nozzle	
Flaps	Aluminum
Islands	Aluminum
Attachment ring	Aluminum
Primary nozzle	
Bulkheads	Nickel
Skin/stringer fairing	Titanium
Forward mount	Steel
Aft mount	Nickel

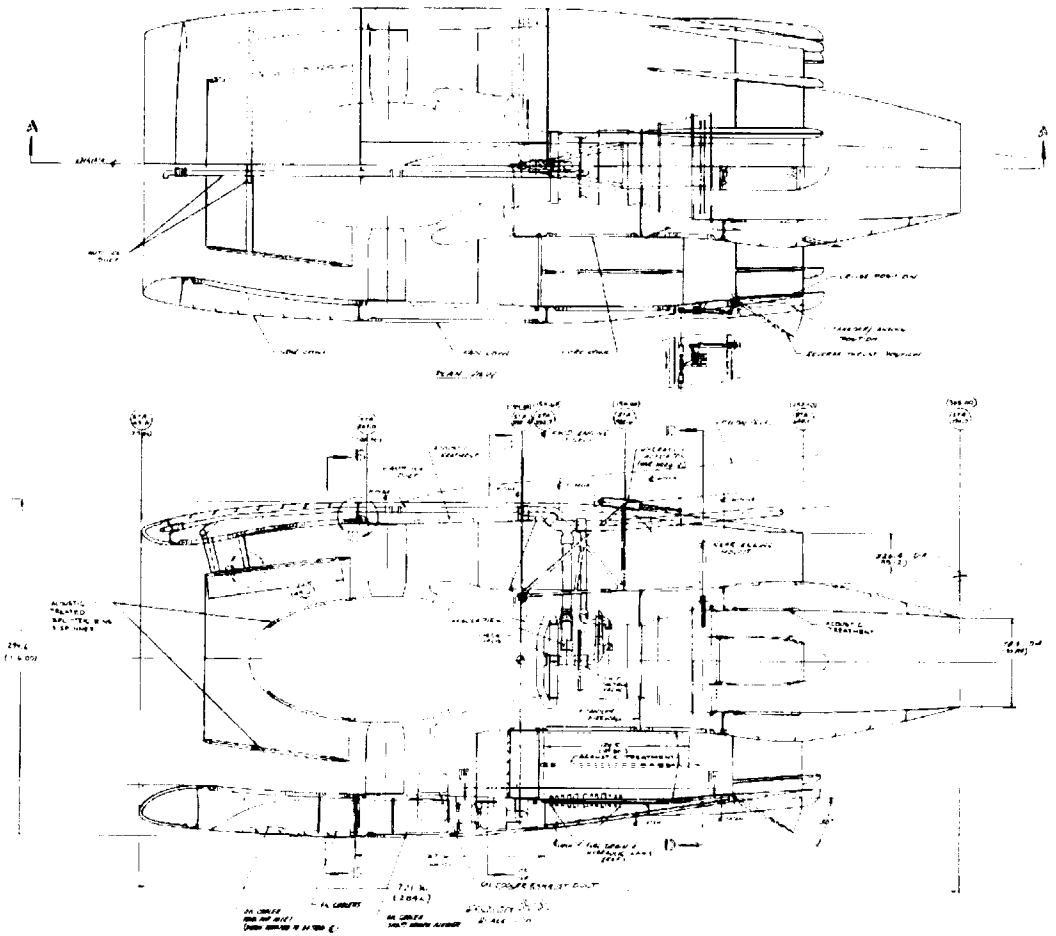

Figure 3b-2. PD287-5 propulsion system installation drawing (UTW-EBF) (Sheet 1 of 2).

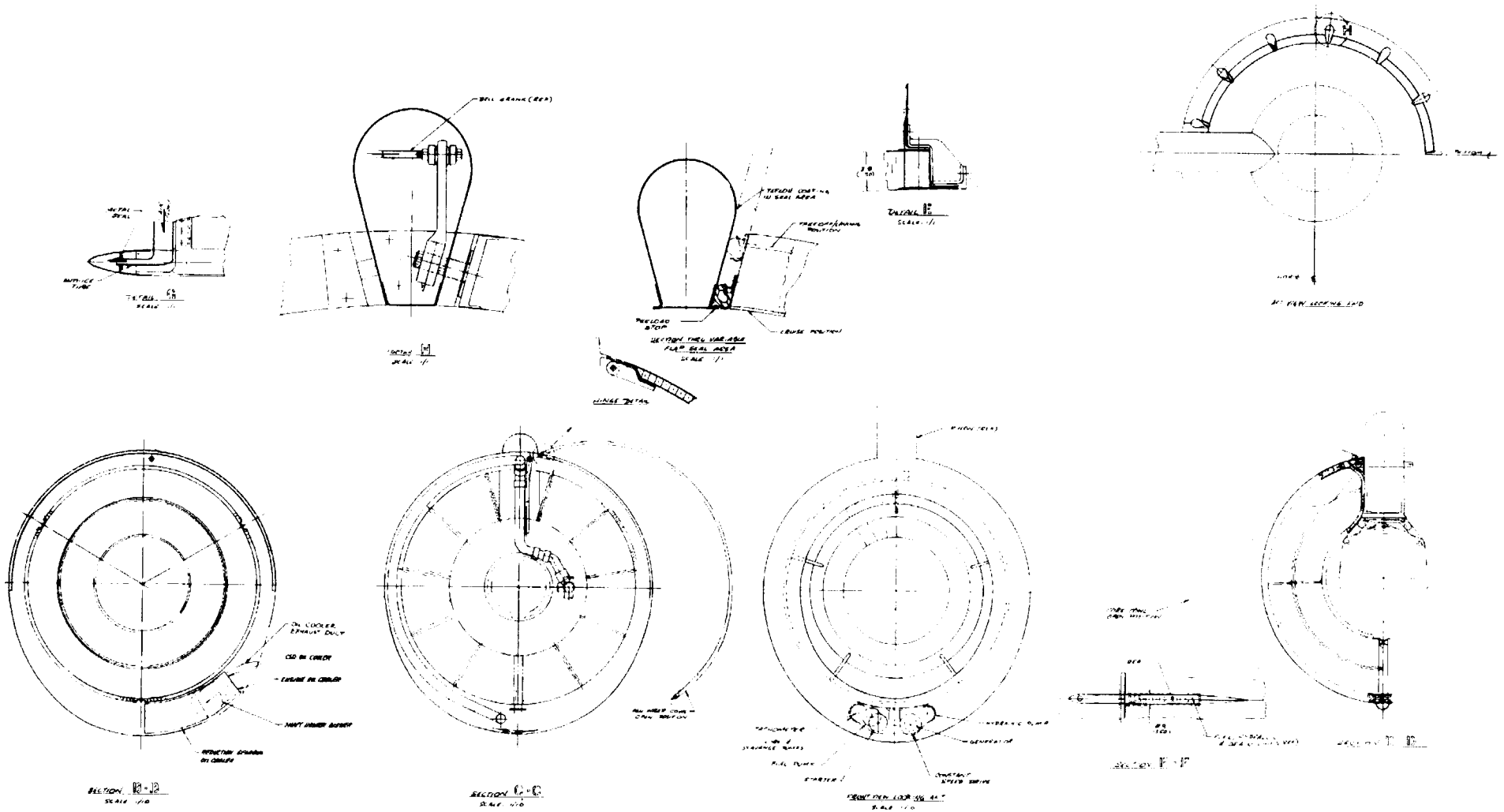

Figure 3b-2. PD287-5 propulsion system installation drawing (UTW-EBF) (Sheet 2 of 2).

The three-stage fan turbine is uncooled and is supported on a roller bearing mounted in the interturbine transition housing and a thrust ball bearing mounted in the rear bearing support. Compressor discharge air is introduced to a cavity behind the third-stage fan turbine wheel to balance the rearward thrust of the turbine assembly and reduce the axial thrust requirements imposed on the ball bearing. The rear bearing support is a Hastelloy S weldment consisting of an inner and outer ring separated by 12 hollow vanes designed to eliminate exit swirl of the turbine exhaust gases. The structure is designed to withstand the total turbine axial thrust load. The fan drive forward extension shaft is attached between the first- and second-stage fan turbine wheels and extends forward to a roller bearing support housed in the fan forward frame.

The engine compressor case has been provided with an air collection manifold and bleed ports at the fifth and seventh compressor stages. Fifth-stage bleed air is used to provide anti-icing air to the splitter and exit guide vanes in the fan housing and is connected through external plumbing and check valves to the compressor discharge bleed ports located on the outer combustor case. The fifth-stage compressor discharge may be used to provide aircraft bleed air service (for cabin conditioning, etc). The seventh-stage bleed system provides cooling air for the second-stage high-pressure turbine vane and wheel and for the fan turbine wheels.

The lubrication system for PD287-5 is shown in Figure 3b-3. This system consists of two independent dry sump oil systems. One oil system provides lubrication, cooling, and filtering for the Q-Fan, a pitch change hydraulic system, and a nozzle actuation system. The other oil system is used to provide the same services for the core engine and fan turbine bearing sumps. Air-oil coolers mounted on the engine fan case provide oil temperature conditioning.

The vent and cooling system shown in Figure 3b2-2 of the Supplement is similar to the GMA100 and provides engine cooling, sump seal pressurization, and thrust balance air with minimum performance penalty. The system uses labyrinth seals to take advantage of their life capability. All engine vent air is routed to the accessory gearbox, passes through a centrifugal air-oil separator, and is vented overboard through a single port. The system combines advantages of minimum effect on engine performance with a minimum number of critical seal locations. The vent and cooling system shown is typical for all QCSEE engines.

The materials used throughout the engine are shown in Figure 3b2-3 of the Supplement to this report. Except for fan blades, the materials shown are typical for all QCSEE engines.

The propulsion system for PD287-5 has been designed for applicability to a UTW STOL aircraft using an EBF high lift wing (Figure 3b-2). The propulsion system design provides a low noise propulsion system of 95 EPNdB operation at 30 m (100 ft) attitude, at sea level static takeoff power, and a 152-m (500-ft) sideline noise measurement point. Maintainability has also been considered a primary design criterion. The design of the fan cowl and bifurcated

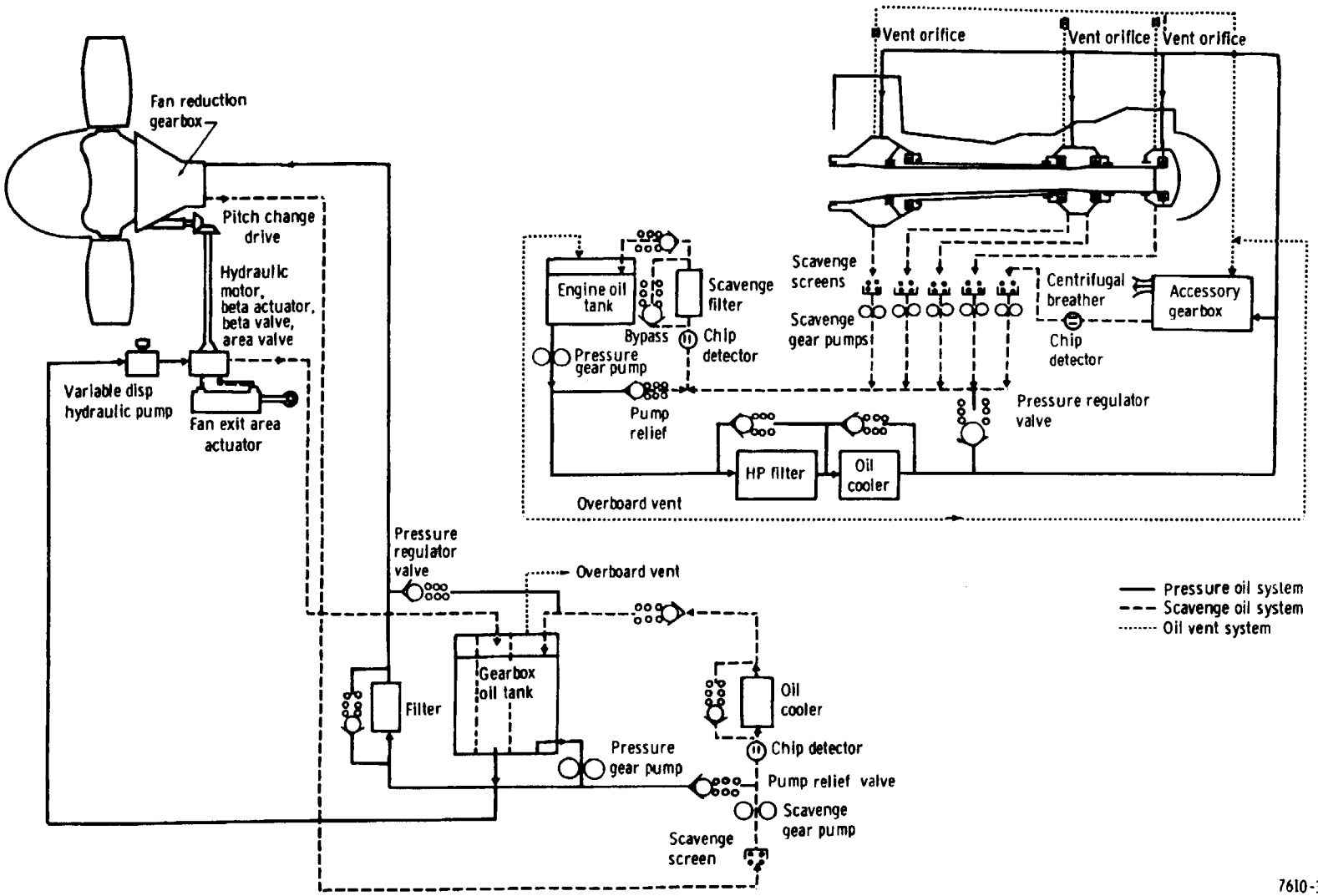

Figure 3b-3. PD287-5, -6, and -7 lubrication system schematic.

fan duct system allows rapid access to the accessories and engine core. The entire propulsion system is readily removed from the pylon. The engine, the engine inlet cowl, and the primary nozzle may be removed without removing the fan cowl and fan duct and nozzle assembly from the pylon. Reverse thrust operation is provided by changing the fan blade pitch angle to reverse pitch and opening the secondary nozzle to form an inlet duct for the reverse fan flow. No thrust reverser or spoiler on the primary stream is necessary because of the effectiveness of the variable pitch fan in reverse and the relatively low thrust of the primary stream.

A detailed discussion of the fuel system, control system, and installation ancillary systems is contained in Subsection 3d7.

PD287-6 PROPULSION SYSTEM (R_F = 1.325—Variable Pitch)

PD287-6 is a high bypass ratio, geared, variable pitch turbofan designed for low noise and low emissions. The engine is mechanically similar to PD287-5. However, the propulsion system installation is markedly different in that PD287-6 is designed for a OTW EBF aircraft. The engine consists of a variable pitch, Q-Fan system driven through a 2.96:1 ratio, planetary star gear system by a three-stage, high-speed fan turbine. The advanced technology GMA100 gas generator forms the core for PD287-6. Engine general arrangement drawings in Figure 3b-4 and Figure 3b-5 show the fan system and the OTW installation. A complete general arrangement drawing showing core gas generator detail is presented in the Supplement to this report (Ref: Figure 3b2-4).

The Q-Fan system consists of 23 blades retained in a fan rotor hub by a double row of ball bearings. The hub is supported on two bearings housed in the fan rotor/gear case similar to the PD287-5. The Q-Fan is designed to produce a pressure ratio of 1.325:1 at design point and operates at a fan tip speed of 282 m/s (925 ft/sec). The major components of the Q-Fan system are similar in type and identical in operation to those already discussed for the PD287-5.

The engine forward frame is similar to the forward frame described for the PD287-5. The core engine and fan turbine components for the PD287-6 are identical to the PD287-5 except for minor turbine airfoil resets. The lubrication system for the PD287-6 is identical to that shown in Figure 3b-3 for the PD287-5.

The area of major difference between the PD287-5 and PD287-6 is the propulsion system installation. The propulsion system for the PD287-6 has been designed for a OTW engine placement EBF STOL aircraft. This installation features a fan duct/nozzle configuration designed to blanket the wing with fan discharge air. Primary gas exits through a cylindrical nozzle above the rectangular secondary nozzle. During takeoff, excess fan air is ducted through a tube below the wing to a spanwise plenum in the wing. This air is used to augment the wing lift system by discharging air through nozzles in the wing trailing edge flap.

Reversing is accomplished by opening a door in the outer skin of the nacelle and exposing the blow-in doors which normally seal the outer wall of the fan duct. Simultaneously with the opening of the outer doors, an inner blocker door closes off the rear fan duct to prevent hot primary gas from flowing up the fan duct. Reversal of the fan blades causes a negative pressure gradient across the exposed blow-in doors; they open allowing air to flow into the annulus area to the rear of the fan.

The fuel system, control system, and installation ancillary systems are similar to the PD287-5 and are explained in detail in subsequent sections of this report.

PD287-7 PROPULSION SYSTEM (R_F = 1.25—Variable Pitch)

The PD287-7 is a high bypass ratio turbofan. This engine is a scaled (0.91 fan, 0.85 core) variation of the PD287-5. The engine general arrangement, structure, components, and systems are similar to the PD287-5 with the variation consisting of introduction of an intermediate pressure compressor stage in the core engine transition duct. This intermediate pressure compressor stage is driven at fan turbine speed and is designed to raise the overall engine pressure ratio to 21:1. A general arrangement drawing showing the fan system of the PD287-7 is shown in Figure 3b-6. A complete general arrangement drawing showing the core gas generator details is presented in the Supplement to this report (Ref: Figure 3b2-5).

An installation drawing for the PD287-7 was not prepared; however, the installation shown in Figure 3b-2 for UTW EBF aircraft or the installation shown in Figure 3b-5 for OTW EBF aircraft would be totally applicable for PD287-7. This includes applicability of the lubrication, fuel, control, and installation ancillary systems.

PD287-11 PROPULSION SYSTEM (R_F = 1.35—Fixed Pitch)

The PD287-11 is a high bypass ratio, geared, fixed pitch turbofan engine designed for low noise-low emission operation. The engine consists of a 1-1/2 stage fan system driven through a 3.4:1 reduction ratio planetary star gear arrangement by a three-stage, high-speed fan turbine. Engine PD287-11 uses the same ten-stage compressor version of the GMA100 gas generator and three-stage fan turbine used in the PD287-5 and PD287-6. An engine general arrangement showing the fan system is shown in Figure 3b-7. Figure 3b-8 is an OTW installation for the PD287-11. A complete general arrangement of the PD287-11 engine is presented in the Supplement to this report (Ref: Figure 3b2-6).

The fan system consists of a two-stage rotor designed for low noise, relatively high pressure ratio operation. The first rotor, containing 20 hollow titanium blades, is designed to develop a pressure ratio of 1.35:1 average from the tip to the bypass splitter when rotating at 239 m/s (784 ft/sec). The second rotor contains 46 hollow titanium blades and rotates at the same speed but is approximately one-half the span of the first rotor blade. This rotor stage boosts the main rotor hub pressure ratio to produce approximately a constant radial pressure distribution aft of the fan system.

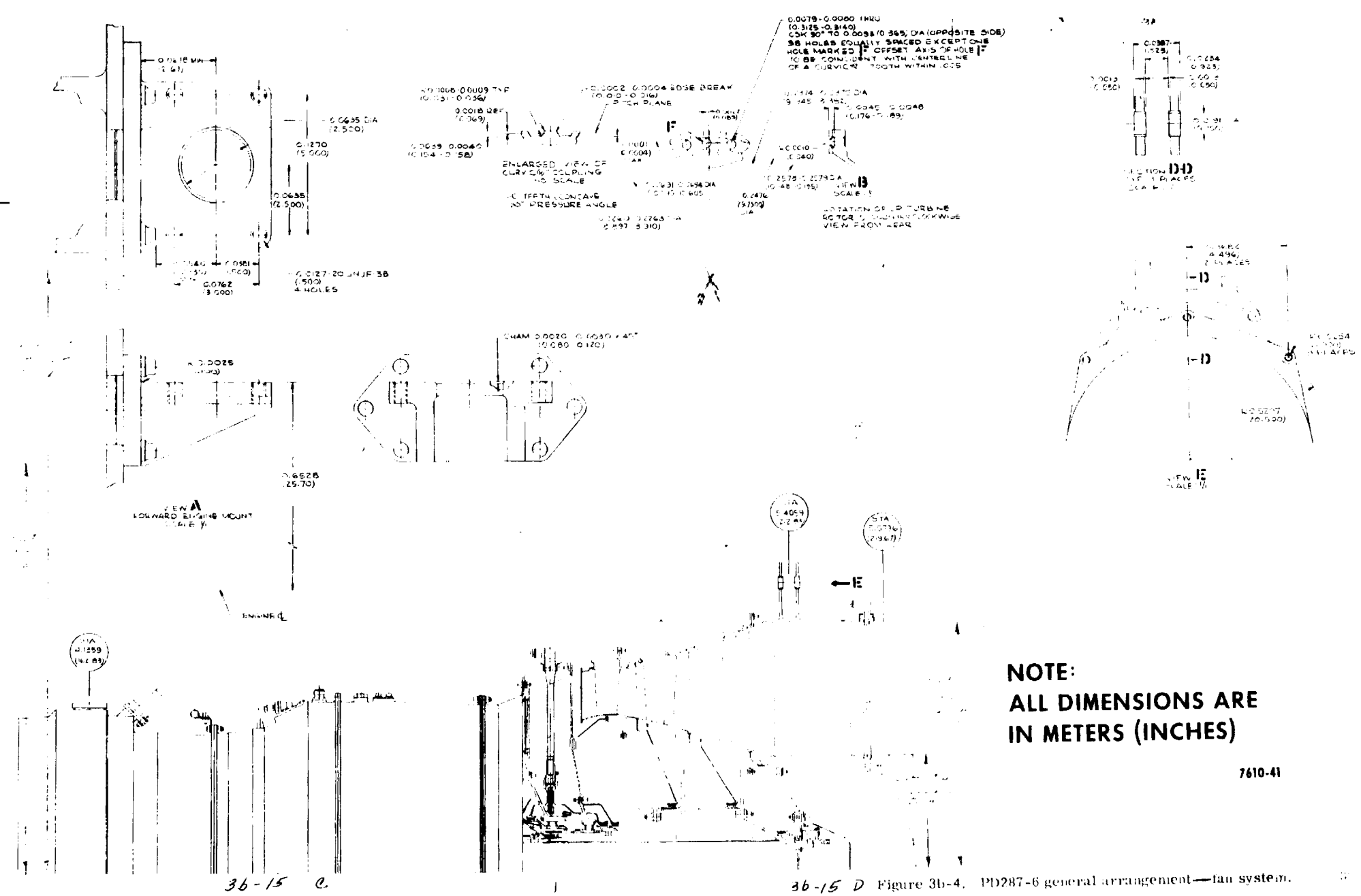

36-15 C

36-15 D Figure 3b-4. PD287-6 general arrangement—fan system.

36-15 A
36-15 B

Nacelle assembly	Material (alloy)
Inlet nose cowl	
Outer barrel	Aluminum
Inner barrel	Aluminum
Nose lip	Aluminum
Lip liner	Titanium
Bulkheads	Titanium
Attachment ring	Aluminum
Suppression ring	Aluminum
Spinner	Aluminum
Forward core cowl and fan ducts	
Fan ducts	Aluminum
Skin/frame	Aluminum
Doors	Aluminum
Fixed core cowl and fan ducts	
Outer fairing	Aluminum
Fan ducts	Aluminum
Primary nozzle	
Inner section	Nickel
Attachment	Nickel
Outer covering	Aluminum
Forward mount	Steel
Aft mount	Nickel
Boundary layer control duct	Aluminum

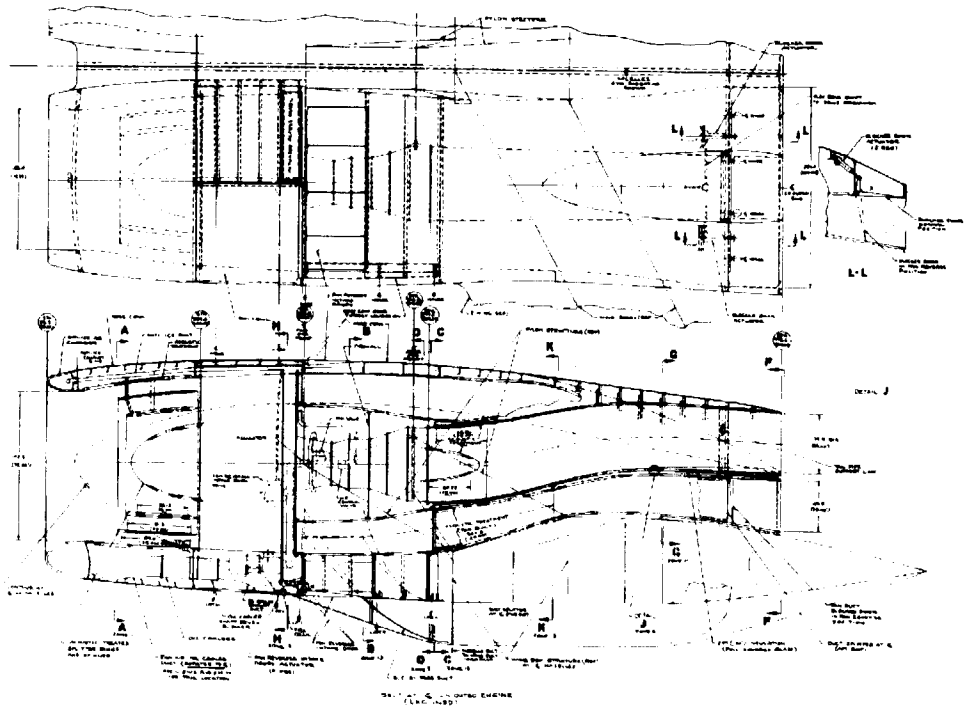

Figure 3b-5. PD287-6 propulsion system installation drawing (OTW). (Sheet 1 of 2)

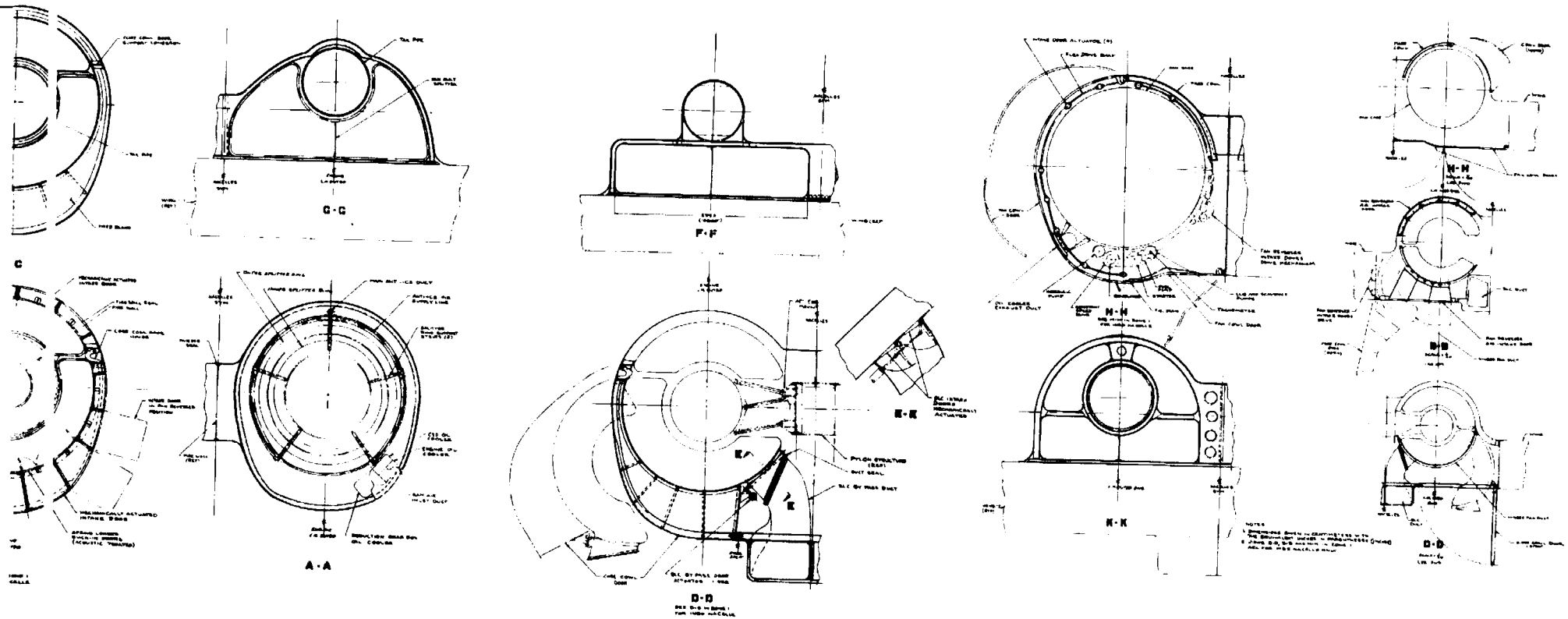

3b-19 A

Figure 3b-5. PD287-6 propulsion system installation drawing (OTW). (Sheet 2 of 2)

3b-19 B

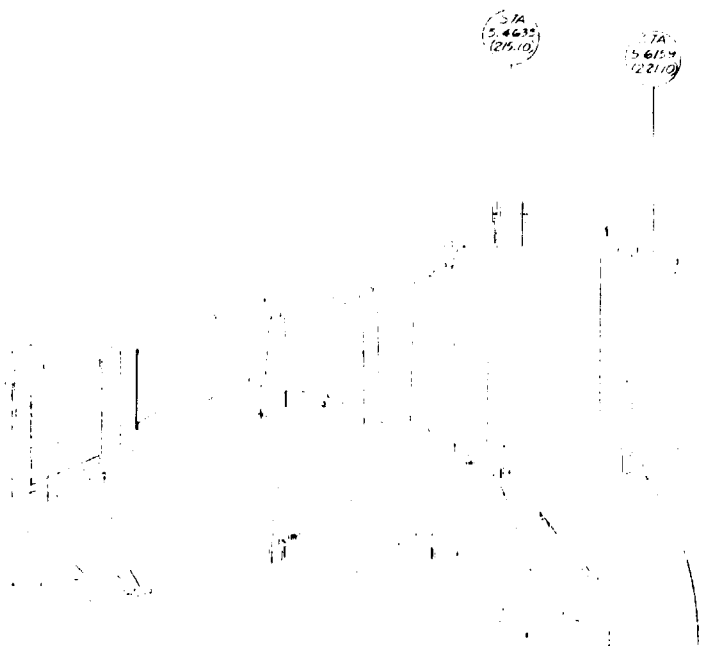

36-21 E

NOTE:
ALL DIMENSIONS ARE IN METERS (INCHES)

36-21 F

NOTE:
ALL DIMENSIONS ARE IN METERS (INCHES)

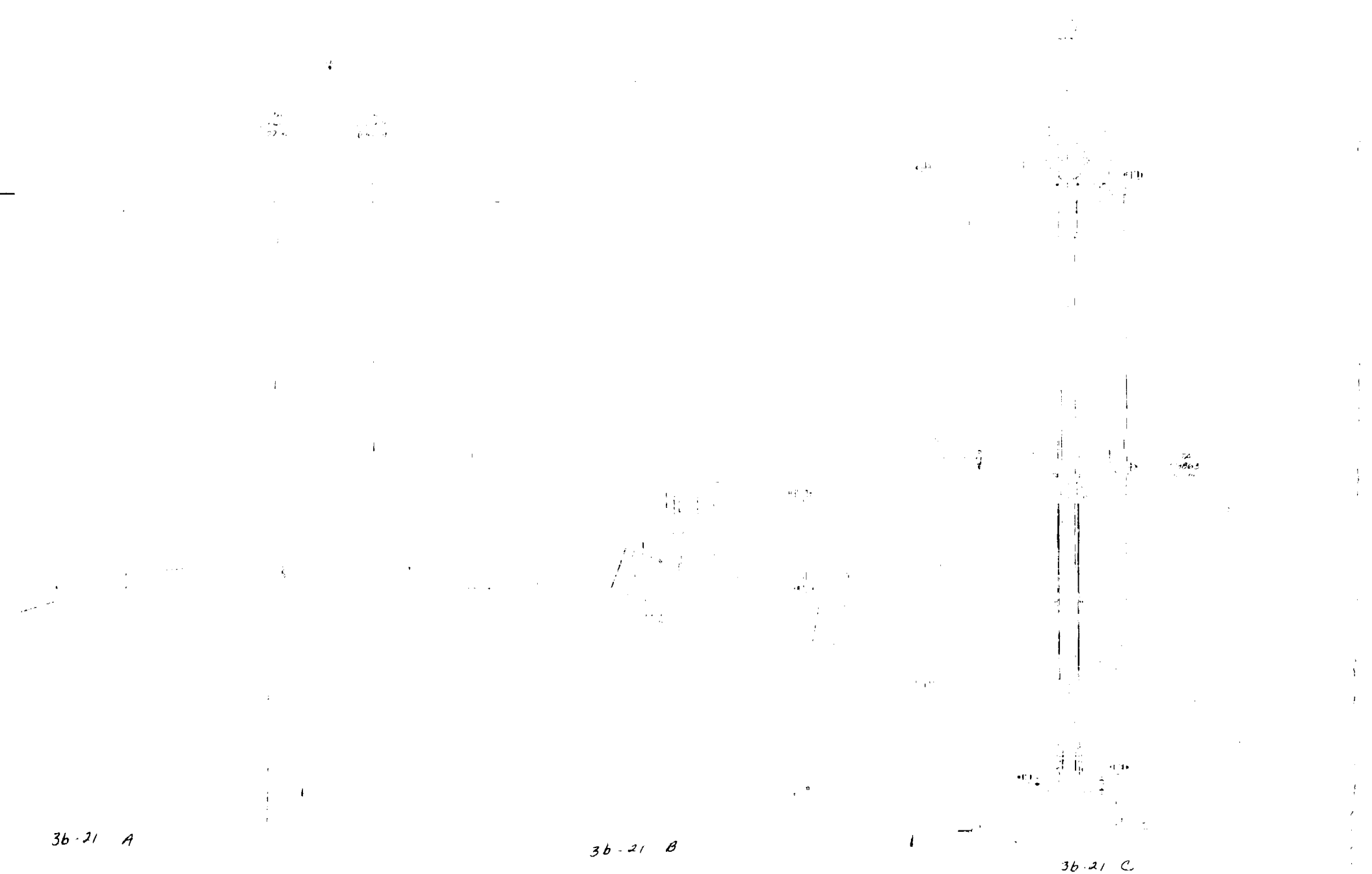

36-21 A

36-21 B

36-21 C

36-21 A

NOTE:
ALL DIMENSIONS ARE IN METERS (INCHES)

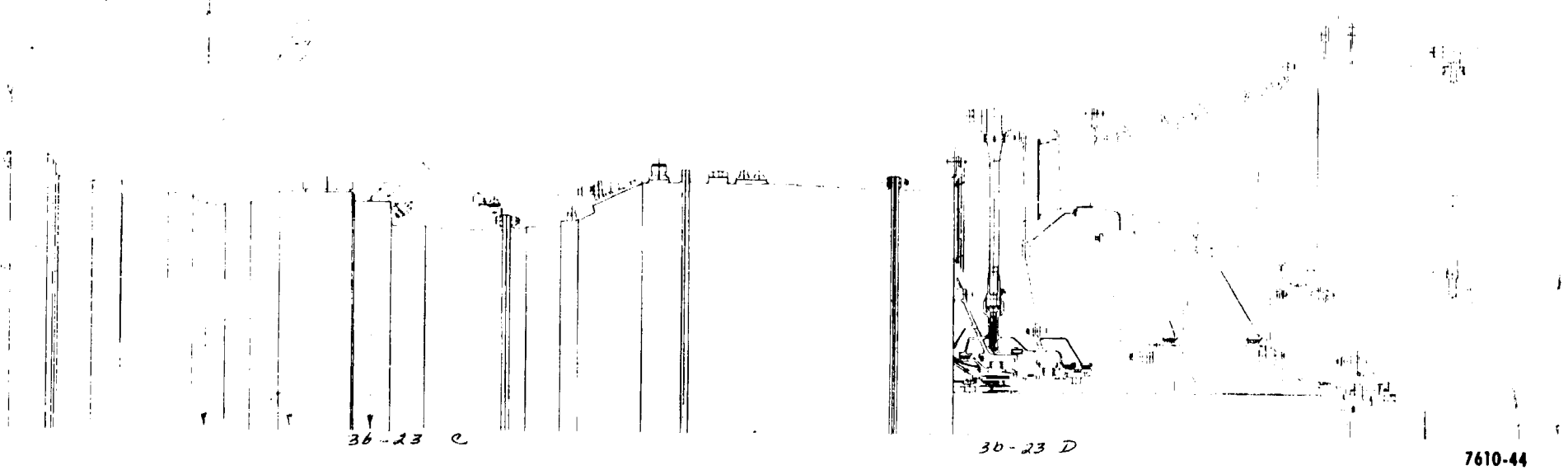

7610-44

Figure 36-7. PD287-11 general arrangement—fan system.

36-13 A

36-23 B

	Material (alloy)
	Aluminum
	Aluminum
	Aluminum
	Titanium
	Titanium
ring	Aluminum
rings	Aluminum
	Aluminum
	Aluminum
	Aluminum
l fan d cts	
	Aluminum
	Aluminum
	Aluminum
	Magnesium
nd fan ucts	
g	Aluminum
	Aluminum
n	Nickel
	Nickel
ing	Aluminum
	Steel
	Nickel
contro luct	Aluminum

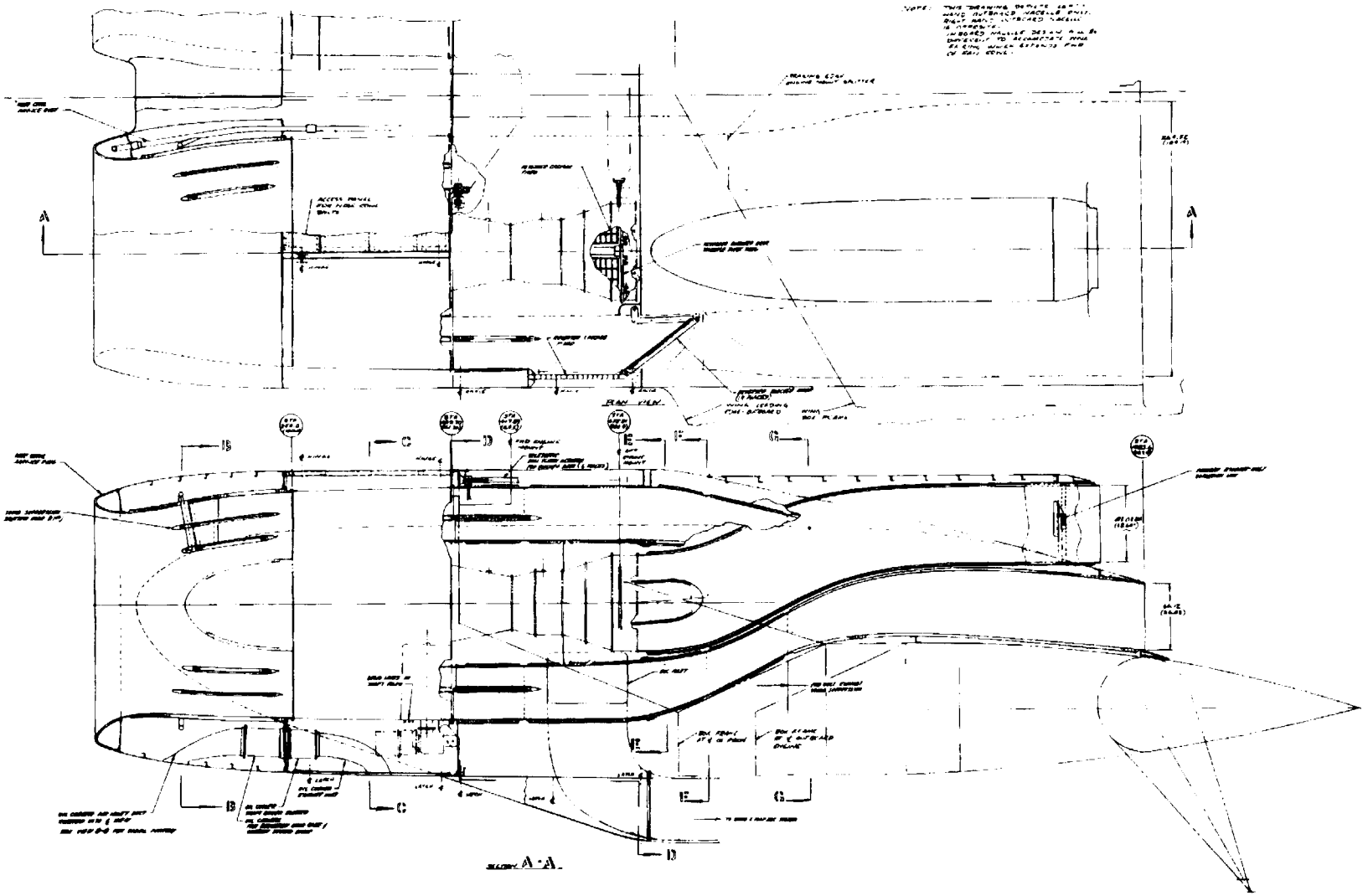

3b-25 A

3b-25 B

Figure 3b-8. PD287-11 propulsion system installation drawing (OTW-EBF). (Sheet 1 of 2)

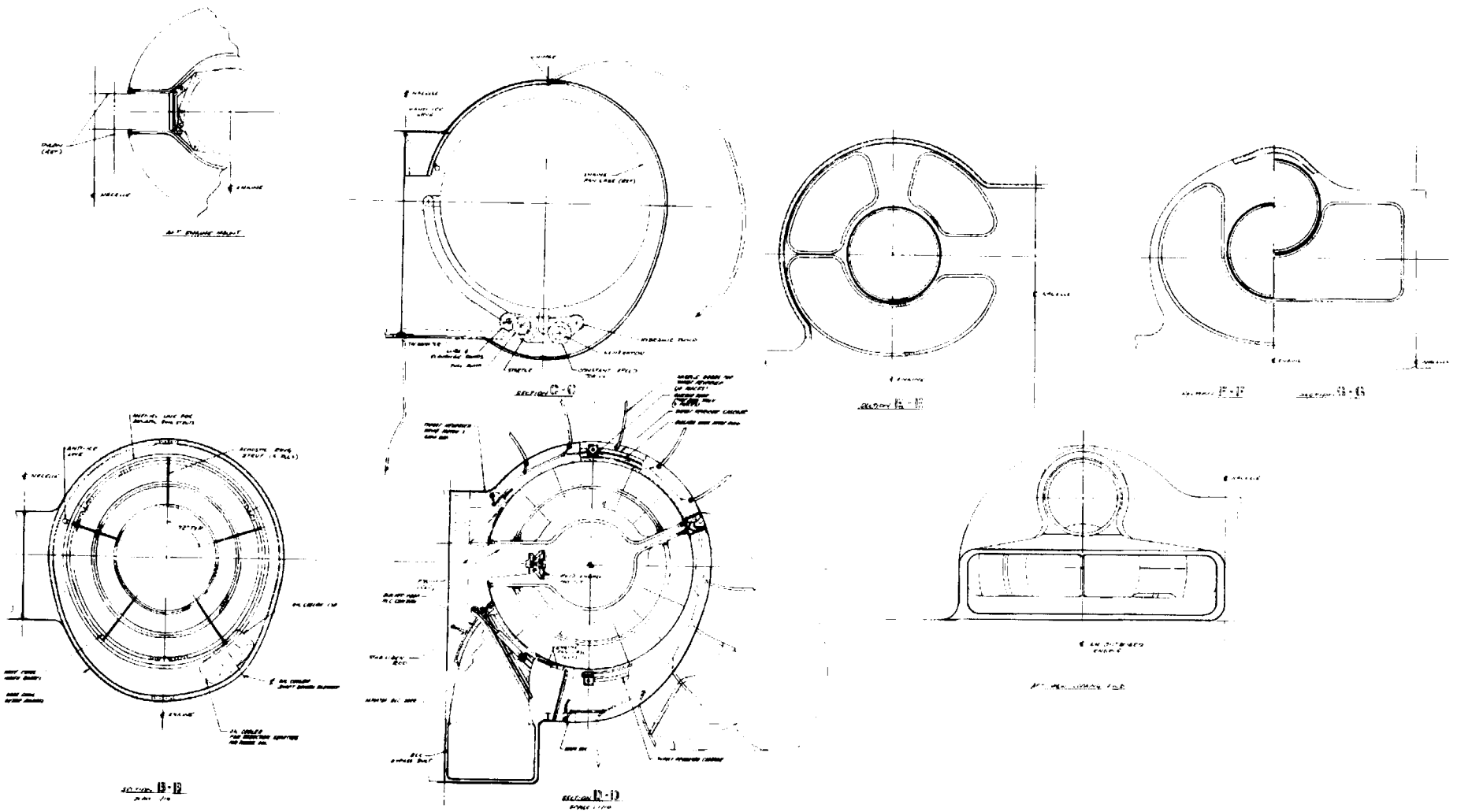

Figure 3b-8. PD287-11 propulsion system installation drawing (OTW-EBF). (Sheet 2 of 2)

The fan is driven by the ring gear of a star planetary gear system mounted in the fan forward frame. This reduction gear system consists of a helical sun gear driven by the fan turbine through extension shafting, five planetary gears supported by dual roller bearings on a stationary planet carrier assembly, and a ring gear attached through splines to the fan drive shaft. Design of the fan reduction gearing is treated in detail in Subsection 3d6. The gear set has been designed with helical gearing to minimize noise generation and to reduce the fan and fan turbine rotor thrust balance requirements. Relatively high pitch helical gearing was selected to minimize noise and heat generation. The fan rotor is supported on a thrust bearing housed in a coned bearing support bolted to a flange in the fan forward frame and a roller bearing supported by the fan forward frame through the stationary planet carrier.

The fan forward frame is similar to the forward frame for the PD287-5; the core engine and fan turbine for the PD287-11 are identical to the PD287-5 and PD287-6 except for minor turbine airfoil resets.

The installation shown for the PD287-11 in Figure 3b-8 is an OTW installation similar in many respects to that for the PD287-6. The areas of major difference are the lubrication and thrust reverser systems.

Lubrication System

The lubrication system for the PD287-11 (Figure 3b-9) is similar to the PD287-5 except that the gear lubrication and engine lubrication systems are integrated. Engine PD287-11 does not have a fan nozzle actuation system. Integration of the gear and engine lube systems will allow minor weight savings because of nonduplication of some lube system components—primarily sensors (i.e., magnetic plugs, filters, ΔP transducers, etc).

Thrust Reverser System

The thrust reverser system for the PD287-11 is the major area of difference relative to the PD287-6. The fan is of fixed pitch configuration. A cascade type thrust reverser, therefore, is included in the propulsion system fan duct. Blocker doors are used to turn the fan air through the reverser cascades. No thrust reverser or thrust spoiler is required on the engine primary flow system.

PD287-51 PROPULSION SYSTEM (R_F = 3.0—Fixed Pitch)

The PD287-51 is a low bypass ratio, direct drive turbofan engine designed for applicability to aircraft employing an AW high lift system to achieve STOL operation. The engine consists of a three-stage fan rotor, an eight-stage compressor version of the GMA100 gas generator, and a three-stage fan turbine. An engine general arrangement featuring the fan system is shown in Figure 3b-10 and a typical AW podded installation is shown in Figure 3b-11. A complete engine general arrangement is shown in the Supplement to this report (Ref: Figure 3b2-7).

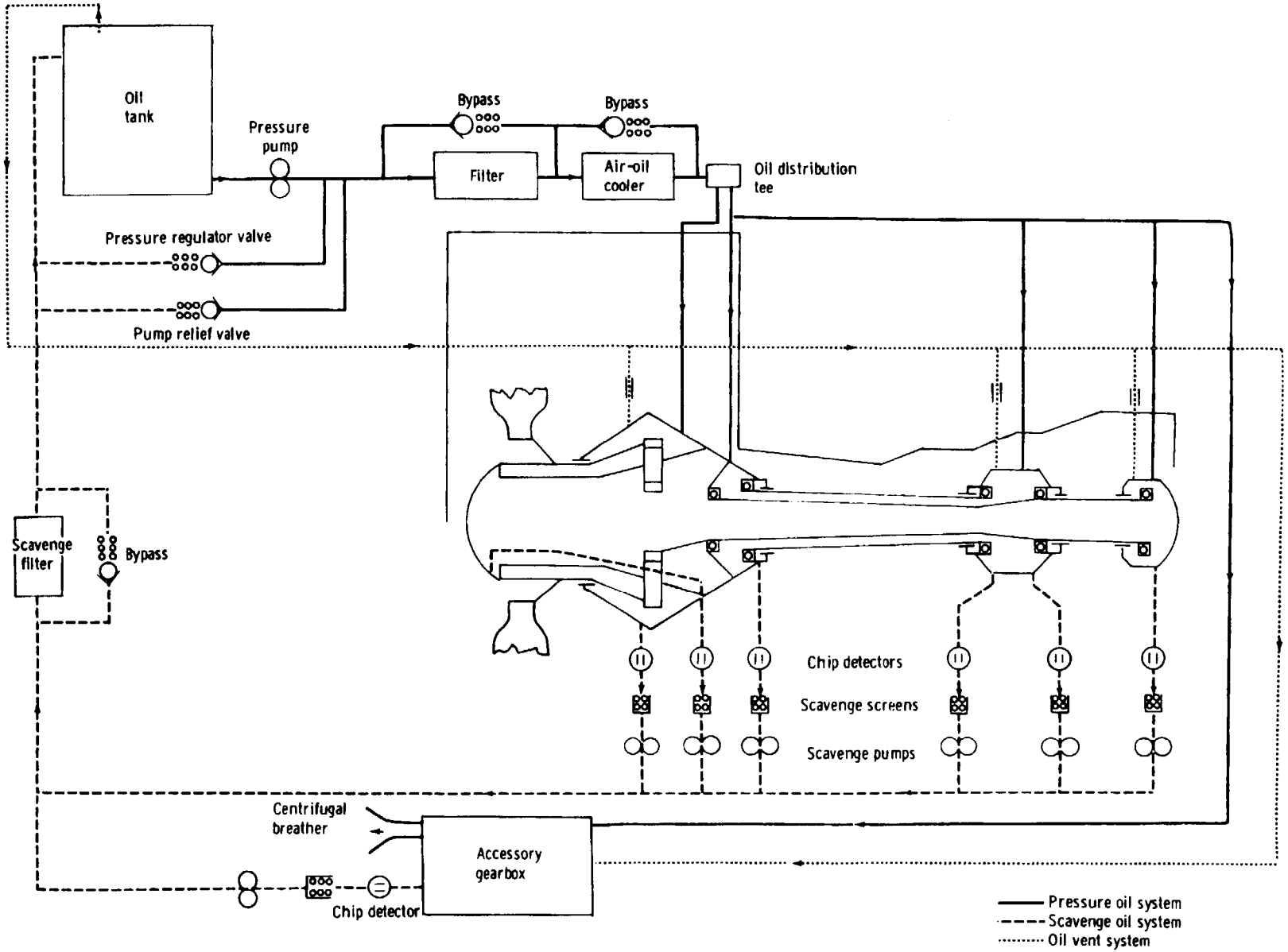

Figure 3b-9. PD287-11 lubrication system schematic.

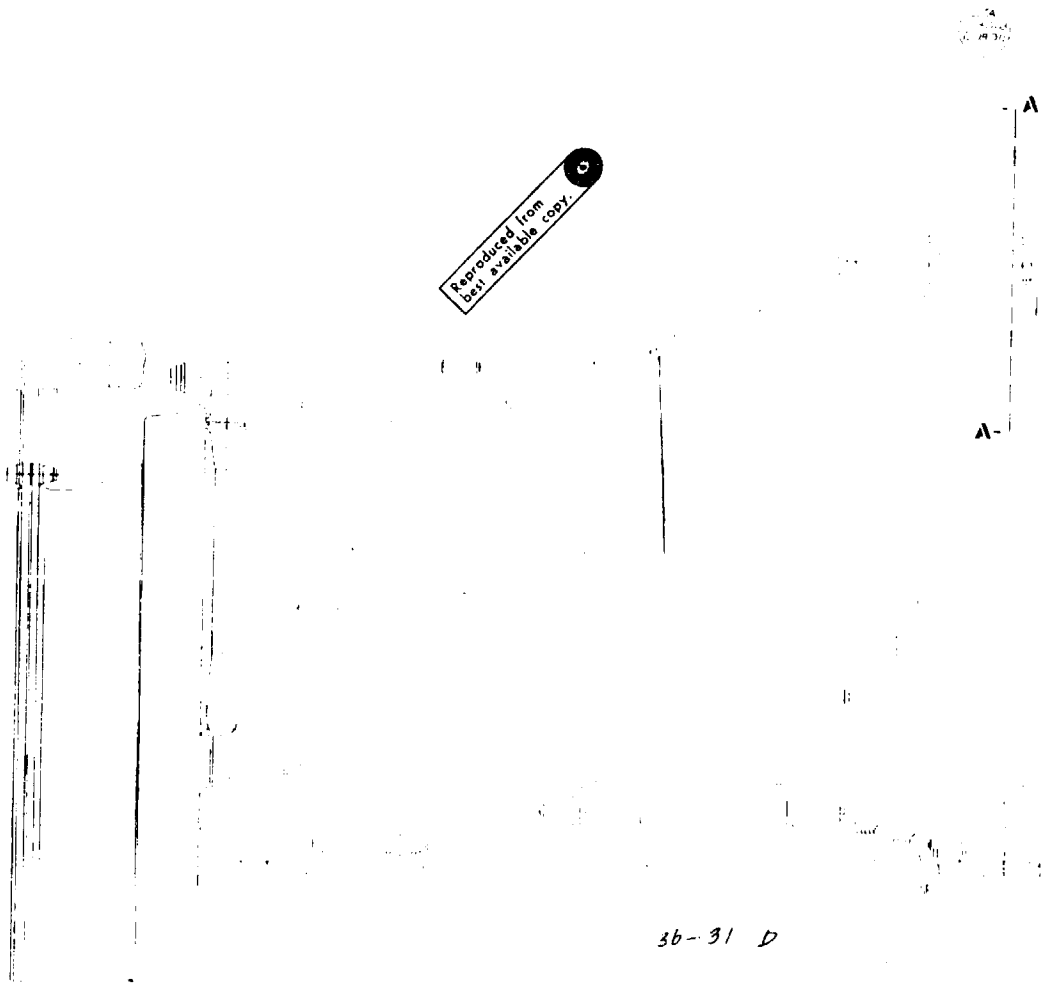

Figure 3b-10. PD287-1 general arrangement—fan system

NOTE:
ALL DIMENSIONS ARE IN METERS (INCHES)

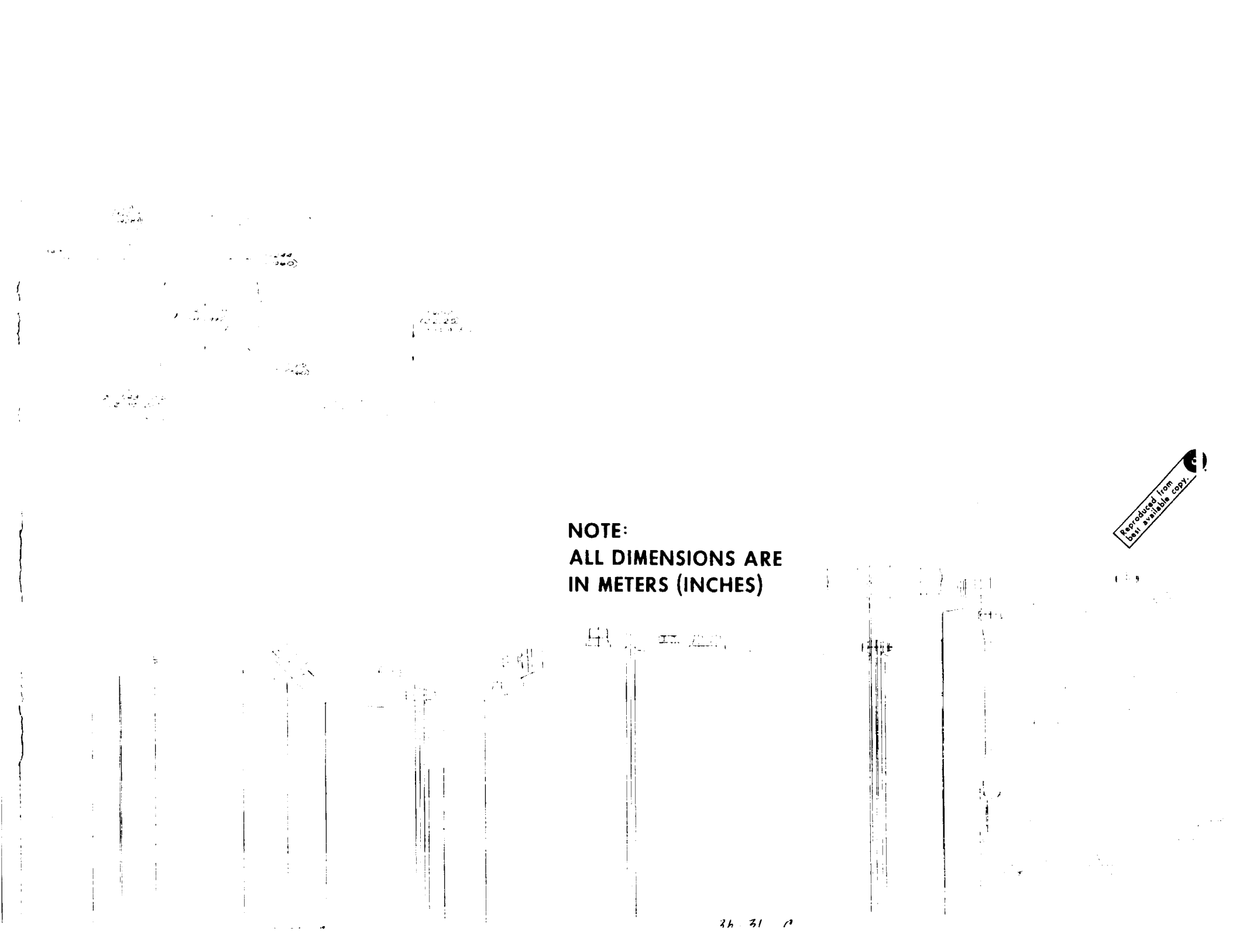

Nacelle assembly	Material (alloy)
Inlet nose cowl	
Outer barrel	Aluminum
Inner barrel	Aluminum
Nose lip	Aluminum
Lip liner	Titanium
Bulkheads	Titanium
Attachment ring	Aluminum
Fan cowl	Aluminum
Fan duct/thrust reverser	
Ducts	Titanium/Aluminum
Outer skin	Titanium/Aluminum
Cascade	Magnesium
Cascade covering	Aluminum
Primary nozzle and thrust spoiler	
Inner section	Nickel
Attachment	Nickel
Bulkheads	Nickel
Skin	Titanium
Spoiler doors	Nickel
Tail cone	Nickel
Forward mount	Steel
Aft mount	Nickel

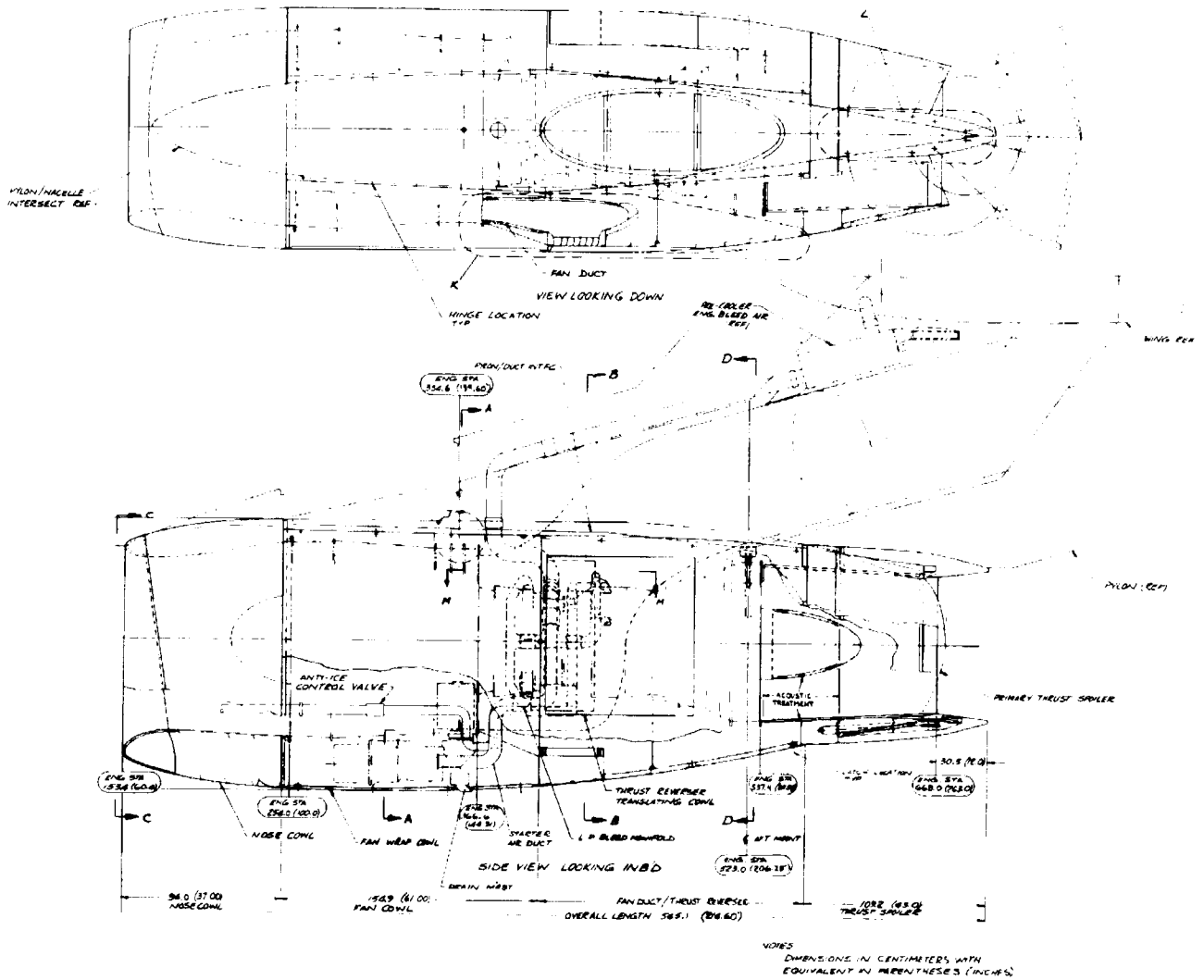

Figure 3b-11. PD287-51 propulsion system installation drawing. (Sheet 1 of 2)

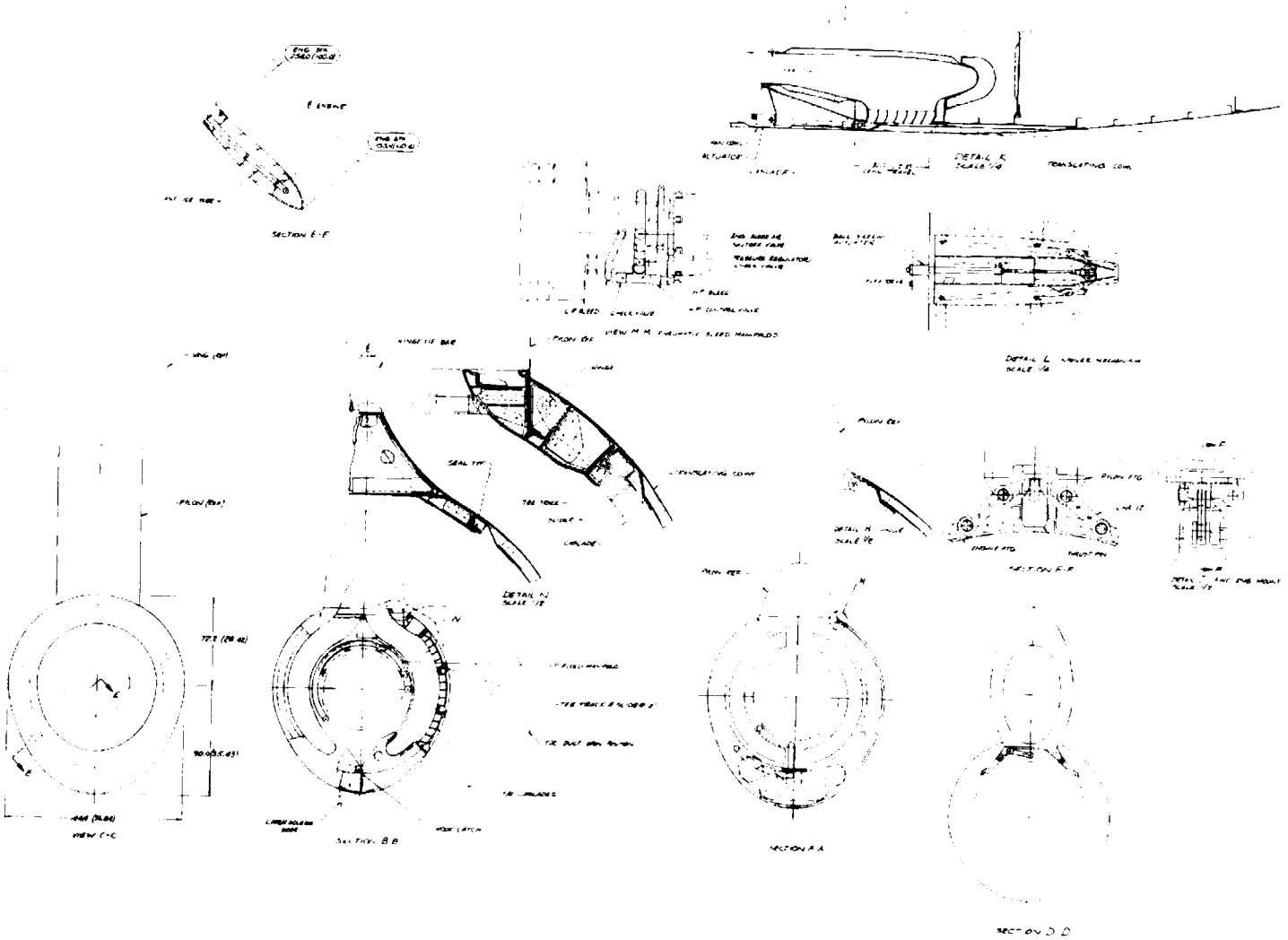

Figure 3b-11. PD287-51 propulsion system installation drawing. (Sheet 2 of 2)

36 35 A

B

The three-stage fan rotor is structurally equivalent to the TF41 LP fan rotor and is designed to produce a 3:1 pressure ratio at 503 m/s (1650 ft/sec) tip speed. The fan assembly features a variable inlet guide vane preceding the first-stage rotor and hollow titanium blades in each rotor stage. The variable inlet vane is designed to produce a sonic noise block forward of the rotor to prevent forward propagation of fan noise. Scheduling of the variable inlet guide vane is controlled by the main engine fuel control to maintain high fan rotor speed over a wide range of operating conditions, thus improving the thrust response time of the engine. The fan rotor is supported on two bearings. The forward support is provided by a roller bearing housed in a bearing support designed as an integral part of the fan first-stage vane housing. Fan rear support is provided by a ball thrust bearing housed in a coned bearing support which is bolted to a flange in the forward fan frame.

The core engine is an eight-stage compressor version of the GMA100 advanced technology gas generator. Forming this configuration involves removal of the first two compressor stages of the GMA100 gas generator and minor configuration changes to the third-, fourth-, and fifth-stage compressor wheels. The basic welded, simply supported core engine rotor concept is retained and the annular combustor and two-stage, air-cooled turbine are identical to those used in the PD287-5, -6, and -11 engines with the exception of minor turbine airfoil resets required for proper component matching.

The three-stage fan turbine is uncooled and is structurally equivalent to the turbines used on the PD287-5, -6, and -11. The turbine rotor is supported on a roller bearing housed in the interturbine transition housing and a roller bearing housed in the rear bearing support. The entire rotor is thrust balanced by introducing seventh-stage compressor air into a cavity aft of the third-stage fan turbine wheel. Residual thrust is reacted by the fan thrust ball bearing located forward.

The rear support structure contains 12 exit guide vane struts designed to reduce exit swirl in the turbine exhaust gas. The support houses the fan turbine rear bearing and is designed to withstand axial loading imposed by the rotor balance piston air load. The configuration is identical to the TF41 rear bearing support.

Engine and customer bleed ports provided on both the engine compressor case and the outer combustor case are identical to the PD287-5, -6, -7, and -11.

The lubrication system for the PD287-51 is shown in Figure 3b-12. This system is a completely integrated system requiring no nacelle interfaces other than for normal filling, monitoring, and draining activities. Oil cooling is provided by a fuel-cooled oil cooler mounted on the fan case. The lubrication system is similar to the TF41 system and is a self-contained, dry sump system compatible with MIL-L-7808 and MIL-L-23699 oil. The system provides lubrication and cooling for all bearings, gears, and splines at all flight conditions and attitudes

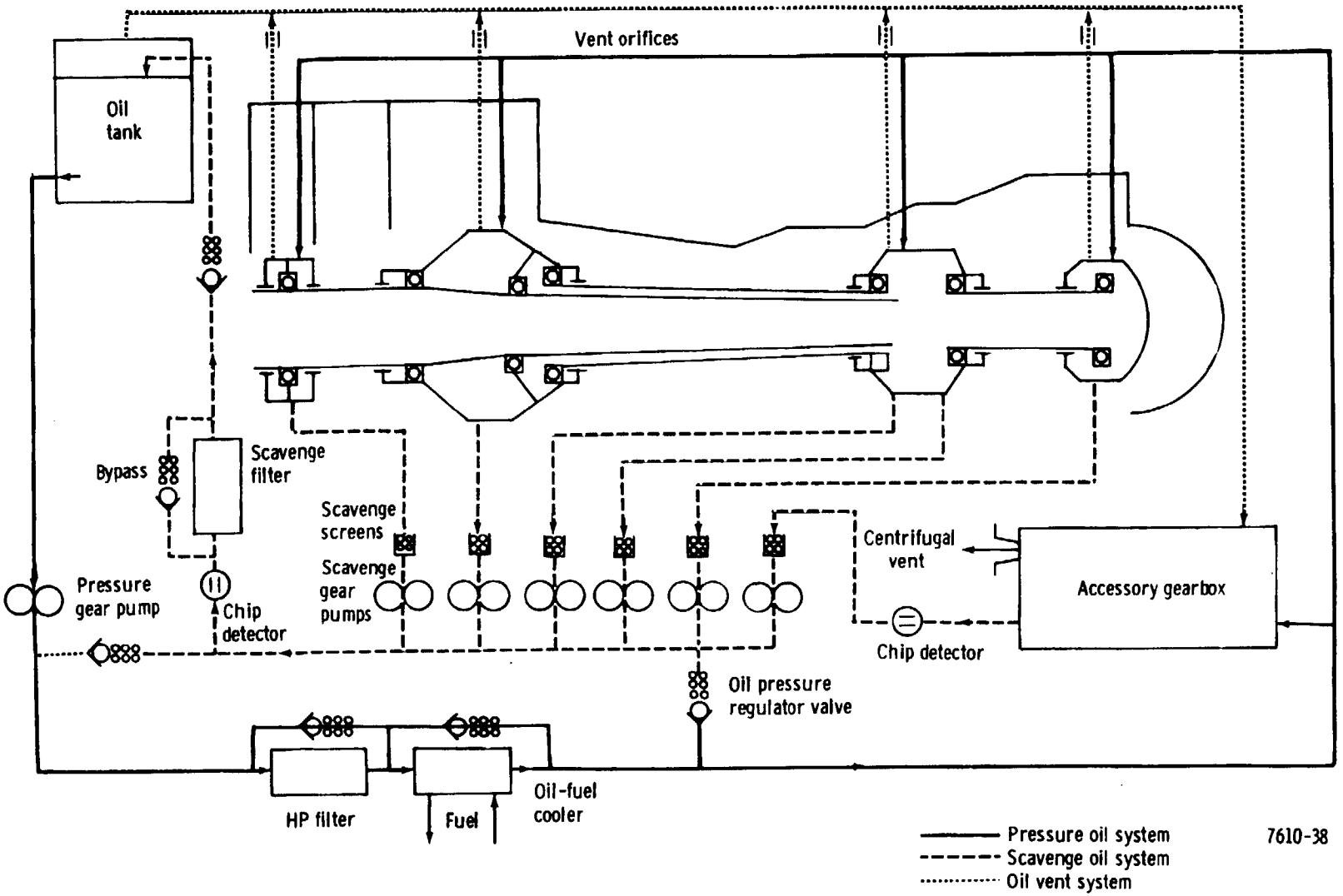

Figure 3b-12. PD287-51 lubrication system schematic.

specified in MIL-E-5007C. The pressure pump size permits pressure regulation at idle speed. The scavenge elements size gives a minimum capacity of twice the oil input to each sump at the idle condition. High-pressure sumps eliminate the possibility of scavenge element cavitation. Oil at regulated pressure is supplied to front support, interturbine support, rear bearing support, and accessory gearbox. A low-pressure system will be used to permit the use of large metering orifices less susceptible to clogging.

Fan discharge air is collected in a fan air duct which transitions from a bifurcated annulus to an elliptical shape at the top of the engine. A cascade-type fan thrust reverser contained in the fan air duct provides reverse thrust capability after landing. A target-type thrust spoiler is provided to spoil primary thrust.

The fuel, control, and installation ancillary systems are discussed in detail in Subsection 3d7.

LP SYSTEM AERODYNAMIC PARAMETERS

The fan and LP turbine aerodynamic design point parameters for the five Task II propulsion systems are shown in Table 3b-I and 3b-II, respectively.

Table 3b-I.

Fan design point parameters.

Design parameters	PD287-5	PD287-6	PD287-7	PD287-11	PD287-51
Fan pressure ratio, R_F	1.25	1.325	1.25	1.35	3.0
Fan tip speed, m/s (ft/sec)	229 (750)	282 (925)	229 (750)	239 (784)	502 (1647)
Efficiency	91.5	90.0	91.5	89.5	82.6
Fan diameter at rotor inlet, m (ft)	2.4 (7.713)	2.1 (7.050)	2.1 (6.87)	2.1 (7.033)	1.14 (3.76)
Rotor shaft power, MW (shp)	14 (18140)	14 (19050)	13 (16,100)	17 (23,375)	21 (28,400)
Specific air flow, $\frac{kg/s}{m^2}\left(\frac{lbm/sec}{ft^2}\right)$	195 (40.0)	195 (40.0)	195 (40.0)	195 (40.0)	195 (40.0)
Inlet stagnation pressure, kN/m^2 (lbf/ft^2)	101 (2116)	101 (2116)	101 (2116)	101 (2116)	101 (2116)
Inlet stagnation temperature, °K(°R)	288 (518.7)	288 (518.7)	288 (518.7)	288 (518.7)	288 (518.7)
Flight Mach number	0	0	0	0	0

Table 3b-II.

LP turbine design point parameters.

Design parameters	PD287-5,6,&11	PD287-7	PD287-51
Number of stages	3	3	3
Stage load coefficients			
First-stage	2.681	2.688	2.170
Second-stage	2.177	2.182	1.870
Third-stage	1.203	1.201	1.456
Number of airfoils			
First-stage vane	52	66	72
First-stage blade	120	114	98
Second-stage vane	66	84	70
Second-stage blade	88	112	84
Third-stage vane	66	76	56
Third-stage blade	70	80	66
Solidity			
First-stage vane	1.042	1.003	1.126
First-stage blade	1.105	1.098	1.137
Second-stage vane	1.173	1.083	1.121
Second-stage blade	1.157	1.099	1.125
Third-stage vane	1.329	1.104	1.135
Third-stage blade	1.056	1.029	1.038
Aspect ratio			
First-stage vane	2.0	2.0	2.0
First-stage blade	3.5	3.5	3.5
Second-stage vane	3.0	3.0	3.0
Second-stage blade	5.0	5.0	5.0
Third-stage vane	4.0	4.0	4.0
Third-stage blade	6.5	6.5	6.5

3c. Noise Characteristics

GROUND RULE CHANGES

Results of the Task I QCSEE parametric studies indicated that the engines most suitable for further study were the 1.25 fan pressure ratio under-the-wing (UTW) EBF, 1.3 to 1.35 fan pressure ratio over-the-wing (OTW) EBF, and 3.0 fan pressure ratio 2-stream engine for augmentor wing (AW) applications. Five engines based on these Task I results were selected for study in Task II. The acoustic design goal in Task II is 95 EPNdB, four engines measured on a 152 m (500 ft) sideline with the aircraft on a straight and level flyby at 41 m/c (80 kt) and 30 m (100 ft) altitude. The ground rules used to calculate the noise levels in Task II are listed in Table 3c-I and are compared with the Task I ground rules.

Table 3c-I.
Comparison of Task I and Task II noise ground rules.

	Task I	Task II
Noise goal unit	PNdB	EPNdB
Fuselage shielding	No	Yes
Ground attenuation	2 conditions only	All conditions
Flap noise technology	Current	-3 PNdB
Takeoff condition:		
Installed thrust, %	100	100
EBF flap angle, rad (deg)	0.35 (20)	0.52 (30)
Approach condition:		
EBF installed thrust, %	50	72
EBF flap angle, rad (deg)	1.1 (60)	1.1 (60)
AW:		
Installed thrust, %	50	55

In addition to these items, the engine bleed requirement to provide air for control surface blowing on EBF aircraft in Task I was eliminated from the Task II study. As a result, the primary and secondary nozzle exit velocities for the Task II study, are increased as shown in Figure 3c-1, with a corresponding increase in jet and flap noise (1 to 3 PNdB).

The calculation of EPNL's is done using the method specified in FAR Part 36, except that the 90 $PNdB_t$ minimum level was deleted from the calculation procedure. The noise time history curves are generated by moving the aircraft past the observer in constant time intervals and calculating the noise level at the observer for each interval as a function of the slant distance and angular relationship between observer and aircraft. The noise methodology used in this preliminary design is presented in the Appendix A to this report.

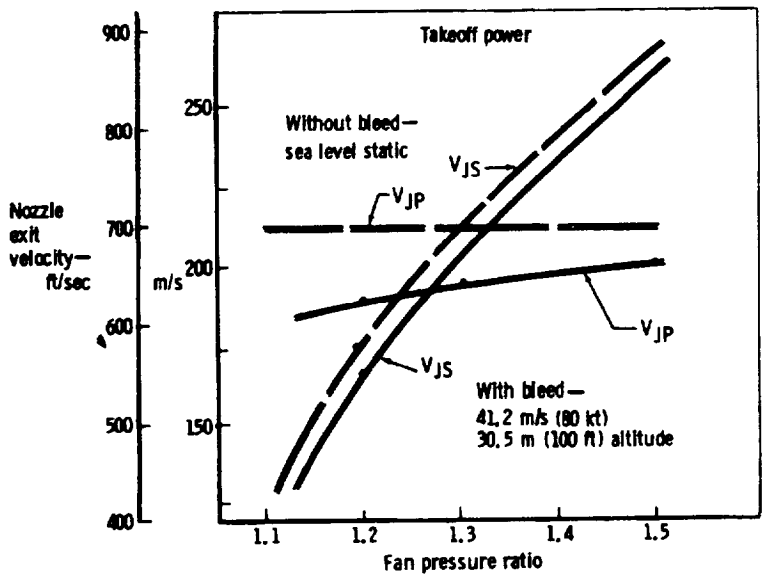

Figure 3c-1. Nozzle exit velocities with and without control surface blowing bleed.

TASK I RESULTS

The results of the Task I EBF noise study are summarized in Figure 3c-2. This figure presents system total and individual source levels as a function of fan pressure ratio. Noise for the Task II engines are superimposed to show the continuity between Tasks I and II. Figure 3c-2 has been revised since its initial presentation in Task I to reflect revised flap noise computation procedures which improved correlation with the NASA Lewis experiments, especially the higher pressure ratios. Q-Fan noise levels originally shown were free-field levels and have been raised 3 db.

TASK II ENGINES

The five engines selected for the Task II study are described in Table 3c-II. These engines, with the exception of the PD287-11, have flow paths similar to those used in Task I and are shown in Figure 3c-3. PD287-5, -6, and -7 have typical Q-Fan flow paths with low number of blades and vanes and with about 2 1/2 projected fan chord spacing. The PD287-7 uses an IP stage to boost the fan hub pressure and increase the engine overall pressure ratio. This stage is located well inside the gooseneck with a treated inlet duct which has a length-to-heighth ratio of about six. The IP stage uses a tip speed of 335 m/s (1100 ft/sec) to produce a pressure ratio of 1.25. IP noise radiated from the core inlet is not significant in terms of the 95-EPNdB goal at a 152-m (500-ft) sideline.

The three fan stages of the PD287-51 are closely spaced to take a fan case length and weight advantage from the attenuation provided by the sonic block inlet vanes (SIV). The spacing from the SIV to the first stage provides diffusion length as well as some control over the first-stage radiated noise.

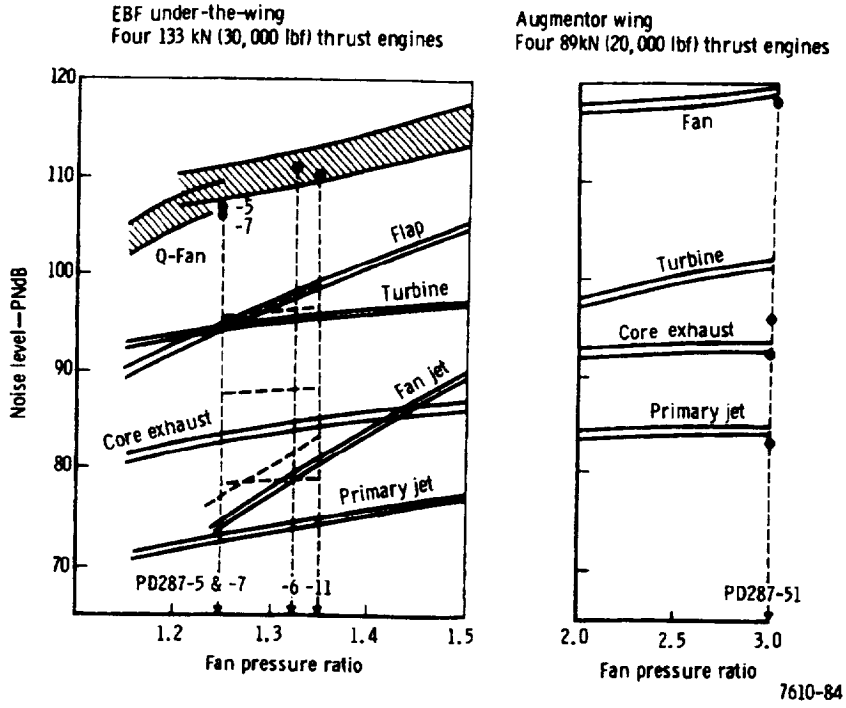

Figure 3c-2. Comparison of Task I and II noise levels—no shielding or extra ground attenuation effects.

Table 3c-II.
Task II engines.

Model description	PD287-5	PD287-6	PD287-7	PD287-11	PD287-51
Fan type	VP-Fan	VP-Fan	VP-Fan	FP-Fan	3-stage
Fan pressure ratio	1.25	1.325	1.25	1.35	3.0
Bypass ratio	17.6	13.8	17.3	12.7	2.5
Fan tip speed, m/s (ft/sec)	229 (750)	282 (925)	229 (750)	239 (784)	502 (1647)
Application	EBF	EBF	EBF	EBF	AW
System noise goal, EPNdB	95	95 OTW 100 UTW	95	95 OTW 100 UTW	95
Unsuppressed (4 engine) system noise, EPNdB	106	110 OTW 112 UTW	105	106 OTW 108 UTW	113

The PD287-11 configuration is shown in Figure 3c-4. This arrangement is based on pre-Task I experience and on the Task I fan tip speed trade study which showed that reducing fan tip speed at the cost of adding a boost stage was beneficial. This configuration provides several benefits: (1) very low tip speeds for a given pressure ratio, (2) reduced fan diameter because of a lower hub/tip ratio, (3) bypass duct heights which are amenable to treatment without requiring a splitter, and (4) reduced noise (about 4 PNdB) compared with an equivalent single-stage fan.

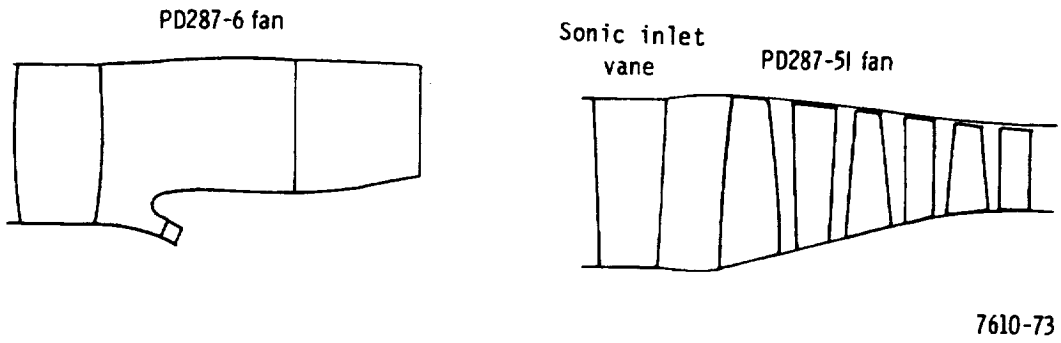

Figure 3c-3. Fan flowpath arrangement for PD287-6 and -51.

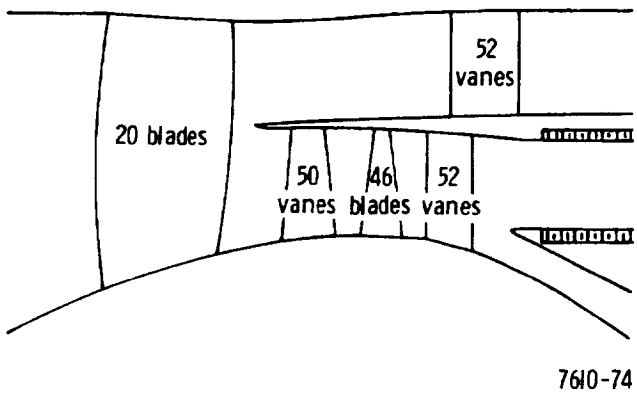

Figure 3c-4. Fan flowpath arrangement for PD287-11.

As in Task I, each engine was analyzed to determine the unsuppressed noise level from each of the several sources as shown in Figure 3c-2. These levels and their associated noise spectrums provide the basis for designing the duct noise suppression treatments.

NOISE SUPPRESSION

Designing duct treatments to meet an EPNdB goal requires that the variable effects of time duration and engine shielding as well as the background or floor effect of flap, jet, and turbine noise must be considered. In general, the combined effect of time duration, engine shielding, and ground attenuation gave 1 to 3 PNdB relief in fan noise suppression requirements. Initial attenuation estimates were made by comparing the unsuppressed source spectrums with a constant noy requirement to meet the suppressed goal. An example of this comparison is shown in Figure 3c-5 for the PD287-6 engine. The goal is shown as a band where the bottom of the band represents a PNdB design goal and the width of the band indicates possible relief for an EPNdB goal. Additional insight into the treatment requirements can be obtained from inspection of the flyby $PNdB_t$ and individual source PNdB time histories as shown in Figures 3c-6 and 3c-7. While fan inlet noise makes an identifiable contribution to the system time

history at about 3 s before flyby, the rear fan radiation noise dominates and will require the greater attenuation. The source comparison indicates the same conclusion and also shows that fan and flap noise have similar slopes before and after flyby. This situation indicates that as fan noise is suppressed and approaches the flap levels the greatest system reduction will occur near flyby. Before and after flyby slopes will remain about constant. The elapsed time between the 10 db down points will be greater for the suppressed system than for the unsuppressed system and the EPNdB level will tend to approach $PNdB_t$ maximum.

The duct suppression designs for each of the engines is given in Table 3c-III and are shown in Figures 3c-8 through 3c-12. The duct designs described are not unique but are a best choice of the treatment length versus number of splitter trade to obtain mechanical simplicity, low weight and duct pressure loss. The treatment weights given in Table 3c-III are relative to an untreated nacelle. Pressure losses, however, are for the whole duct and include inlet recovery and losses because of the untreated portion of the duct as well as treatment loss. The suppression provided by these treatments is shown in Figures 3c-13 through 3c-19. These illustrations show peak flyby 1/3 octave spectrums for the unsuppressed systems as well as the 95-EPNdB spectrums for all engines and the 100-EPNdB spectrums for the UTW PD287-6 and -11 installations. While fan suppression to near the flap impingement noise levels is required to about 2 kHz or beyond, the use of low-noise fans has held the peak sound pressure attenuation requirements to about 15 to 25 db. Peak flyby noise for the unsuppressed and suppressed EBF systems occurred at nearly the same observed angle so that the decrease in flap noise level (low-frequency bands) is primarily because of a nozzle exit velocity decrease caused by duct treatment pressure losses. The apparent change in wing noise shown for the augmentor wing installation (Figure 3c-19) is caused by a large change between the angles of peak sideline noise for fan inlet noise and wing noise. The fan inlet dominates the unsuppressed AW configuration while the wing dominates the suppressed AW configuration.

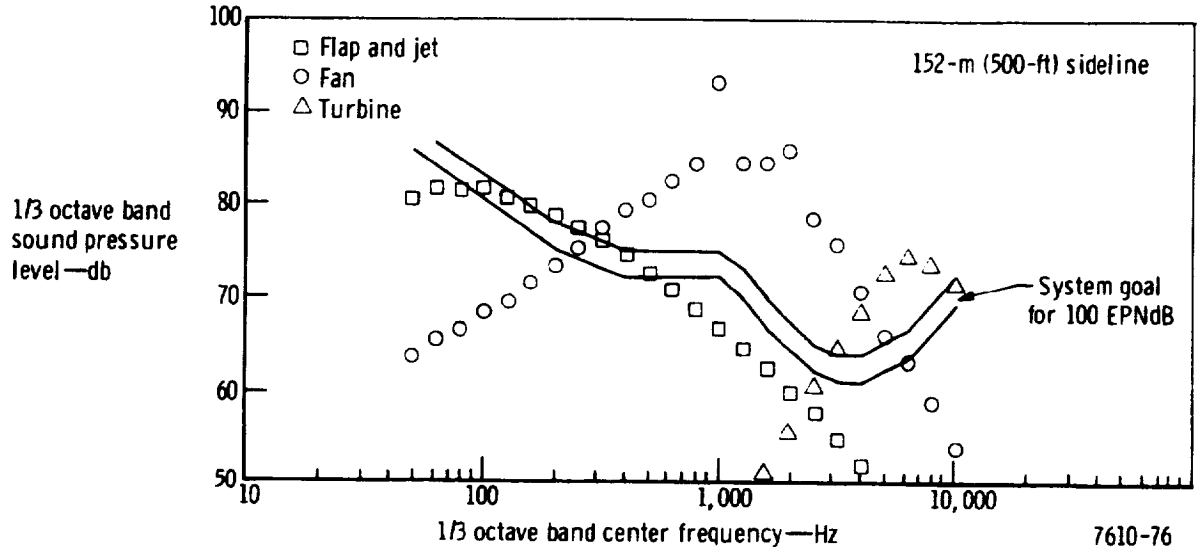

Figure 3c-5. Attenuation requirements for PD287-6 UTW configuration.

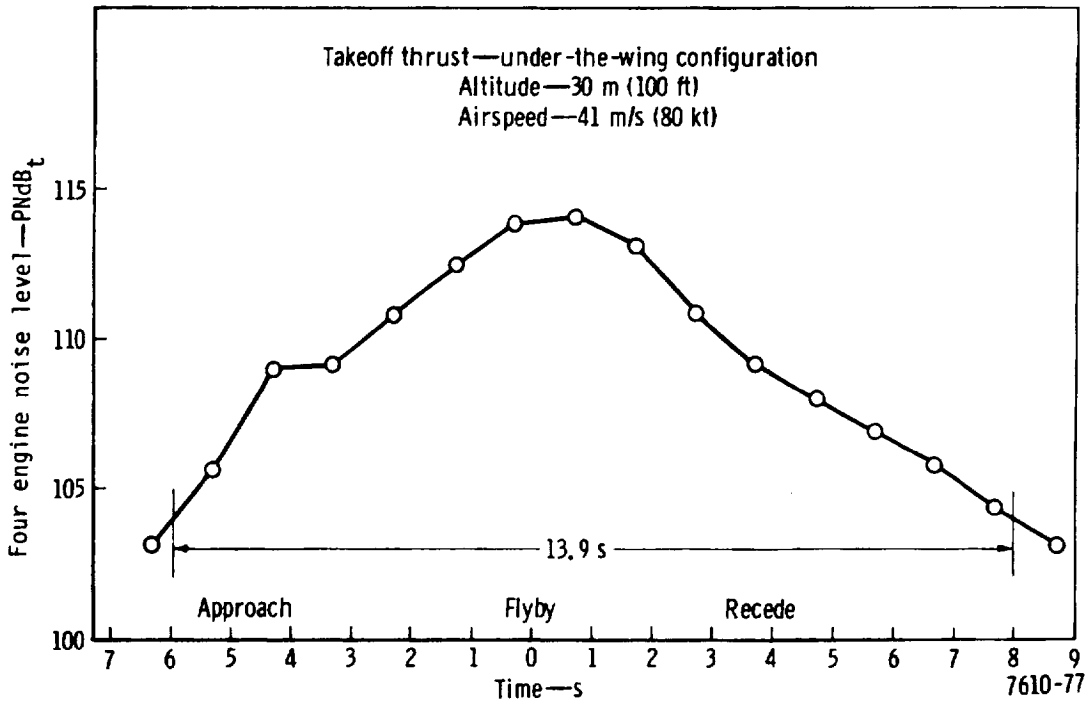

Figure 3c-6. PD287-6 straight and level flyby time history at 152-m (500-ft) sideline.

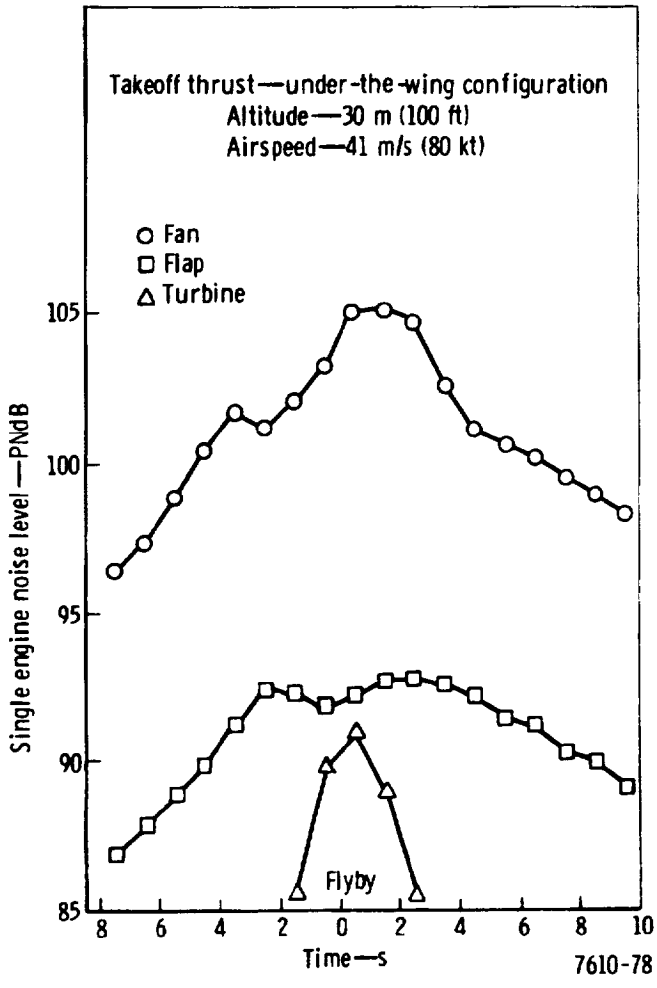

Figure 3c-7. PD287-6 unsuppressed source time histories at 152-m (500-ft) sideline for straight and level flyby.

Table 3c-III.

95- and 100-EPNdB duct suppression designs for Task II engines.

95-EPNdB duct suppression designs for Task II engines

		PD287-5			PD287-6 (OTW)			PD287-7			PD287-11 (OTW)			PD287-51		
		Fan			Fan			Fan			Fan			Fan		
		Inlet	Bypass	Turbine	Inlet	Bypass	Turbine	Inlet	Bypass	Turbine	Inlet	Bypass	Turbine	Inlet	Bypass	Turbine
No. of splitters		1	1	0	2	0	0	1	1	0	2	1**	0	Sonic inlet guide vane		0
Splitter thickness, cm (in.)‡		6.0(2.36)	10.4(4.08)	---	4.0(1.56)	---	---	3.9(1.52)	7.8(3.08)	---	3.5(1.4)	7.8(3.08)	---			
Splitter length, cm (in.)		124(49)	124(49)	---	81(32)	---	---	51(20)	91(36)	---	99(39)	126(50)	---			
Wall length, cm (in.)		150(59)	124(49)	51(20)	107(42)	305(120)	109(43)	76(30)	91(36)	64(25)	125(49)	126(50)	109(93)			46(18)
Design	h/c	0.45	0.56	1.9	0.64	1.26	4.0	0.84	0.81	1.8	0.72	0.84	4.4			2.7
	Z/ρc R	1.4	0.30	1.0	1.8	0.40	2.1	2.35	0.30	0.86	2.0	0.35	2.3			1.3
	Z/ρc -jX	1.1	0.20	0.74	1.4	0.31	1.3	2.20	0.20	0.83	1.8	0.20	0.9			1.2
	Open area ratio	0.03	0.20	0.08	0.02	0.20	0.042	0.025	0.20	0.10	0.03	0.20	0.038			0.08
	Backing depth, cm (in.)	2.9(1.14)	5.1(2.0)	1.0(0.4)	1.9(0.74)	3.8(1.5)	0.64(0.25)	1.8(0.72)	3.8(1.5)	1.0(0.4)	1.7(0.67)	3.8(1.5)	0.64(0.25)			1.0(0.4)
	Sheet thickness, cm (in.)	0.08(0.032)	1.3*(0.50)	0.08(0.032)	0.05(0.02)	0.5*(1.2)	0.08(0.032)	0.08(0.032)	0.5*(0.2)	0.08(0.032)	0.08(0.032)	0.5*(0.2)	0.08(0.032)			0.08(0.032)
	Hole dia, cm (in.)	0.25(0.1)	0.13(0.05)	0.25(0.1)	0.13(0.05)	0.64(0.25)	1.24(0.096)	0.25(0.10)	0.76(0.3)	0.25(0.10)	0.13(0.05)	0.76(0.3)	0.24(0.096)			0.25(0.10)
Takeoff pressure loss, ΔP/P†		0.0116	0.025	0.0044	0.0140	0.0183	0.005	0.0087	0.0148	0.005	0.0162	0.0205	0.007			0.002
Weight, kg (lbm)		84(183)	120(274)	0 (0)	93(205)	0 (0)	0 (0)	29(66)	82(188)	0 (0)	93(213)	61(135)	0 (0)			0 (0)

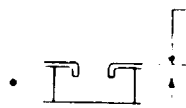

**Extension of fan case flow splitter, 51 cm (20 in.) in fan case.
†Total ΔP/P includes lip loss and duct geometry effects.
‡Based on 0.08-cm (0.032-in.) skin and 0.04-cm (0.016 in.) septum.

100-EPNdB duct suppression designs for Task II engines

	PD287-5			PD287-6 (UTW)			PD287-7			PD287-11 (UTW)		
	Fan			Fan			Fan			Fan		
	Inlet	Bypass	Turbine	Inlet	Bypass	Turbine	Inlet	Bypass	Turbine	Inlet	Bypass	Turbine
No. of splitters	0	0	0	1	0	0	0	0	0	1	1**	0
Splitter thickness, cm (in.)‡	---	---	---	4.0(1.56)	---	---	---	---	---	3.1(1.22)	7.8(3.08)	---
Splitter length, cm (in.)	---	---	---	46(18)	---	---	---	---	---	81(32)	76(30)	---
Wall length, cm (in.)	64(25)	64(25)	38(15)	61(24)	178(70)	51(15)	51(20)	51(20)	51(20)	102(40)	114(45)	38(15)
Takeoff pressure loss†	0.0082	0.010	0.0033	0.0123	0.018	0.0017	0.0077	0.009	0.0028	0.0118	0.020	0.0024
Weight, kg (lbm)	0 (0)	0 (0)	0 (0)	25(56)	0 (0)	0 (0)	0 (0)	0 (0)	0 (0)	36(80)	24(45)	0 (0)

†Total ΔP/P includes lip loss and duct geometry effects.
‡Based on 0.08-cm (0.032-in.) skin and 0.04-cm (0.016-in.) septum.
**Extension of fan case flow splitter, 51 cm (20 in.) in fan case.

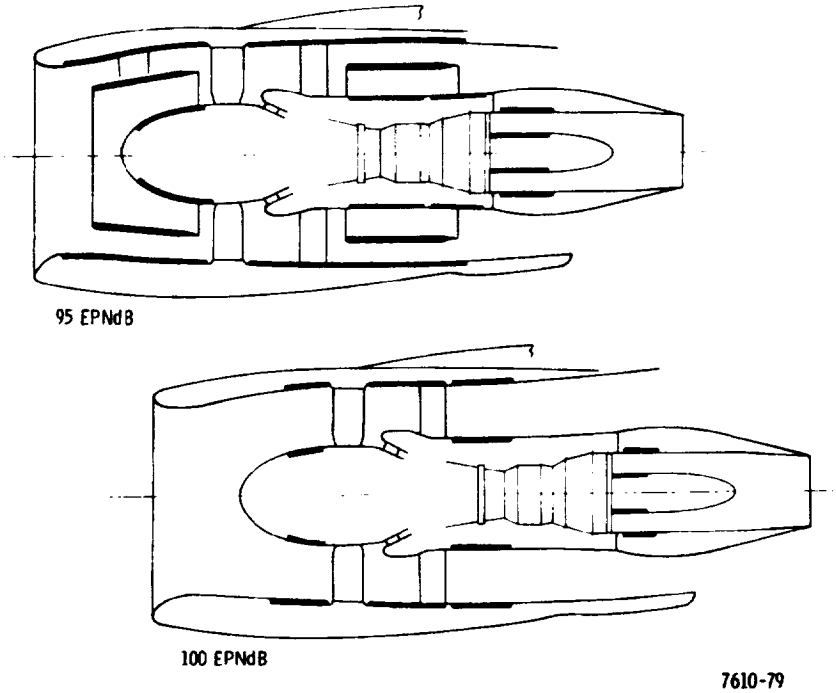

Figure 3c-8. PD287-5 suppression treatment for 95 and 100 EPNdB.

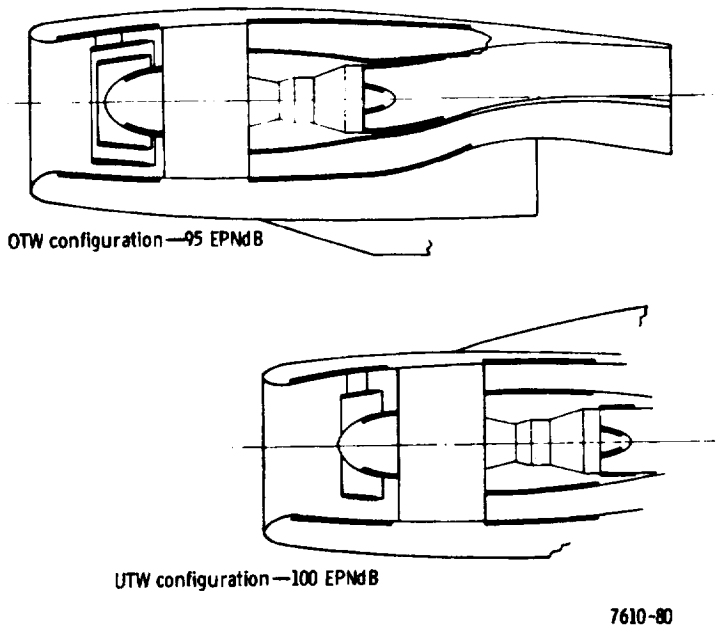

Figure 3c-9. PD287-6 suppression treatment for 95 and 100 EPNdB.

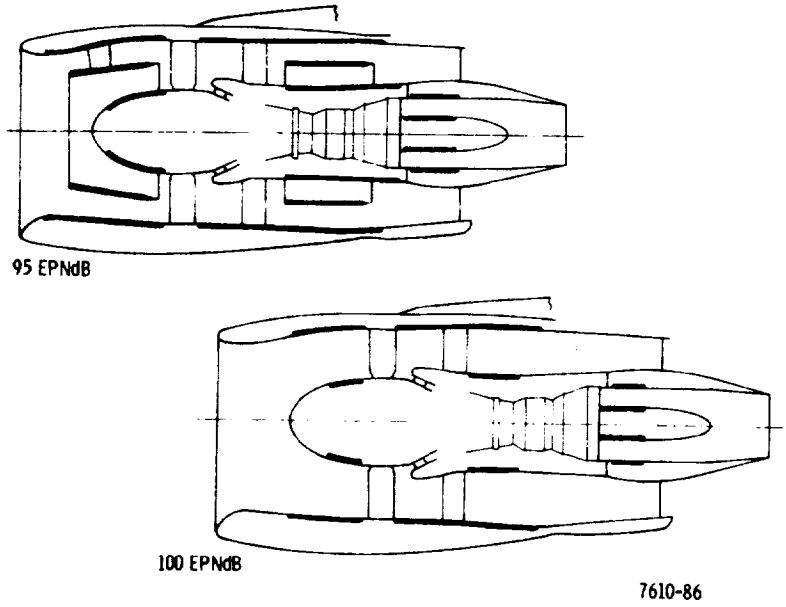

Figure 3c-10. PD287-7 suppression treatment for 95 and 100 EPNdB.

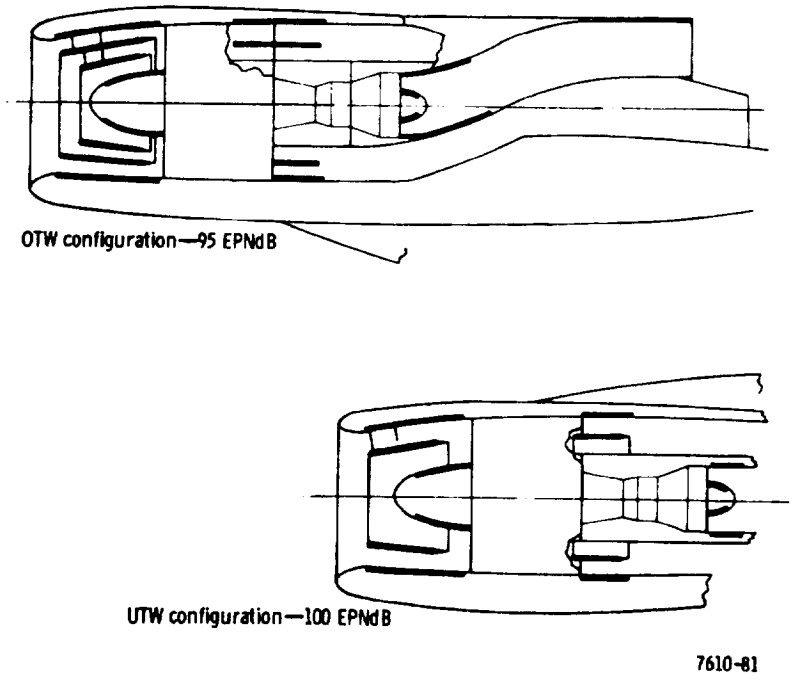

Figure 3c-11. PD287-11 suppression treatment for 95 and 100 EPNdB.

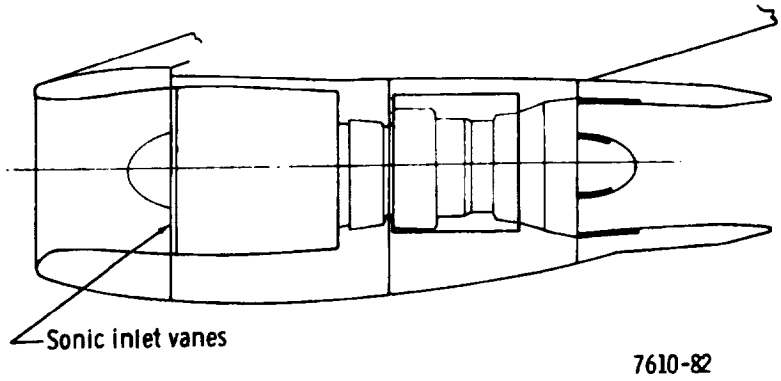

Figure 3c-12. PD287-51 suppression treatment for 95 EPNdB.

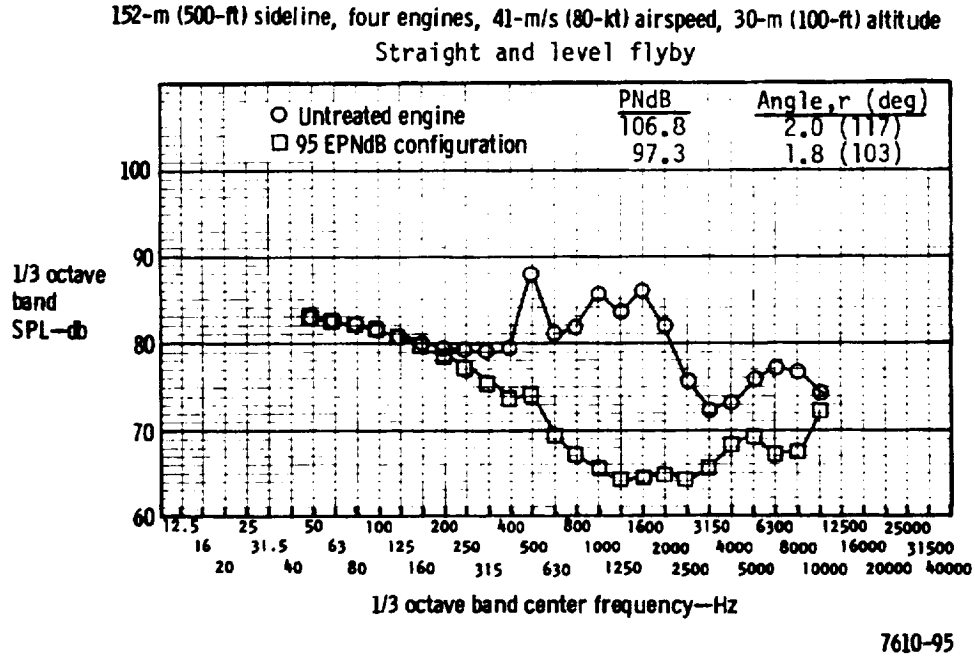

Figure 3c-13. PD287-5 peak suppressed and unsuppressed 1/3 octave band spectrums.

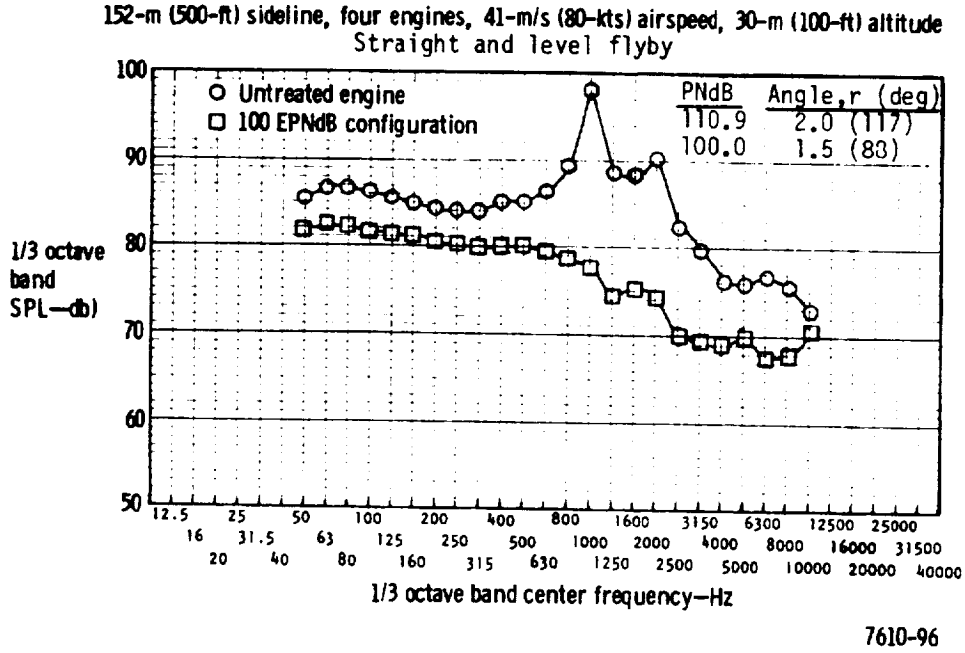

Figure 3c-14. PD287-6 UTW peak suppressed and unsuppressed 1/3 octave band spectrums.

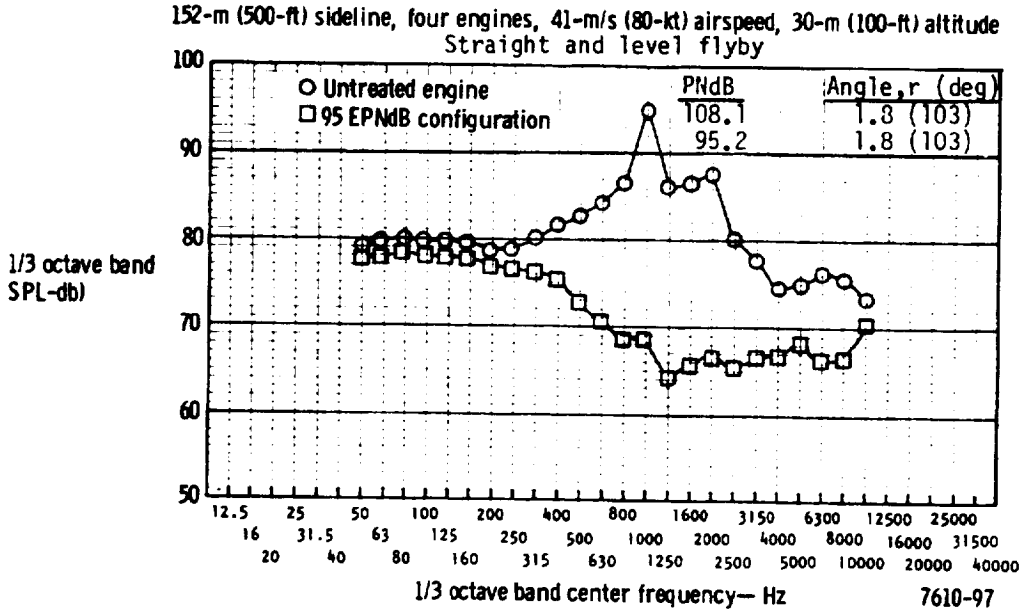

Figure 3c-15. PD287-6 OTW peak suppressed and unsuppressed 1/3 octave band spectrums.

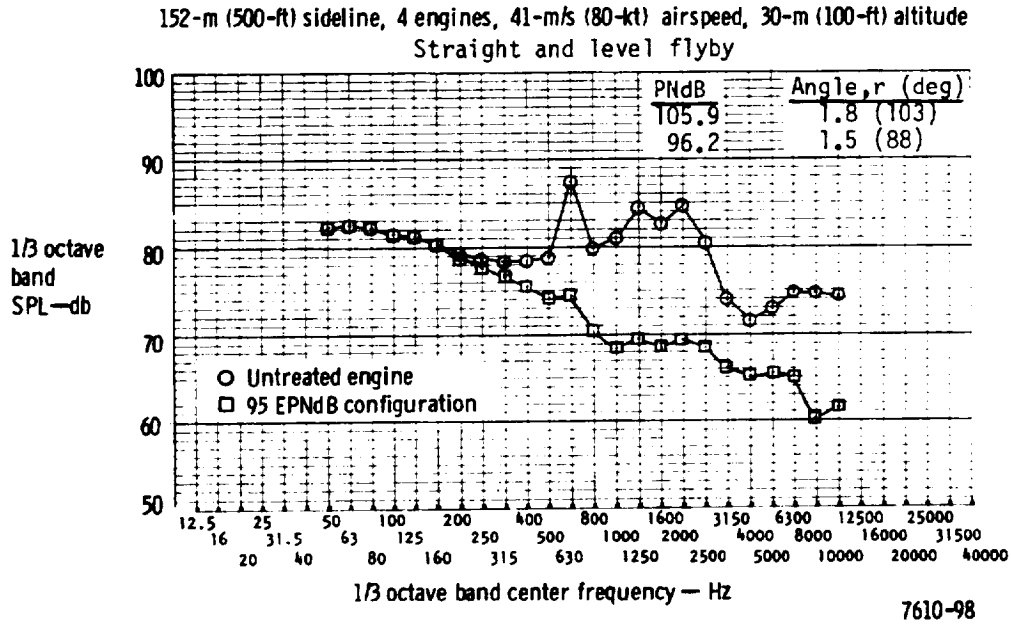

Figure 3c-16. PD287-7 UTW peak suppressed and unsuppressed 1/3 octave band spectrums.

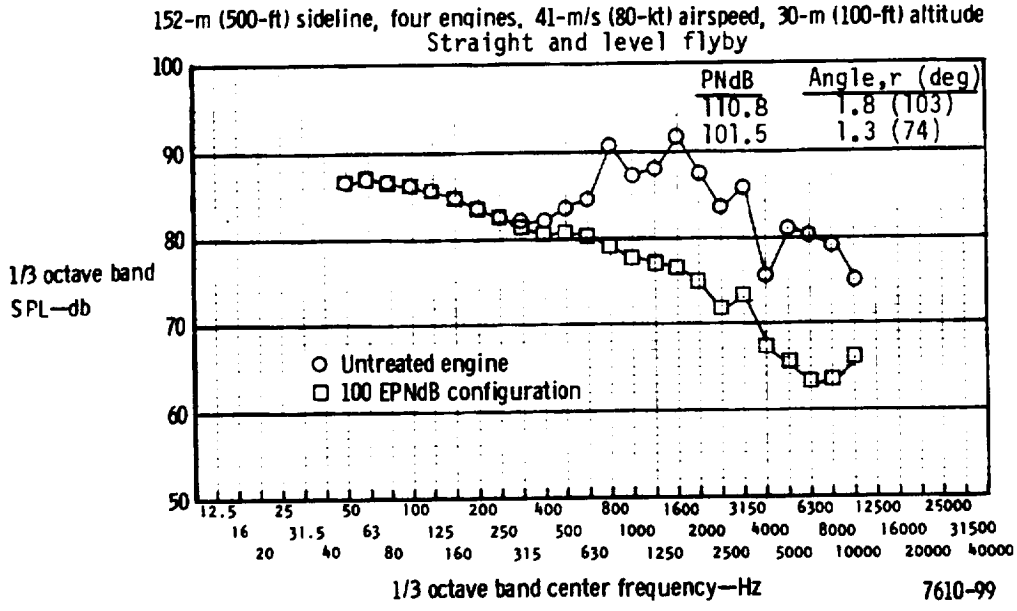

Figure 3c-17. PD287-11 UTW peak suppressed and unsuppressed 1/3 octave band spectrums.

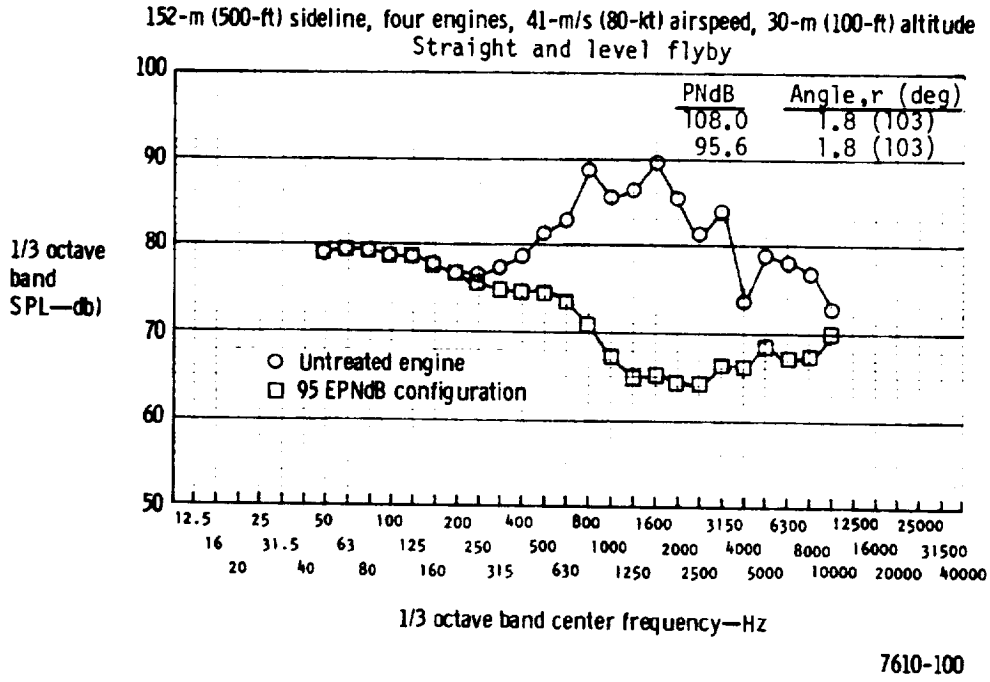

Figure 3c-18. PD287-11 OTW peak suppressed and unsuppressed 1/3 octave band spectrums.

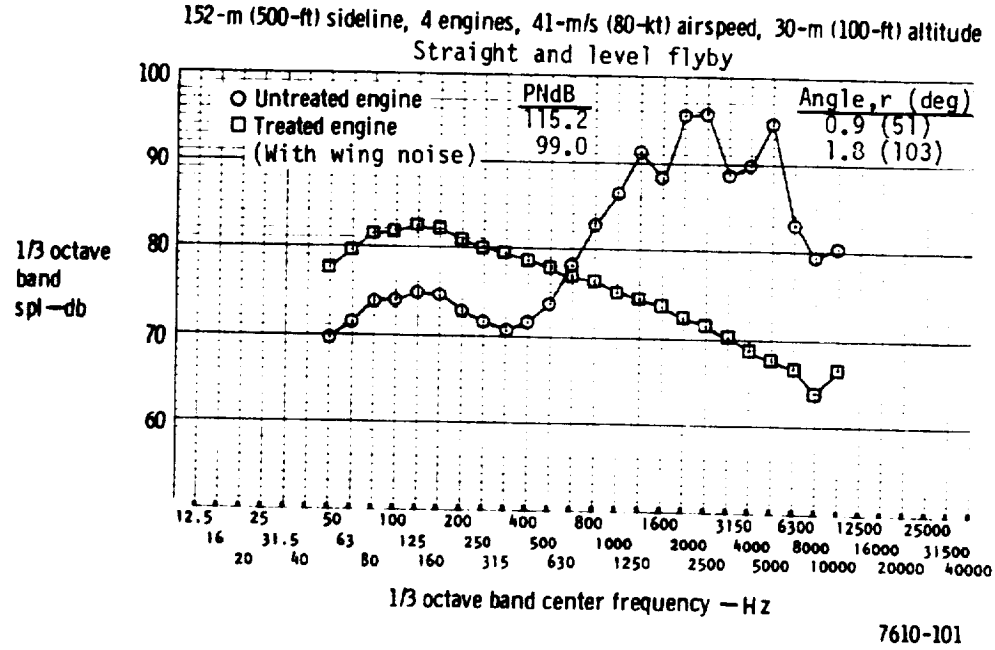

Figure 3c-19. PD287-51 peak suppressed and unsuppressed 1/3 octave band spectrums.

EPNL CONTOURS

Contours of equal-level EPNL at 90, 95, and 100 EPNdB were generated for each of the Task II engines using the flight description shown in Figure 3c-20. Takeoff is made with constant flight and engine conditions but approach consists of deceleration and constant condition legs. Approach contours were approximated by generating two sets of contours: one for constant 25% thrust and decreasing airspeed from 51 to 41 m/s (100 to 80 kt) and one for the constant condition final leg. The two sets of contours were combined to produce the contours shown in Figures 3c-21 through 3c-26. The two leg approach reduces contour areas for all configurations.

Generating contours for the AW aircraft presented a special problem in that only a limited description of wing noise was available. Data from NASACR-114285, Design Integration and Noise Studies for Jet STOL Aircraft, Vol III, were used to obtain wing generated noise. Figure 3c-27 shows the 1/3 octave spectrum and UTW PNdB distribution used. A minor level decrement (4 db) was required to obtain the directed goal of 92 EPNdB for the wing noise alone. Flap impingement noise has a similar spectrum, as shown in Figures 3c-13 through 3c-18, but a very different PNdB distribution. Figure 3c-28 compares the UTW PNdB distribution for AW and EBF lift systems. The narrow radiation path of the AW noise produces a sharply peaked PNdB time history which will convert to a lessor EPNdB than EBF lift noise having the same peak PNdB.

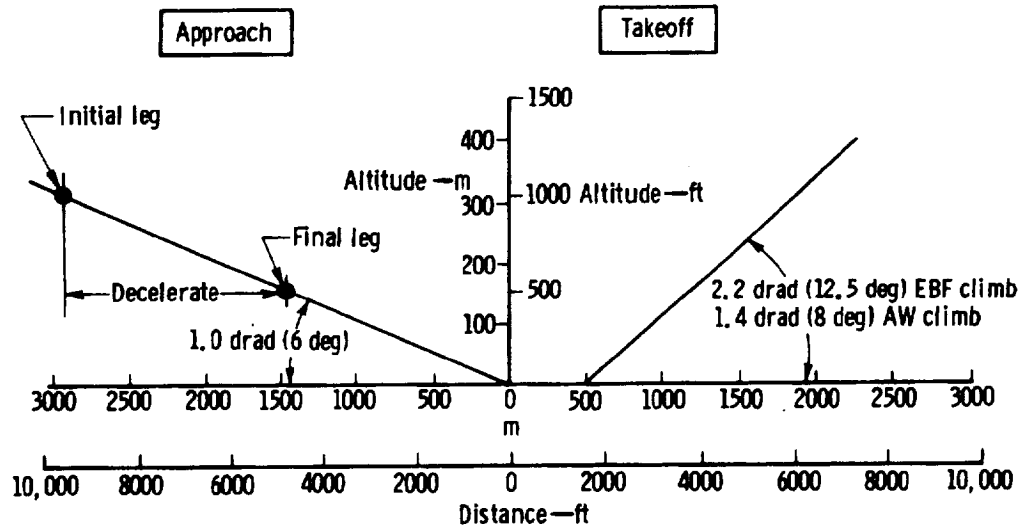

Final Leg Approach Power Settings

Configuration	Percent of max installed thrust at 41 m/s (80 kt)
EBF	72
OTW	72
AW	55

Aircraft configurations

		Takeoff	Approach	
			Initial leg	Final leg
Airspeed	m/s (kt)	41(80)	51(100)	41(80)
Flap setting	rad (deg)	0.5 (30)	0.6 (35)	1 (60)
Thrust setting	% max	100	25	---

7610-87

Figure 3c-20. Flight path and thrust requirements for EPNL contours.

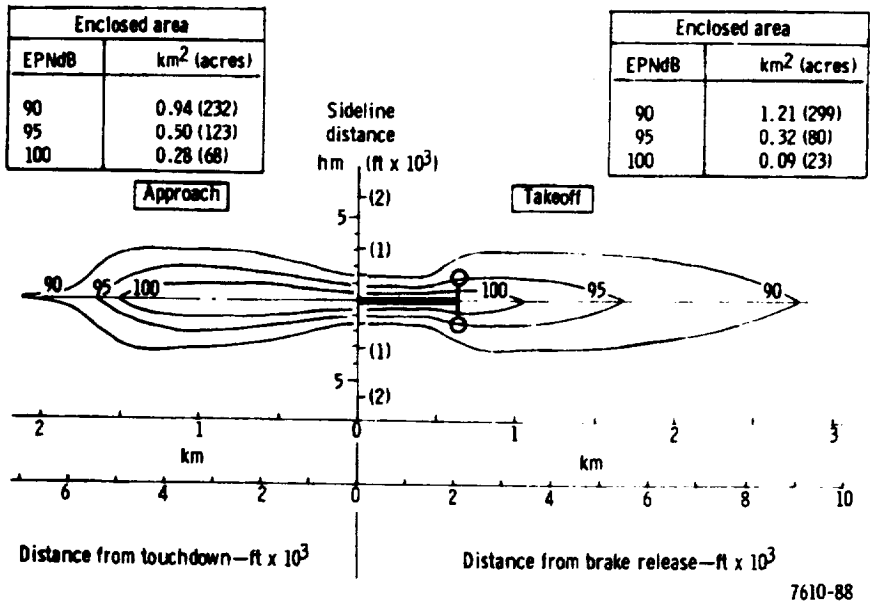

Figure 3c-21. EPNL contours for PD287-5 UTW.

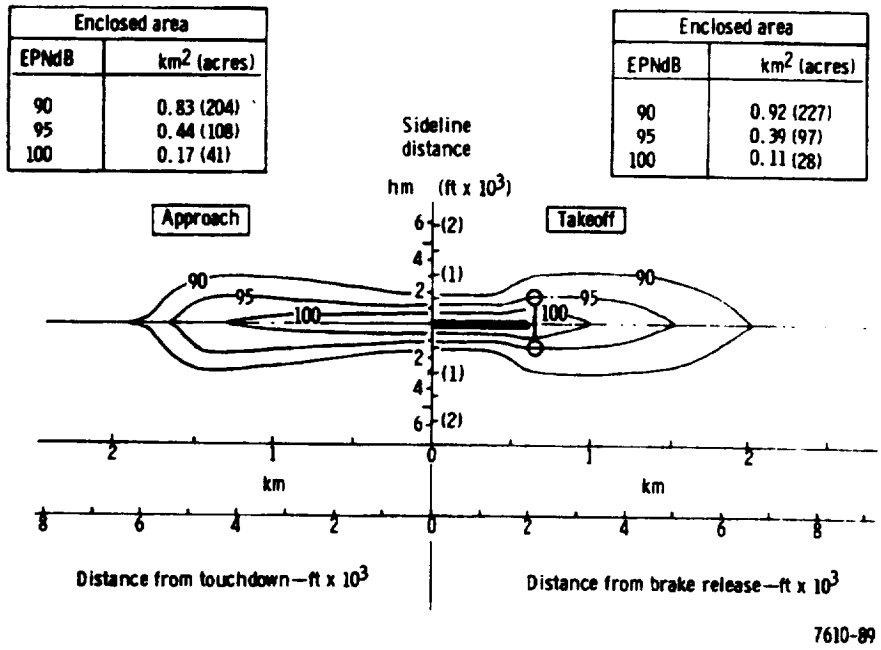

Figure 3c-22. EPNL contours for PD287-6 OTW.

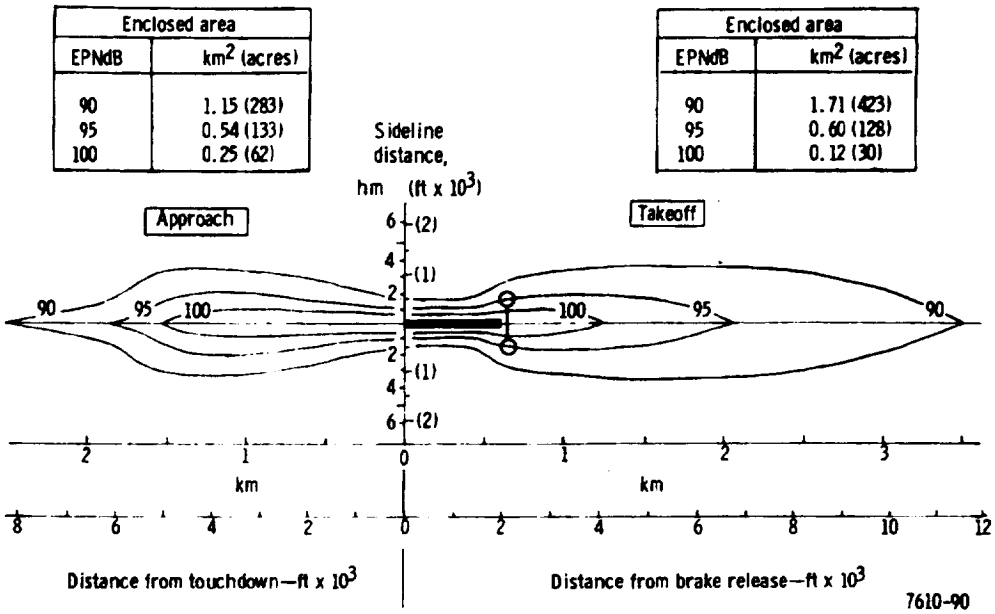

Figure 3c-23. EPNL contours for PD287-7.

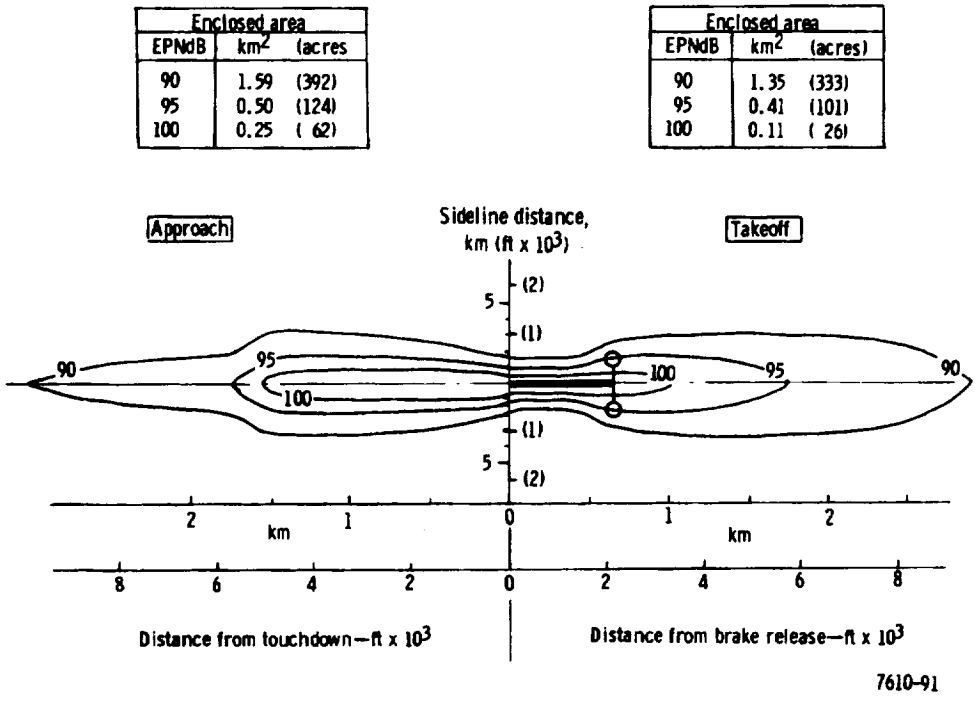

Figure 3c-24. EPNL contours for PD287-11 OTW.

Full sonic block	
Enclosed area	
EPNdB	km^2 (acres)
90	0.47 (115)
95	0.20 (49)
100	0.05 (13)

Partial sonic block	
Enclosed area	
EPNdB	km^2 (acres)
90	1.06 (262)
95	0.45 (111)
100	0.15 (36)

Enclosed area	
EPNdB	km^2 (acres)
90	2.44 (605)
95	0.66 (164)
100	0.18 (45)

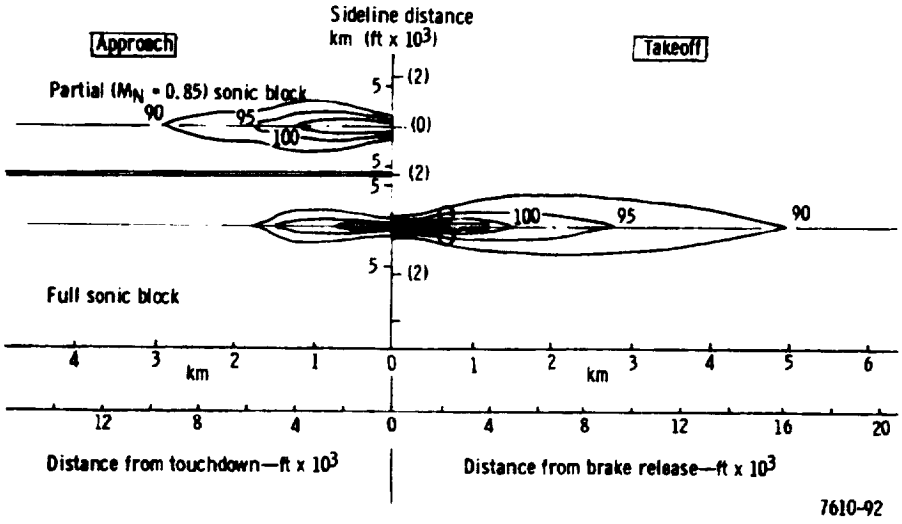

Figure 3c-25. EPNL contours for PD287-51.

Enclosed area	
EPNdB	km^2 (acres)
90	1.57 (388)
95	0.75 (186)
100	0.40 (98)

Enclosed area	
EPNdB	km^2 (acres)
90	5.10 (1260)
95	1.40 (345)
100	0.55 (136)

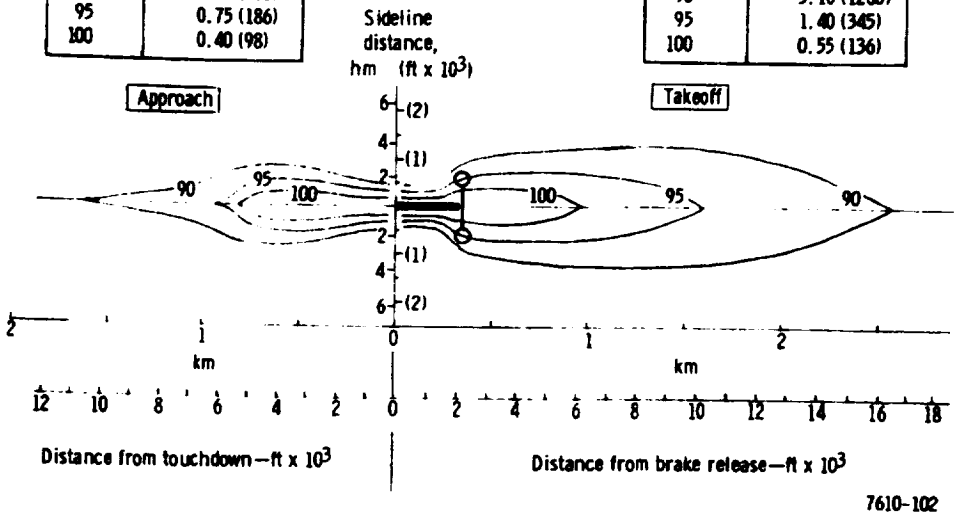

Figure 3c-26. EPNL contours for PD287-6 UTW.

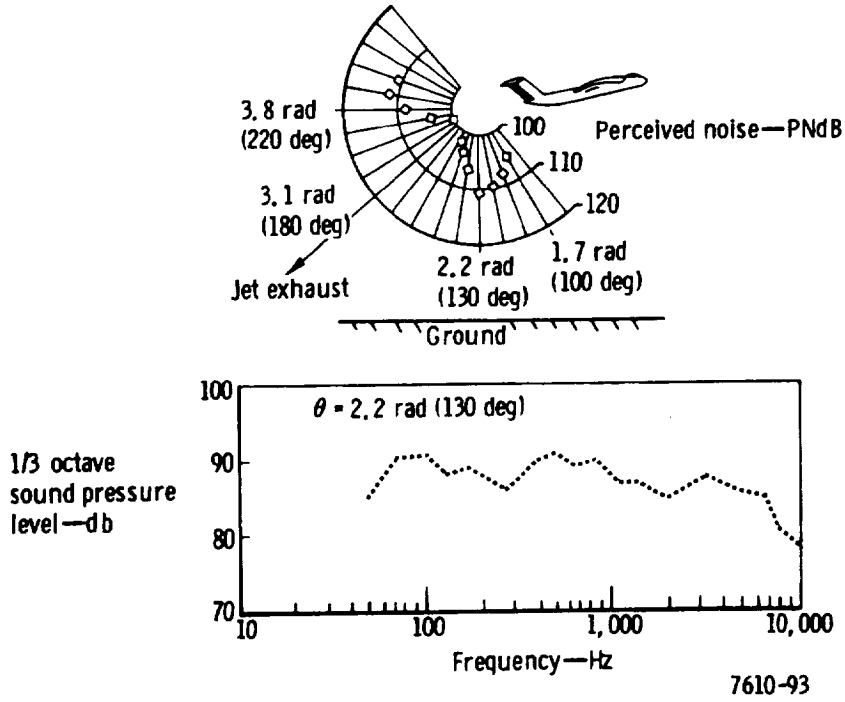

Figure 3c-27. AW noise at 98 m (320 ft) for four 89 kN (20, 000 lbf) thrust engines.

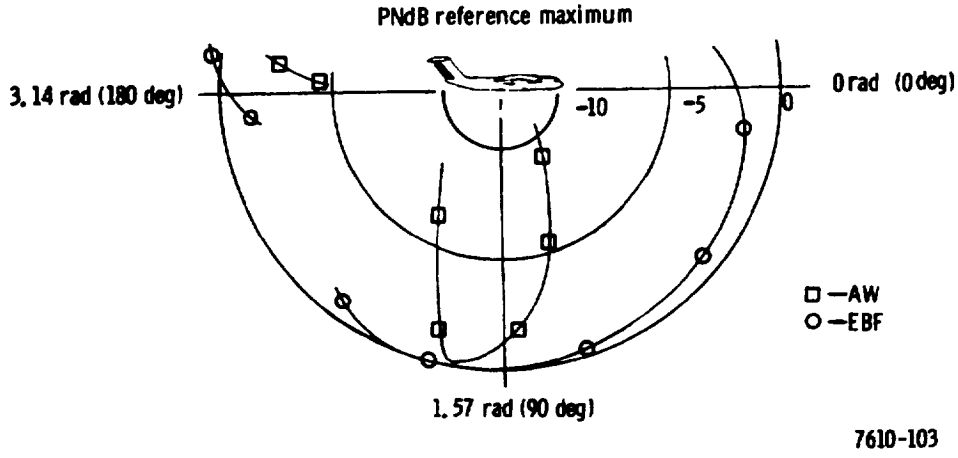

Figure 3c-28. PNdB distribution for AW and EBF lift system noise.

A dual set of contours were generated for the augmentor wing installation to determine if the full choke was required in the inlet vanes during approach. This comparison is made (Figure 3c-26) and shows that a partial sonic block (M_N = 0.85) will meet the approach attenuation requirements.

NOISE REDUCTION AND ENGINE GROWTH

Flap impingement noise is the primary constraint currently limiting EBF systems to fan pressure ratios of about 1.25 for UTW and about 1.35 for OTW applications. These pressure ratios combined with the primary nozzle velocity limit of about 213 m/s (700 ft/sec) result in engine bypass ratios in the range of 13 to 18 which are quite sensitive to duct treatment pressure losses. In addition to fans with reduced noise generation characteristics, three areas can be exploited to improve EBF system performance.

Flap Impingement Noise

Current experiments have shown noise reductions with forward velocity, treated (porous) flap leading and/or trailing edges, and trailing edge blowing. The results of these experiments indicate that the 3-PNdB technology decrement used in Task II is realistic and probably conservative. An additional 3-PNdB reduction would raise the fan pressure limit to about 1.3 and 1.4 for UTW and OTW installations. Trailing edge blowing shows the potential for even larger reductions but an evaluation of the effect of the air supply requirement is needed to assess the merit of this approach.

Primary Nozzle Velocity

An increase in primary nozzle exit velocity is desired because of the resulting decrease in bypass ratio (for constant thrust and fan pressure ratio) and reduced sensitivity to duct pressure losses. The magnitude of the increase possible is both configuration and technology dependent. If the primary stream does not impinge on the flap system as in the PD287-6 and -11 OTW installations or if a variable attitude nozzle is used to direct the primary streams below the flaps, an increase of about 30 m/s (100 ft/sec) can be realized. With development of technology to control core exhaust noise, the increase for the nonimpinging primary stream can be raised about 91 m/s (300 ft/sec). The result would not only be a decrease in bypass ratio but also an increase in thrust/airflow ratio indicating a reduction in engine size. This development would directly benefit AW as well as EBF systems.

Partial Sonic Block

Task I and II results show that the application of a partial choke inlet (M_N = 0.85 to 0.9) to EBF fans is desirable from a weight and pressure loss viewpoint. Current test results also show that the inlet attenuation (15 to 20 PNdB) provided by a partial block is sufficient to meet the 95-EPNdB goal.

Application of partial choke inlet vanes to engines similar to the PD287-11 would result in a net increase in engine thrust/weight ratio and in addition would substantially improve engine thrust response.

Engine growth can be obtained in a number of ways. Supercharging the core will allow an increase in fan pressure ratio or a fan of larger size. Increased turbine temperature can also be used and a nonflap impinging primary stream will allow an increase in primary stream velocity for thrust growth. These elements can be used in combination to obtain 25% growth and still maintain a 95-EPNdB system.

NOISE SUMMARY

Each engine was evaluated at the 41-m/s (80-kt), 31-m (100-ft) altitude take-off power condition to determine the base propulsion system noise and engine suppression requirements. In addition, each engine was evaluated in the suppressed mode at several operating conditions as shown in Table 3c-IV to determine if the 95-EPNdB goal would be met in all modes of operation.

As given in Table 3c-IV, changes in altitude, airspeed, and engine power setting are involved, all of which affect the propulsion system noise as follows.

- Forward speed affects jet noise through the relative velocity effect and has a reducing effect on flap noise. Airspeed has a direct bearing on EPNL through time duration.
- Altitude has a direct bearing on the sideline noise levels because slant distance is affected. In addition to the distance change, engine and flap noise directivity, shielding, and extra ground attenuation effects are influenced by altitude changes.
- Engine power setting has a direct bearing on engine and lift system noise generation. While the two are interdependent to a strong degree changes in lift system configuration (i.e., flap angle) can materially affect the propulsion system total noise even at a constant power setting.

Changes in fan inlet and bypass duct attenuations also occur with engine power setting changes. Duct designs are built around the take-off suppression requirements and reflect the spectral and duct Mach number requirements at that condition. At reduced power settings, the duct Mach numbers are reduced and the duct suppression tuning and attenuation are affected. Inlets attenuation is reduced and the peak tends to move away from the fan passing tones as their frequencies are reduced. The inverse is true for the bypass duct treatment. Attenuation levels are increased somewhat and the peak tends to follow the fan passing tone frequency reduction.

Changes in duct attenuation as the result of power level changes have been included in the analysis and are reflected in the propulsion system levels shown in Table 3c-IV.

Table 3c-IV.

Propulsion system noise at several operating conditions.

152-m (500-ft) sideline

Condition	Thrust, %	Altitude, m (ft)	Airspeed, m/s (kt)	Noise levels, EPNdB						
				PD287-5	PD287-6		PD287-7	PD287-11		PD287-51
				UTW	OTW	UTW	UTW	OTW	UTW	AW
Takeoff	100	30 (100)	41 (80)	95	95	100	95	95	100	95
Takeoff	100	0	0	96*	96*	100*	95*	97*	100*	101*
Takeoff	100	0	61 (130)	89	90	93	89	90	94	86
Approach	EBF 72 AW 55	152 (500)	41 (80)	97	95	100	96	97	101	91
Reverse	35	0	21 (40)	100	107	107	101	100	101	110

*PNdB levels at zero forward speed.

Source Noise Levels for Task II Engines

The techniques for predicting noise generation and suppression described in Appendix A were used in Tasks I and II. A complete description of system noise in terms of the individual source levels was obtained for each engine installation at the several required operating conditions. Souce levels for the Task II engines are summarized in Tables 3c-V through 3c-IX. Levels for front and rear radiated noise are shown for several flight conditions (straight and level flybys) and several ground conditions. Three primary effects—other than distance and engine thrust changes—are responsible for the source trends shown. These effects are:

- Forward velocity effect on externally blown flap noise (-3db)
- Increasing shielding effect with decreasing altitude
- Increasing extra ground attenuation with decreasing altitude

Conversion of Four-Engine System EPNL to Single-Engine Test Stand PNdB

Task II ground rules required that extra ground attenuation and shielding effects be included in the noise analysis. These effects have been isolated to show their impact on the system EPNdB and additional data were generated to provide a rationale to link single-engine test stand demonstration noise levels to four-engine system EPNL. Table 3c-X summarizes this information.

Table 3c-V.

PD287-5 noise breakdown at peak front and rear PNdB.

Takeoff 100% thrust 0.26/0.52 rad (15/30 deg) flap					Four engine levels at 152-m (500-ft) sideline												
Alt		Airspeed		Mode	Peak front noise, PNdB—0.9-1.1 rad (50-60 deg)						Peak rear noise, PNdB—1.7-1.9 rad (100-110 deg)						Noise—EPNdB
m	(ft)	m/s	(kt)		Fan	Flap	Turbine	Jet	Core	Total	Fan	Flap	Turbine	Jet	Core	Total	
31	(100)	41	(80)	Bare*	98.2	92.7	82.8	71.8	80.9	100.6	105.3	91.8	93.0	77.4	85.7	106.8	106.4
31	(100)	41	(80)	Suppressed	87.0	89.3	71.3	69.2	78.6	92.1	88.1	90.5	89.1	75.5	84.9	97.3	94.3
0	(0)	0	(0)	Suppressed	80.0	90.8	63.7	72.4	77.1	92.4	86.6	91.1	88.4	77.7	83.4	96.3	
0	(0)	61	(130)	Suppressed	80.0	86.8	63.7	64.5	77.1	87.4	86.9	89.8	88.4	69.2	83.4	95.2	89.0
Approach 72% thrust 0.55/1.1 rad (30/60 deg) flap																	
151	(500)	41	(80)	Suppressed**	82.2	93.9	72.5	59.2	67.4	96.0	79.7	92.4	84.0	64.1	71.4	94.0	96.5
Reverse thrust 35% thrust 0 rad (0 deg) flap (Engine at 100% cond)																	
0	(0)	21	(40)	Suppressed**	90.4	None	62.1	70.3	77.0	91.3	95.6	None	88.4	76.0	83.4	98.1	100.0

*Base condition—duct treatments designed at this condition.

**Fan noise reflects treatment attenuation change caused by duct M_N change.

Table 3c-VI.

PD287-6 noise breakdown at peak front and rear PNdB OTW configuration.

Takeoff 100% thrust 0.26/0.52 rad (15/30 deg) flap					Four engine levels at 152-m (500-ft) sideline											
					Peak front noise, PNdB—0.9-1.1 rad (50-60 deg)						Peak rear noise, PNdB—1.7-1.9 rad (100-110 deg)						Noise—EPNdB
Alt m	Alt (ft)	Airspeed m/s	Airspeed (kt)	Mode	Fan	Flap	Turbine	Jet	Core	Total	Fan	Flap	Turbine	Jet	Core	Total	
31	(100)	41	(80)	Bare*	102.8	84.4	80.9	77.5	81.9	103.9	106.5	87.1	90.0	82.3	86.6	108.0	109.5
31	(100)	41	(80)	Suppressed	88.9	81.3	75.5	73.5	80.1	91.2	90.3	82.0	86.7	77.6	84.0	95.2	95.4
0	(0)	0	(0)	Suppressed	84.2	80.6	60.7	75.5	78.6	85.4	91.5	82.0	88.3	79.7	82.5	93.6	
0	(0)	61	(130)	Suppressed	84.2	77.6	60.7	60.4	78.6	85.4	91.5	80.5	87.8	72.3	82.5	95.5	96.9
Approach 72% thrust 0.55/1.1 rad (30/60 deg) flap											Note: Peak at 2.4 rad (140 deg)						
151	(500)	41	(80)	Suppressed**	83.8	85.1	68.9	60.4	70.9	88.5	80.9	90.3	64.0	65.7	73.3	91.8	94.9
Reverse thrust 35% thrust 0 rad (0 deg) flap (Engine at 100% cond)																	
0	(0)	21	(40)	Suppressed**	91.8	None	60.9	70.1	79.0	93.3	103.3	None	87.5	78.0	84.0	105.4	107.4

*Base condition—duct treatments designed at this condition.

**Fan noise reflects treatment attenuation change caused by duct M_N change.

Table 3c-VII.

PD287-7 noise breakdown at peak front and rear PNdB UTW configuration.

Takeoff 100% thrust 0.26/0.52 rad (15/30 deg) flap					Four engine levels at 152-m (500-ft) sideline												
					Peak front noise, PNdB—0.9-1.1 rad (50-60 deg)						Peak rear noise, PNdB—1.7-1.9 rad (100-110 deg)						Noise-EPNdB
Alt m	Alt (ft)	Airspeed m/s	Airspeed (kt)	Mode	Fan	Flap	Turbine	Jet	Core	Total	Fan	Flap	Turbine	Jet	Core	Total	
31	(100)	41	(80)	Bare*	96.7	91.0	78.1	72.6	80.4	99.5	104.1	90.9	91.1	76.8	85.2	105.9	105.4
31	(100)	41	(80)	Suppressed	91.3	90.2	71.5	70.8	78.1	94.8	92.1	89.8	82.7	74.6	84.4	96.2	95.5
0	(0)	0	(0)	Suppressed	84.7	90.0	60.0	72.5	76.5	91.0	88.6	91.1	83.0	78.4	83.0	91.5	
0	(0)	61	(130)	Suppressed	85.1	87.0	60.0	63.3	76.5	88.4	86.0	88.3	83.0	68.3	83.0	92.1	89.0
Approach 72% thrust 0.5/1.1 rad (30/60 deg) flap																	
151	(500)	41	(80)	Suppressed**	85.3	93.7	70.7	59.6	67.0	95.2	84.5	91.1	82.2	64.2	71.0	93.6	96.0
Reverse thrust 35% thrust 0 rad (0 deg) flap (Engine at 100% cond)																	
0	(0)	21	(40)	Suppressed**	91.1	None	57.6	71.5	76.5	91.7	97.5	None	82.8	75.1	83.0	99.1	100.9

*Base condition—duct treatments designed at this condition.

**Fan noise reflects treatment attenuation change caused by duct M_N change.

Table 3c-VIII.

PD287-11 noise breakdown at peak front and rear PNdB OTW configuration.

Takeoff 100% thrust 0.26/0.52 rad (15/30 deg) flap					Four engine levels at 152-m (500-ft) sideline												
					Peak front noise, PNdB—0.9-1.1 rad (50-60 deg)						Peak rear noise, PNdB—1.7-1.9 rad (100-110 deg)						
Alt		Airspeed		Mode													Noise—EPNdB
m	(ft)	m/s	(kt)		Fan	Flap	Turbine	Jet	Core	Total	Fan	Flap	Turbine	Jet	Core	Total	
31	(100)	41	(80)	Bare*	104.1	85.2	80.8	78.7	82.0	105.0	106.6	86.2	92.6	82.8	87.2	108.0	107.9
31	(100)	41	(80)	Suppressed	90.6	84.2	75.2	76.7	81.0	93.2	89.7	85.2	86.9	80.8	86.0	95.6	95.3
0	(0)	0	(0)	Suppressed	85.9	82.9	60.4	81.0	79.2	87.0	91.8	84.1	88.1	82.5	84.3	96.8	
0	(0)	61	(130)	Suppressed	85.9	80.0	60.4	68.2	79.2	87.0	91.6	83.1	87.8	74.4	84.3	94.9	89.7
Approach 72% thrust 0.55/1.1 rad (30/60 deg) flap											Note: Peak rear at 2.4 rad (140 deg)						
151	(500)	41	(80)	Suppressed**	88.6	87.2	69.6	65.6	70.0	92.0	75.6	92.2	68.2	69.2	79.1	92.5	96.5
Reverse thrust 35% thrust 0 rad (0 deg) flap (Engine at 100% cond)					Reverser						Reverser						
0	(0)	21	(40)	Suppressed**	86.3	None	60.4	89.0		90.3	92.9	None	87.6	98.1		100.4	99.7

*Base condition—duct treatments designed at this condition.

**Fan noise reflects treatment attenuation change caused by duct M_N change.

Table 3c-IX.

PD287-51 noise breakdown at peak front and rear PNdB AW configuration.

Takeoff 100% thrust 0.52 rad (30 deg) flap					Four engine levels at 152-m (500 ft) sideline												
Alt		Airspeed		Mode	Peak front noise, PNdB—0.9-1.1 rad (50-60 deg)						Peak rear noise, PNdB—1.7-1.9 rad (100-110 deg)						Noise—EPNdB
m	(ft)	m/s	(kt)		Fan	Wing	Turbine	Jet	Core	Total	Fan	Wing	Turbine	Jet	Core	Total	
31	(100)	41	(80)	Bare	113.2	---	83.0	76.2	86.1	113.6	106.6	---	94.5	79.9	90.9	108.1	112.5*
31	(100)	41	(80)	Suppressed	78.2	90.6	74.4	76.2	86.1	88.9	71.6	97.5	85.9	79.9	90.9	93.5	93.8* 94.6
0	(0)	0	(0)	Suppressed	65.8	85.9	61.2	80.0	82.1	86.5	72.1	99.6	85.9	83.8	89.9	100.8	
0	(0)	61	(130)	Suppressed	66.3	79.0	60.2	69.0	82.1	81.3	71.2	91.0	84.7	72.1	89.9	92.2	85.6
Approach 35% thrust 1.1 rad (60 deg) flap																	
151	(500)	41	(80)	Suppressed	73.4	93.4	70.3	48.8	69.2	93.7	66.4	86.9	82.8	52.6	73.1	90.4	91.3
Reverse thrust 35% thrust 0 rad (0 deg) flap (Engine at 100% cond)					Reverser						Reverser						
0	(0)	21	(40)	Suppressed	78.2	None	74.4	109.4		100.5	72.5	None	84.7	109.0		111.5	110.1

*Engine only.

Table 3c-X.

Converting 152-m (500-ft) and 95 EPNdB aircraft levels to suppressed single-engine test stand levels at 46-m (150-ft) polar.

(Changes shown reflect peak noise levels at each condition.)

Condition	PD287-5	PD287-6	PD287-7	PD287-11	PD287-51
Base line, 31-m (100-ft) alt, 152-m (500-ft) sideline, 41-m/s (80-kt) flyby (four-engine), EPNdB	94.3	95.4	95.5	95.3	94.6
Effect of extra ground attenuation on:					
Level	+0.4	+0.3	+0.4	+0.4	+0.2
Duration	+0.8	+1.4	+1.1	+2.7	+0.4
EPNdB-to-PNdB$_t$ duration correction	+2.3	-0.5	-0.4	-1.8	+4.0
PNdB$_t$-to-PNdB tone correction	-1.4	0.0	0.0	0.0	0.0
Shielding effect	+1.7	+1.7	+1.7	+1.7	+1.7
Four-engine-to-single-engine effect	-6.0	-6.0	-6.0	-6.0	-6.0
41-m/s (80-kt)-to-0 m/s forward velocity effect	+1.1	+0.3	+0.6	+0.3	+0.2
31-m (100-ft) alt, 152-m (500-ft) sideline to 46-m (150-ft) polar	+14.0	+18.1	+15.1	+20.5	+14.0
Engine only—no flap or wing noise	-2.2	-3.0	-3.8	-6.2	-5.4
Peak single-engine test stand level at 46-m (150-ft) polar, PNdB	105.0	107.7	104.2	106.9	103.7

3d. Component Definitions

3d1. Nacelles

Rohr Industries, Incorporated conducted the preliminary design and analysis of the nacelles for the five Task II propulsion systems. Table 3d1-I presents a weight breakdown for the nacelle components and total structure and nacelle weights for the five systems.

PD287-5 NACELLE DESCRIPTION

The PD287-5 propulsion pod shown in Figure 3b-2 is a UTW, pylon-mounted installation in which the secondary and primary airstreams exhaust from the nacelle in a conventional way. The nacelle consists of the following major assemblies.

Inlet Nose Cowl

The inlet nose cowl consists of an aluminum alloy honeycomb inner barrel and an aluminum skin/frame outer barrel. The nose lip is of aluminum alloy with an inner liner of titanium alloy. The lip is closed out with a titanium alloy bulkhead to form the anti-ice "D" duct. An aft bulkhead of titanium alloy joins the inner and outer barrels and an anti-icing hot air duct pierces both bulkheads to feed the D duct. An aluminum alloy attach ring is joined to the inner barrel and mates with the engine. Carried within the inlet duct on five struts is a ring of structural aluminum alloy, honeycomb, double "sandwich." The outer skins of this and the inner skin of the nose cowl inner barrel are perforated for sound suppression. The leading edge of the acoustic ring is served by a hot air feed to prevent icing.

Fan Cowl

The fan cowl is an aluminum alloy honeycomb bondment hinged at the pylon and latched at its lower center line. The fan cowl interfaces with the nose cowl forward and the fan duct aft.

Fan Duct

This assembly consists of an inner and outer duct wall of aluminum alloy, bonded, honeycomb sandwich. Mounted within the duct is a ring of aluminum alloy, honeycomb, double sandwich supported from the inner and outer walls by sheet aluminum alloy struts. The wetted surfaces of the duct and ring are perforated for sound suppression. An outer fairing of skin/frame aluminum is mounted to the outer duct wall by aluminum sheet metal bulkheads. The assembly is hinged to the pylon and latches together at its lower center line.

Variable Fan Nozzle

Mounted to the fan duct assembly is the variable area fan nozzle consisting of 12 aluminum alloy honeycomb flaps supported on aluminum alloy "islands." The islands contain the actuating mechanism and mount to an aluminum alloy ring on the aft end of the fan duct.

Table 3d1-I.
QCSEE nacelle weight summary.

Component	PD287 component weight, kg (lbm)				
	-5	-6	-7	-11	-51
Structure					
Nose cowl including splitter	308 (678)	307 (676)	241 (531)	375 (826)	83 (182)
Fan cowl	98 (216)	89 (196)	79 (174)	73 (160)	53 (117)
Fan reverser	---	---	---	---	124 (274)
Primary spoiler	---	---	---	---	170 (375)
Fan duct	---	397 (876)	---	390 (859)	94 (208)
Fan duct including splitter and outer cowl	308 (837)	---	300 (661)	---	---
Fan variable nozzle and fairing	87 (192)	---	68 (151)	---	---
Tailpipe and core cowl	134 (296)	---	103 (228)	---	---
Tail cone (bullet)	34 (76)	---	33 (72)	---	5 (11)
All structure from fan cowl to engine aft flange	---	419 (923)	---	417 (919)	---
Tailpipe including tail cone	---	231 (510)	---	229 (505)	---
Aft nacelle	---	156 (344)	---	148 (326)	---
Aft engine mount	12 (27)	29 (65)	10 (22)	29 (65)	25 (55)
Total structure	1053 (2322)	1628 (3590)	834 (1839)	1660 (3660)	554 (1222)
Thrust reverser pneumatic system	---	125 (276)	---	84 (185)	125 (276)
Variable fan nozzle area control system	12 (27)	---	10 (22)	---	---
EBU equipment (per equipment list)	298 (657)	298 (657)	285 (629)	285 (629)	242 (533)
Miscellaneous (brackets, plumbing, wiring, etc)	151 (332)	151 (334)	151 (332)	152 (336)	150 (330)
Total nacelle	1514 (3338)	2203 (4857)	1280 (2822)	2182 (4810)	1071 (2361)

Primary Nozzle and Fairing

The primary nozzle is a brazed nickel alloy honeycomb assembly of three welded panels attached to the engine flange and has a titanium skin/stringer fairing mounted on nickel alloy bulkheads.

A tail cone assembly of brazed nickel alloy honeycomb is mounted off the engine within the nozzle. The wetted skin of the nozzle and plug are perforated for sound suppression.

Engine Forward Flight Mount

The engine forward flight mount consists of a pylon fitting of high-strength, low-alloy steel and bolts to the engine mount pad.

Engine Aft Flight Mount

This assembly consists of a pylon fitting and three links arranged to resist vertical side and torque loads. The links interface to the engine mount lugs on the turbine casing. The links and fitting are of high-strength nickel alloy.

PD287-6 NACELLE DESCRIPTION

The PD287-6 propulsion pod shown in Figure 3b-5 is a twin-engine, OTW installation. The nacelle consists of the following major assemblies.

Inlet Nose Cowl

The inlet nose cowl consists of an aluminum alloy honeycomb inner barrel and an aluminum skin/frame outer barrel. The nose lip is of aluminum alloy with an inner liner of titanium alloy. The lip is closed out with a titanium alloy bulkhead to form the anti-ice D duct. An aft bulkhead of titanium alloy joins the inner and outer barrels and an anti-ice hot air duct pierces both bulkheads to feed the D duct. An aluminum alloy attach ring is joined to the inner barrel and mates with the engine. Carried within the inlet duct on five struts are two rings of aluminum alloy, honeycomb, double sandwich. The outer skins of these and the inner skin of the nose cowl inner barrel are perforated for sound suppression. The leading edges of the acoustic rings are served by a hot air feed to prevent icing.

A nose spinner attached to the engine is built up of aluminum alloy honeycomb panels with perforated skins for sound suppression.

Fan Cowl

The fan cowl is in three pieces: an upper aluminum alloy skin/frame and two hinged aluminum alloy honeycomb doors. The skin/frame attaches to the engine fan case and terminates at the upper center line of the nacelle. One hinged door hinges to the fixed portion and latches to the other door which is hinged to the lower edge of the pylon.

Forward Core Cowl and Fan Ducts

This assembly consists of two parts: an upper, fixed portion attached to the pylon and a side-hinged portion latched at the bottom to the pylon. Fan ducts of aluminum alloy honeycomb are carried within the cowling which is of aluminum skin and frame construction.

The forward end of the cowls are fitted with mechanically actuated doors of aluminum alloy honeycomb and the corresponding part of the duct outer wall is fitted with a spring-loaded door. These doors form the reverse flow passage for the variable pitch fan. In the lower duct outer wall is an opening which interfaces with the boundary layer control bypass duct. The wetted skins in the fan ducts are perforated for sound suppression.

Fixed Core Cowl and Fan Ducts

This assembly consists of an outer fairing of aluminum skin and frame attached to the pylon and containing the fan ducts. These ducts enclose the primary tailpipe and are of aluminum alloy honeycomb, the forward section of which has perforated skins for sound suppression. At the aft end there is a hinged door to close the fan duct in reverse thrust mode.

Primary Tailpipe

The primary tailpipe attaches to the engine and is of brazed nickel alloy honeycomb for the forward section with perforated skins for sound suppression. The aft part of the tailpipe is of nickel alloy skin frame construction. The entire outer surface of the duct is covered with insulation to shield the surrounding aluminum structure.

Engine Forward Flight Mount

The engine forward flight mount consists of a pylon fitting of high-strength, low-alloy steel and bolts to the engine mount pad.

Engine Aft Flight Mount

This mount consists of a pylon fitting and three links arranged to resist vertical side and torque loads. The links interface to the engine mount lugs on the turbine casing. The links and fitting are of high-strength nickel alloy.

Boundary Layer Control Bypass Duct

This duct consists of an aluminum skin/frame section with a mechanically actuated shutoff door. It interfaces with the airframe at the wing front spar.

PD287-11 NACELLE DESCRIPTION

The PD287-11 propulsion pod shown in Figure 3b-8 is a twin-engine, OTW installation. The nacelle consists of the following major assemblies.

Inlet Nose Cowl

The inlet nose cowl consists of an aluminum alloy honeycomb inner barrel and an aluminum skin/frame outer barrel. The nose lip is of aluminum alloy with an inner liner of titanium alloy. The lip is closed out with a titanium alloy bulkhead to form the anti-ice D duct. An aft bulkhead of titanium alloy joins the inner and outer barrels and an anti-ice hot air duct pierces both bulkheads to feed the D duct. An aluminum alloy attach ring is joined to the inner barrel and mates with the engine. Carried within the inlet duct on five struts are two rings of aluminum alloy, honeycomb, double sandwich. The outer skins of these and the inner skin of the nose cowl inner barrel are perforated for sound suppression. The leading edges of the acoustic rings are served by a hot air feed to prevent icing.

A nose spinner attached to the engine is built up of aluminum alloy honeycomb panels with perforated skins for sound suppression.

Fan Cowl

The fan cowl is in three pieces: an upper aluminum alloy skin/frame and two hinged aluminum alloy honeycomb doors. The skin/frame attaches to the engine fan case and terminates at the upper center line of the nacelle. One door hinges to the fixed portion and latches to the other door which is hinged to the lower edge of the pylon.

Forward Core Cowl and Fan Ducts

This assembly consists of two parts: an upper fixed portion attached to the pylon and a side-hinged portion latched at the bottom to the pylon. Fan ducts of aluminum alloy honeycomb are carried within the cowling which is of aluminum skin and frame construction. The forward end of the cowls are fitted with a thrust reverser mechanism. Inner aluminum alloy honeycomb doors are hinged to a translating ring and linked to the duct inner wall. External doors of aluminum alloy honeycomb cover fixed magnesium cascade castings. In the lower duct outer wall is an opening which interfaces with the boundary layer control bypass duct. In the forward end

of the fan duct there is a ring of double-faced, aluminum alloy, honeycomb which aligns with a corresponding ring in the engine.

The wetted skin of the fan duct and ring are perforated for sound suppression.

Fixed Core Cowl and Fan Ducts

This assembly consists of an outer fairing of aluminum skin and frame attached to the pylon and containing the fan ducts. The ducts enclose the primary tailpipe and are of aluminum alloy honeycomb, the forward section of which has perforated skins for sound suppression.

Primary Tailpipe

The primary tailpipe is of brazed nickel alloy honeycomb for the forward section with perforated skins for sound suppression. The aft part of the tailpipe is of nickel alloy skin frame construction. The entire outer surface of the duct is covered with insulation to shield the surrounding aluminum structure.

Engine Forward Flight Mount

The engine forward flight mount consists of a pylon fitting of high-strength low-alloy steel and bolts to the engine mount pad.

Engine Aft Flight Mount

This mount consists of a pylon fitting and three links arranged to resist vertical side and torque loads. The links interface to the engine mount lugs on the turbine casing. The links and fitting are of high-strength nickel alloy.

Boundary Layer Control Bypass Duct

This duct consists of an aluminum skin/frame section with a mechanically actuated shutoff door. It interfaces with the airframe at the wing front spar.

PD287-51 NACELLE DESCRIPTION

The PD287-51 propulsion pod shown in Figure 3b-11 is a UTW, pylon-mounted installation in which the entire secondary airstream is ducted up to the wing via the pylon and the primary airstream exhausts from the nacelle in a conventional manner. The nacelle consists of the following major assemblies.

Inlet Nose Cowl

The inlet nose cowl consists of an aluminum alloy inner and outer barrel skin stiffened with aluminum alloy frames. The nose lip is of aluminum alloy with an inner liner of titanium alloy. The lip is closed with a titanium alloy bulkhead to form the anti-ice D duct. An aft bulkhead of titanium alloy joins the inner and outer barrels and an anti-icing hot air duct pierces both bulkheads to feed the D duct. An aluminum alloy attach ring is joined to the inner barrel and mates with the engine.

Fan Cowl

The fan cowl is an aluminum alloy honeycomb bondment hinged at the pylon and latched at its lower center line. The fan cowl interfaces with the nose cowl forward and the fan duct/thrust reverser aft.

Fan Duct/Thrust Reverser

This assembly consists of kidney-shaped ducts of titanium alloy skins and an aluminum alloy honeycomb core which interface with the engine flanges and the pylon. Between these ducts and the pylon is a "Y" duct assembly which attaches to the aft engine flight mount and the fan case adjacent to the forward engine flight mount. Hinges in the Y duct carry the kidney-shaped duct and reverser assembly which is latched at the lower center line. The reverser consists of a forward torsion box structure to which is bolted magnesium alloy cascade castings. An external translating sleeve of aluminum alloy honeycomb fairs the cascades.

The outer skin of the assembly is of aluminum alloy up to the firewall and titanium alloy skin and frame aft of the firewall.

Primary Nozzle and Thrust Spoiler

The primary nozzle is a brazed, nickel alloy, honeycomb assembly of three welded panels attached to the engine flange—the inner skin of the panels being perforated for sound suppression. Mounted to this nozzle is a forward fairing consisting of two nickel alloy sheet metal bulkheads and a titanium alloy skin. Two spoiler doors of nickel alloy skin and frame construction are attached to the nozzle via 422 Cres steel links and an investment cast Cres link box which also contains the spoiler actuator mechanism. The link box attaches to longerons on the nozzle and houses the ballscrew actuator for the spoiler. A nickel alloy, honeycomb, brazed tail cone is mounted within its nozzle on the engine.

Engine Forward Flight Mount

The engine forward flight mount consists of a pylon fitting which carries a thrust pin and two support links. A fitting attaches to the engine to receive the thrust pin and links. The material for these components is high-strength, low-alloy steel.

Engine Aft Flight Mount

This assembly consists of a pylon fitting and three links arranged to resist vertical side and torque loads. The links attach to the engine mount lugs on the turbine casing. The links and fitting are of high-strength nickel alloy.

PD287-5, -6, -11, -51 NACELLE SYSTEMS

Fire Detection System

This system provides dual loop, redundant, fire and overheat detection within the nacelle. Each loop consists of continuous element detectors functionally independent but adjacent to each other to provide the redundant coverage.

The elements are routed to cover areas where combustibles might accumulate as well as overall sensing of an overheat condition anywhere in the nacelle. Fire-resistant wiring is used to connect the sensing elements to quick disconnects on the pylon/nacelle firewall.

Generator Cooling

Fan air is tapped off the fan air duct and ducted to the generator. A collector shroud at the opposite end of the generator mates with an exhaust duct mounted on the forward cowl door which leads the cooling air overboard. Both the inlet duct and the outlet duct are divided and equipped with bulb-type "donut" seals to accommodate the differential motion of the accessory gearbox with respect to the fan duct and nacelle floors.

Constant-Speed Drive Cooler

The constant-speed drive for the generator requires cooling provisions for the lubricating oil. An air-oil cooler (located in the nose cowl with inlet and outlet ports projecting through the cowl side walls) is connected to the constant-speed drive unit on the accessory gearbox with flex hoses. Connections to the two units are such that cross installation cannot be made.

Pneumatic System

A schematic of the pneumatic system is shown in Figure 3d1-1. This system consists of a compressor high-stage bleed manifold, low-stage bleed manifold, nose cowl anti-icing, starter air supply, cabin air supply, and various valves and regulators.

The high-stage manifold is mounted to four bleed ports on the engine and terminates in a control valve on the horizontal center line of the engine left side. The low-stage manifold is mounted to two engine bleed ports and terminates in a check valve opposing the high-stage control valve. A tee duct bridges the gap between these valves and is routed over the top of the engine, through the pylon nacelle firewall, and into the precooler in the pylon. This tee duct contains the system shutoff valve and the combination pressure regulator and check valve.

The starter air duct is teed into this system downstream of the system shutoff valve. It is routed down the right side of the engine to the starter located on the vertical center line of the engine in the accessory gearbox. Venting is into the engine compartment. This system permits starting any engine from a ground cart and furnishes air to the cabin air conditioning system, also permits cross feed of starting air from one engine to another.

The nose cowl anti-icing system is teed into the high-stage manifold up stream of the control valve. A shutoff valve is in this line for anti-icing control. The duct is routed forward through the nose cowl and into the D ring which acts as a plenum distributing the hot air around nose cowl lip. The air is bled into the cowl structure and overboard through a vent on the bottom.

Cooling air for the precooler is taken from the bypass fan duct and through a control valve which is modulated by a temperature sensor in the cabin air supply duct downstream of the precooler. The cooling air is dumped overboard through vents in the pylon.

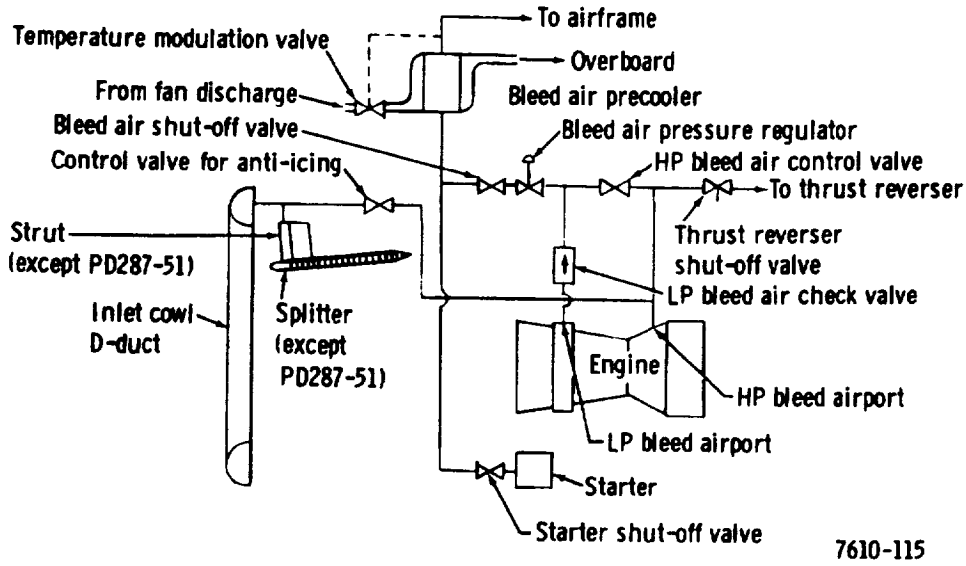

Figure 3d1-1. Pneumatic system schematic.

Engine Lubrication System

The engine lube system is furnished with the engine. The Rohr task is limited to furnishing instrumentation to monitor the performance of the system.

Oil Pressure Transmitter and Low-Pressure Warning Switch

This equipment is mounted on brackets furnished by Rohr and connected by 0.64-cm (0.025-in.) tubing to a single boss on the engine. Both units are vented by tubing to the accessory gearbox.

Scavenge Filter "P" Switch

This switch is mounted on brackets furnished by Rohr and connected by 0.64-cm (0.25-in.) tubing to bosses on the scavenge filter furnished with the engine.

Oil Temperature Sensor

This sensor is located on a boss in the line upstream of the scavenge oil filter.

Oil Quantity Transmitter

This filter is located on a pad provided on the lube oil tank.

Hydraulic System

A schematic of the hydraulic power for the aircraft is shown in Figure 3d1-2. The hydraulic system is supplied by eight 21-MN/m^2 (3000-psi), 0.0028-m^3/s (45-gpm), engine-driven hydraulic pumps mounted on the forward side of the engine accessory gearbox. Flex hoses with fire sleeves for the pressure and the case drain lines are routed from the pump to an engine-mounted filter module which provides separate filtration for them. The filter module contains a pressure switch on the pressure side and a temperature switch on the case drain side. Differential pressure indicators on both sides give visual indication of clogged filters. Check valves (integral with the module) minimize fluid spillage during removal and replacement of the filter elements.

The case drain and pressure lines are routed from the filter module around the core engine to the pylon/nacelle interface which consists of a threaded tube coupling for the case drain line and a self-sealing, quick-disconnect coupling for the pressure line. Check valves in the case drain and pressure lines on the pylon side of the firewall prevent loss of fluid from the airframe hydraulic system in the event of a hydraulic line rupture within the nacelle or removal of the engine.

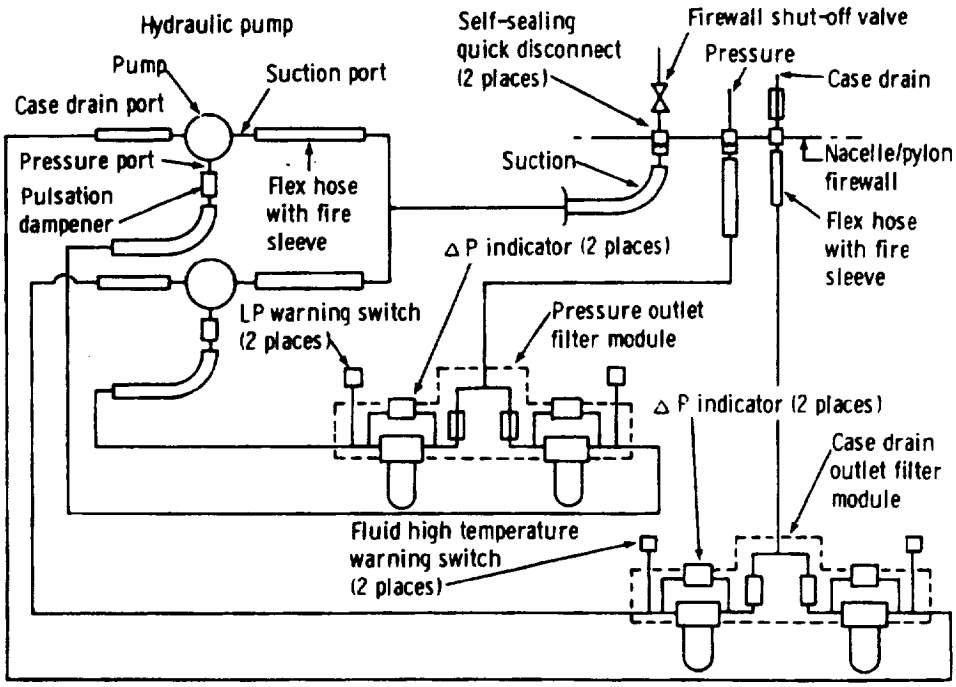

Figure 3d1-2. Hydraulic system schematic.

A hydraulic suction line from the airframe system is routed from the pylon around the core engine to connect with the suction port on the hydraulic pump. The pylon/nacelle interface connection is a self-sealing, quick-disconnect coupling. A firewall shutoff valve on the pylon side of the firewall provides for isolation of the nacelle. In the event of an engine fire, the valve is automatically closed by the signal that activates the fire extinguisher system and may be manually closed for hydraulic system malfunctions.

Fuel System

A schematic of the fuel system in the nacelle is shown in Figure 3d1-3. This system transfers the fuel from the nacelle/pylon firewall to the fuel pump furnished with the engine. It contains instrumentation to monitor the performance of various elements of the system integral with the engine and after engine shutdown provides a means to return residual fuel to the fuel tanks.

A flex hose with fire shielding is attached to a self-sealing quick-disconnect on the pylon/nacelle firewall. This supply line is routed to the fuel pump on the forward side of the accessory gearbox. The following portion of the fuel system is part of the engine. The following paragraphs describe the instrumentation and residual fuel return furnished with the engine buildup.

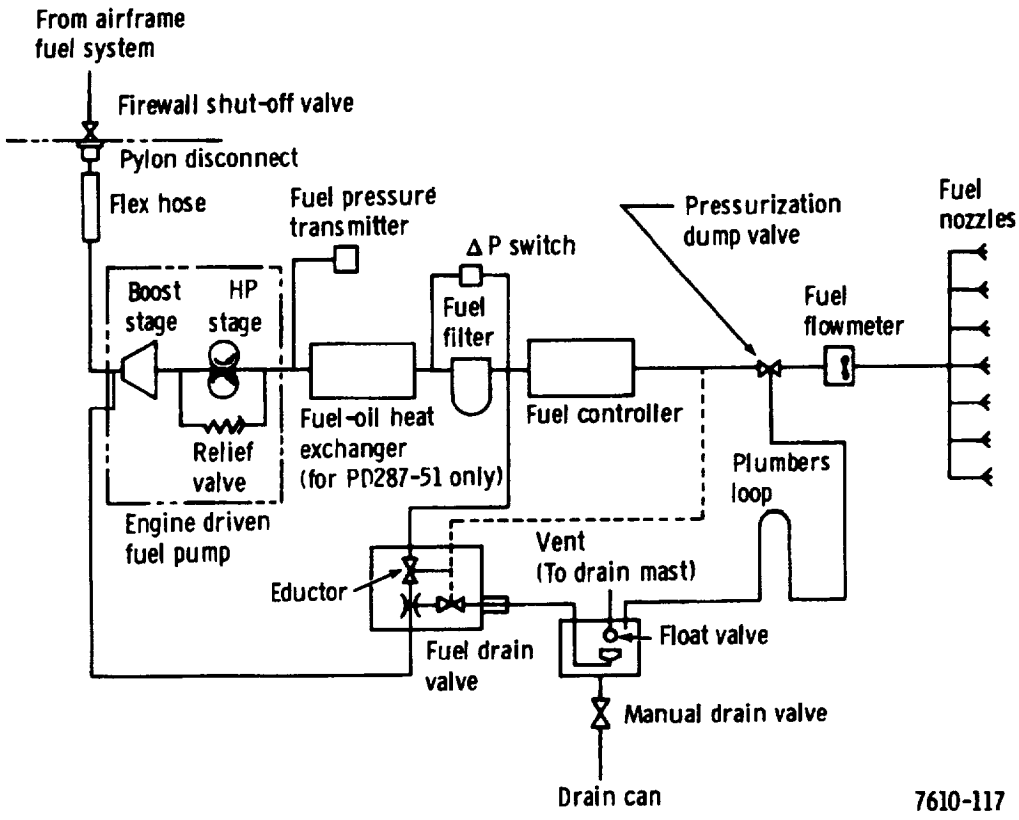

Figure 3d1-3. Fuel system schematic.

The fuel pump is a two-stage unit that raises fuel pressure from approximately 412 kN/m^2 (60 psi) as received from the fuel transfer system to approximately 6.89 MN/m^2 (1000 psi), depending on engine rpm. The fuel is then routed through a fuel oil heat exchanger (PD287-51 only), through a fuel filter, and to the fuel controller. The controller meters fuel to the engine in accordance with power demand and engine-operating conditions; it shuts off fuel flow for engine shutdown. From the controller, fuel passes through the pressurizing and dump valve and into the fuel manifold where it is distributed to the nozzles in the combustion chamber. The pressurizing and dump valve, on signal from the fuel controller, opens fuel to the fuel manifold for engine operation and at shutdown permits fuel to drain from the manifold to prevent erratic shutdown and coking.

The engine buildup includes a pressure transmitter mounted on brackets and connected to a pressure port on the fuel pump. A fuel flowmeter is also mounted on brackets and plumbed between the pressurizing and dump valve and the fuel manifold, and a ΔP switch is plumbed across the fuel filter.

The drain from the pressurizing and dump valve is connected to a drain can by means of a looped drain line, the top of the loop being below the lowest point of the fuel manifold but above the flowmeter to keep the latter wet. The drain can is sized to permit three aborted engine starts and subsequent draining of the fuel manifold.

A drain control valve, incorporating an eductor, is located downstream of the drain can. Its operation depends on the slow pressure decay of the fuel pump as a result of the inertia of the rotor in the engine to which the fuel pump is directly geared.

High pressure fuel, tapped from between the filter and the controller, is used to power the eductor. Fuel is removed from the drain can and returned to the main fuel pump inlet. The drain control valve is controlled by fuel pressure sensed downstream of the controller. This pressure closes both the high pressure port and the inlet port from the drain can. When the controller shuts off the fuel both ports will open to put the eductor in operation.

The drain can contains a float valve which shuts off flow to the drain control valve before the fuel in the can is exhausted. This action prevents vapor lock in the eductor and possibly air being induced into the fuel system.

PD287-5 Variable Fan Exit Nozzle

A schematic of the PD287-5 variable fan exit nozzle system is shown in Figure 3d1-4. The variable nozzle is employed to match the nozzle area with engine performance at various speeds and altitudes. In addition, the nozzle flaps are opened to approximately 0.52 rad (30 deg) in the thrust reverse mode. Thrust reversing is accomplished by changing the pitch of the fan and reversing the airflow through the fan duct. Opening the nozzle flaps to approximately 0.52 rad (30 deg) simulates a bell mouth inlet for low velocity airflow.

The flaps are operated by a single hydraulic actuator located in the pylon and working through a system of bell cranks and push-pull rods. The system is so designed as to eliminate the series stack up of tolerances normally associated with a large number of bell cranks and push-rods.

This system is capable of infinite modulation of the flaps, rapid response, and self-correction if the flaps drift out of position or are subjected to external loads trying to force them out of position.

Power and control of the system is furnished by the fan pitch control unit on the engine. A mechanical feedback of the flap actuation is supplied for the thrust control system as well as the engine.

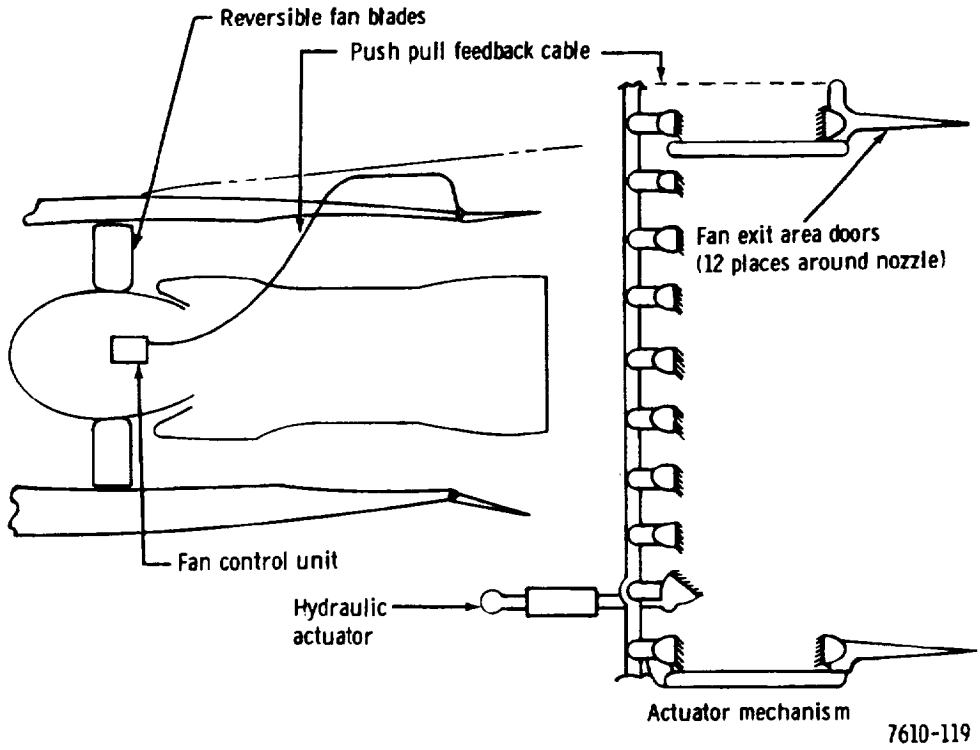

Figure 3d1-4. PD287-5 variable area nozzle system schematic.

PD287-6 Thrust Reverser System

Thrust reversing is accomplished by changing the pitch of the bypass fan to reverse the airflow in the fan duct. Reingestion of primary engine exhaust gas is blocked by closing a door at the fan nozzle. Air is supplied to the fan for thrust reverse by opening doors in the cowling just aft of the engine fan.

The door actuation system is powered by an air motor which draws the airflow from the engine pneumatic system.

Control of the door actuation system is furnished by the fan pitch control unit on the engine. Mechanical and electrical feedback is supplied to the engine control unit. The engine control unit coordinates throttle position, fan blade angle, and fan duct door openings.

PD287-11 Thrust Reverser System

Thrust reverse is accomplished by diverting fan air through cascades in the side of the fan duct. The cascades are fixed in place and covered by doors on the outside of the nacelle and

on the inside of the fan duct. Actuation of the doors is powered from the engine bleed air system by an air motor. The inside doors are driven by ball screw shafts which translate a ring on which the doors are pivoted. Each door is restrained by a link which pulls the doors into the fan duct to block the fan air. At the same time a lever system opens the outer nacelle doors.

Control of the system is accomplished by means of a mixer box and directional control valve. The mixer box is connected to the throttle, reverser control, and the boundary layer control actuator. The BLC system is shut off during thrust reverse.

PD287-51 Thrust Reverser System

A schematic of the PD287-51 thrust reverser system is shown in Figure 3d1-5. This system has two major subsystems: a thrust reverser for the fan air exhaust and a thrust spoiler for the gas turbine exhaust. A single pneumatic drive unit powers both subsystems. Control of the system is interlocked with the engine control system.

High-stage bleed air is used to power the air motor. The torque of this motor is fed through a reversing gearbox controlled by the deploy or stow signal from the flight deck. Flexible shafting is routed from the reversing gear to transfer gearboxes—one for the fan thrust reverser and one for the gas turbine thrust spoiler. From these gearboxes, flexible shafting is routed circumferentially around the nacelle to series-mounted, right-angle drives.

Ball screw linear actuators deploy or stow the reverser and spoiler simultaneously.

A mechanical feedback system controls a brake to prevent damage from overruns plus locking the system in the desired position. This feedback signal is also available for integration into the engine control system. Position indicator switches provide a signal when the system is deployed or stowed.

COMPOSITE MATERIALS

For the Phase II QCSEE effort—which will have a manufacturing span from late calendar 1973 through early 1975—use of composites must be based on current technology. The weight savings for the PD287-5 and -51 nacelles based on current composite technology is shown in Table 3d1-II. The use of composites employing current technology is of particular significance because such use does not increase costs. With additional development, greater weight savings could be obtained, but costs will probably increase. Considering existing technology, composites would be employed generally in place of the aluminum structures in current use (e.g., the inlet cowl, fan cowl, noise suppression face sheets, thrust reverser cowl, and variable exhaust nozzle component parts).

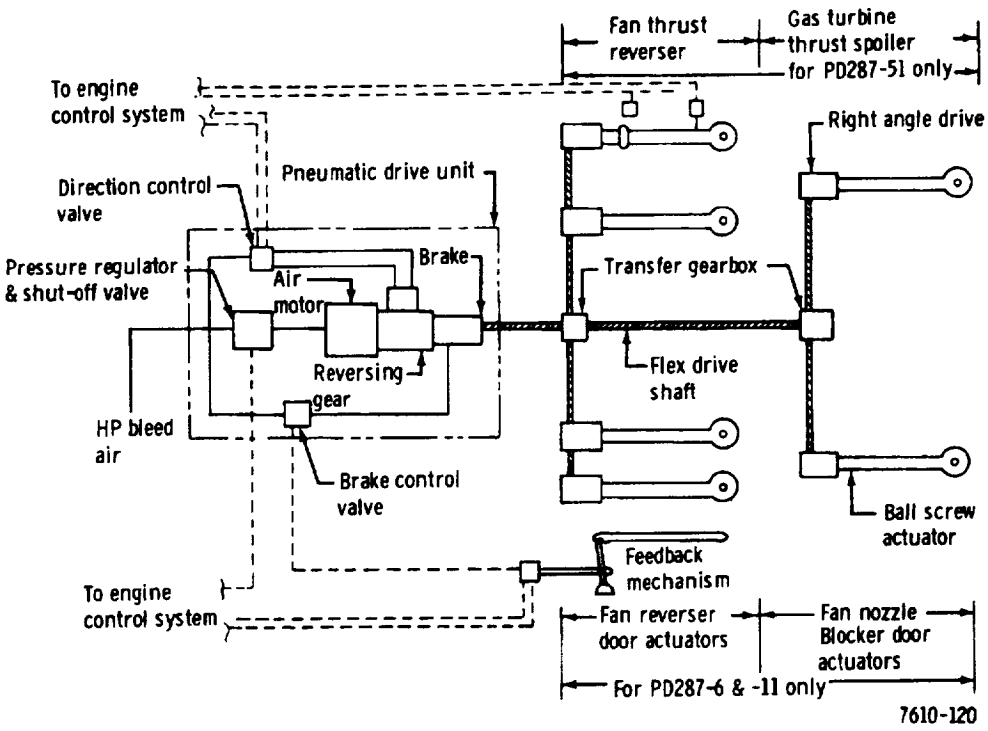

Figure 3d1-5. Reverser and spoiler system schematic.

The fan duct for the PD287-51 AW propulsion system is designed as a bonded honeycomb structure with titanium skins and aluminum core. Because of the duct shape and high internal pressures, this combination was lighter than aluminum skins. This area of the nacelle lends itself to use of composites and the weight savings are considerable—approximately 26.5%. In spite of the higher material costs, the overall costs are less with composites because of the much simpler tooling and the reduced number of detail parts.

Weight savings can be obtained by making the face sheets of the noise suppression panels from composites. Before this can be accomplished, however, considerable development work is necessary.

The greatest potential application of composites for weight saving is probably the aircraft pylon, which is outside the scope of Task II work.

Table 3d1-II
Nacelle composite weight savings.

	PD287-5	PD287-51
Structural weight		
Conventional structure, kg (lbm)	1053 (2322)	554 (1222)
Composites, kg (lbm)	943 (2080)	500 (1102)
Saving, %	10.4	9.7
Total weight		
Conventional structure, kg (lbm)	1514 (3338)	1071 (2361)
Composites, kg (lbm)	1404 (3096)	1016 (2241)
Saving, %	7.2	5.1

NACELLE AERODYNAMICS

Inlet Selection

The aerodynamic criteria for selecting the inlet geometry for the Task II engines were:

- High-static pressure recovery
- Tolerance to high-upwash angles induced by wing lift
- Compatibility with the inlet acoustic treatment
- 5% airflow growth capability
- Acceptable forebody cruise drag

Nacelle forebody dimensional criteria of 0.5 L/D and 0.8 D_{HL}/D_{max} [1]* were selected as goals for minimum cruise drag with adjustments made for acoustic treatment and low-speed internal performance.

The inlet throat was sized for a corrected mass flow/area of 205 kg/s · m^2 (42 lbm/sec-ft^2) at sea level static takeoff power to provide 5% airflow growth before deviating from a bellmouth loss curve as shown in Figure 3d1-6 and obtained from Blackaby and Watson.[2] This curve is used for growth margin sizing only.

The design point for the internal inlet lines is a maximum power wave off at a Mach number of 0.136 which results in an effective upwash angle of 0.628 rad (36 deg) as shown in Albers.[3]

*Superscript numbers refer to the references listed at the end of this subsection.

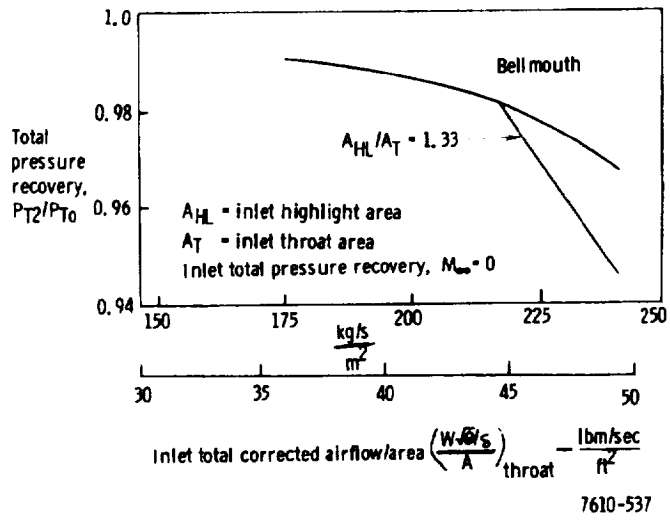

Figure 3d1-6. Bellmouth loss curve.

The basic inlet shape is a NACA-1 Series forebody with a 2:1 ellipse from highlight to throat followed by a subsonic diffuser. The internal diffusion angles and lip thicknesses are based on crosswind velocities and induced upwash angles. The bottom lip thicknesses and diffusion angles are selected, using potential flow and boundary layer analyses to avoid flow separation in the diffuser. The lower lip thickness and diffusion (together with the inlet throat size) determined the side and upper lip location and diffusion angles.

The cowl coordinates were developed by using three Rohr computer programs: Bodytest, Axinlet and Blayer. Accurate inlet coordinates calculated by Bodytest are input to program Axinlet. Program Axinlet is an incompressible potential flow solution that combines unblocked, blocked, and crossflow solutions to determine inlet surface pressures and velocities at various free stream Mach numbers, mass flow ratios, and angles of attack.

The velocity ratios from Axinlet are input to program Blayer. Program Blayer calculates the boundary layer parameters which include the laminar flow portion, transition, turbulent flow portion, and separation point. Separation is predicted in the turbulent boundary layer where the incompressible form factor—displacement thickness/momentum thickness ($H_i = \delta^*/\theta$)—reaches 2.8.

The first inlet analyzed had a lip thickness ratio of 0.13 with a NACA-1 Series contour from D_{HL} to D_{max} and a 2:1 ellipse from D_{HL} to D_T. The equivalent conical diffuser half angle was 0.0916 rad (5.25 deg). The cowl was run in program Axinlet at angles of attack from 0 to 0.8725 rad (0 to 50 deg) in 0.1745 rad (10 deg) increments. Boundary layer analysis indicated separation occurring at less than 0.5235 rad (30 deg). To avoid separation, the lower lip thickness was increased to a ratio of 0.20 and the internal diffusion angle was reduced to 0.0436 rad (2.5 deg). Figures 3d1-7 and 3d1-8 show the resulting surface velocity profiles,

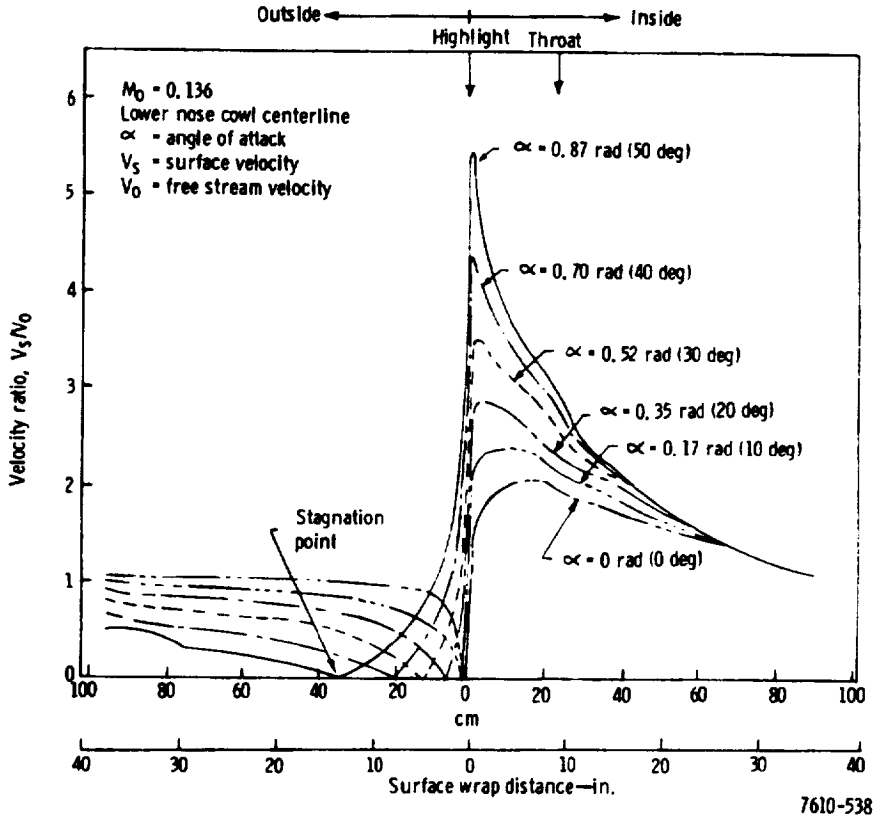

Figure 3d1-7. Inlet surface velocity characteristics.

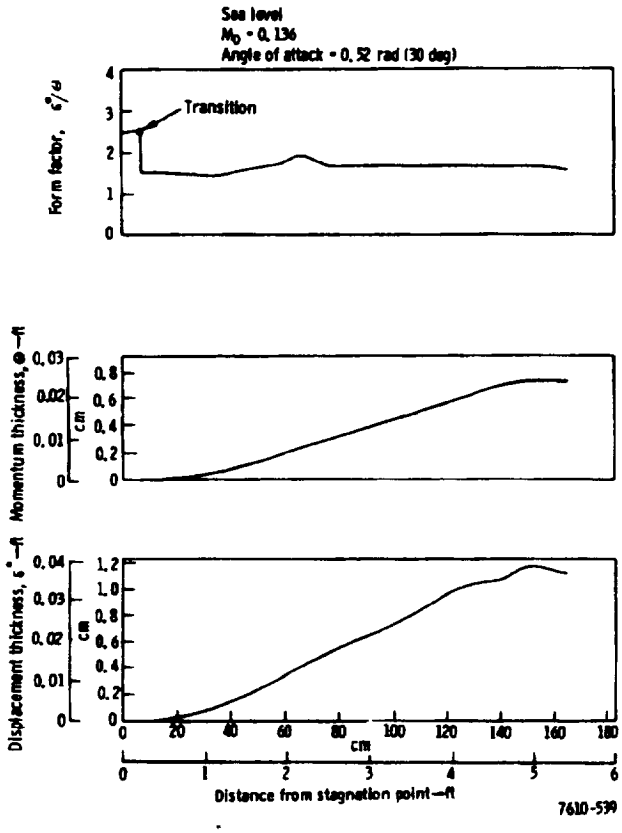

Figure 3d1-8. Inlet boundary layer thickness.

boundary layer form factor, and momentum and displacement thicknesses for 0.5235 rad (30 deg) case at a Mach number of 0.136. This final configuration—indicating no separation at an upwash angle of 0.5235 rad (30 deg) with possible separation at 0.698 rad (40 deg)—was selected as meeting the stated criteria of 0.628 rad (36 deg). To minimize the overall contraction ratio—A_{HL}/A_T—and subsequent cruise drag, the lip thickness was reduced to a ratio of 0.13 on the side to 0.11 on the top, resulting in an A_{HL}/A_T of 1.366 overall contraction ratio. The detailed comparisons of the inlet forebody design parameters for the PD287-5, -6, -11, and -51 are shown in Table 3d1-III.

Table 3d1-III.
Inlet/forebody design parameters.

Parameters	PD287-5	PD287-6	PD287-11	PD287-51
Inlet throat corrected airflow/area, $kg/s \cdot m^2$ ($lb/sec\text{-}ft^2$)	205 (42)	205 (42)	205 (42)	205 (42)
Throat Mach number	0.61	0.61	0.61	0.61
Inlet lip thickness ratio (y/R_{HL})				
Top	0.11	0.11	0.11	0.11
Side	0.13	0.13	0.13	0.13
Bottom	0.20	0.20	0.20	0.20
Overall contraction ratio (A_{HL}/A_T)	1.366	1.366	1.366	1.366
Forebody dia ratio (D_{HL}/D_{max})	0.84	0.77	0.79	0.77
Forebody length/dia ratio (L/D_{max})	0.67	0.67	0.67	0.62
Forebody contour	NACA-1-84-67	NACA-1-77-67	NACA-1-79-67	NACA-1-77-62

A_{HL} - Highlight area, m^2 (ft^2)
A_T - Throat area, m^2 (ft^2)
D_{HL} - Highlight dia, m (ft)
D_{max} - Nacelle maximum dia, m (ft)
D_T - Throat diameter, m (ft)
L - Inlet length—highlight to engine face, m (ft)
R_{HL} - Highlight radius, m (ft)
y - Lip thickness—($R_{HL} - R_T$), m (ft)

Nacelle external lines were based on fairing the external line required to enclose the fan case and engine accessories, fan exit diameter, sound suppression treatment of the fan exit duct fan nozzle area, and a maximum external boattail angle of approximately 0.157 rad (9 deg).

Core cowl lines were based on fan nozzle area, core engine length, core engine sound suppression treatment, primary nozzle area, and a maximum boattail angle of 0.2617 rad (15 deg).

Internal Performance Loss Analysis

The objective of the internal performance loss analysis was to estimate the pressure losses associated with the inlet, fan, and primary ducts designed for each engine concept and to predict the increase in internal pressure loss caused by noise-reduction design features.

Method of Analysis

Calculation of internal pressure losses was accomplished with the aid of an IBM 360 computer program recently developed at Rohr. In this program, each duct under investigation (e.g., inlet or fan duct) is divided into a number of segments and losses are calculated for each segment using well-known fluid flow relationships. Individual segment losses are summed to arrive at the total pressure loss for each duct. Types of losses considered include friction drag, ring, splitter and strut profile drag, inlet lip losses, duct expansion and contraction losses, and losses caused by duct turning and branching. The methods used in calculating these losses follow.

Skin Friction Losses

Skin friction losses are evaluated, using the standard equation for friction drag of a flat plate, $D_{frict} = C_{fq} S_{wet}$.[4] The drag correction to account for the three-dimensional effects of the duct (i.e., increase of friction losses caused by surface curvature) is of negligible magnitude for full-scale aircraft ducting and consequently was not used in this program. The friction coefficient, C_f, is calculated for smooth, untreated surfaces by the Prandtl-Schlichting skin friction formula, $C_f = \frac{0.455}{(\log R_L)\, 2.58}$,[5] and for Rohr's perforated plate acoustical material by a method recommended by Hoerner.[4] This method results in the equation $C_f{}^1 = X_1 C_f + X_2\ C_D$ where X_1 is the percentage of plate area which is smooth and X_2 is the percentage of open area caused by perforations. C_f is as defined earlier for smooth surfaces and C_D is the drag coefficient of the hole. Average values of C_D can be obtained from Hoerner[4] for various hole geometries. Empirical skin friction coefficient data are available for other types of acoustic material and may be inserted into the program in tabular form.

Skin friction coefficients calculated for smooth, untreated surfaces are corrected by a roughness factor, E, to be representative of the surface finish found in most aircraft ducting. A correction for compressibility effects is made, using the equation, $C_{f_{comp}} = C_{f_{inc}} \left\{1 - 0.12\ M^2\right\}$.

Duct segments are chosen small enough that cross-sectional area changes within the segment are minimized. In a constant area duct, the drag force per unit surface area/per unit length is balanced and is equal to pressure loss per unit cross-sectional area/per unit length. Thus the pressure loss for each segment is calculated by dividing segment friction drag by segment cross-sectional area.

Ring, Splitter, and Strut Profile Drag

The calculation of profile or total drag for rings or splitters inserted into the inlet, fan, or primary ducts is based on a method by Hoerner.[4] In this method, the profile drag of an airfoil is related to its friction drag by the equation $C_p = C_f \left[1 + 2\frac{(t)}{s} + 60\frac{t}{(s)}4\right]$ where t is ring or splitter thickness and s is ring length. The friction coefficient, C_f[1], is obtained by calculating a basic friction coefficient as before and modifying this coefficient by an empirical factor relating theoretical, acoustically-treated flat-plate friction coefficients to those determined for representative rings and splitters during full-scale engine nacelle tests. The pressure loss is then calculated, using the relation $P = \frac{C_p q S_{wet}}{A_{cs}}$. S_{wet} is the wetted surface area of the ring, A_{cs} is the cross-sectional flow area at that particular segment and q is the dynamic pressure at that segment.

Inlet Lip Losses

Pressure losses occur at the inlet lip as a result of high local velocities and separation as the outer layer of the entering air flows over the lip profile. These losses are a direct function of the amount of turning the air must accomplish as it enters the inlet. During moderate to high speed flight, the air streamtube entering the inlet is limited to a column of air directly in front of the inlet. The entering air streamlines have to bend only slightly, consequently lip losses are negligibly small. During static operation, air is drawn into the inlet from the sides as well as the front. The layer of entering air next to the inlet lip surface must turn through a much larger angle over a short distance for the typical flight-type inlet and separation occurs. Thus, lip losses are a maximum during static operation and decrease as flight speeds increase. Experience with subsonic inlets have shown that, typically, lip losses decrease to an insignificant level at velocities around 41 m/s (80 kt).[2] The pressure loss caused by the inlet lip during static operation was estimated, using the relation $\Delta P_{lip} = 0.02q$[6] where q is the dynamic pressure at the inlet throat.

Duct Expansion and Contraction Losses

Losses caused by changes in duct flow area were computed, using standard incompressible flow equations and empirical curves.[7] The pressure losses resulting from sudden contraction or expansion or gradual contraction of the duct flow area were calculated using the expression $\Delta P = K_T q$ where q is the velocity head (dynamic pressure) in the smaller area section. K_T is a loss coefficient described by a set of separate empirical values which depend on whether

sudden contraction, sudden expansion, or gradual contraction is being considered. For gradual duct area expansion—such as in an inlet diffuser—the pressure loss is calculated by the expression $\Delta P = CK_T q$ where K_T is the coefficient of sudden expansion, q is the dynamic pressure in the smaller area section, and C is an empirical diffuser expansion factor. This diffuser expansion factor is used to correct the loss coefficient (K_T) given for sudden expansion to obtain values appropriate for gradual expansion.

Bend and Branch Duct Losses

Bend losses, the losses incurred as a result of duct turning, were calculated using the relationship $\Delta P = C'K_{T_{90}} q$. In this equation, q is the dynamic pressure in the duct upstream of of the bend, $K_{T_{90}}$ is the empirical loss coefficient for a 1.57 rad (90 deg) bend and C' is a factor used to correct the loss coefficient ($K_{T_{90}}$) for bends other than 1.57 rad (90 deg). Values of C' and $K_{T_{90}}$ were obtained.[7]

The pressure loss caused by mixing in converging branches may be estimated from curves.[7] The dynamic pressure, q, is upstream of the converging or diverging branch.

Results and Discussion

The internal pressure losses have been calculated for the inlet, fan, and primary ducts of the PD287-5, -6, -11, and -51 engine nacelles. Acoustic treatment was not employed on the PD287-51 nacelle, the -5 nacelle has treatment added in each duct, and the -6 and -11 have treatment in the inlet and fan ducts only.

Inlet, fan collector, and primary duct pressure losses for the PD287-51 nacelle are presented in Figures 3d1-9, 3d1-10, and 3d1-11 as a function of corrected mass flow. Inlet pressure losses are shown with and without inlet lip loss. The curve with lip loss represents static engine operation while the curve without lip loss represents flight operation at speeds equal to or exceeding 41 m/s (80 kt). Pressure losses for operation at speeds between 0-41 m/s (0-80 kt) can be estimated by a linear interpolation between these two curves. An examination of Figures 3d1-9 and 3d1-11 show inlet and primary duct pressure losses consistent with that expected for typical inlet and primary duct design. Fan collector duct pressure losses (Figure 3d1-10) are significant. They are a direct result of the complex collector duct geometry required to make the transition from a bifurcated duct at the fan case to a single duct above the engine.

Pressure losses are shown in Figures 3d1-12, 3d1-13, and 3d1-14 for the PD287-5 engine nacelle with no inlet, fan, or primary duct acoustic treatment. These pressure losses are consistent in magnitude with that expected for typical well-designed inlet, fan, and primary ducts. Pressure losses for the -5 nacelle with acoustic treatment are shown in Figures 3d1-15, 3d1-16, and 3d1-17. A brief analysis of calculated inlet acoustic treatment losses was made to check their validity. This analysis showed close agreement between these calculated losses

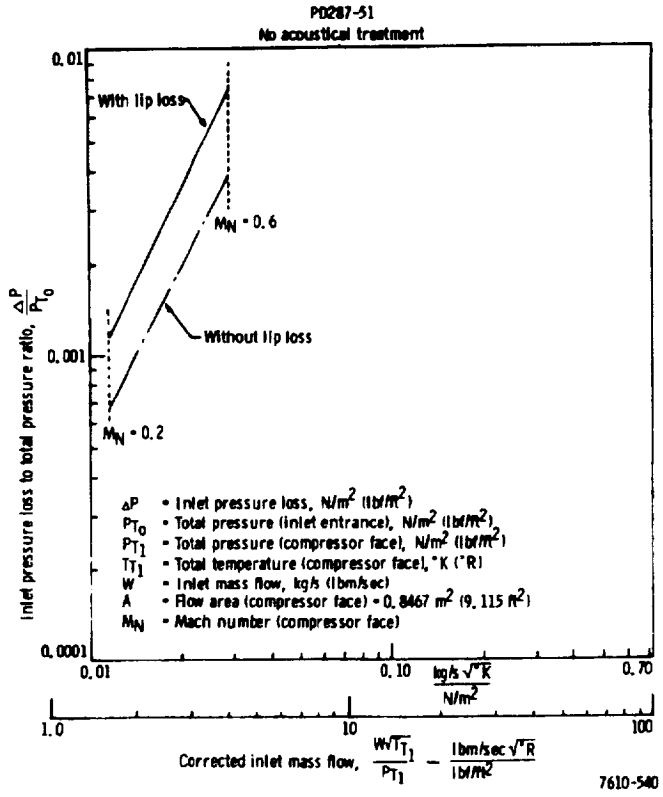

Figure 3d1-9. PD287-51 inlet internal performance.

and full-scale inlet test results when adjustments were made for differences in Mach number, dynamic pressure, ring surface area, and inlet cross-sectional area.

Internal pressure losses are shown in Figures 3d1-18, 3d1-19, and 3d1-20 for the PD287-6 nacelle without acoustic treatment and in Figures 3d1-21, 3d1-22, and 3d1-23 for the -6 inlet, fan, and primary ducts with acoustic treatment. Pressure losses for the PD287-11 nacelle with and without acoustic treatment are shown in Figures 3d1-24 through 3d1-29. The following observations can be made in comparing losses associated with the various configurations.

- Fan duct losses for the PD287-6 and -11 engines are higher than those for the -5. This is a result of the increased fan duct length, and the greatly increased complexity of duct geometry (addition of duct branching, bifurcation, and bends) necessitated by the OTW placement of the -6 and -11 nacelles.
- Primary duct losses for the PD287-6 and -11 engines are higher than those for the -5 engine because of increased length and addition of bends to facilitate OTW placement.
- Treated inlet losses are smaller for the PD287-5 engine than for the -6 and -11 engines. This is primarily a result of one ring being used in the -5 inlet acoustic treatment while two rings are used in the -6 and -11 inlets.

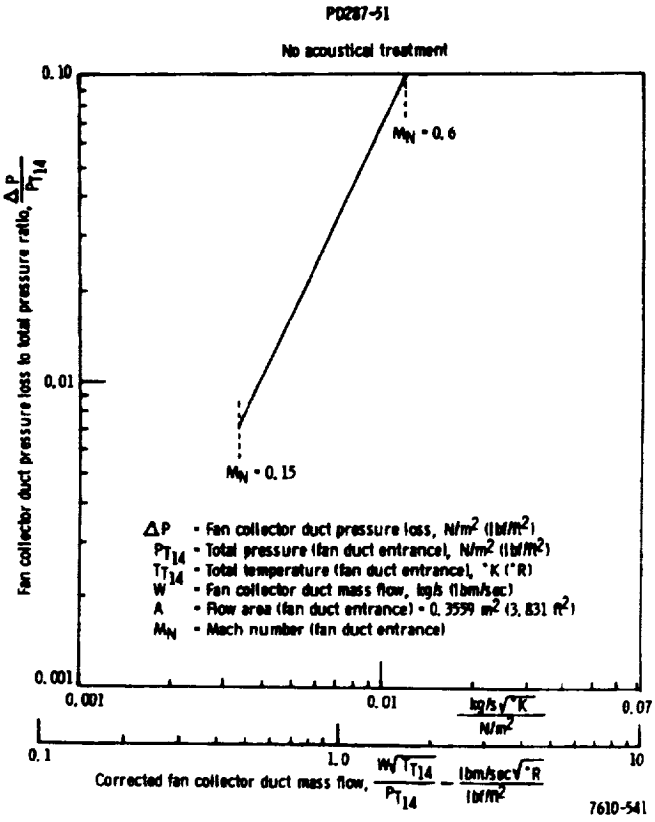

Figure 3d1-10. PD287-51 fan collector duct internal performance.

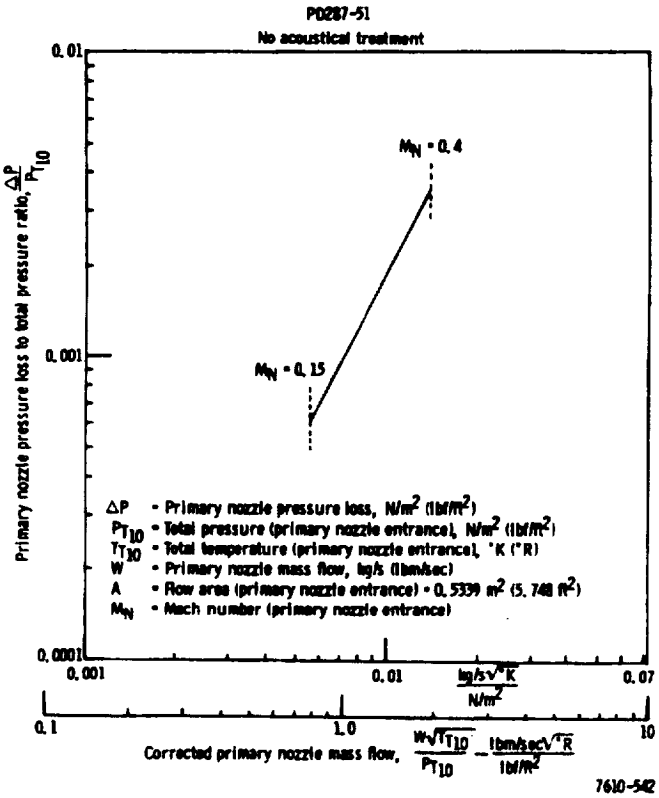

Figure 3d1-11. PD287-51 primary nozzle internal performance.

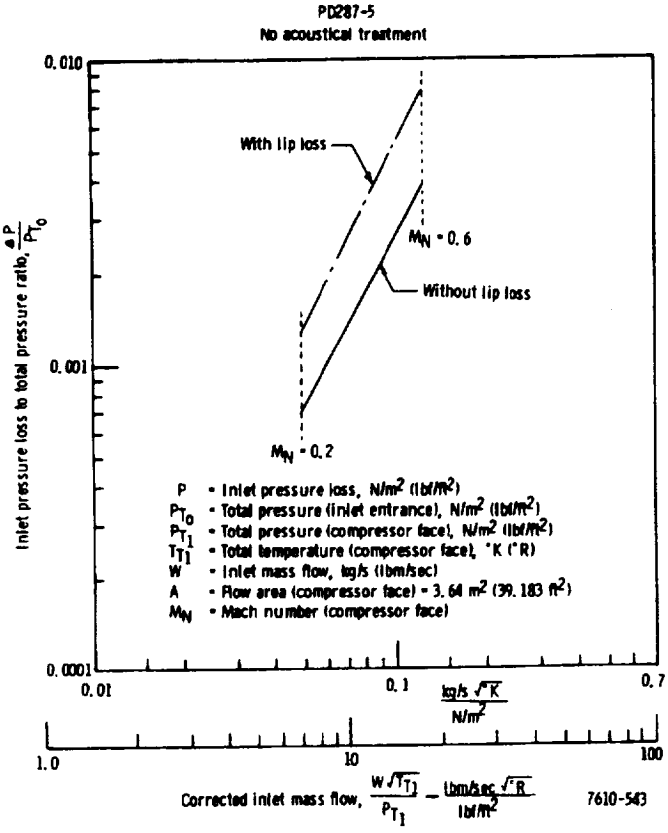

Figure 3d1-12. PD287-5 inlet internal performance.

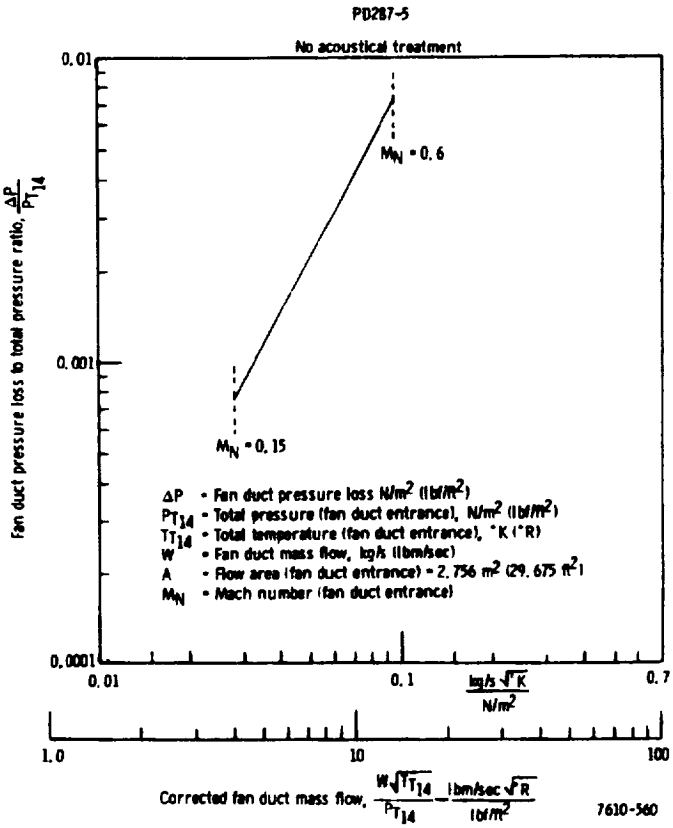

Figure 3d1-13. PD287-5 fan duct internal performance.

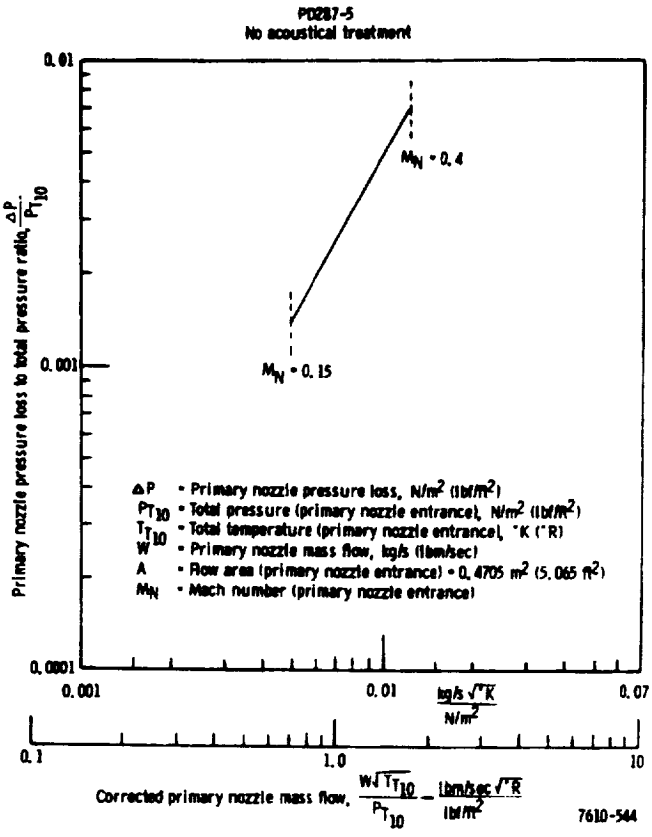

Figure 3d1-14. PD287-5 primary nozzle internal performance.

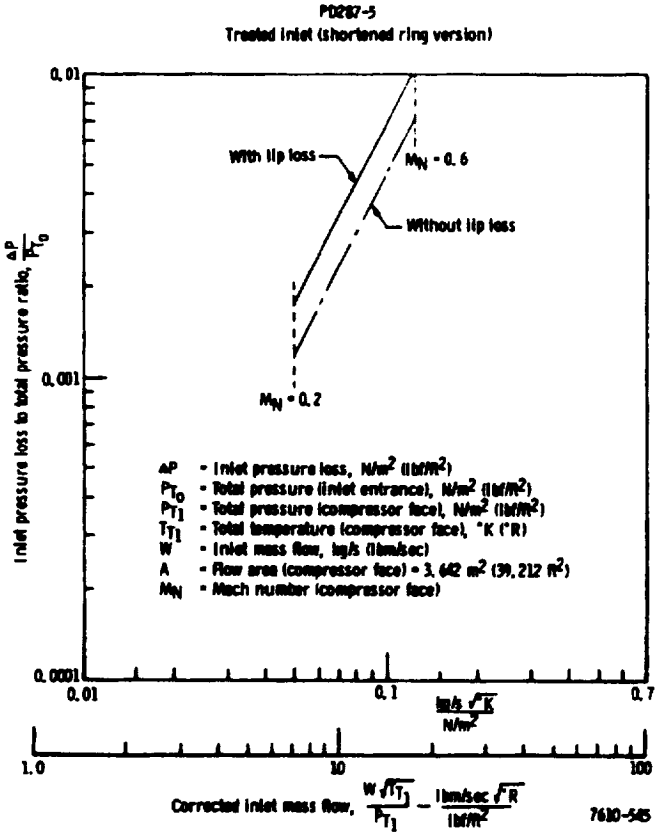

Figure 3d1-15. PD287-5 inlet internal performance.

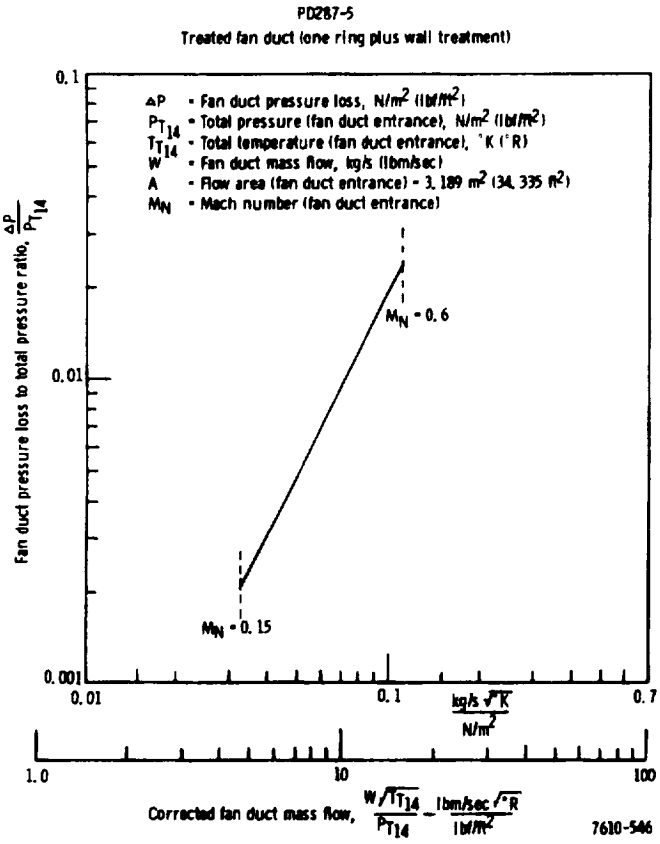

Figure 3d1-16. PD287-5 fan duct internal performance.

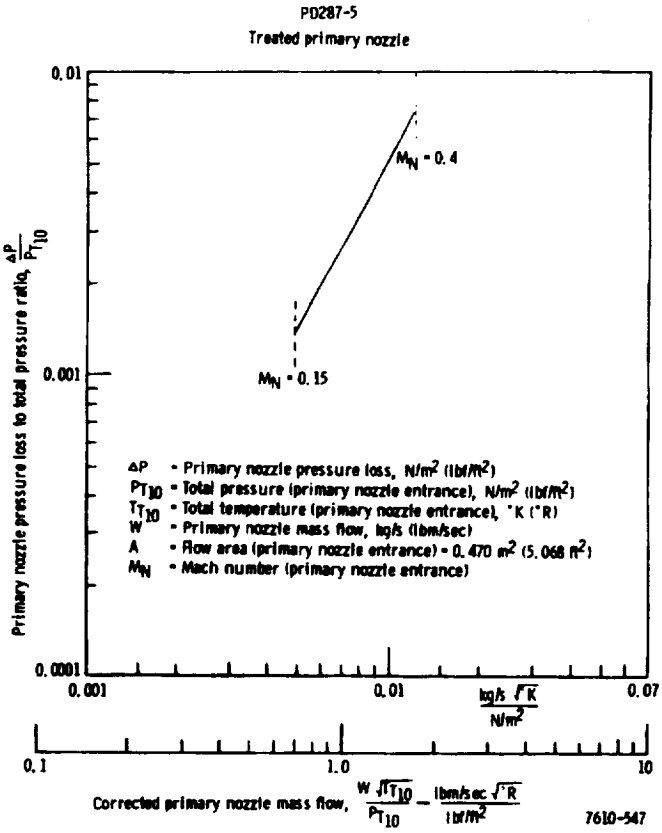

Figure 3d1-17. PD287-5 primary nozzle internal performance.

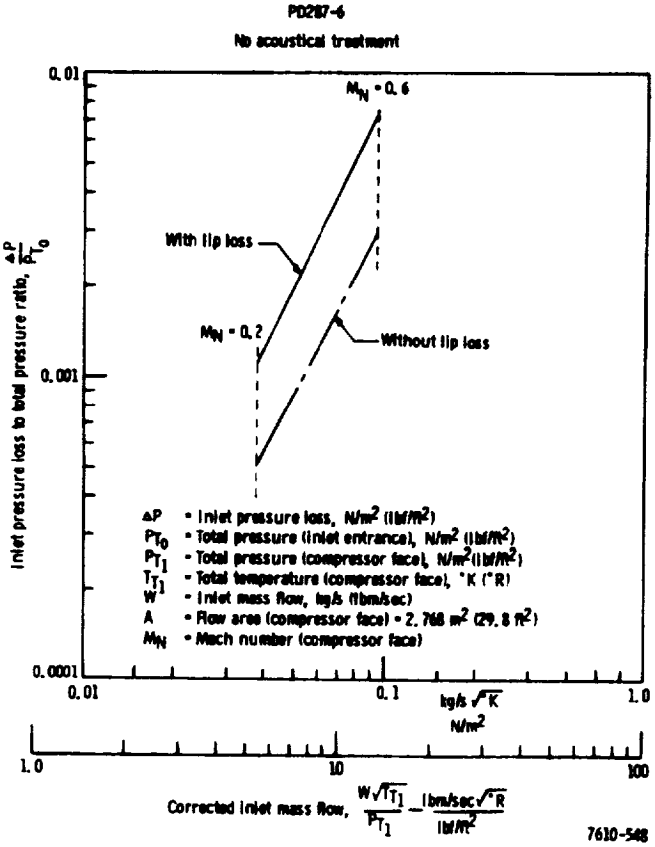

Figure 3d1-18. PD287-6 inlet internal performance.

Figure 3d1-19. PD287-6 fan duct internal performance.

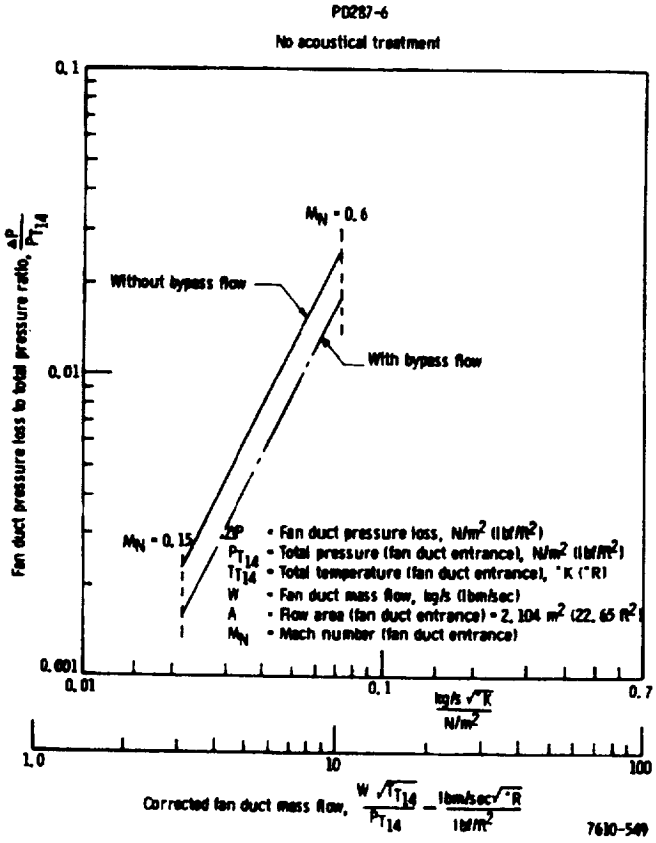

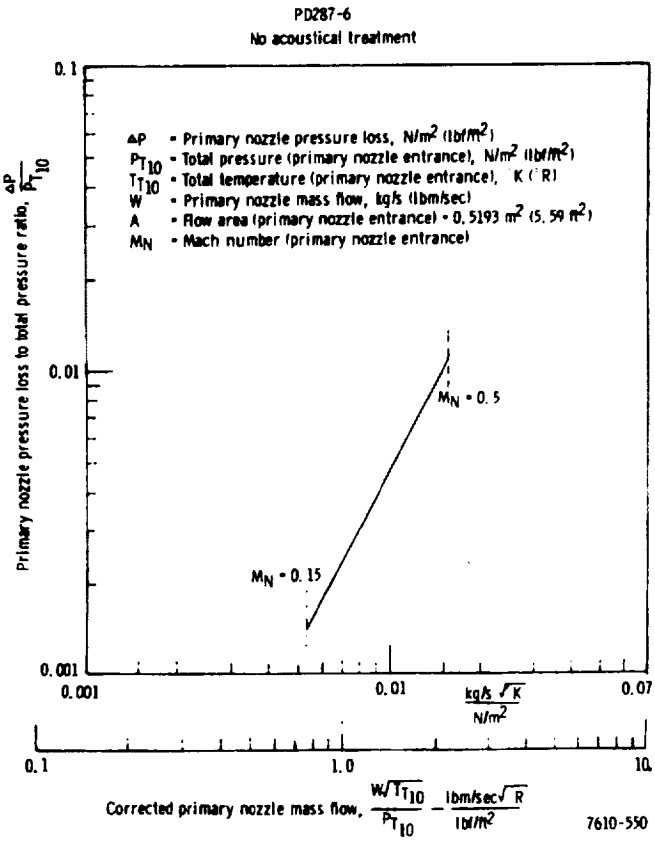

Figure 3d1-20. PD287-6 primary nozzle internal performance.

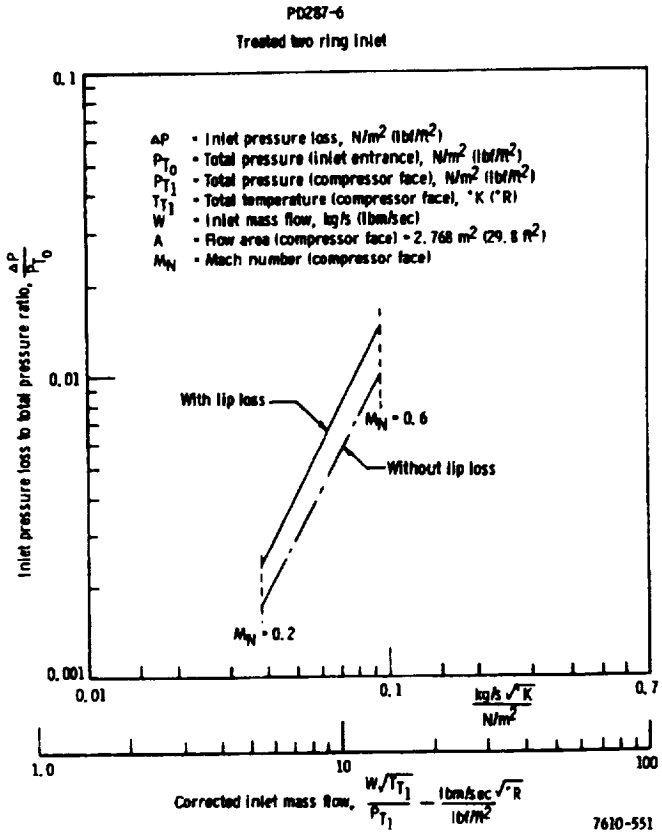

Figure 3d1-21. PD287-6 inlet internal performance.

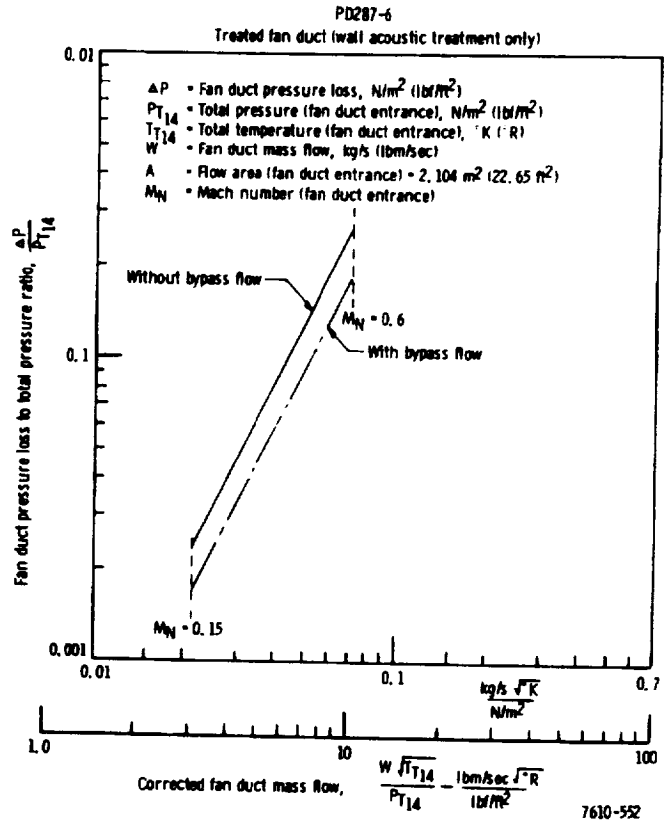

Figure 3d1-22. PD287-6 fan duct internal performance.

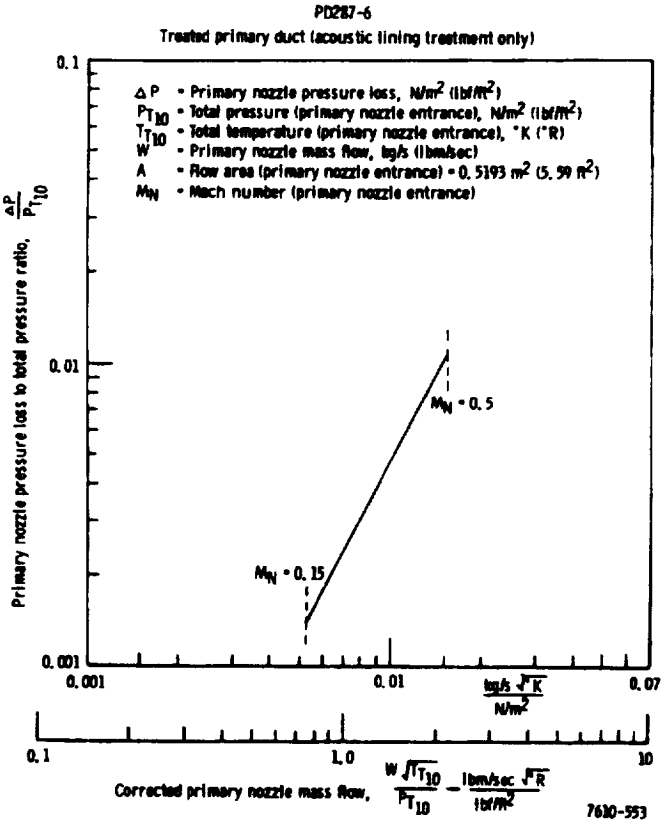

Figure 3d1-23. PD287-6 primary nozzle internal performance.

Figure 3d1-24. PD287-11 inlet internal performance.

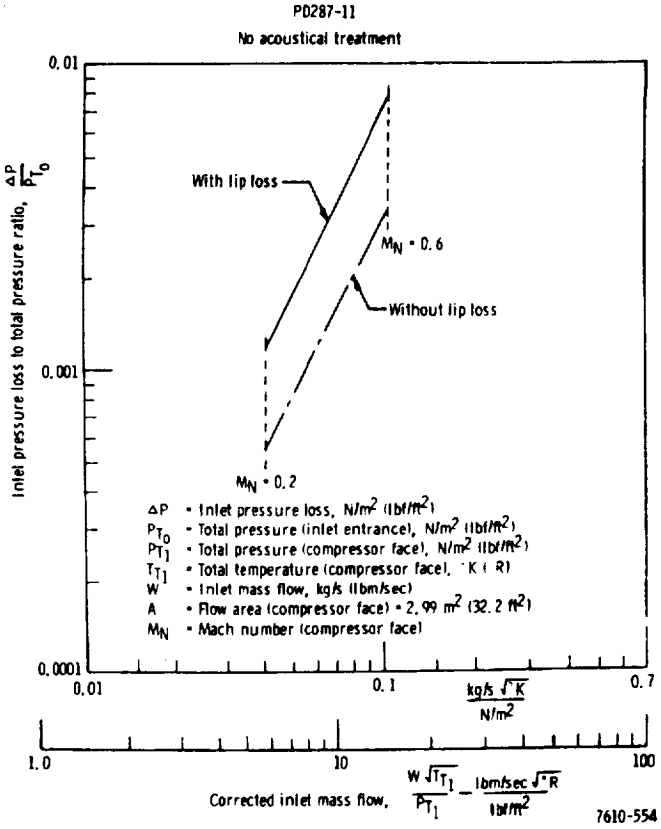

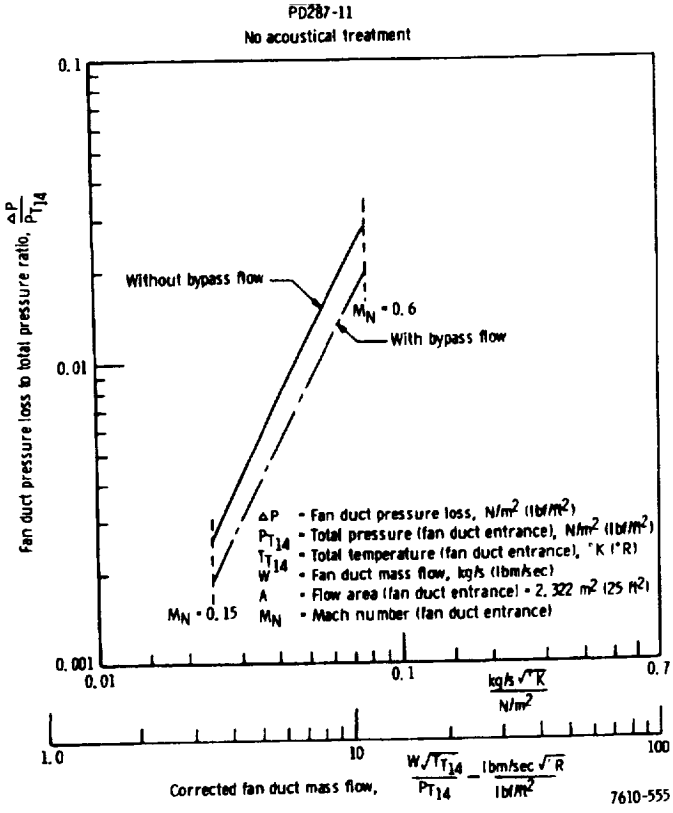

Figure 3d1-25. PD287-11 fan duct internal performance.

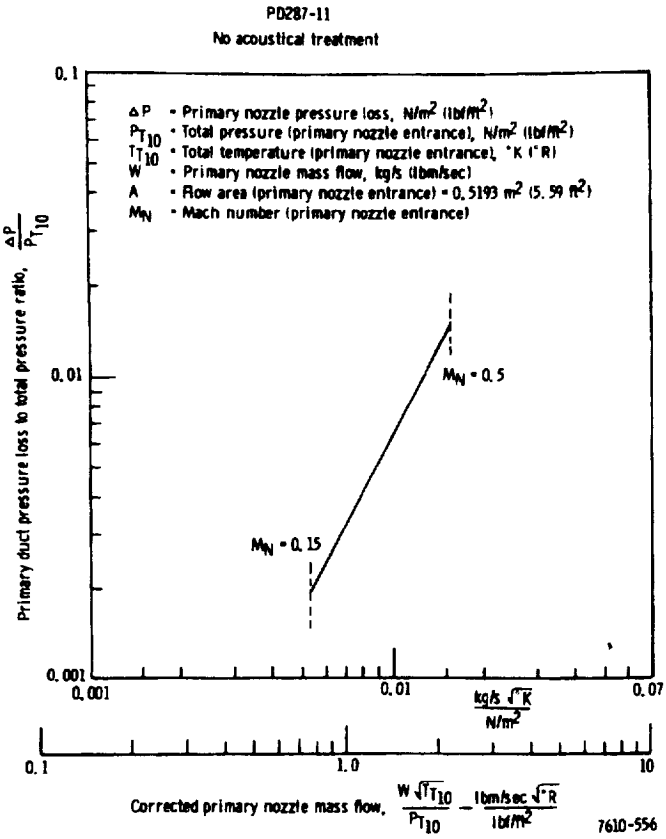

Figure 3d1-26. PD287-11 primary nozzle internal performance.

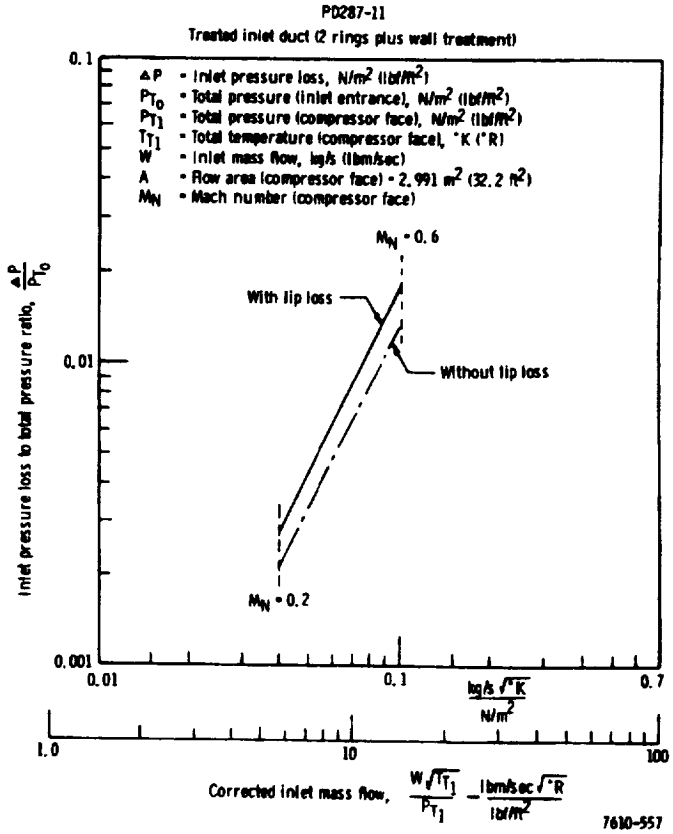

Figure 3d1-27. PD287-11 inlet internal performance.

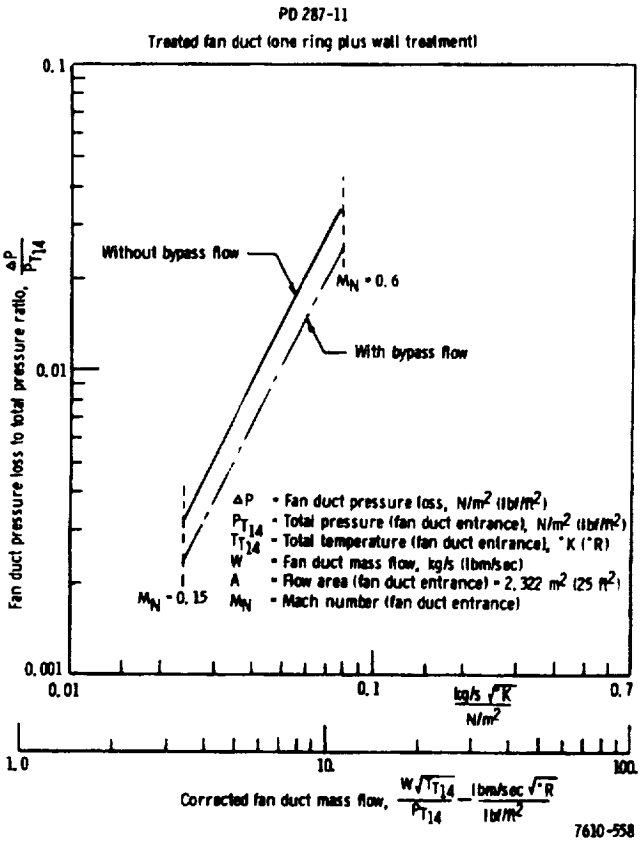

Figure 3d1-28. PD287-11 fan duct internal performance.

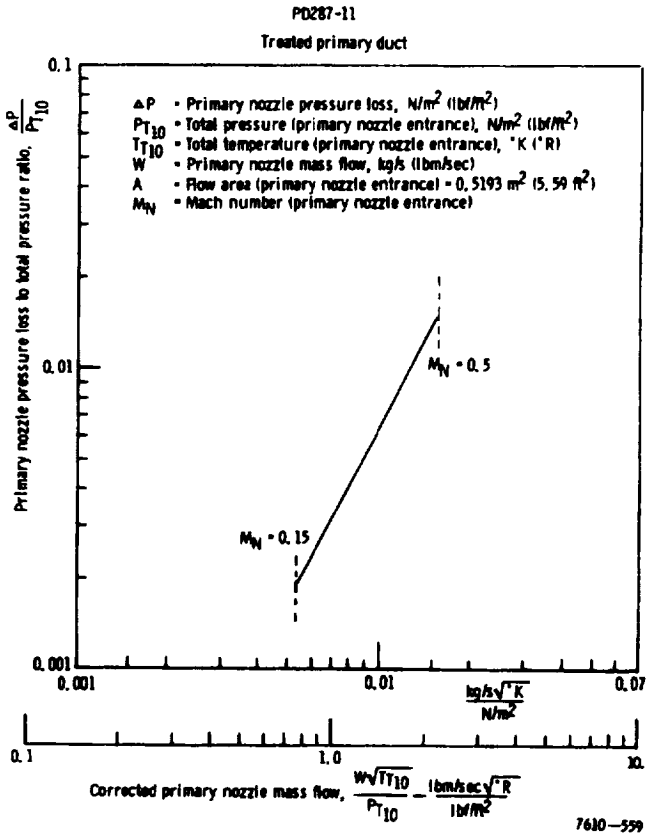

Figure 3d1-29. PD287-11 primary nozzle internal performance.

- The difference in pressure loss is very small between treated and untreated ducts when acoustic treatment is limited to an acoustical lining (perforated plate over honeycomb sandwich). This agrees very well with results observed during full-scale testing at the Rohr Brown Field test facility.
- PD287-6 fan duct pressure losses are lower than those of the -11 fan duct. The -11 fan duct design has bends which turn the flow through a larger angle than that required by the -6 duct. In addition, the treated version of the -11 fan duct has a short acoustical ring while the -6 duct has wall treatment only.
- The PD287-6 primary duct losses are lower than those of the -11 primary because of the sharper-angled bends used in the -11 primary duct design.

Exhaust Nozzles

Nozzle performance of the four selected Task II engines is described by thrust and discharge coefficients which are defined as:

$$\text{Thrust coefficient} = \frac{\text{measured thrust}}{\text{ideal thrust based on measured mass flow}}$$

$$= \frac{F\ (\text{measured})}{W\ (\text{measured}) \times V\ (\text{ideal})/g}$$

$$\text{Discharge coefficient} = \frac{\text{measured mass flow}}{\text{ideal mass flow}}$$

$$= \frac{W\ (\text{measured})}{\rho \times A \times V\ (\text{ideal})}$$

These thrust and discharge coefficients are based on experimental data whenever possible and reflect internal configuration, external configuration, primary and secondary jet interaction, and external flow effects. Researching the available published data resulted in the exploration of publications which cover conical and plug nozzle performance[1,2,3,4] with and without external flow [8,9] and two representative high bypass propulsion systems.[10,11]

The first configuration is for the variable pitch engine installed in a UTW location (PD287-5 and -7) with a variable annular fan nozzle and fixed convergent primary nozzle. The fan nozzle thrust and discharge coefficients shown in Figures 3d1-30 and 3d1-31 are from Poland and Schwanebeck[10] with substantiation of external flow field effects from Yarker and Stanhope.[11] The same thrust and discharge coefficients were used for the variable fan nozzle in the open and closed position as a result of the very small change in nozzle convergence angle.

The variable pitch engines (PD287-5 and -7) primary nozzle thrust and discharge coefficients are shown in Figures 3d1-32 and 3d1-33 and are obtained from Kutney[9] and Poland and Schwanebeck,[10] respectively. Thrust coefficients are from Kutney.[9]

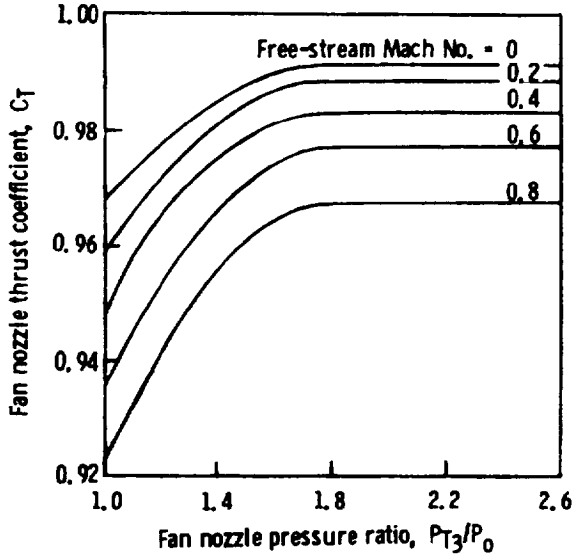

Figure 3d1-30. Fan nozzle thrust coefficient.

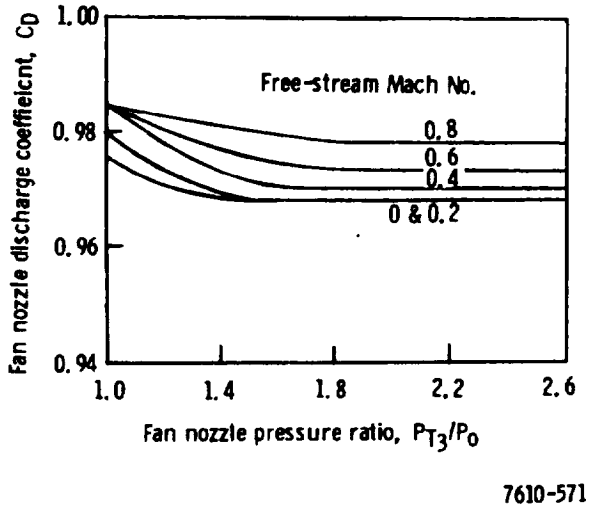

Figure 3d1-31. Fan nozzle discharge coefficient.

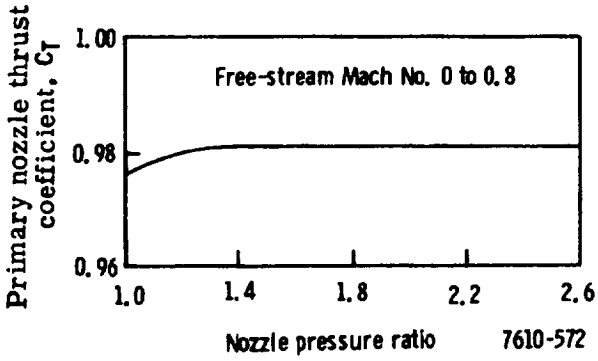

Figure 3d1-32. Primary nozzle thrust coefficient.

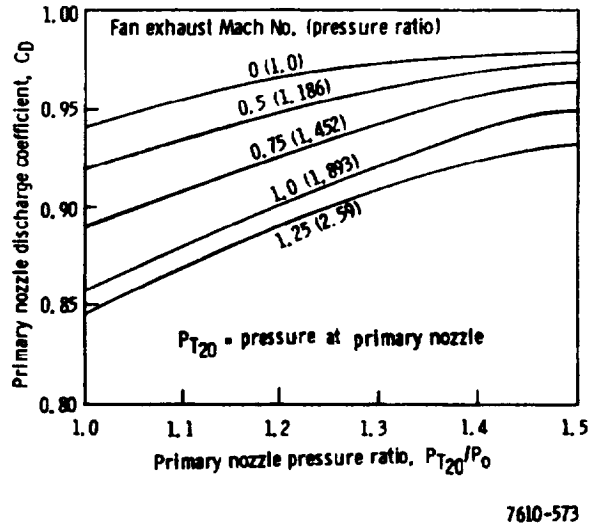

Figure 3d1-33. Primary nozzle discharge coefficient.

The second configuration is for the PD287-51 AW engine. The primary and fan nozzle discharge coefficients are presented in Figures 3d1-34 and 3d1-35 and were developed from Gray and Wilsted[8] and Kutney[9] with the static discharge coefficient from Gray and Wilsted and the external flow effects from Kutney.

The third configuration is for the PD287-6 Q-Fan installed in the OTW location. Preliminary analysis of the fan and primary nozzle configurations were made, based on the aerodynamic requirement of a 4:1 fan nozzle aspect ratio located forward of the flap hinge point. Thrust coefficients were estimated by analyzing the boundary layer in fan nozzles and primary nozzles which are circular, rectangular, separate, and combined rectangular. From this comparison, the separate nozzles with a circular primary and a rectangular fan nozzle appeared to give the minimum decrease in area coefficient with the additional benefit of less wetted area in the primary and fan duct and subsequent lower friction losses. The performance of the primary nozzle is shown in Figures 3d1-32 and 3d1-34 using Gray and Wilsted[8] and Kutney.[9] Figures 3d1-32 and 3d1-35 present the fan nozzle thrust and discharge coefficient which were developed from Gray and Wilsted and Kutney with an adjustment in the discharge coefficient from circular to rectangular.

The fourth nozzle configuration is for the PD287-11 engine and follows the ground rules established on the PD287-6 and uses the same nozzle performance curves given in Figures 3d1-32 and 3d1-34 for the primary and Figures 3d1-32 and 3d1-35 for the fan nozzle. The small difference in nozzle length and area between the PD287-6 and -11 installations resulted in negligible changes in area coefficient and justify the use of the same nozzle performance curves for both configurations.

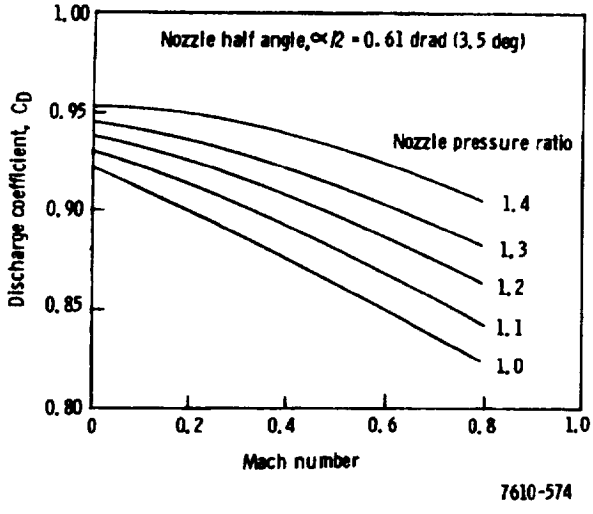

Figure 3d1-34. Primary nozzle discharge coefficient.

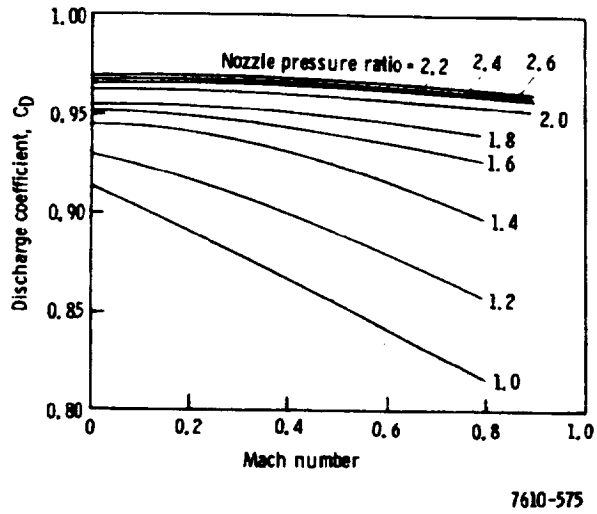

Figure 3d1-35. Fan nozzle discharge coefficient.

Thrust Reversers

Thrust reverser requirements for the Task II engines were defined by Denington[12] as 35% of the sea level static takeoff thrust during ground roll. The two variable pitch engines, PD287-5 and -6, meet these requirements with a reversible pitch fan while the fixed pitch engines require thrust reversers. The NASA ground rules further limit the thrust reverser plume to the side and top of the nacelle, excluding the lower quadrant and minimizing ground impingement which creates foreign object damage and reduced visibility on wet runways.

PD287-51 Thrust Reverser

The reversal of the bypass air on PD287-51 is accomplished in the collector duct in the nacelle, and the primary spoiler or reverser is mounted on the primary tailpipe. The bypass air is blocked by a valve in the pylon ducting. This geometry is unique but can be demonstrated as required. See Figure 3b-11 for reverser details.

The selected system is a primary target spoiler and a 42% effective bypass cascade reverser covering 2.97 rad (170 deg) of the total periphery—1.48 rad (85 deg) per side with capability for ±0.26 rad (±15 deg) vectoring in the radial direction. The internal surface of the cascade blades are recessed in the duct wall and left exposed to the bypass flow. This results in a 0.27% increase in total pressure loss or 0.10% decrease in bypass net thrust at cruise when the reverser is stowed. This result is considered a reasonable trade for the reduced weight, cost, and complexity of internal doors covering the cascade opening.

Development of the thrust reversal system to achieve an overall installed thrust reverser effectiveness of 35% requires a 42% installed effectiveness of the bypass flow and a 100% spoiled primary. The bypass cascade is sized (based on two-dimensional cascade test data from Wickline[13]) with allowances for flow vectoring, leakage, installation losses, and structural supports. The final cascade includes a 10% overall area factor of conservatism to ensure acceptable engine/thrust reverser matching and proper plume shaping. The cascade area of 0.52 m^2 (800 $in.^2$) is evenly distributed on each side of the nacelle in 1.48-rad (85 deg) segments to satisfy the NASA ground rules which restricts the lower 1.57 rad (90 deg) because of ground impingement, foreign object damage, and reduced visibility on wet runways. The blade design for this unit is of constant thickness with circular arcs and a blade exit angle of 0.54 rad (31 deg). The inflow angle will be varied to provide minimum losses and the exit will be vectored to shape the plume and prevent reingestion at low cutoff speeds.

PD287-11 Thrust Reverser

The thrust reverser requirements for the PD287-11 to give a 35% total effectiveness were determined analytically. The thrust ratio of 13.3 (fan thrust/primary thrust) results in an unspoiled primary stream and a 45% effective fan thrust reverser. Evaluating the configuration and considering the unique features of the OTW installation, a cascade fan thrust reverser

was located in the constant area duct section over a total perimeter of 3.14 rad (180 deg). Development of the required cascade area from two-dimensional test data and including the blockage caused by cascade blades, resulted in a total cascade face area of 2.97 m^2 (4600 $in.^2$). These data (obtained from Wickline[13]) are based on the measured test data shown in Figure 3d1-36. Thrust reverser effectiveness was arrived at from the measured cascade efficiency data shown in Figure 3d1-37. These data show that cascade efficiency can achieve levels of 90% or above to permit the prediction of cascade thrust reverser performance. Cascade efficiency is defined as:

$$N_C = \frac{\text{(reverse thrust/forward thrust)}}{\text{Cos } \beta_2}$$

where β_2 = cascade blade exit angle

The fan flow is blocked and directed into the cascades with internal doors and the reverser efflux gets further direction from the longitudinal vanes to direct the plume and minimize reingestion.

Thrust Reverser Reingestion Analysis

The incipient reingestion of cascade reverser flow into the inlet is analyzed for plane inviscid flows by transforming a simplified geometry into the real axis of an auxiliary plane (t-plane) as shown in Figure 3d1-38. The whole flow field of the physical plane now corresponds to the upper half of the t-plane. In this t-plane, the inlet is represented by a sink at M and the flow through the cascade is represented by uniform source distributions along the cascade openings. The strength of the sources in the individual openings is adjusted so that the flow is smooth at tips of the vanes C_1, C_2, etc. The total mass flow through the cascade is equated to the reverser mass flow while the inlet mass flow determines the strength of the sink at M. By an appropriate choice of the t-plane coordinates for the points corresponding to such points in the physical plane as the cowl nose (N), the upstream edge of the reverser port (D), etc, the correct correspondence between the physical and t-planes is established for given geometrical parameters in the physical plane. Then the flow in the t-plane can be simply described as the flow caused by a sink at M and source distributions along the cascade openings. From this, the incipient reingestion properties can be determined.

The analysis is applied to the geometry shown in Figure 3d1-39. The incipient reingestion results are obtained by varying the free-stream velocity over the range 3.048 to 45.72 m/s (10 to 150 ft/sec) and the reverser mass flow over the range 117.2 to 162.6 kg/s (258.4 to 360.7 lbm/sec).

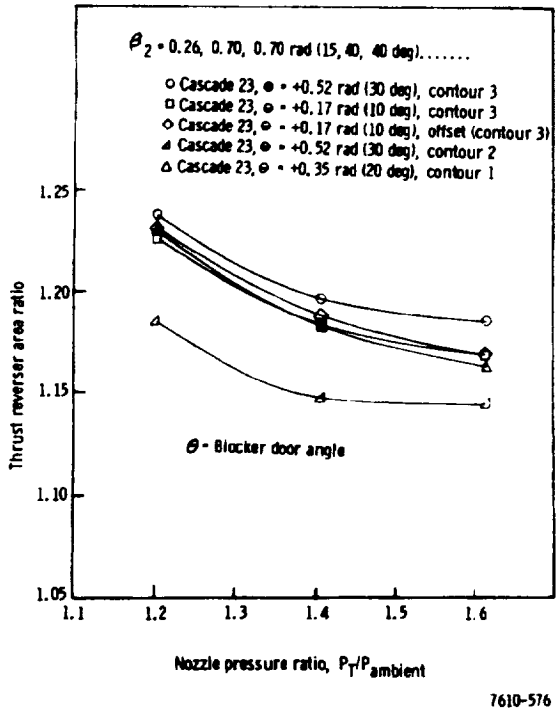

Figure 3d1-36. Influence of nozzle pressure ratio on thrust reverser area ratio.

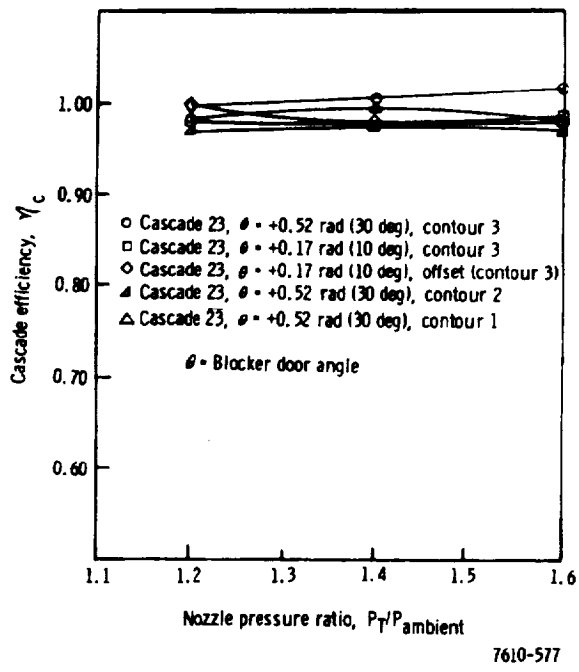

Figure 3d1-37. Measured cascade efficiency data.

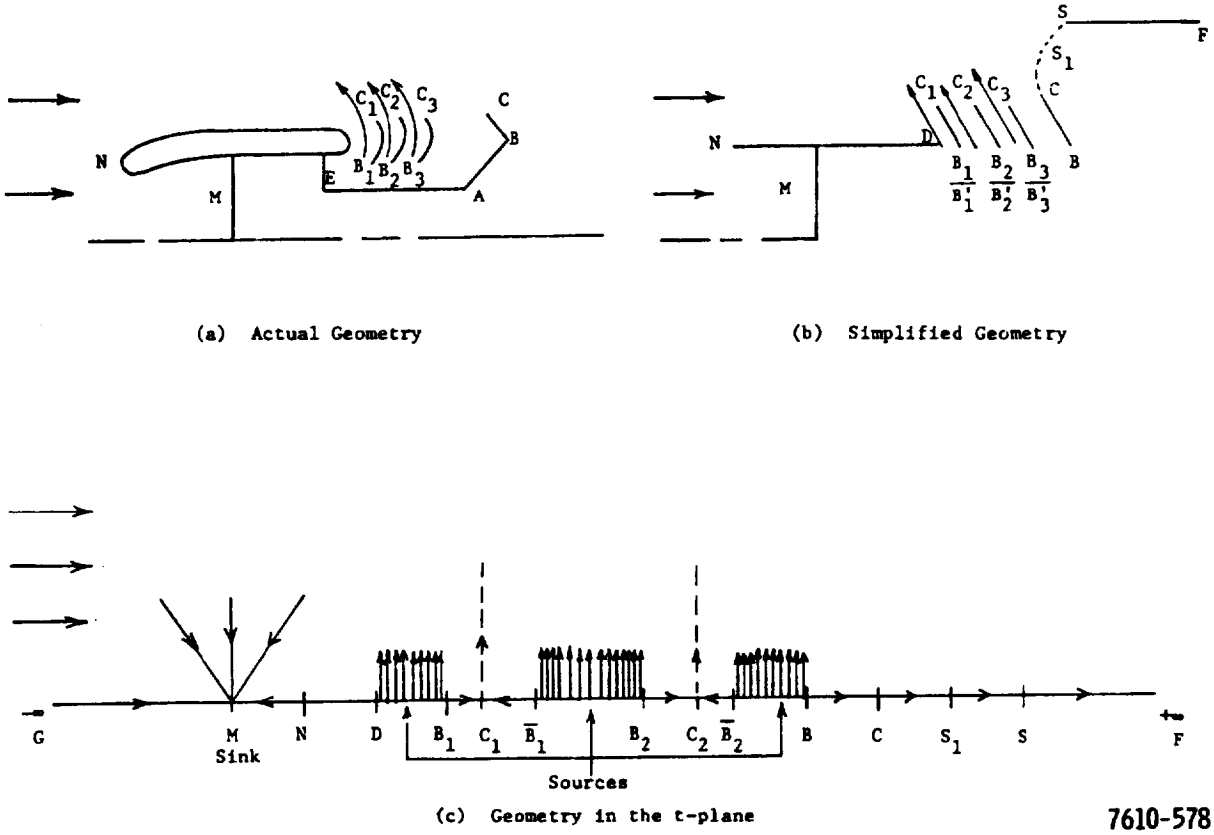

Figure 3d1-38. Cascade reverser flow geometry comparison.

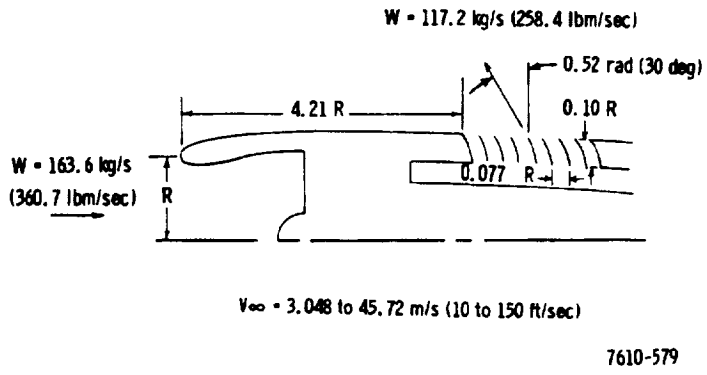

Figure 3d1-39. Analyzed geometry.

The results are presented in Figures 3d1-40 through 3d1-46. Figures 3d1-40 through 3d1-42 show $\dot{m}_i/\dot{m}_R$ for incipient reingestion as a function of free-stream velocity V_∞ for various values of reverser mass flow, $\dot{m}_R$. Each illustration contains the results for a reverser with all vanes at the same angle as well as with the angle for the first vane being decreased. Figures 3d1-40 through 3d1-42 are, respectively, for cascade angles 2.6, 2.4, and 2.1 rad (150, 135, and 120 deg) relative to the free stream. From these illustrations, the free stream velocity can be obtained for incipient reingestion for the given values of $\dot{m}_i/\dot{m}_R$ and $\dot{m}_R$.

For example, from Figure 3d1-42, for $\dot{m}_R$ = 117.2 kg/s (258.4 lbm/sec) and $\dot{m}_i/\dot{m}_R$ = 1.4 with β = 2.1 rad (120 deg) (design case of the DDA program), the free-stream velocity for incipient reingestion is found to be 10.4 m/s (34 ft/sec). However, if the first vane angle is decreased to 1.6 rad (90 deg) while keeping the other angles at 2.1 rad (120 deg), the incipient reingestion speed decreases to 6.4 m/s (21 ft/sec). Thus, decreasing the first vane angle decreases the incipient reingestion speed considerably.

Figures 3d1-40 and 3d1-41 give similar results for β = 2.6 and 2.4 rad (150 and 135 deg). For the 2.6 rad (150 deg) case and again at design values of $\dot{m}_R$ and $\dot{m}_i/\dot{m}_R$ from Figure 3d1-40, the incipient reingestion speeds increase to 13.4 m/s (44 ft/sec) and 10.4 m/s (34 ft/sec) for equal and unequal cascade angles.

The results shown in Figures 3d1-40 through 3d1-42 are cross plotted in Figures 3d1-43 through 3d1-46 to show the effects of cascade angles. Figures 3d1-43 and 3d1-44 give the results for fixed $\dot{m}_i$ with varying $\dot{m}_i/\dot{m}_R$ while Figures 3d1-45 and 3d1-46 give the results for fixed $\dot{m}_i/\dot{m}_R$. All these illustrations also show the effects of decreasing the first vane angle. Figures 3d1-43 and 3d1-44 show that for fixed $\dot{m}_i$, the incipient reingestion speed varies approximately linearly with the cascade angle for all values of $\dot{m}_i/\dot{m}_R$. However, the effects of varying $\dot{m}_i/\dot{m}_R$ become insignificant above a cascade angle of 2.6 rad (150 deg). Figures 3d1-45 and 3d1-46 show that for fixed $\dot{m}_i/\dot{m}_R$, the incipient reingestion speed is not linearly related to the cascade angle. However, when the first vane angle is decreased, the linear relation seems reestablished.

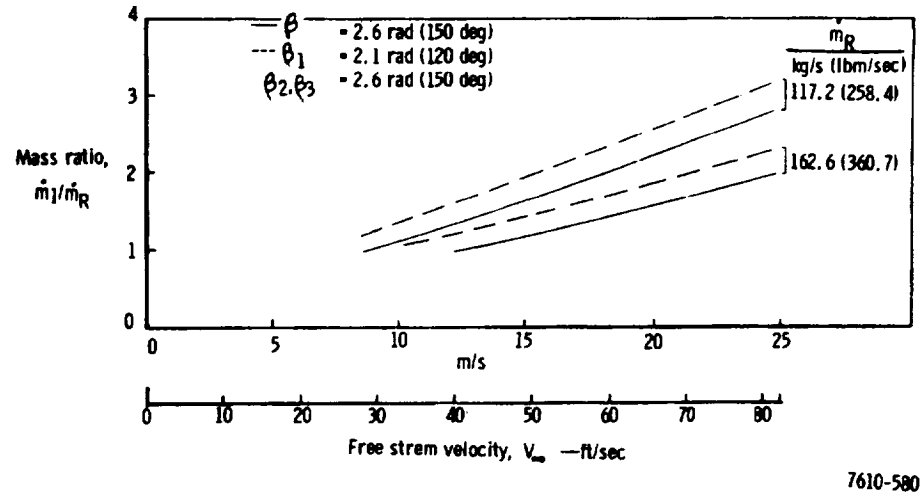

Figure 3d1-40. Results of reingestion analysis.

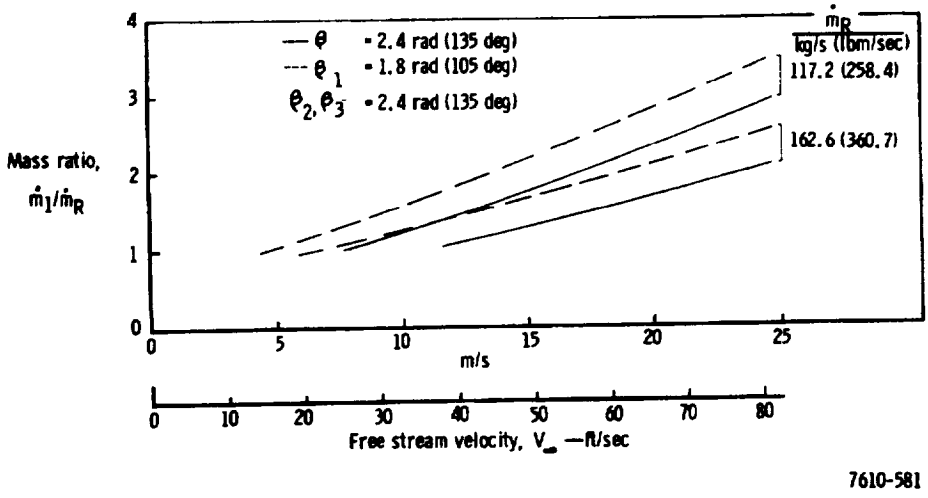

Figure 3d1-41. Results of reingestion analysis.

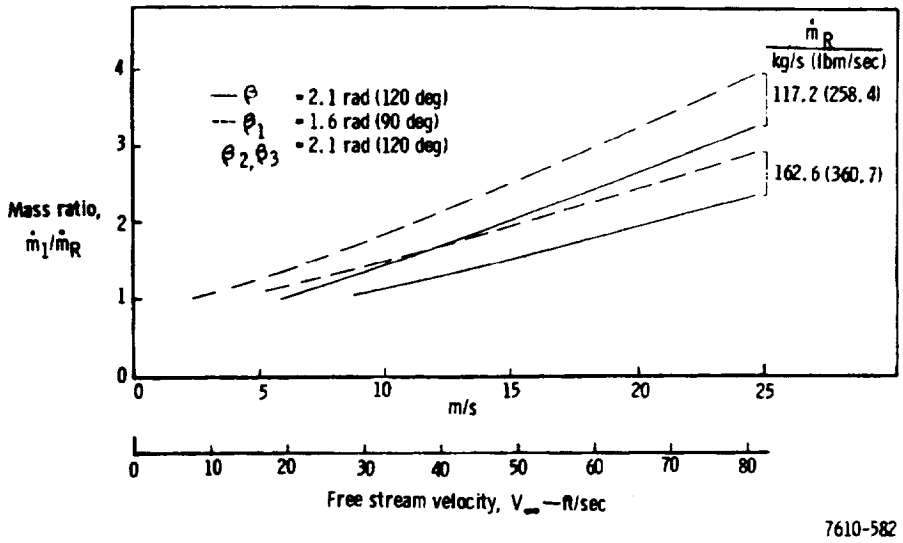

Figure 3d1-42. Results of reingestion analysis.

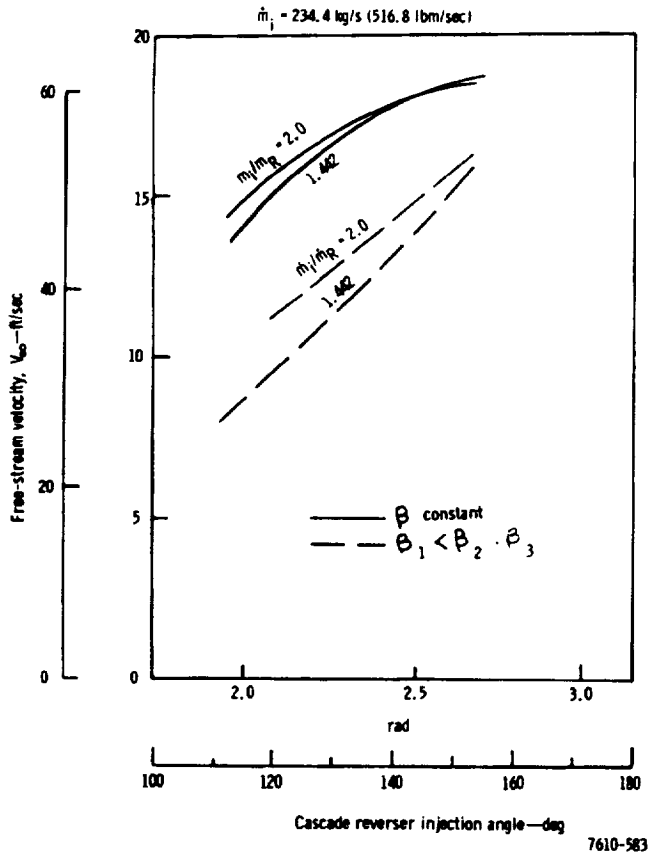

Figure 3d1-43. Results of reingestion analysis.

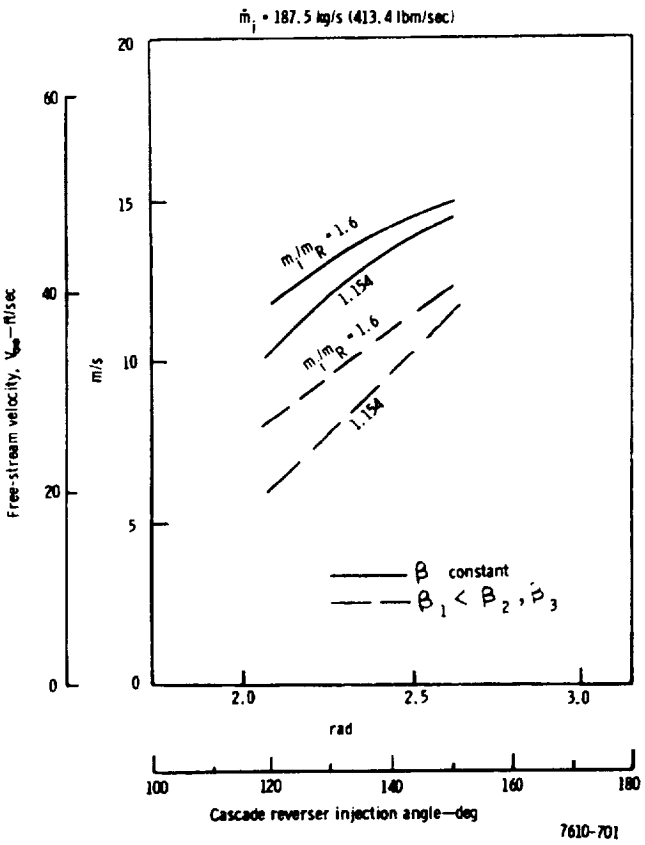

Figure 3d1-44. Results of reingestion analysis.

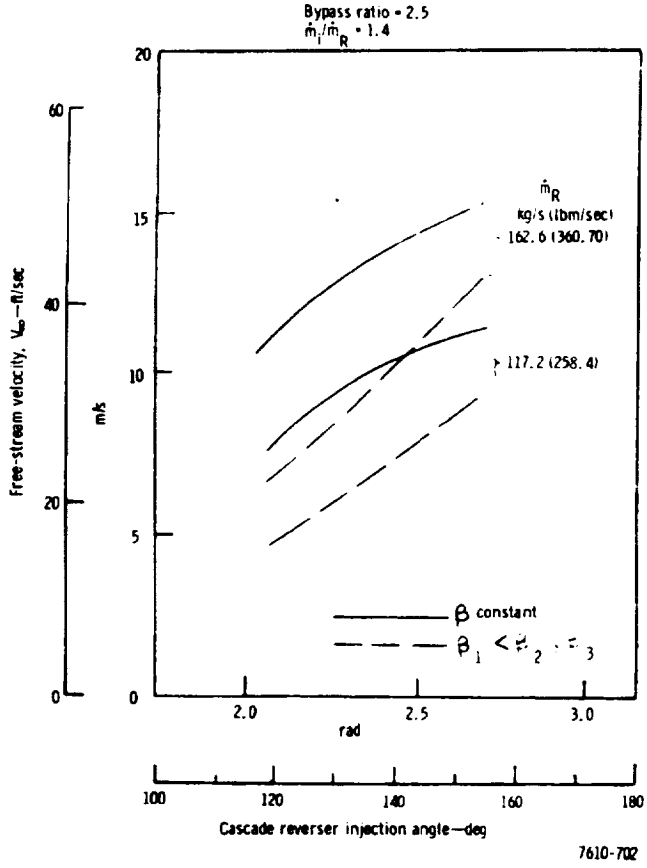

Figure 3d1-45. Results of reingestion analysis.

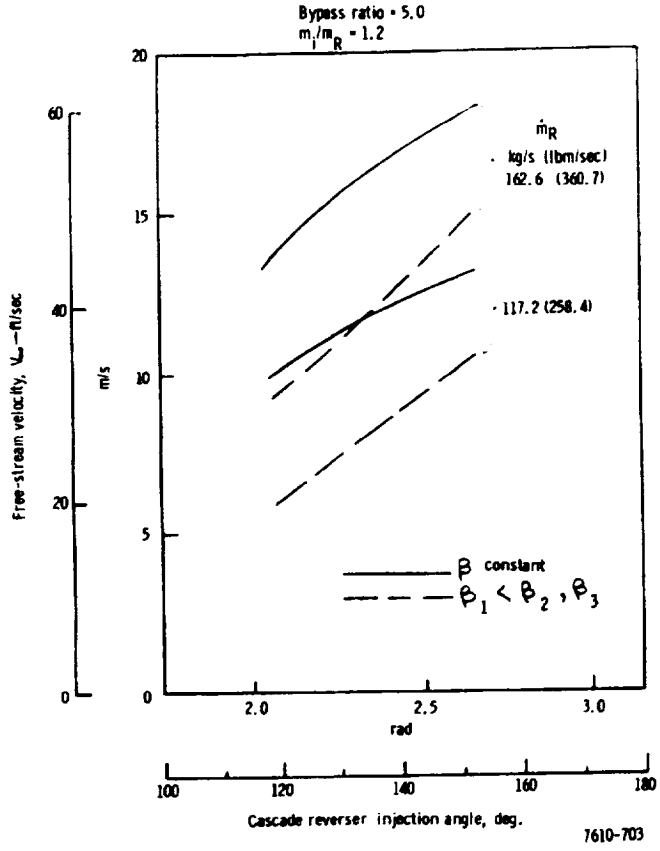

Figure 3d1-46. Results of reingestion.

Further calculations have been done for essentially the same cowl geometry as Figure 3d1-39, but with the inlet mass flow increased to 578 kg/s (1275 lbm/sec) and the reverser mass flow increased to 536 kg/s (1181 lbm/sec). With the cascade angle at 2.2 rad (127 deg) relative to the free stream, incipient reingestion occurs at a free-stream velocity of 37 m/s (120 ft/sec). With the first vane angle reduced to 1.6 rad (90 deg), incipient reingestion would occur at a free-stream velocity estimated to be 22.6 m/s (74 ft/sec).

STRESS ANALYSIS

Emphasis in preliminary design was placed on aerodynamic and acoustic design. Sufficient stress analysis was performed to establish feasibility when combined with experience. This discussion presents a brief preliminary stress analysis for the PD287-5, -51, -11, and -6 nacelles. For the -5 and -51, each major nacelle component is treated individually with a separate discussion preceding the analysis of each component. The discussions contain a structural and functional description of the component, a description of load paths, and a brief statement of Rohr experience in the area of this particular component. Generally, conventional materials are shown because the composite materials are not demonstrated. However, in an advanced technology program, composites would be incorporated (see Table 3d1-II).

The analysis that follows the discussion identifies the external loads and temperatures that would be applied to the particular component and usually contains a brief stress analysis of a major subcomponent. All components of the PD287-6 and -11 nacelles, except for the fan ducts, are similar to the corresponding components on the -5 and -51 nacelles. In these cases, a reference is made to the -5 and -51 analysis. Because of the similarity of -6 and -11 fan ducts, they are treated as one.

The final design and analysis of these nacelles would include an accurate determination of the external loads and corresponding temperature environment. These external loads would be used with the NASTRAN computer program to determine the solution of the internal loads. The final analysis would contain ultimate stress, fail safe, and sonic and static fatigue analysis of all nacelle components and subcomponents.

PD287-5 Nacelle

Nose Cowl

The nose cowl is an interchangeable aerodynamic fairing assembly which has the function of diffusing and stabilizing the inlet airflow to the fan and core sections of the engines. In addition, the nose cowl serves as a sound attenuator. It is mounted on the forward face of the engine fan case.

The nose cowl assembly is comprised of an outer and inner barrel interconnected in front by a curved panel (leading edge lip) and is interconnected further aft by two bulkhead webs. This entire structure is attached to the engine fan case by means of fittings which are located radially on the inner barrel aft end. The outer barrel is an aluminum skin supported approxi- every 20.3 cm (8 in.) by an aluminum Z-shaped ring. The inner barrel is an acoustic sandwich which has aluminum face sheets bonded to an aluminum core. The inner face sheet is perforated for the purpose of sound attenuation. An inner ring is supported inside of the inner barrel by means of five struts. This inner ring is an acoustically treated aluminum sandwich and is required only for sound attenuation. Both the leading edge lip skin of the overall cowl and the leading edge lip skin of the inner ring have anti-ice systems. The forward bulkhead is an unstiffened titanium web in the shape of an annular disk. The rear bulkhead is a stiffened web, also in the shape of an annular disk. It is stiffened by Z-shaped, commercially pure titanium stiffeners. The fittings, which are mounted on the inner barrel, are stainless steel castings.

Figures 3d1-47 and 3d1-48 show the results of the preliminary stress analysis on the PD287-5 nose cowl resulting from aerodynamic and acceleration loads.

Rohr has designed, analyzed, and manufactured nose cowls of similar configurations for the DC-10, -20, and -30 aircraft.

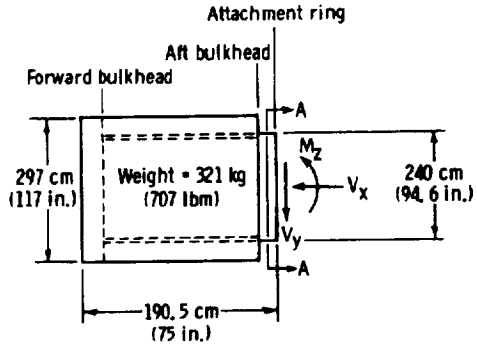

Determine max interface loads with engine fan case.

The following loads are reaction loads on the aft flange of the nose cowl:

$V_X = 1,491 \frac{N}{cm} \times 3.81 \text{ cm} = 5,680 \text{ N } (1,275 \text{ lbf})$ ultimate

$V_Y = 7,192 \frac{N}{cm} \times 3.81 \text{ cm} = 27,400 \text{ N } (6,150 \text{ lbf})$ ultimate

$M_Z = 9,344 \frac{N \cdot m}{cm} \times 3.81 \text{ cm} = 35,600 \text{ N} \cdot \text{m } (315,000 \text{ in.-lbf})$ ultimate

7610-121

Figure 3d1-47. PD287-5 nose cowl stress analysis.

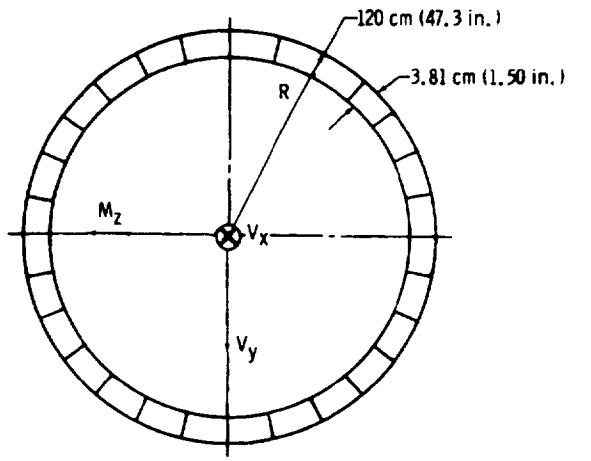

Inner barrel configuration—aluminum honeycomb sandwich
Inner skin—0.13-cm (0.05-in.) 2014-T6 AL 3% perforated
Outer skin—0.05-cm (0.02-in.) 2014-T6 AL
Core—1.91-cm (0.75-in.) hex and 0.008-cm (0.003-in.) foil

} These were set by sound attenuation requirements.

$$f_c = \frac{V_x}{A} + \frac{M}{\pi R^3 t}$$

$f_c = 4.83\ MN/m^2$ (701 lbf/in.^{2})

Therefore, aerodynamic loads are not critical for this configuration of the inner barrel.

7610-122

Figure 3d1-48. PD287-5 nose cowl stress analysis.

Fan Cowl

The fan cowl doors are basically two curved honeycomb panels that wrap around the engine. The doors are hinged at three places from the pylon and are latched at three places on the lower center line. The functions of the fan cowl doors are to provide a fairing enclosing the fan case of the engine and also to allow access to all major engine accessories.

The panels are constructed of 2.5 cm (1-in.) thick 5056 aluminum honeycomb core with 0.48 cm (3/16 in.) cells and 0.0025 cm (0.001-in.) thick foil. The outer face sheet is a 0.102 cm (0.040 in.), 2024-T81 clad sheet, chem-milled down to a basic 0.05 cm (0.020 in.) except at hinge and latch locations, etc. The inner face sheet is a 0.05 cm (0.020 in.), 2014-T6 face sheet. The latches and hinges are 17-4PH stainless steel castings. The U-bolts that attach the latches are Inco 718.

Figures 3d1-49 and 3d1-50 show the results of the preliminary stress analysis on the PD287-5 fan cowl.

The internal pressure loads and external air loads are reacted through the honeycomb structure and are transmitted into the pylon leading edge through the hinge fittings. A pressure relief door is provided to protect against nacelle overpressurization.

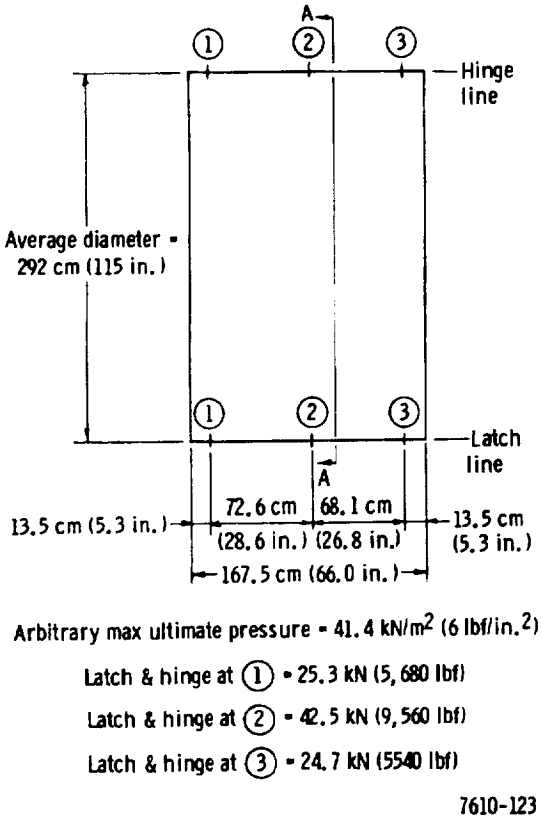

Figure 3d1-49. PD287-5 fan cowl stress analysis.

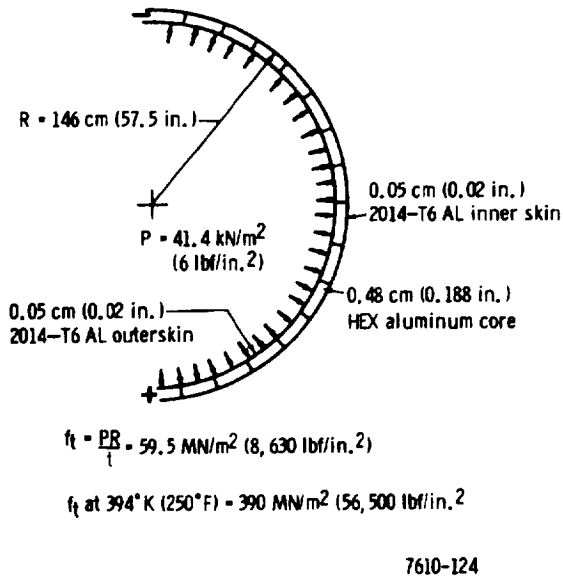

Figure 3d1-50. PD287-5 fan cowl stress analysis.

Rohr has designed, analyzed, and manufactured fan cowls of similar configurations for the DC-10, -20, and -30 aircraft.

Fan Duct and Nozzle Door

Figures 3d1-51 through 3d1-53 show the results of the preliminary stress analysis on the PD287-5 fan duct and nozzle door.

This door has an integral duct for the fan air and also has a flap system at its aft end which serves as a variable nozzle. The doors are hinged at three places from the pylon and are latched at three places on the lower center line.

The outer wall of the door is a fairing which is a skin and frame configuration. The inner walls, which form the duct, are an aluminum honeycomb sandwich. The door also contains a sound suppression ring which is supported inside of the duct. It also is an aluminum honeycomb sandwich. For all aluminum sandwiches, the face sheet gages vary from 0.05 to 0.127 cm

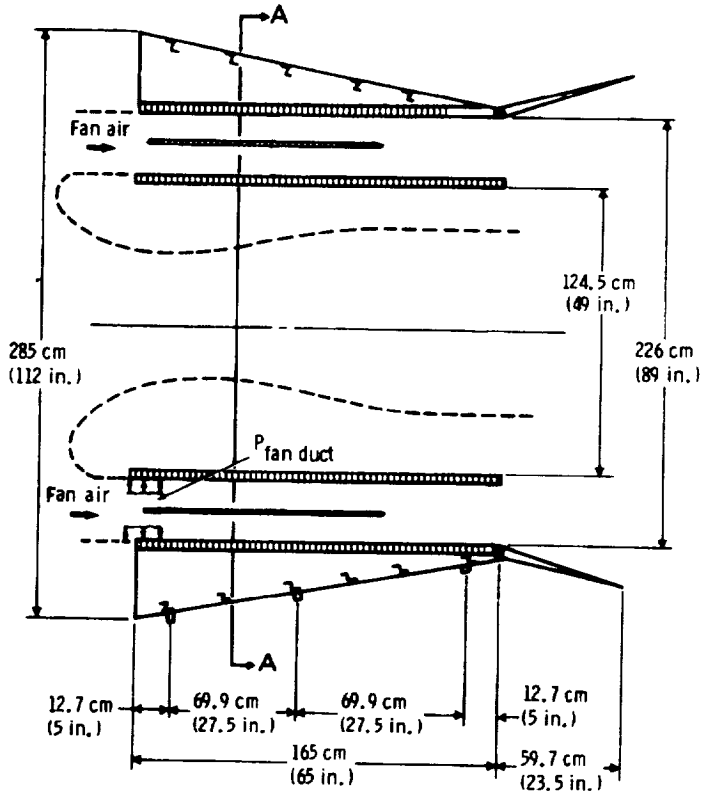

Figure 3d1-51. PD287-5 fan duct and nozzle door stress analysis.

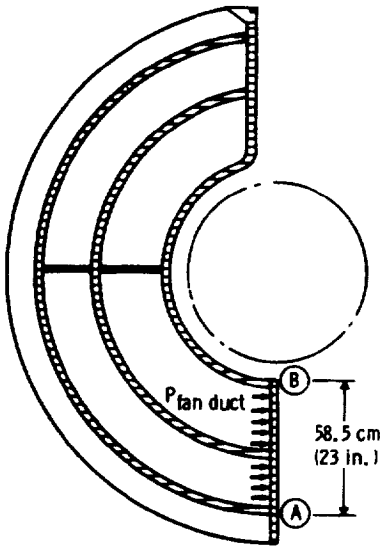

Fan duct pressure = 25.5 kN/m^2 (3.7 lbf/in.^{2})

Check end plate (A) - (B) as a fixed-fixed beam for duct pressures.

7610-126

Figure 3d1-52. PD287-5 fan duct and nozzle door stress analysis.

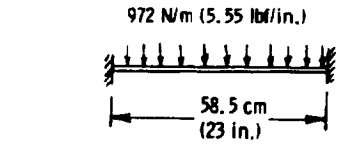

$M_{max} = \frac{wl^2}{12}$ = 27.7 N·m (245 in.-lbf)

f_t at 394°K (250°F) = 389 MN/m^2 (56,500 lbf/in.^{2})

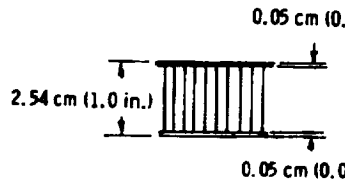

$M_{allowable} = A f_t h$ = 125.5 N·m (1,110 in.-lbf)

7610-127

Figure 3d1-53. PD287-5 fan duct and nozzle door stress analysis.

(0.020 to 0.050 in.); the sandwich height is 3.81 cm (1.50 in.); and the cell size is either 1.27 or 1.91 cm (1/2 or 3/4 in.) with 0.0076 cm (0.003 in.) foil. One face sheet of the sandwich is perforated for sound suppression purposes. The percentage of open area is 2%. The latches and hinges are 17-4PH stainless steel castings. The U bolts that attach the latches are Inco 718.

The internal pressure loads and external air loads are reacted through the honeycomb structure and are transmitted into the pylon leading edge through the hinge fittings. A pressure relief door is provided to protect against nacelle overpressurization.

Rohr has designed, analyzed, and manufactured aluminum honeycomb sandwich fan ducts of similar complexity for the DC-8 aircraft.

Engine Mounts

The forward and aft engine mounts as shown schematically in Figure 3d1-54 form a fail-safe system of beams and links attaching the engine to the pylon.

The forward mount has two bolts to react vertical loads and pitching moments. It also has a thrust pin which reacts side loads, fore and aft loads, and yawing moments.

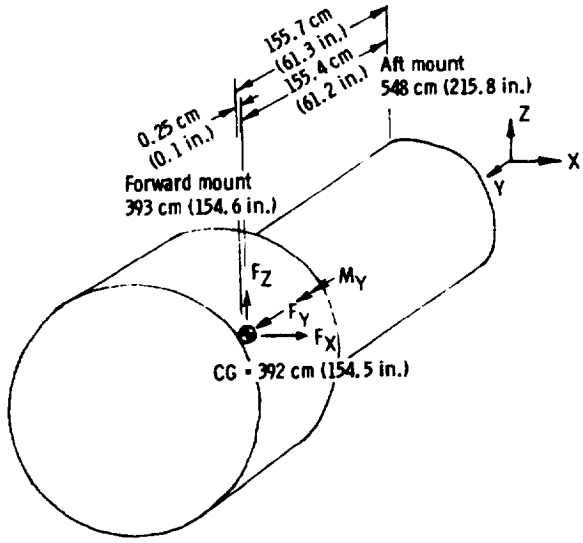

Engine weight	= 2,010 kg (4,400 lbm)
Engine buildup system weight	= 1,560 kg (3,420 lbm)
Total weight	= 3,570 kg (7,820 lbm)

Assume that cg coincides with engine cg and that the engine buildup system weight is reacted by the engine mounts into the pylon.

7610-128

Figure 3d1-54. PD287-5 engine mount analysis.

The aft mount system is composed of a beam that attaches to the pylon and three links that attach the beam to the engine. The beam and link assembly consist of fore and aft beam halves bolted together, giving fail-safe capability. The aft mount is designed to react vertical and side loads and pitching, yawing, and rolling moments.

The aft mount is designed so that it cannot react any fore and aft external loads. This is to allow for thermal expansion of the engine in the fore and aft direction.

The material used for the mounts is Inco 718, a nickel base alloy. With the exception of the Inco 718 pins, which connect the links to the engine, all fasteners are made of H-11, a high-strength steel alloy. Table 3d1-IV shows the loads calculated at various conditions for this mounting system.

Rohr has designed, analyzed, and manufactured engine mounts similar to this configuration for the C-5A and the DC-10 aircraft.

Table 3d1-IV.
Assumed ultimate load conditions.

Condition No.	Condition description	Loads at engine CG			
		F_x	F_y	F_z	M_y
1	12g Forward crash	0	417,000N (93,800 lbf)	0	0
2	Max 5g side (outboard) and 1.5g down	174,000N (39,100 lbf)	0	-52,200N (-11,730 lbf)	0
3	Max 5g side (inboard) and 1.5g down	-174,000N (-39,100 lbf)	0	-52,200N (-11,730 lbf)	0
4	Max 8g down and thrust (1.5g × max thrust)	0	195,000N (43,800 lbf)	-278,000N (-62,500 lbf)	0
5	Max 8g down and drag (1.5g)	0	-52,100N (-11,700 lbf)	-278,000N (-62,500 lbf)	0
6	Max 5g up and thrust (1.5g × max thrust)	0	195,000N (43,800 lbf)	174,000N (39,100 lbf)	0
7	Max 5g up and drag (1.5g)	0	-52,100N (-11,700 lbf)	174,000N (39,100 lbf)	0
8	Max limit thrust × 2.25	0	292,000N (65,700 lbf)	0	0
9	Max limit reverse thrust × 2.25	0	-102,300N (-23,000 lbf)	0	0
10	Max seizure torque M_y and 1.5g down	← (Not enough engine data) →			

Notes: These loads will be resolved to the forward and aft engine mounts.
These loads exceed FAA requirements. Reference: Early STOL Aircraft Studies.

Tail Cone and Tail Pipe Assembly

The PD287-5 tail cone and tail pipe assembly shown in Figure 3d1-55 provide an acoustically treated passageway for the core engine air. The tail cone and the inner wall of the tail pipe assembly are brazed steel honeycomb with perforated face sheets for sound attenuation. The outer wall is a 6Al-4V-Ti skin and frame configuration and is supported from the inner wall by two 6Al-4V-Ti bulkheads.

Both the tail cone and tail pipe assembly are cantilevered off the aft end of the engine. Because the pressure loads are essentially symmetrical around the circumference, the static stresses are low as shown in Figure 3d1-56.

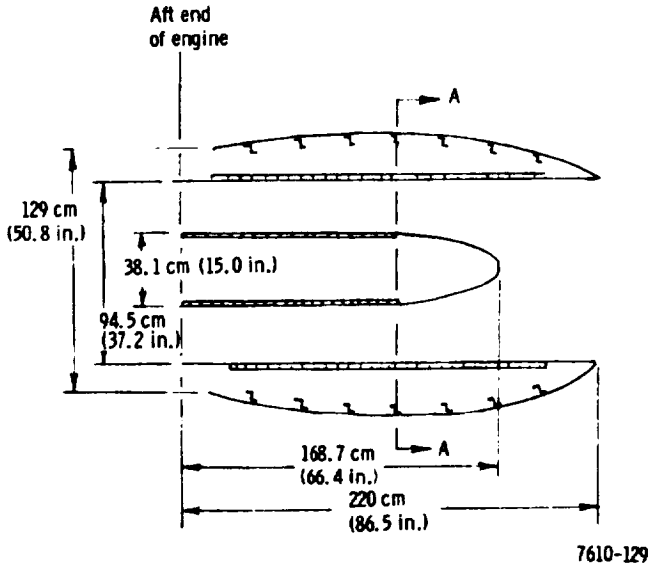

Figure 3d1-55. PD287-5 tail cone and tail pipe assembly schematic.

Pressure = 9.65 kN/m^2 (1.4 lbf/in.^{2}) limit
= 14.5 kN/m^2 (2.1 lbf/in.^{2}) ultimate
Temperature = 811°K (1000°F)

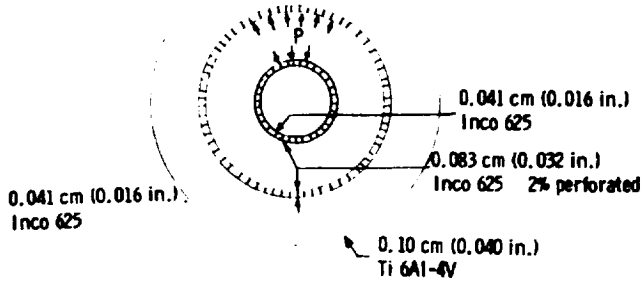

$$F_c = \frac{PR}{t} = 2270 \text{ kN/m}^2 \text{ (329 lbf/in.}^2\text{)}$$

7610-130

Figure 3d1-56. PD287-5 tail cone and tail pipe assembly analysis.

Rohr has design, analysis, and manufacturing experience in tail pipes, tail cones, and brazed steel honeycomb for the DC-9, 737, DC-10 and 747 aircraft.

PD287-51 Nacelle

Nose Cowl

The nose cowl is an interchangeable aerodynamic fairing assembly which has the function of diffusing and stabilizing the inlet airflow to the fan and core sections of the engines. It is mounted on the forward face of the engine fan case.

The nose cowl assembly is comprised of an outer and inner barrel interconnected in front by a curved panel (leading edge lip) and interconnected further aft by two bulkhead webs. This entire structure is attached to the engine fan case by means of an attach ring which is located on the aft end of the inner barrel. The inner and outer barrels are aluminum skins supported approximately every 17.6 cm (7 in.) by aluminum Z-shaped rings. The leading edge lip skin of the overall cowl has an anti-ice system. The forward bulkhead is an unstiffened titanium web in the shape of an annular disk. The rear bulkhead is a stiffened web, also in the shape of an annular disk. It is stiffened by Z-shaped, commercially pure titanium stiffeners. The attach ring is a machined steel forging. Figures 3d1-57 and 3d1-58 show the results of the preliminary stress analysis on the PD287-51 nose cowl.

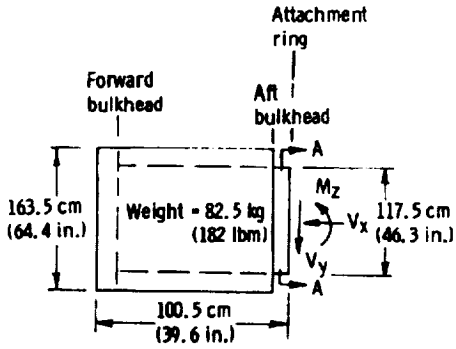

Determine maximum interface loads with engine fan case.

The following loads are reaction loads on the aft flange of the nose cowl:

$V_x = \frac{N}{cm} \times 3.81\ cm = 668\ N\ (150\ lbf)$

$V_y = \frac{N}{cm} \times 3.81\ cm = 3,000\ N\ (675\ lbf)$

$M_z = \frac{N \cdot m}{cm} \times 3.81\ cm = 1,695\ N \cdot m\ (15,000\ in.\text{-}lbf)$

7610-131

Figure 3d1-57. PD287-51 nose cowl stress analysis.

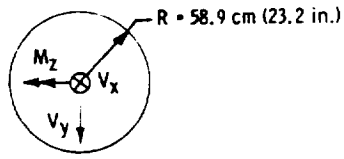

Inner barrel configuration—aluminum skin and aluminum ring frames
Skin—0.16 cm (0.063 in.) 2024-T42
Frames—0.16 cm (0.063 in.) 2024-T42

$$f_c = \frac{V_x}{A} + \frac{MR}{\pi R^3 t}$$

$f_c = 1.08\ MN/m^2\ (157\ lbf/in.^2)$

Therefore, aerodynamic loads are not critical for this configuration of the inner barrel.

7610-132

Figure 3d1-58. PD287-51 nose cowl stress analysis.

Rohr has designed, analyzed, and manufactured nose cowls of similar configurations for the DC-10, -20, and -30 aircraft.

Fan Cowl

The fan cowl doors are basically two curved honeycomb panels that wrap around the engine. The doors are hinged at three places from the pylon and are latched at three places on the lower center line. The functions of the fan cowl doors are to provide a fairing enclosing the fan case of the engine and also to allow access to all major engine accessories.

The panels are constructed of one inch thick 5056 aluminum honeycomb core with 0.48 cm (3/16 in.) cells and 0.0025 cm (0.001 in.) thick foil. The outer face sheet is an 0.102 cm (0.040 in.) 2024-T81 clad sheet, chem-milled down to a basic 0.05 cm (0.020 in.) except at hinge and latch locations, etc. The inner face sheet is an 0.05 cm (0.020 in.) 2014-T6 face sheet. The latches and hinges are 17-4PH stainless steel castings. The U bolts that attach the latches are Inco 718.

The internal pressure loads and external air loads are reacted through the honeycomb structure and are transmitted into the pylon leading edge through the hinge fittings. A pressure relief door is provided to protect against nacelle overpressurization. Figures 3d1-59 and 3d1-60 show the results of the preliminary stress analysis on the PD287-51 fan cowl.

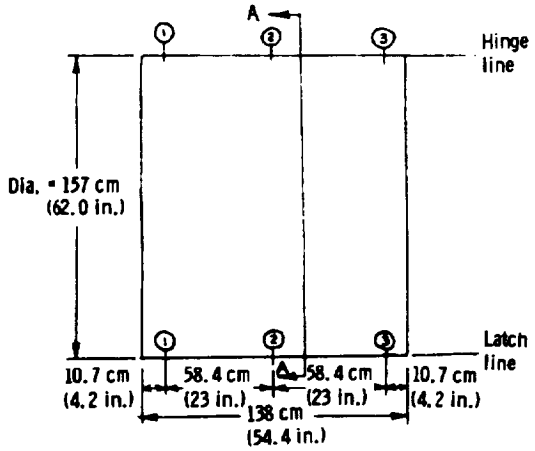

Arbitrary max ultimate pressure = 41.4 kN/m^2 (6 lbf/in.^{2})

Latch and hinge at ① = 11.25 kN (2,530 lbf)
Latch and hinge at ② = 19.05 kN (4,280 lbf)
Latch and hinge at ③ = 11.25 kN (2,530 lbf)

7610-133

Figure 3d1-59. PD287-51 fan cowl stress analysis.

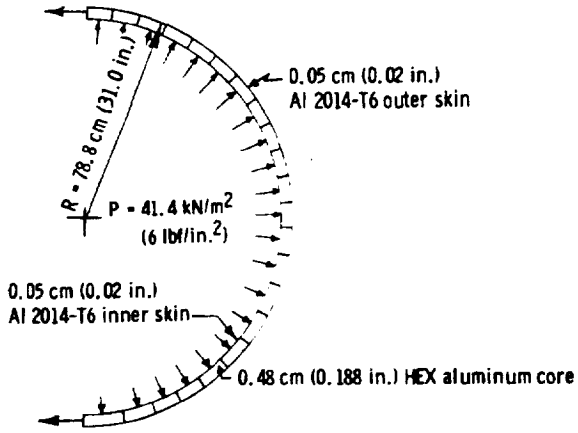

$f_t = \frac{PR}{t}$ = 32.1 MN/m^2 (4,650 lbf/in.^{2})

f_t at 394°K (250°F) = 390 MN/m^2 (56,500 lbf/in.^{2})

7610-134

Figure 3d1-60. PD287-51 fan cowl stress analysis.

Rohr has designed, analyzed and manufactured fan cowls of similar configurations for the DC-10, -20, and -30 aircraft.

Fan Reverser Door

This cowl door, shown in Figure 3d1-61, has an integral duct which carries the fan air from the fan case to a matching duct in the pylon. The pylon duct has a valve which can shut off the fan air. By opening a translating sleeve on the outer surface, this air is exited out of a cascade which is an integral part of the duct. This exiting of fan air gives the thrust reverse capability. The doors are hinged and latched at four places. The hinge attach points are on an "apron" system, which ties into the fan case at the front end and into the aft engine mount at the aft end.

The outer wall of the cowl door serves as a fairing and also houses the translating sleeve. This fairing and sleeve are aluminum honeycomb sandwich structures; the inner walls which form the duct are sandwich structures. The sandwich has aluminum core adhesively bonded to titanium face sheets. The cascade, which is an integral part of the fan duct, is an aluminum casting. The latches and hinges are 17-4PH stainless steel castings. The U bolts that attach the latches are Inco 718.

The internal pressure loads and external air loads are reacted through the sandwich structure to the apron system. The apron system takes the loads through the fan case and mount system into the pylon. Pressure relief doors are provided to protect against nacelle overpressurization. Figures 3d1-62 and 3d1-63 show the results of the preliminary stress analysis on the PD287-51 fan reverser door.

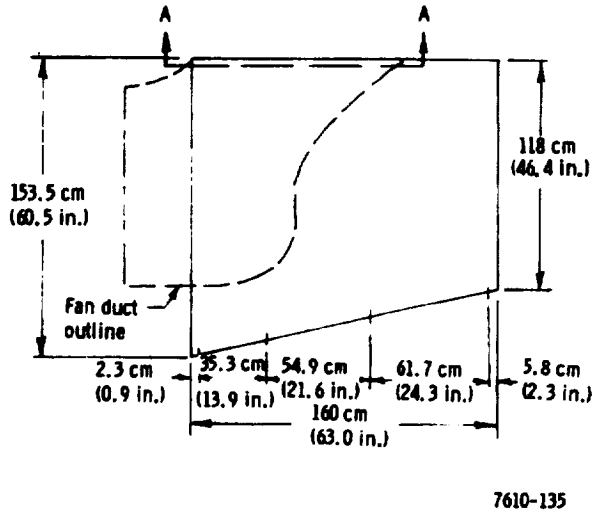

Figure 3d1-61. PD287-51 fan reverser door schematic.

Fan duct pressure = 206 kN/m^2 (30 lbf/in.^{2})

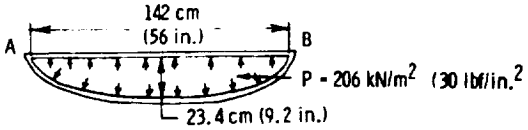

For bending moments, Wall A - B is somewhere between a fixed-fixed beam and a wall of an ellipse.

Bending in the wall of an ellipse.

$M = \frac{P}{2}(R^2 - \rho^2)$

M = −665 N·m (5,880 in.-lbf)

a = 1/2 major dia of ellipse = 71.1 cm (28 in.)

b = 1/2 minor dia of ellipse = 23.4 cm (9.2 in.)

ρ = radius of fictitous circle = $\frac{a+b}{2}$ = 47.3 cm (18.2 in.)

7610-531

Figure 3d1-62. PD287-51 fan reverser door stress analysis.

Bending moment in a fixed-fixed beam

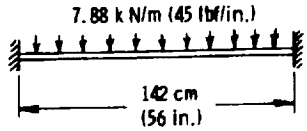

$M_{max} = \frac{Wl^2}{12}$ = 1330 N·m (11,760 in.-lbf)

As an approximation of the bending moment in the duct wall, take an average of the above two values.

M = 997 N·m (8,820 in.-lbf)

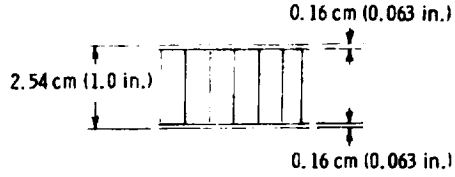

$M_{allowable} = Ph = f_t Ah$ = 950 N·m (8,410 in.-lbf)

f_t at 394°K (250°F) = 985 MN/m^2 (142,500 lbf/in.^{2})

7610-532

Figure 3d1-63. PD287-51 fan reverser door stress analysis.

Rohr has designed, analyzed, and manufactured aluminum honeycomb sandwich fan ducts of similar complexity for the DC-8 aircraft. Also Rohr has manufactured sandwich structure with aluminum core adhesively bonded to titanium face sheets for the inlet of the F-14A aircraft.

Engine Mounts

The forward and aft engine mounts are shown schematically in Figure 3d1-64 and form a fail-safe system of beams and links attaching the engine to the pylon.

The forward mount has two links to react vertical loads and pitching moments. It also has a thrust pin which reacts side loads, and fore and aft loads, and yawing moments.

The aft mount system is composed of a beam that attaches to the pylon and three links that attach the beam to the engine. The beam and link assembly consist of fore and aft beam halves bolted together, giving fail-safe capability. The aft mount is designed to react vertical and side loads and pitching, yawing, and rolling moments.

The aft mount is designed so that it cannot react any fore and aft external loads. This is to allow for thermal expansion of the engine in the fore and aft direction.

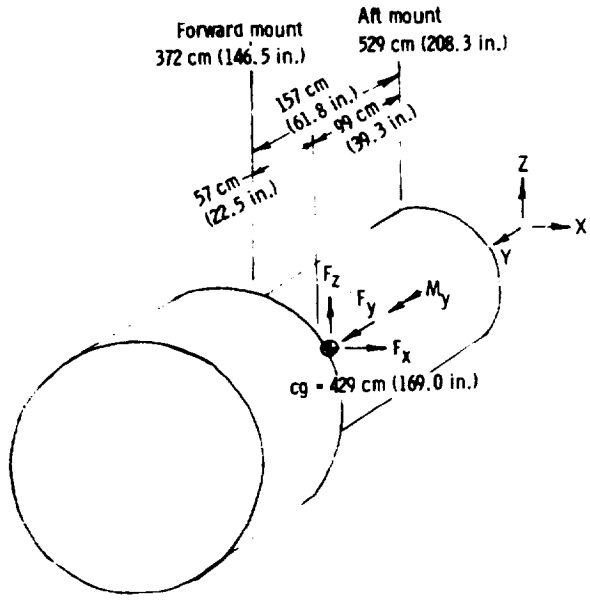

Engine weight	= 1195 kg (2, 634 lbm)
Engine buildup system weight	= 1130 kg (2, 487 lbm)
Total pod weight	= 2325 kg (5, 121 lbm)

Assume that pod cg coincides with engine cg and that all engine buildup system weight is reacted by the engine mounts into the pylon.

7610-533

Figure 3d1-64. PD287-51 engine mount analysis.

The material used for the mounts is Inco 718, a nickel base alloy. With the exception of the Inco 718 pins, which connect the links to the engine, all fasteners are made of H-11, a high-strength steel alloy. Table 3d1-V shows the loads calculated at various conditions for this mounting system.

Rohr has designed, analyzed, and manufactured engine mounts similar to this configuration for the C-5A and the DC-10 aircraft.

Primary Thrust Reverser

Figure 3d1-65 shows the PD287-51 primary thrust reverser system. The thrust reverser is a target type in which the target doors are flush to the outside contour in the faired position. The doors are driven by hydraulic actuators operated by the utility system. The linkage is designed such that in event of the loss of system pressure in the forward thrust position, the doors will remain in that position; and if loss of system pressure occurs in reverse thrust, the doors will remain in the reverse thrust position.

Table 3d1-V.
Assumed ultimate load conditions.

Condition No.	Condition description	Loads at engine CG F_x	F_y	F_z	M_y
1	12g forward crash	0	274,000N (61,500 lbf)	0	0
2	Max 5g side (outboard) and 1.5g down	114,000N (25,600 lbf)	0	-34,200N (-7,680 lbf)	
3	Max 5g side (inboard) and 1.5g down	-114,000N (-25,600 lbf)	0	-34,200N (-7,680 lbf)	0
4	Max 8g down and thrust (1.5g × max thrust)	0	97,300N (21,840 lbf)	-182,000N (-40,900 lbf)	0
5	Max 8g down and drag (1.5g)	0	-34,200N (-7,680 lbf)	-182,000N (-40,900 lbf)	0
6	Max 5g up and thrust (1.5g × max thrust)	0	97,300N (21,840 lbf)	114,000N (25,600 lbf)	0
7	Max 5g up and drag (1.5g)	0	-34,200N (-7,680 lbf)	114,000N (25,600 lbf)	0
8	Max limit thrust × 2.25	0	145,500N (32,700 lbf)	0	0
9	Max limit reverse thrust × 2.25	0	-72,900N (-16,350 lbf)	0	0
10	Max seizure torque M_y and 1.5g down	← (Not enough engine data) →			

Notes: These loads will be resolved to the forward and aft engine mounts.
These loads exceed FAA requirements.

The thrust reverser linkage couples the doors to the actuator and carries the weight and reverse thrust loads of the doors in both the faired and reverse thrust positions. Link material is forged A-286, machined for weight and stiffness control.

The support structure is mounted on the engine tailpipe and carries the reverse thrust loads and inertia loads for the doors and linkage. The tailpipe is supported by the engine aft flange. The aft support fitting is a 17-4PH Cres casting. The forward support fitting is a 4340 steel forging. All other structures are 2024-T42 aluminum except for the tailpipe attach angle which is PH15-7 mo Cres steel.

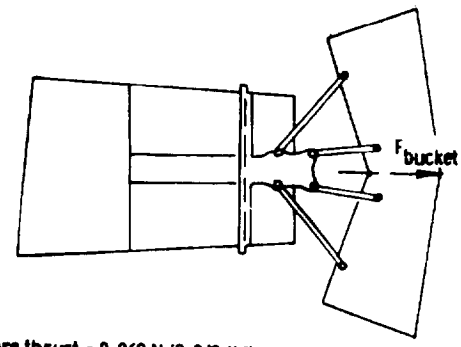

Max core thrust = 9,960 N (2,240 lbf)

$F_{bucket} = (1+R) Fg + D_{base}$

Fg = gross thrust
R = reverse thrust efficiency = 0.50 (assumed)

$D_{base} = q_0 (\bar{a} \times A_{buckets\ projected})$

F_{bucket} = 17,150 N (3,860 lbf) at M_N = 0.9 and
4,572 m (15,000 ft) inadvertent deployment.

7610-534

Figure 3d1-65. PD287-51 primary thrust reverser analysis.

The thrust reverser doors block the engine exhaust gases and deflect them forward. The doors are supported by four links with spherical ball joints on the door end of the links. The support fittings are 17-4PH Cres castings. The door structure is A-286, except the outside skin which is 2024-T42 aluminum.

Rohr has designed, analyzed, and manufactured thrust reversers of similar configurations for the DC-9, 737, and Sabreliner aircraft.

PD287-6 and -11 Nacelles

Nose Cowl

These nose cowls are nearly identical to the PD287-5 nose cowl in both structural configuration and overall dimensions.

Fan Cowl

These fan cowls are nearly identical to the PD287-5 fan cowl in both structural configuration and overall dimensions.

Engine Mounts

These engine mounts are identical in structural description and function to those for the PD287-5 and -51 except they are mounted on the side of the engine instead of on the top of the engine.

Fan Duct Door

The fan duct door performs three functions. It carries fan air from the fan case to the fixed fan duct by means of a kidney-shaped duct integral with the door. A matching upper kidney-shaped duct is in the fixed structure. A BLC bypass duct interfaces with intake doors in the wall of the duct. The intake doors are mechanically actuated and, when opened, allow fan air to enter the BLC bypass duct and eventually be blown over the trailing edge of the wing. The BLC bypass duct is supported by the wing structure and is not part of the fan duct door. Both the PD287-6 and -11 have fan reverser capability but this is accomplished in different ways. The -6 has a variable pitch fan which sucks air from the fan duct. The fan duct obtains air through suck-in doors in the duct wall and mechanically-actuated doors on the outer surface. The -11 has a series of blocker doors within the duct which forces the air through a cascade structure which is an integral part of the duct. The cascade is nominally closed off by a translating door on the outer surface.

Fixed Aft Fan Ducts

The fixed fan duct carries the fan air from the fan duct door and exits it at the end of the nacelle. The duct starts as two separate kidney-shaped ducts. The upper one bifurcates and wraps around the exhaust pipe as it extends aft and then blends into the lower duct. The one duct becomes rectangular in cross-section. The ducts are supported above the wing box by three bulkheads. The lower duct has a splitter (Figure 3d1-80) which runs its entire length down its center line. The duct is constructed of aluminum honeycomb sandwich with perforated face sheets for the purpose of sound attenuation.

The internal pressures are self-equilibrating except the offset of the center lines of the fan duct causes an overturning moment which is coupled out between the bulkheads. Figures 3d1-66 and 3d1-67 show the results of the preliminary stress analysis on the PD287-6 and -11 aft fan ducts.

Rohr has designed, analyzed, and manufactured a fan duct of similar complexity and configuration for the DC-8 aircraft.

Sonic Fatigue

Specific sonic fatigue analyses were not performed during this phase. However, a general overview of the designs was maintained to ensure that the structural concepts presented are basically compatible with the expected acoustic loading, based on Rohr experience. The following discussion briefly describes Rohr background and approach in the sonic fatigue design of nacelle structures.

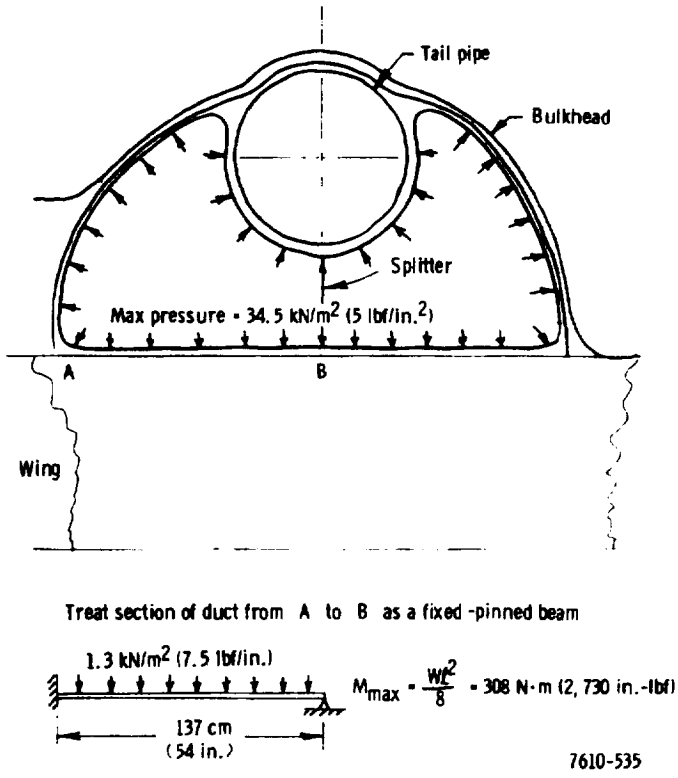

Figure 3d1-66. PD287-6 and -11 fixed aft fan duct stress analysis.

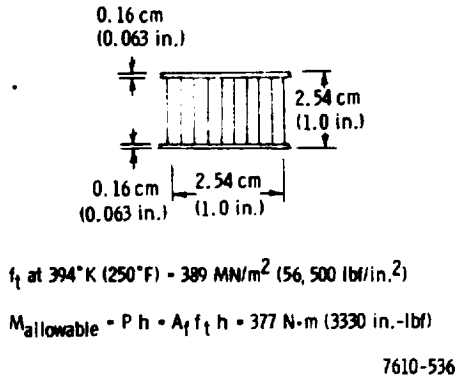

Figure 3d1-67. PD287-6 and -11 fixed aft fan duct stress analysis.

Considerable nacelle response data have been generated from full-scale engine ground tests, flight tests, and progressive wave tube tests. Different nacelles have been subjected to engine testing to determine the response to acoustic loading (fan noise) of each major structural component. These investigations have included acoustical and conventional honeycomb sandwich structures in addition to stiffened-skin structures. Comparable structures have been subjected to progressive wave tube testing for comparison with a wider range of structures (metallic and nonmetallic). Holehouse and Hallam[14,15] detail some of the full-scale testing and Holehouse[16] gives progressive wave tube data for a range of acoustical sandwich designs.

Rohr sonic fatigue analysis has been based on using sound spectrum levels rather than overall levels. This is particularly important where fan noise is concerned. Where the acoustic load spectrum shows a predominant peak at the fan blade passing frequency, sonic fatigue resistance is evaluated in consideration of forced response at the blade passing frequency in addition to resonant response at appropriate combination tone frequencies.

Semiempirical design techniques have been developed from the test data just described and applied to new designs. Subsequent full-scale tests and service experience have confirmed the efficacy of these techniques. Rohr Structures Manual[17] provides the analytical basis.

REFERENCES

1. Stanhope, F. W.: The Performance of NACAl Intakes. Rolls-Royce Report IAR 85002, 1968.

2. Blackaby, J. R. and Watson, E. C.: An Experimental Investigation at Low Speeds of the Effects of Lip Shape on the Drag and Pressure Recovery of a Nose Inlet in a Body of Revolution. NACA TN 3170, April 1954.

3. Albers, J. A.: Predicted Upwash Angles at Engine Inlets for STOL Aircraft. NASA TMX-2593, July 1972.

4. Hoerner, S. F.: Fluid-Dynamic Drag. Published by author, 1965.

5. Schlichting, H.: Boundary Layer Theory. Sixth Edition, McGraw-Hill, New York, 1968.

6. Henry, John R.: Design of Power Plant Installations—Pressure Loss Characteristics of Duct Components. NACA ARR No. L4F26, June 1944.

7. SAE Aero-Space Applied Thermodynamics Manual, February 1960.

8. Grey, R. E. and Wilsted, H. D.: Performance of Conical Jet Nozzles in Terms of Flow and Velocity Coefficients. NACA TN-1757, 1948.

9. Kutney, J. T. et al: Lift/Cruise Fan Exhaust System Research Program. TRECOM TR 64-49, General Electric Company, September 1964.

10. Poland, D. T. and Schwanebeck, J. C.: Turbofan Fan Thrust Determination for the C-5A. AIAA Paper No. 70-611, June 1970.

11. Yarker, A. and Stanhope, F.: Altitude Testing of High Bypass Ratio Fan Engines. SAE Paper No. 690655, October 1969.

12. Denington, R. J.: Aircraft Mission Characteristic Update for Task II of the QCSEE Studies. NASA LERC. 21 August 1972.

13. Wickline, R. J.: Cascade Thrust Reverser Design Procedure. Rohr Corporation TN 832-053, February 1971.

14. Holehouse, I.: Sonic Fatigue of Aircraft Structures Due to Jet Engine Fan Noise. International Conference on Current Developments in Sonic Fatigue. University of Southampton, England, July 1970.

15. Hallam, R. and Holehouse, I.: Engine Testing of Acoustic Sandwich Structure. Rohr Report No. 24-4030, January 1970.

16. Holehouse, I.: Sonic Fatigue of Acoustical Sandwich. Rohr Report 814-0017, June 1970.

17. Rohr Structures Manual—sonic fatigue design section.

AERODYNAMIC DESIGN

The aerodynamic design data on the PD287-11 and -51 fans, the PD287-7 IP compressor, and compressor system stability are presented in subsection 3d2 of the Supplement to this report.

PD287-11

Four candidate configurations were studied for the PD287-11 fan before a final selection was made. The configurations include the following:

- Single-stage fan
- Single-stage fan with boost stage operating at fan turbine speed
- Single-stage fan with boost stage operating at fan speed
- Single-stage fan with half stage operating at fan speed

The second and third configurations were eliminated early in the study. The fan plus boost stage operating at turbine speed was mechanically feasible but rather complicated structurally. The fan plus boost stage operating at fan speed was rejected because of the combined effects of high fan tip speed and high boost stage inlet radius ratio. More detailed studies were performed on the single-stage and the stage-and-a-half configurations. The design point aerodynamics of these configurations are given in Tables 3d2-I and 3d2-II. Included in the tables are values for inlet and exit Mach numbers, inlet and exit air angles, and diffusion factors. These values are recorded for hub, mean, and tip stations for both rotors and stators. The single-stage rotor tip Mach number is slightly supersonic at 1.022. The rotor turning is 1.3 drad (7.3 deg) past axial at the hub and varies radially between 7.6 drad (43.7 deg) and 2.1 drad (12.2 deg). The max rotor diffusion factor is 0.521 and occurs at the mean station. The core stator for this configuration has a max inlet Mach number of 0.784 at the hub, where the turning is 7.6 drad (43.6 deg) and the diffusion factor is 0.448. The maximum bypass stator inlet Mach number of 0.662 also occurs at the hub station. The corresponding levels of air turning and diffusion factor are 7.6 drad (43.4 deg) and 0.510.

The stage-and-a-half fan rotor inlet Mach numbers are all subsonic. The rotor tip inlet relative Mach number is 0.932. Fan rotor turning varies between 6.2 drad (35.53 deg) and 4.0 drad (22.82 deg) hub-to-tip. Turning at the hub is 1.1 drad (6.54 deg) past axial and the diffusion factor level is only 0.191. Max rotor diffusion factor is 0.51. The core stator (Stator 1) inlet Mach numbers vary between 0.776 and 0.748. The bypass stator (Stator 3) inlet Mach numbers vary between 0.773 and 0.668. The max turning for this row is 6.6 drad (37.61 deg) occurring at the hub where the diffusion factor is less than 0.5.

PD287-7 IP Compressor

Table 3d2-III gives the important design numbers for the PD287-7 IP stage. Included in the table are inlet and exit relative Mach numbers and air angles and diffusion factors. The rotor inlet relative Mach numbers vary from 0.949 at the hub to 1.092 at the tip. Rotor turning is low varying spanwise between 1.5 drad (8.44 deg) to 0.6 drad (3.69 deg). The diffusion factors

Table 3d2-I.

PD287-11 stage-and-a-half design numbers.

		Rotor 1	Stator 1	Rotor 2	Stator 2	Stator 3 (bypass)
Inlet relative Mach No.	Hub	0.640	0.776	0.595	0.688	0.733
	Mean	0.790	0.770	0.675	0.580	0.693
	Tip	0.932	0.748	0.696	0.557	0.668
Exit relative Mach No.	Hub	0.661	0.495	0.534	0.501	0.489
	Mean	0.549	0.569	0.605	0.505	0.522
	Tip	0.633	0.586	0.650	0.510	0.504
Inlet relative air angle, drad (deg)	Hub	5.1 (28.99)	5.7 (32.62)	5.7 (32.46)	6.8 (38.88)	6.6 (37.61)
	Mean	7.3 (42.08)	6.4 (36.87)	5.6 (31.80)	3.7 (21.00)	6.1 (35.09)
	Tip	8.9 (51.07)	6.7 (38.58)	6.0 (34.43)	3.0 (17.07)	6.0 (34.37)
Exit relative air angle, drad (deg)	Hub	-1.1 (-6.54)	1.2 (6.80)	-1.0 (-5.87)	0	0
	Mean	1.0 (5.57)	1.7 (9.48)	4.3 (24.90)	0	0
	Tip	4.9 (28.25)	2.3 (12.98)	5.9 (33.53)	0	0
Diffusion factor	Hub	0.191	0.499	0.314	0.472	0.495
	Mean	0.511	0.444	0.178	0.259	0.426
	Tip	0.499	0.424	0.105	0.222	0.445

Table 3d2-II.
PD287-11 single-stage design numbers.

		Rotor 1	Stator 1	Stator 2 (bypass)
Inlet relative Mach No.	Hub	0.727	0.784	0.662
	Mean	0.849	0.746	0.610
	Tip	1.022	0.727	0.567
Exit relative Mach No.	Hub	0.616	0.566	0.452
	Mean	0.551	0.557	0.483
	Tip	0.663	0.524	0.476
Inlet relative air angle, drad (deg)	Hub	6.4 (36.4)	7.6 (43.6)	7.6 (43.4)
	Mean	8.2 (47.0)	7.2 (41.4)	6.6 (37.6)
	Tip	9.5 (54.6)	7.3 (41.7)	6.2 (35.5)
Exit relative air angle, drad (deg)	Hub	-1.3 (-7.3)	0	0
	Mean	3.9 (22.6)	0	0
	Tip	7.4 (42.4)	0	0
Diffusion factor	Hub	0.395	0.488	0.510
	Mean	0.521	0.463	0.416
	Tip	0.481	0.497	0.396

are also low ranging from a max of 0.368 at the hub to 0.301 at the tip. Stator Mach numbers vary from 0.467 to 0.449 at the inlet and from 0.396 to 0.437 at the exit. The stator turning is 5.8 drad (33.02 deg) at the hub and 4.8 drad (27.22 deg) at the tip. The corresponding values for stator diffusion factors are 0.330 and 0.205.

Table 3d2-III.
PD287-7 IP stage design numbers.

	Inlet Mach No.	Exit Mach No.	Inlet air angle, drad (deg)	Exit air angle, drad (deg)	Diffusion factor
Rotor					
Hub	0.949	0.670	10.9 (62.21)	9.4 (53.77)	0.368
Mean	1.024	0.765	11.2 (63.90)	10.3 (59.03)	0.312
Tip	1.092	0.828	11.3 (64.90)	10.7 (61.21)	0.301
Stator					
Hub	0.467	0.396	5.8 (33.02)	0	0.330
Mean	0.448	0.419	5.0 (28.40)	0	0.235
Tip	0.449	0.437	4.8 (27.22)	0	0.205

MECHANICAL DESIGN

The preliminary mechanical design of the fixed-pitch fans addressed three major areas of concern:

- Fan forward frame structural requirements
- Fan case containment requirements
- First-stage blade and wheel configuration:
  - Attachment stress
  - Airfoil stress
  - Disk stress
  - Dynamic vibration analysis

The preliminary design studies completed in the first two areas of concern are applicable to all Task II engines; however, the studies pertaining to blade and wheel configurations are limited to Task II engines PD287-11 and -51. A detailed analysis of the fan blades and wheel configuration for the variable pitch engines PD287-5, -6, and -7 is contained in Section 3d.

Fan Forward Frame Structural Requirements

The fan forward frame is the main structural engine element and provides support for the fan casing, inlet cowl, fan air ducts, fan rotor and gear assembly, and the high pressure core rotor thrust bearing. This structural support was configured to develop maximum stiffness to prevent performance degradation due to excessive clearances. The circular splitter, which separates bypass and core airflow, is an extremely stiff box section designed as a space truss to develop rotational stiffness, prevent shell ovalization at the compressor inlet, and control fan blade/case clearance. The engine forward mount is bolted to the rear wall of the circular splitter box section on all high bypass ratio EBF engines. The AW (PD287-51) engine thrust mount is bolted to the outer case of the fan support similar to the TF41. All of the forward supports are designed as an aluminum casting.

An exhaustive analysis of the deflection characteristics at various loading conditions of the entire fan case/forward support structure/fan rotor was beyond the scope of the preliminary design activity. In order to configure a reasonable forward support structure for weight analysis, it was necessary to make some simplifying assumptions relative to allowable structural deflections under normal flight loads.

The forward support structure for PD287-5 was selected for preliminary design analysis since it was the largest in diameter. The allowable deflection of the fan case at a position over the fan blade was selected to be 0.13 cm (0.050 in.). Nominal operating fan blade tip clearance is 0.38 cm (0.150 in.). A dimensional tolerance error allowance of 0.26 cm (0.100 in.) was estimated leaving an allowable maximum deflection of 0.13 cm (0.050 in.) before blade tip rub occurs.

The loading condition selected simulated a STOL takeoff and resulted in a 158 kN·m (1,400,000 in.-lb) moment imposed as a force couple at the fan case flange and reacted at the forward engine mount. The entire structure was modeled as a series of isoparametric quadrilateral finite elements and analyzed in an existing finite element analysis computer program. The structural model is shown in Figure 3d2-1.

The results indicated a fan case deflection of approximately 0.09 cm (0.035 in.) relative to the fan rotor support flange in the area above the fan blade. This result was sufficient to demonstrate structural feasibility.

All Task II QCSEE engines will comply with the containment requirements defined in FAA Advisory Circular No. AC33-1B. The containment requirements for the fan cases were established based on criteria developed to meet the containment requirements of MIL-E-5007C, which are equivalent to FAA requirements.

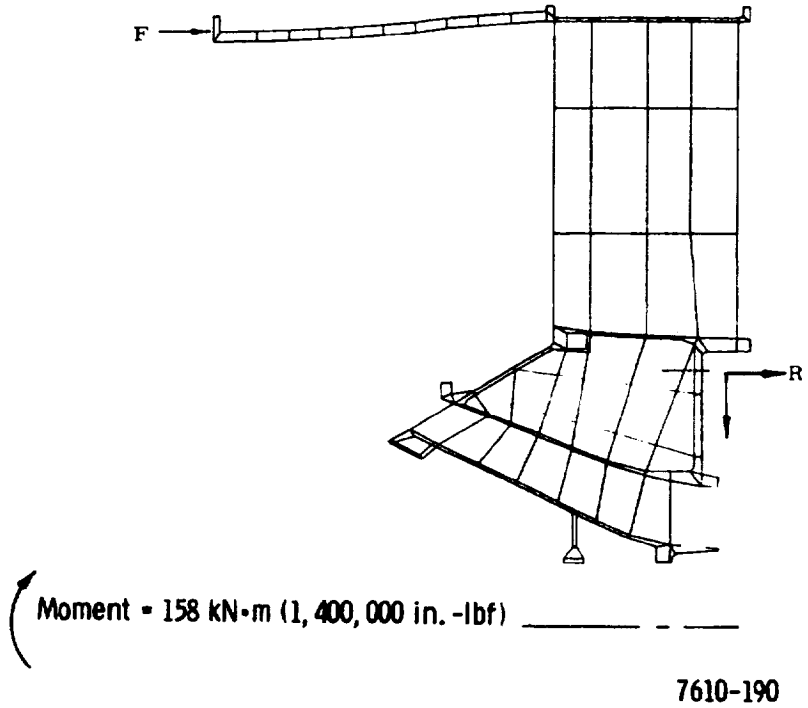

Figure 3d2-1. EBF forward frame finite element representation.

Substantiation of conformance with these containment requirements is based on an analytical relationship developed empirically and validated by developmental and service experience. This relationship equates the energy of the failed portion of a blade with the containment capability of the engine casing wall(s) which the failed blade must penetrate to escape from the engine. This relationship can be expressed as

$$E = k\, U\, e\, t^{2.5}$$

where:

- k = constant depending on units, 6.21×10^5 (3.26×10^6)
- E = failed blade energy, N•m (ft-lb_f)
- U = wall material ultimate tensile strengh, kN/m^2 ($lb_f/in.^2$)
- e = material elongation, %
- t = material thickness, cm (in.)

The material properties are defined at the maximum operating temperature of the casing wall, which is assumed to be at nominal thickness. The energy of the failed blade is calculated at the maximum operating speed. On the variable pitch fan blades, it was assumed that the blade spar would not fail but that the entire shell, including the fill and the leading edge sheaths, could separate from the spar. On the fixed pitch fans (PD287-11 and -51), failure was assumed to occur above the platform releasing the entire airfoil.

A summary of the required fan case thicknesses is given in Table 3d2-IV.

Table 3d2-IV.
Case containment thickness.

PD287-5	0.61 cm (0.241 in.) titanium
PD287-6	0.51 cm (0.201 in.) titanium
PD287-7	0.61 cm (0.241 in.) titanium
PD287-11	1.07 cm (0.42 in.) titanium
PD287-51	
1st stage	1.02 cm (0.40 in.) aluminum
2nd stage	0.71 cm (0.28 in.) aluminum
3rd stage	0.66 cm (0.26 in.) aluminum

In the EBF engines, the fan case is a 2.54-cm (1.00-in.) thick titanium honeycomb composite. The section modulus is more than equivalent to that required for containment in solid material. In addition, the inlet cowl bolt flange is placed above the blade to provide additional protection.

It is felt that the honeycomb material will be adequate considering the load spreading capability of honeycomb in conjunction with the tendency of the composite blade shells to shatter on impact. The casing above the fan blades on the AW engine (PD287-51) is solid aluminum at the required thickness.

Blade and Wheel Configuration—Fixed-Pitch Engines

A detailed discussion of the preliminary design of the variable pitch, Q-Fan blade and rotor configuration is contained in Section 3d3. This section will present the results of the preliminary design analysis utilized to configure the critical—i.e., first blade and wheel assembly, for Task II QCSEE engines PD287-11 and -51.

Design and Allowable Stresses

The fan design criteria used to establish the fan configuration was based on TF41 experience and the following design life requirements:

- Design life, 72 Ms (20,000 hr)—17,700 cycles
- Duty cycle
  - Maximum power operation—2.3% of total time
  - Climb power operation—6.5% of total time
  - Cruise power operation—91.2% of total time

- Environmental temperature distribution
  - Ambient temperature, 305°K (90°F) or higher—17.5% of time
  - Ambient temperature, 289°K (60°F) or higher—82.5% of time

Table 3d2-V compares the maximum stress levels of the first-stage rotor of PD287-11 with the allowable stresses previously determined. Tables 3d2-VI through 3d2-VIII are similar data applicable to the first, second, and third stages for PD287-51.

Vibration and Flutter

Figure 3d2-2 and 3d2-3 show, respectively, the results of a preliminary vibration analysis of PD287-11 and -51 first-stage fan blade/wheel combination. These analyses indicate that there are no damaging response modes in the operating range. The potential response point where the first bend mode is coincident with second engine order vibration is well above idle speed and below flight operation speed in both cases. The first-stage fan blades for both engines have also been analyzed and found to have sufficient flutter margin throughout the engine operating range as shown in Figures 3d2-4 and 3d2-5 (separation between the stall flutter boundary and estimated surge line show this margin).

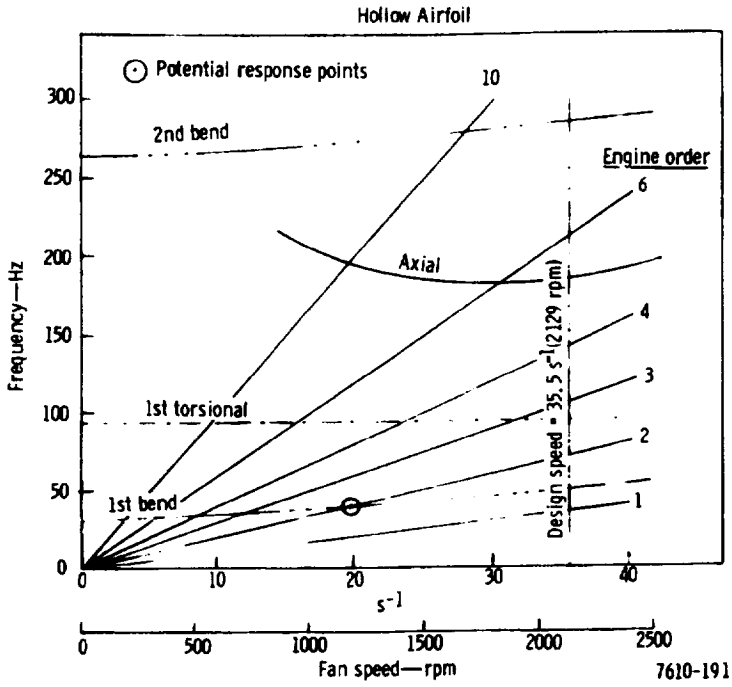

Figure 3d2-2. PD287-11 first-stage fan blade and frequency characteristics.

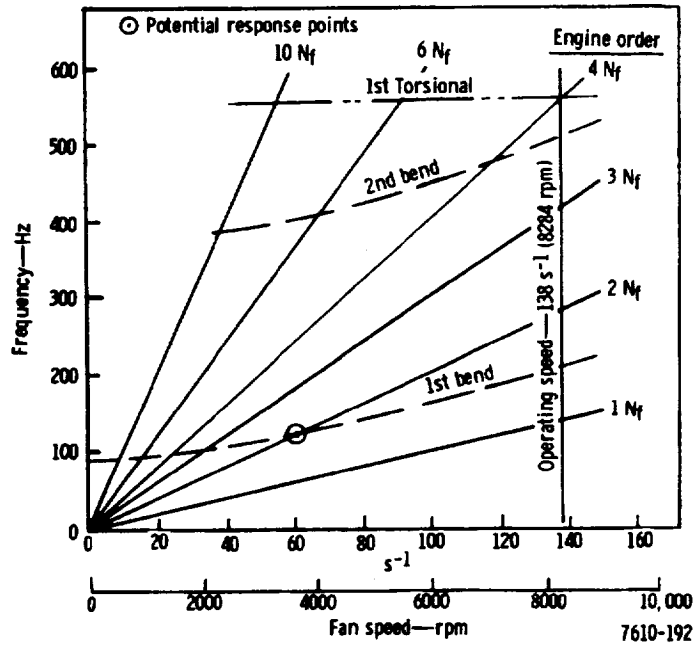

Figure 3d2-3. PD287-51 first-stage fan blade/disk frequency characteristics.

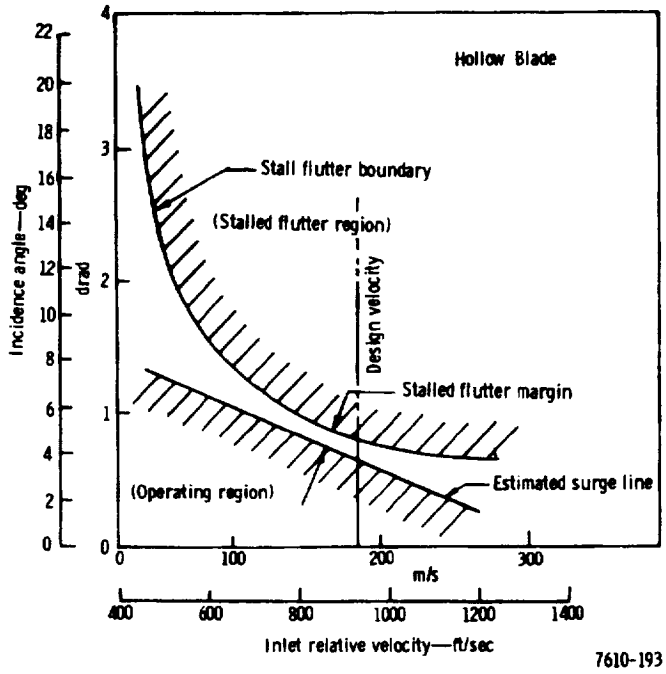

Figure 3d2-4. PD287-11 first-stage fan blade stall flutter margin.

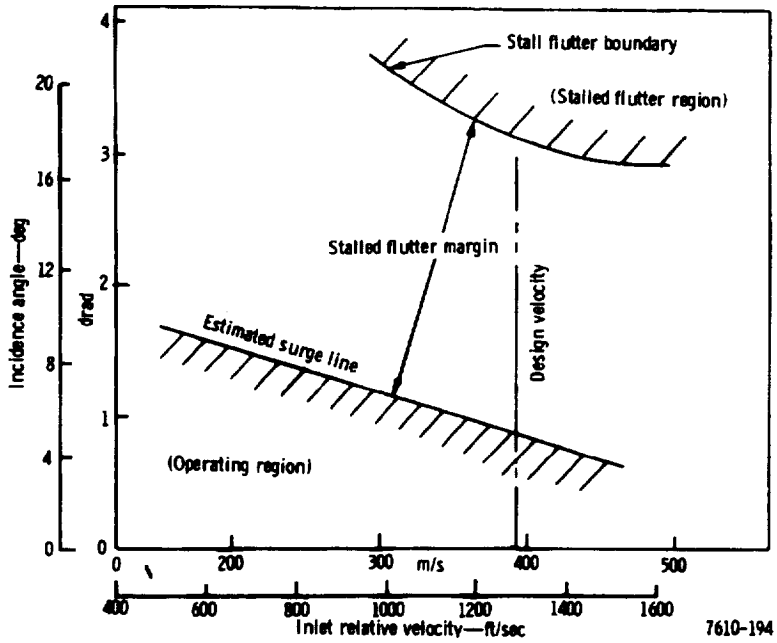

Figure 3d2-5. PD287-51 first-stage blade stall flutter margin.

Table 3d2-V.

PD287-11 first-stage hollow blade and wheel stresses.

Type of stress	Criteria, % 0.2% yield	Criteria, % Ultimate	Allowable stress, MN/m^2 (ksi)	Preliminary design stress, MN/m^2 (ksi)
Blade airfoil				
Direct tensile	60	---	462 (67)	110 (16)
Blade stalk				
Direct tensile	40	---	310 (45)	145 (21)
Blade attachment				
Bearing	50	---	386 (56)	303 (44)
Shear	45	35	296 (43)	97 (14)
Tensile	35	---	269 (39)	34 (5)
Heywood-Neuber fillet (17,000 cycles)	---	---	683 (99)	---
Fillet peak stress (17,000 cycles)	---	---	586 (85)	407 (59)
Wheel lug				
Bearing	50	---	386 (56)	303 (44)
Shear	45	35	296 (43)	76 (11)
Tensile	35	---	269 (39)	34 (5)
Heywood-Neuber fillet (17,000 cycles)	---	---	683 (99)	---
Fillet peak stress (17,000 cycles)	---	---	586 (85)	359 (52)
Wheel disk				
Average hoop	80	65	545 (79)	255 (37)
Web hoop	85	---	655 (95)	283 (41)
Rim hoop (17,000 cycles)	---	---	441 (64)	221 (32)
Bore hoop (17,000 cycles)	---	---	683 (99)	283 (41)
Web radial	85	---	655 (95)	179 (26)

Table 3d2-VI.

PD287-51 first-stage hollow blade and wheel stresses.

Type of stress	Criteria, % 0.2% yield	Criteria, % Ultimate	Allowable stress, MN/m^2 (ksi)	Preliminary design stress, MN/m^2 (ksi)
Blade airfoil				
Direct tensile	60	---	462 (67)	441 (64)
Blade stalk				
Direct tensile	40	---	310 (45)	117 (17)
Blade attachment				
Bearing	50	---	386 (56)	379 (55)
Shear	45	35	296 (43)	117 (17)
Tensile	35	---	269 (39)	248 (36)
Heywood-Neuber fillet (17,000 cycles)	---	---	683 (99)	---
Fillet peak stress (17,000 cycles)	---	---	586 (85)	586 (85)
Wheel lug				
Bearing	50	---	386 (56)	379 (55)
Shear	45	35	296 (43)	193 (28)
Tensile	35	---	269 (39)	165 (24)
Heywood-Neuber fillet (17,000 cycles)	---	---	683 (99)	---
Fillet peak stress (17,000 cycles)	---	---	586 (85)	586 (85)
Wheel disk				
Average hoop	80	65	545 (79)	531 (77)
Web hoop	85	---	655 (95)	648 (94)
Rim hoop (17,000 cycles)	---	---	441 (64)	400 (58)
Bore hoop (17,000 cycles)	---	---	683 (99)	676 (98)
Web radial	85	---	655 (95)	648 (94)

Table 3d2-VII.

PD287-51 second-stage hollow blade and wheel stresses.

Type of stress	Criteria, % 0.2% yield	Criteria, % Ultimate	Allowable stress, MN/m^2 (ksi)	Preliminary design stress, MN/m^2 (ksi)
Blade airfoil				
Direct tensile	60	---	462 (67)	---
Blade stalk				
Direct tensile	40	---	310 (45)	110 (16)
Blade attachment				
Bearing	50	---	386 (56)	379 (55)
Shear	45	35	296 (43)	159 (23)
Tensile	35	---	269 (39)	159 (23)
Heywood-Neuber fillet (17,000 cycles)	---	---	683 (99)	---
Fillet peak stress (17,000 cycles)	---	---	586 (85)	579 (84)
Wheel lug				
Bearing	50	---	386 (56)	379 (55)
Shear	45	35	296 (43)	152 (22)
Tensile	35	---	269 (39)	131 (19)
Heywood-Neuber fillet (17,000 cycles)	---	---	683 (99)	---
Fillet peak stress (17,000 cycles)	---	---	586 (85)	579 (84)
Wheel disk				
Average hoop	80	65	545 (79)	565 (82)
Web hoop	85	---	655 (95)	648 (94)
Rim hoop (17,000 cycles)	---	---	441 (64)	427 (62)
Bore hoop (17,000 cycles)	---	---	683 (99)	676 (98)
Web radial	85	---	655 (95)	634 (92)

Table 3d2-VIII.

PD287-51 third-stage hollow blade and wheel stresses.

Type of stress	Criteria, % 0.2% yield	Criteria, % Ultimate	Allowable stress, MN/m^2 (ksi)	Preliminary design stress, MN/m^2 (ksi)
Blade airfoil				
Direct tensile	60	---	462 (67)	---
Blade stalk				
Direct tensile	40	---	310 (45)	117 (17)
Blade attachment				
Bearing	50	---	386 (56)	352 (51)
Shear	45	35	296 (43)	83 (12)
Tensile	35	---	269 (39)	159 (23)
Heywood-Neuber fillet (17,000 cycles)	---	---	683 (99)	---
Fillet peak stress (17,000 cycles)	---	---	586 (85)	579 (84)
Wheel lug				
Bearing	50	---	386 (56)	352 (51)
Shear	45	35	296 (43)	214 (31)
Tensile	35	---	269 (39)	90 (13)
Heywood-Neuber fillet (17,000 cycles)	---	---	683 (99)	---
Fillet peak stress (17,000 cycles)	---	---	586 (85)	579 (84)
Wheel disk				
Average hoop	80	65	545 (79)	572 (83)
Web hoop	85	---	655 (95)	648 (94)
Rim hoop (17,000 cycles)	---	---	441 (64)	427 (62)
Bore hoop (17,000 cycles)	---	---	683 (99)	676 (98)
Web radial	85	---	655 (95)	648 (94)

3d3. Variable Pitch Fans

Three of the five propulsion systems selected for preliminary design during Task II used variable pitch fans (Q-Fans). The Q-Fan engines were:

- PD287-5: 1.25 fan pressure ratio
- PD287-6: 1.325 fan pressure ratio
- PD287-7: 1.25 fan pressure ratio (scaled core)

Hamilton Standard Division (HSD) of United Aircraft Corporation was responsible for the aerodynamics, acoustics, and mechanical design of PD287-5 and -6, while DDA scaled the 1.25 fan pressure ratio data provided by HSD for the PD287-7 propulsion system.

Figures 3d3-1 and 3d3-2 show the resulting preliminary designs of the 1.25 and 1.325 fan pressure ratio Q-Fans, respectively. Both systems are variable pitch fans with approximately 1.7 rad (100 deg) of blade angle travel from ground idle to full reverse pitch. Both systems have a forward mounted gear reduction system which reduces the low-pressure turbine speed by gear ratios of 3.89:1 for the 1.25 R_F and 2.96:1 for the 1.325 R_F fan designs. The pitch change mechanism is a mechanical gear harmonic drive which is powered by a hydraulic motor located in the fan Beta (blade angle) control unit.

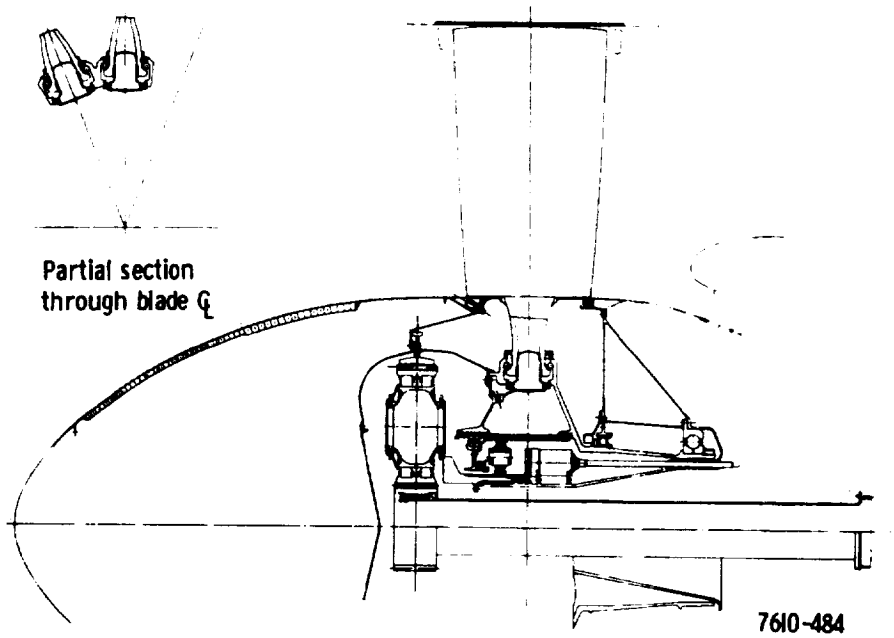

Figure 3d3-1. PD287-5 (1.25 R_F) Q-Fan layout.

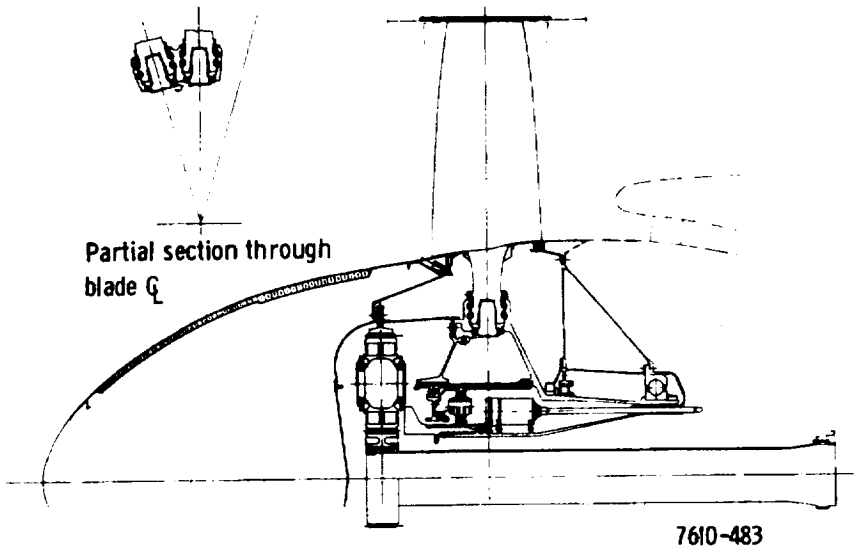

Figure 3d3-2. PD287-6 (1.325 R_F) Q-Fan layout.

The fans have the following design point characteristics:

Design parameters	PD 287-5	PD287-6
Fan pressure ratio, R_F	1.25	1.325
Fan power, MW (shp)	13.5 (18,140)	14.2 (19,050)
Fan tip speed, m/s (ft/sec)	229 (750)	282 (925)
Specific air flow, $\frac{kg/s}{m^2}$ $\left(\frac{lbm/sec}{ft^2}\right)$	195.3 (40)	195.3 (40)
Fan tip diameter, m (ft)	2.35 (7.71)	2.15 (7.05)

The aerodynamic and mechanical design of the Q-Fan is supported by an advanced axial flow fan aerodesign method and a continuous series of engineering investigations over the past four years. This approach covers:

- Several wind tunnel tests (including reverse thrust)
- Discussions and joint studies with engine, nacelle, and aircraft manufacturers
- Mechanical design trade-off studies
- Numerous aerodynamic designs with the manufacture of five different configurations
- Two models and two current full-scale acoustic tests
- Development of an acoustic prediction method
- Design, fabrication, and test (in process) of a 36 kN (8000-lbf) thrust class Q-Fan Demonstrator engine

The low-pressure ratio, variable pitch, Q-Fan concept is a relatively new subsonic propulsion approach. However, most of the major component technology discussed herein is based on proved concepts evolving from turboprop and ducted propeller experience.

AERODYNAMICS

The aerodynamics of the Q-Fan designs are presented in Subsection 3d3 of the Supplement to this report.

Blade Analysis

Velocity vector diagrams calculated at the leading and the trailing edges of each blade row were used to design the rotor and the stator blades. The establishment of the design vector diagrams and the aerodynamic flow path is an iterative solution which was completed for each of the two Q-Fans, using estimated streamlines and blade row loading distributions. An axisymmetric streamline analysis, outlined in the following paragraphs, was used to obtain the velocity vectors from which the rotor and stator blade elements were selected. The final selections of the loadings, flow paths and blade geometries were based on achieving high performance and low noise while remaining compatible with mechanical and engine matching constraints including inlet distortion.

The aerodynamic method of analysis used in the design of the two Q-Fans uses continuity, energy, and radial equilibrium equations. These equations account for streamline curvature and radial gradients of enthalpy and entropy but neglect the viscous terms in the following equation of motion:

$$C_m \frac{\partial C_m}{\partial m} \sin\phi + \frac{C_m^2}{R_c} \cos\phi - \frac{C_u^2}{r} + \frac{1}{\rho} \frac{\partial P}{\partial r} = 0$$

where

R_c is the streamline radius of curvature

and, $R_c = \frac{\partial \phi}{\partial m}$

and, $C_m = C_x^2 + C_r^2$

The definitions of these terms are shown on the general vector diagram of Figure 3d3-3.

The Q-Fan rotors have been designed with no flow convergence for the PD287-5 and with about 4% area convergence at the root for the PD287-6. Both Q-Fans have root convergence for the

fan duct stators and both have area convergence through the engine inlet stators. The degree of convergence selected for each blade row was to control velocity levels and profiles and to keep the blade loadings (diffusion factors) at levels that would yield adequate predicted surge margins. The design point diffusion factors for the two Q-Fans are listed in Table 3d3-I, which divides the flow into stream tubes with the fourth stream tube dividing the primary and secondary airflows.

As can be seen in Table 3d3-I, the PD287-6 diffusion factors are generally lower than those for the PD287-5. The diffusion factor is defined as:

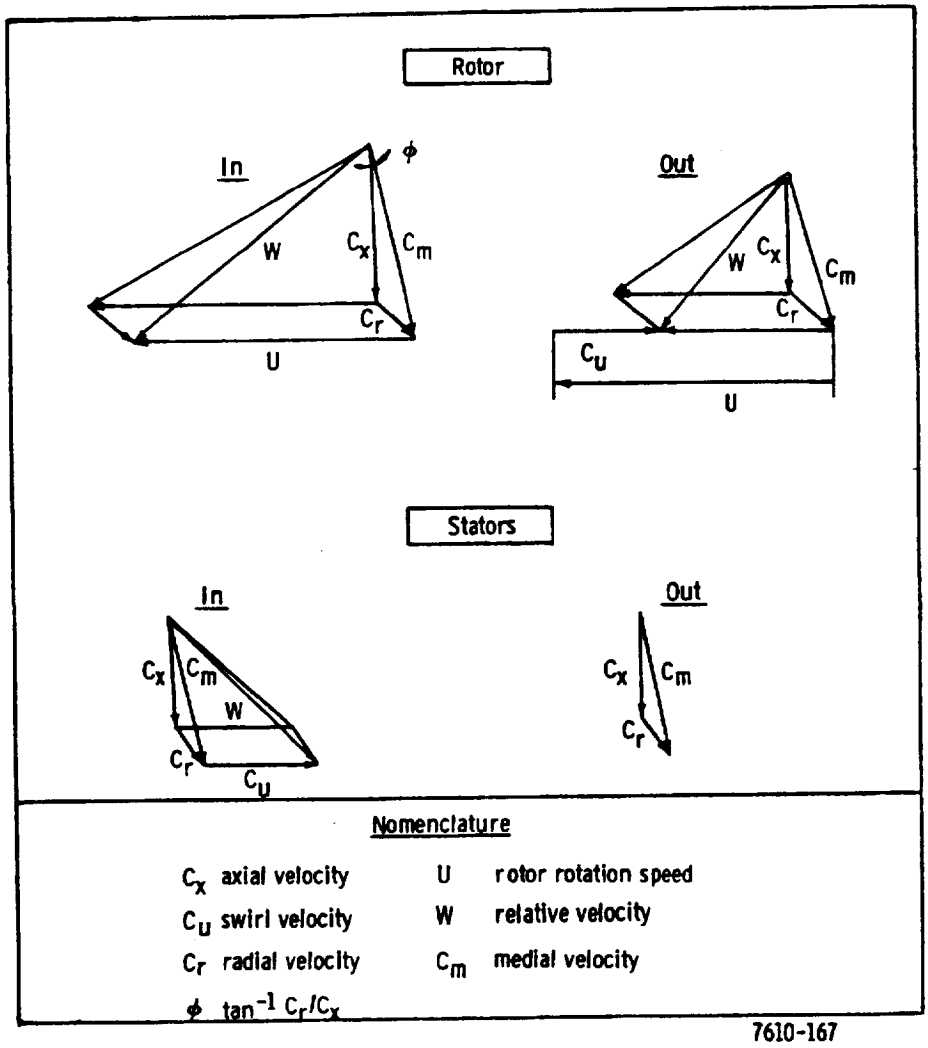

Figure 3d3-3. Vector diagram.

$$D_{rotor} = 1 - \frac{W_o}{W_i} + \frac{C_{u_o}}{2\,w_i}\,(\tau/b), \text{ and } D_{stator} = 1 - \frac{C_o}{C_i} + \frac{r_o C_{u_o} - r_o C_{u_i}}{2\,C_i\,(r_i + r_o)}\,(\tau/b)$$

where

r = local radius
W = relative velocity
C = absolute velocity
C_u = tangential velocity

and where subscripts

i = inlet to blade row
o = outlet from blade row
τ/b = gap/chord ratio

The principal velocity, pressure, and temperature distributions for the two Q-Fans at the design points are listed in Tables 3d3-II through 3d3-XIII. The data are presented for the entrance and exit to each blade row. These data are for stream tubes which divide the bypass airflow and the core engine airflow into equal increments.

Table 3d3-I.
Q-Fan design point diffusion factors.

Flow (%)		Design point diffusion factors					
		Rotor		Fan duct stators		Engine inlet stators	
PD287-5	PD287-6	PD287-5	PD287-6	PD287-5	PD287-6	PD287-5	PD287-6
0.00	0.00	0.344	0.483	---	---	0.449	0.409
53.12	53.95	0.532	0.483	0.359	0.317	---	---
100.00	100.00	0.478	0.459	0.338	0.282	---	---

Table 3d3-II.

1.25 R_F fan stage leading edge data.

Flow (%)	$\frac{r}{R_o}$ (%)	C_x m/s	C_x (ft/sec)	C_r m/s	C_r (ft/sec)	C_u m/s	C_u (ft/sec)	$M_{N_{rel}}$	ϕ drad	ϕ (deg)
0	46.2	179.92	(590.29)	1.92	(6.29)	0.0	(0.0)	0.631	0.10	(0.61)
53.12	79.6	188.66	(618.97)	6.33	(20.78)	↓	↓	0.796	0.34	(1.92)
100.00	100.0	185.14	(607.43)	3.25	(10.67)	↓	↓	0.893	0.18	(1.01)

Flow (%)	$\frac{r}{R_o}$ (%)	P N/m^2	P (lbf/ft^2)	T °K	T (°R)	P_{o_1} N/m^2	P_{o_1} (lbf/ft^2)	T_{o_1} °K	T_{o_1} (°R)
0	46.2	82831.50	(1729.97)	272.00	(489.63)	101314.56	(2116.00)	288	(518.70)
53.12	79.6	81115.19	(1694.13)	270.37	(486.70)	↓	↓	↓	↓
100.00	100.0	81820.50	(1708.86)	271.04	(487.91)	↓	↓	↓	↓

Table 3d3-III.

1.25 R_F fan stage trailing edge data.

Flow (%)	$\frac{r}{R_o}$ (%)	C_x m/s	C_x (ft/sec)	C_r m/s	C_r (ft/sec)	C_u m/s	C_u (ft/sec)	$M_{N_{rel}}$	ϕ drad	ϕ (deg)
0	46.2	172.81	(566.97)	3.50	(11.49)	104.48	(342.78)	0.516	0.20	(1.16)
53.12	80.2	161.41	(529.57)	11.76	(38.59)	118.24	(387.91)	0.512	0.73	(4.17)
100.00	100.0	159.59	(523.59)	-0.43	(-1.42)	101.24	(332.15)	0.596	0.03	(0.16)

Flow (%)	$\frac{r}{R_o}$ (%)	P N/m^2	P (lbf/ft^2)	T °K	T (°R)	P_o/P_{o_1}	T_o/T_{o_1}	η ad
0	46.2	89281.88	(1864.69)	278.83	(501.92)	1.12700	1.03822	0.91076
53.12	80.2	102413.31	(2138.95)	289.79	(521.65)	1.27673	1.07518	0.96249
100.00	100.0	105473.63	(2202.86)	293.46	(528.26)	1.27900	1.08021	0.90879

Table 3d3-IV.

1.25 R_F fan duct stator leading edge data.

Flow (%)	$\frac{r}{R_o}$ (%)	C_x m/s	C_x (ft/sec)	C_r m/s	C_r (ft/sec)	C_u m/s	C_u (ft/sec)	$M_{N_{abs}}$	ϕ drad	ϕ (deg)
6.24	57.9	146.39	(480.28)	5.30	(17.38)	101.10	(331.71)	0.525	0.36	(2.07)
53.12	84.3	164.70	(540.35)	0.17	(0.54)	112.53	(369.18)	0.584	0.01	(0.06)
100.00	103.3	154.80	(507.87)	-2.25	(-7.39)	97.97	(321.43)	0.532	-0.14	(-0.83)

Flow (%)	$\frac{r}{R_o}$ (%)	P N/m^2	P (lbf/ft^2)	T °K	T (°R)	P_o N/m^2	P_o (lbf/ft^2)	T_o °K	T_o (°R)
6.24	57.9	96737.63	(2020.41)	285.74	(514.36)	116745.13	(2438.27)	301.53	(542.79)
53.12	84.3	102650.38	(2143.90)	289.98	(522.00)	129351.13	(2701.56)	309.81	(557.70)
100.00	103.3	106827.00	(2231.13)	294.53	(530.19)	129581.25	(2706.36)	311.27	(560.31)

Table 3d3-V.

1.25 R_F fan duct stator trailing edge data.

Flow (%)	$\frac{r}{R_o}$ (%)	C_x m/s	C_x (ft/sec)	C_r m/s	C_r (ft/sec)	C_u m/s	C_u (ft/sec)	$M_{N_{abs}}$	ϕ drad	ϕ (deg)
6.24	64.1	137.58	(451.39)	9.07	(29.74)	-0.72	(-2.36)	0.402	0.66	(3.77)
53.12	86.6	191.07	(626.88)	4.58	(15.02)	0.67	(2.21)	0.558	0.24	(1.37)
100.00	102.6	188.31	(617.81)	-0.25	(-0.82)	1.64	(5.39)	0.548	-0.01	(-0.08)

Flow (%)	$\frac{r}{R_o}$ (%)	P N/m^2	P (lbf/ft^2)	T °K	T (°R)	P_o/P_{o_1}	T_o/T_{o_1}	η_{ad}
6.24	64.1	102349.19	(2137.61)	292.06	(525.73)	1.12948	1.04644	0.76359
53.12	86.6	104303.44	(2178.42)	291.61	(524.92)	1.27222	1.07518	0.94807
100.00	102.6	104641.00	(2185.48)	293.59	(528.49)	1.26698	1.08021	0.87276

Table 3d3-VI.

1.25 R_F fan engine inlet guide vane leading edge data.

Flow (%)	$\frac{r}{R_o}$ (%)	C_x m/s	C_x (ft/sec)	C_r m/s	C_r (ft/sec)	C_u m/s	C_u (ft/sec)	$M_{N_{abs}}$	ϕ drad	ϕ (deg)
0	42.2	161.45	(529.70)	-55.61	(-182.43)	114.29	(374.96)	0.614	-3.44	(-19.00)
2.08	44.1	151.66	(497.58)	-62.11	(-203.78)	118.29	(388.11)	0.603	-4.09	(-22.27)
4.16	45.9	145.62	(477.77)	-65.70	(-215.55)	121.06	(397.19)	0.597	-4.51	(-24.28)
6.24	47.7	141.81	(465.25)	-53.12	(-174.27)	122.88	(403.15)	0.579	-3.74	(-20.53)

Flow (%)	$\frac{r}{R_o}$ (%)	P N/m^2	P (lbf/ft^2)	T °K	T (°R)	P_o N/m^2	P_o (lbf/ft^2)	T_o °K	T_o (°R)
0	42.2	88487.31	(1848.10)	278.11	(500.63)	114181.50	(2384.73)	299.16	(538.52)
2.08	44.1	89994.38	(1879.57)	279.68	(503.46)	115050.06	(2402.87)	300.05	(540.12)
4.16	45.9	91104.88	(1902.77)	280.80	(505.48)	115906.00	(2420.75)	300.84	(541.54)
6.24	47.7	93043.19	(1943.25)	282.57	(508.65)	116745.13	(2438.27)	301.53	(542.79)

Table 3d3-VII.

1.25 R_F fan engine inlet guide vane trailing edge data.

Flow (%)	$\frac{r}{R_o}$ (%)	C_x m/s	C_x (ft/sec)	C_r m/s	C_r (ft/sec)	C_u m/s	C_u (ft/sec)	$M_{N_{abs}}$	ϕ drad	ϕ (deg)
0	38.2	138.94	(455.84)	-70.46	(-231.18)	0.00	(0.00)	0.459	-5.07	(-26.89)
2.08	40.2	145.01	(475.74)	-64.84	(-212.74)	-0.25	(-0.83)	0.467	-4.47	(-24.09)
4.16	42.0	152.12	(499.07)	-62.30	(-204.40)	-0.27	(-0.87)	0.484	-4.09	(-22.27)
6.24	43.7	142.41	(467.22)	-91.23	(-299.31)	-0.25	(-0.81)	0.498	-6.40	(-32.64)

Flow (%)	$\frac{r}{R_o}$ (%)	P N/m^2	P (lbf/ft^2)	T °K	T (°R)	P_o/P_{o1}	T_o/T_{o1}	η_{ad}
0	38.2	96836.13	(2022.47)	287.06	(516.75)	1.10412	1.03822	0.75243
2.08	40.2	97154.19	(2029.11)	287.47	(517.48)	1.11373	1.04130	0.75794
4.16	42.0	96917.19	(2024.16)	287.37	(517.29)	1.12266	1.04403	0.76466
6.24	43.7	97002.88	(2025.95)	287.27	(517.12)	1.13405	1.04644	0.78931

Table 3d3-VIII.

1.325 R_F fan stage leading edge data.

Flow (%)	$\frac{r}{R_o}$(%)	C_x m/s	C_x (ft/sec)	C_r m/s	C_r (ft/sec)	C_u m/s	C_u (ft/sec)	$M_{N_{rel}}$	ϕ drad	ϕ (deg)
0	48.0	192.19	(630.56)	33.06	(108.46)	0.0	(0.0)	0.722	1.72	(9.76)
53.95	80.4	186.48	(611.83)	11.49	(37.68)	↓	↓	0.891	0.62	(3.52)
100.00	100.0	184.74	(606.12)	0.26	(0.86)	↓	↓	1.021	0.01	(0.08)

Flow (%)	$\frac{r}{R_o}$(%)	P N/m^2	P (lbf/ft^2)	T °K	T (°R)	P_{o_1} N/m^2	P_{o_1} (lbf/ft^2)	T_{o_1} °K	T_{o_1} (°R)
0	48.0	79868.94	(1668.10)	269.18	(484.55)	101314.56	(2116.00)	288.15	(518.70)
53.95	80.4	81495.00	(1702.06)	270.74	(487.35)	↓	↓	↓	↓
100.00	100.0	81903.75	(1710.60)	271.12	(488.05)	↓	↓	↓	↓

Table 3d3-IX.

1.325 R_F fan stage trailing edge data.

Flow (%)	$\frac{r}{R_o}$(%)	C_x m/s	C_x (ft/sec)	C_r m/s	C_r (ft/sec)	C_u m/s	C_u (ft/sec)	$M_{N_{rel}}$	ϕ drad	ϕ (deg)
0	51.2	155.54	(510.31)	18.21	(59.75)	132.44	(434.52)	0.463	1.17	(6.68)
53.95	81.9	167.09	(548.19)	20.23	(66.36)	120.22	(394.44)	0.586	1.21	(6.90)
100.00	100.0	140.41	(460.67)	-1.72	(-5.64)	98.04	(321.64)	0.665	-0.12	(-0.70)

Flow (%)	$\frac{r}{R_o}$(%)	P N/m^2	P (lbf/ft^2)	T °K	T (°R)	P/P_o	T/T_o	η_{ad}
0	51.2	94986.44	(1983.83)	286.24	(515.26)	1.200304	1.066124	0.81084
53.95	81.9	108094.63	(2257.61)	294.52	(530.16)	1.36218	1.09608	0.96150
100.00	100.0	109208.75	(2280.87)	301.07	(541.96)	1.27220	1.09556	0.74564

Table 3d3-X.

1.325 R_F fan duct stator leading edge data.

Flow (%)	$\frac{r}{R_o}$(%)	C_x m/s	C_x (ft/sec)	C_r m/s	C_r (ft/sec)	C_u m/s	C_u (ft/sec)	$M_{N_{abs}}$	ϕ drad	ϕ (deg)
7.95	65.8	169.24	(555.26)	2.38	(7.80)	108.98	(357.54)	0.592	0.14	(0.80)
53.95	86.7	176.30	(578.43)	3.21	(10.53)	113.61	(372.73)	0.610	0.18	(1.04)
100.00	104.0	120.15	(394.20)	1.88	(6.18)	94.27	(309.27)	0.437	0.16	(0.90)

Flow (%)	$\frac{r}{R_o}$(%)	P N/m^2	P (lbf/ft^2)	T °K	T (°R)	P_o N/m^2	P_o (lbf/ft^2)	T_o °K	T_o (°R)
7.95	65.8	98804.69	(2063.58)	288.10	(518.61)	125208.44	(2615.03)	308.27	(554.96)
53.95	86.7	107317.63	(2241.38)	293.91	(529.07)	138008.38	(2882.37)	315.84	(568.54)
100.00	104.0	113049.63	(2361.09)	304.06	(547.35)	128892.31	(2691.97)	315.69	(568.27)

Table 3d3-XI.

1.325 R_F fan duct stator trailing edge data.

Flow (%)	$\frac{r}{R_o}$(%)	C_x m/s	C_x (ft/sec)	C_r m/s	C_r (ft/sec)	C_u m/s	C_u (ft/sec)	$M_{N_{abs}}$	ϕ drad	ϕ (deg)
7.95	70.9	147.60	(484.24)	-0.39	(-1.29)	-1.55	(-5.07)	0.427	-0.03	(-0.15)
53.95	89.4	197.36	(647.52)	3.82	(12.54)	-0.70	(-2.28)	0.572	0.19	(1.11)
100.00	104.0	162.40	(532.82)	-0.24	(-0.80)	0.57	(1.86)	0.466	-0.02	(-0.09)

Flow (%)	$\frac{r}{R_o}$(%)	P N/m^2	P (lbf/ft^2)	T °K	T (°R)	P_o/P_{o_1}	T_o/T_{o_1}	η ad
7.95	70.9	107824.44	(2251.96)	297.44	(535.42)	1.20636	1.06991	0.78846
53.95	89.4	110070.69	(2298.88)	296.42	(533.59)	1.35624	1.09608	0.94730
100.00	104.0	110484.56	(2307.52)	302.55	(544.61)	1.26530	1.09556	0.72825

Table 3d3-XII.

1.325 R_F fan engine inlet guide vane leading edge data.

Flow (%)	$\frac{r}{R_o}$(%)	C_x m/s	C_x (ft/sec)	C_r m/s	C_r (ft/sec)	C_u m/s	C_u (ft/sec)	$M_{N_{abs}}$	ϕ drad	ϕ (deg)
0	51.2	151.09	(495.69)	-13.50	(-44.30)	132.44	(434.52)	0.593	-0.89	(-5.11)
2.65	53.3	153.97	(505.16)	-21.23	(-69.66)	128.77	(422.48)	0.594	-1.38	(-7.85)
5.30	55.2	158.18	(518.96)	-26.93	(-88.36)	126.70	(415.68)	0.602	-1.70	(-9.66)
7.95	57.0	164.40	(539.37)	-14.54	(-47.70)	125.63	(412.16)	0.611	-0.88	(-5.05)

Flow (%)	$\frac{r}{R_o}$(%)	P N/m^2	P (lbf/ft^2)	T °K	T (°R)	P_o N/m^2	P_o (lbf/ft^2)	T_o °K	T_o (°R)
0	51.2	95865.25	(2002.19)	286.99	(516.61)	121607.75	(2539.83)	307.20	(553.00)
2.65	53.3	96704.13	(2019.71)	287.13	(516.86)	122791.31	(2564.55)	307.44	(553.41)
5.30	55.2	97060.38	(2027.15)	286.98	(516.60)	123998.75	(2589.77)	307.82	(554.10)
7.95	57.0	97321.50	(2032.60)	286.85	(516.36)	125208.44	(2615.03)	308.30	(554.96)

Table 3d3-XIII.

1.325 R_F fan engine inlet guide vane trailing edge data.

Flow (%)	$\frac{r}{R_o}$(%)	C_x m/s	C_x (ft/sec)	C_r m/s	C_r (ft/sec)	C_u m/s	C_u (ft/sec)	$M_{N_{abs}}$	ϕ drad	ϕ (deg)
0	50.5	160.11	(525.30)	-20.65	(-67.76)	-2.79	(-9.17)	0.469	-1.29	(-7.35)
2.65	52.4	162.70	(533.80)	-23.40	(-76.78)	-1.10	(-3.60)	0.478	-1.44	(-8.19)
5.30	54.2	165.46	(542.84)	-26.18	(-85.89)	0.24	(0.77)	0.487	-1.76	(-8.99)
7.95	56.0	165.62	(543.36)	-33.55	(-110.08)	2.02	(6.64)	0.492	-2.03	(-11.45)

Flow (%)	$\frac{r}{R_o}$(%)	P N/m^2	P (lbf/ft^2)	T °K	T (°R)	P_o/P_{o_1}	T_o/T_{o_1}	η_{ad}
0	50.5	103033.00	(2151.89)	294.21	(529.61)	1.18278	1.06612	0.74402
2.65	52.4	103495.31	(2161.55)	293.97	(529.18)	1.19465	1.06392	0.77986
5.30	54.2	103885.19	(2169.69)	293.83	(528.93)	1.20633	1.06825	0.80754
7.95	56.0	104749.50	(2187.74)	294.06	(529.35)	1.21964	1.06991	0.83579

COMPONENT DESIGN

The Q-Fans for Task II included a 1.25 R_F and a 1.325 R_F design as shown by the preliminary design layouts of Figures 3d3-1 and 3d3-2. The design point characteristics of these Q-Fans are given in Table 3d3-XIV.

Table 3d3-XIV.
Q-Fan design point characteristics.

Parameters	1.25 R_F	1.325 R_F
Fan tip diameter, m (ft)	2.35 (7.71)	2.15 (7.05)
Fan blade inlet hub/tip ratio	0.46	0.48
Number of blades	17	23
Number of fan duct EGV's	11	15
Fan shp, MW (shp)	13.5 (18,140)	14.3 (19,200)
Tip speed, m/s (ft/s)	229 (750)	282 (925)
Gear ratio	3.89	2.96

The Q-Fan design major assemblies consists of the rotor assembly (blades, disk, and retention), gear-train assembly, pitch change actuator assembly, and support structure assembly. Subsection 3d3 of the Supplement to this report contains discussions of the Q-Fan component weights, the blade loadings and stresses, and the power transmission bearings.

Rotor Assembly

Blade Construction and Materials

The general character of the spar-shell blade is shown in Figure 3d3-4. The spar is the central structural member and is made from one piece of titanium tubing from the round, flanged retention area to the flattened tip. The spar is proportioned in width and wall thickness to provide a proper balance between durability, dynamic response, and weight. The shell completely encloses the spar, forms the outer airfoil contour, and is only semistructural in comparison to the spar. It is made from layers of preimpregnated boron-epoxy tape, compacted,

and cured as a detail. The number and orientation of the layers are varied along the blade length in proportion to the spar dimensions. The shell halves are bonded to each other and to the spar with a flocked epoxy adhesive. The leading edge of the shells are protected from foreign object damage by a stainless steel sheath which covers about 25% chord on the face side and 10% chord on the camber side. The sheath is bonded to the spar-shell assembly and is solid from the leading edge back to about 5% chord to provide blend repair. The flanks of the shells are coated with polyurethane. Both the shell and spar cavities are filled with a foamed-in-place polyurethane filler.

Blade Geometry

The important geometric characteristics of the blade are shown in Figures 3d3-21 and 3d3-24 of the Supplement to this report for PD287-5 and -6, respectively. A cross section of the leading edge protection at the 0.8 radius is shown in Figure 3d3-5. This general geometry—which applies to the entire blade length—has evolved from experimental evaluations of various leading edge shapes over the spectrum of foreign objects ranging from sand to two-pound birds. The combination of this leading-edge geometry, a boron-epoxy shell, and a solid titanium spar and retention is believed capable of ingesting the full scope of foreign objects currently specified in FAA Advisory Circular 33.

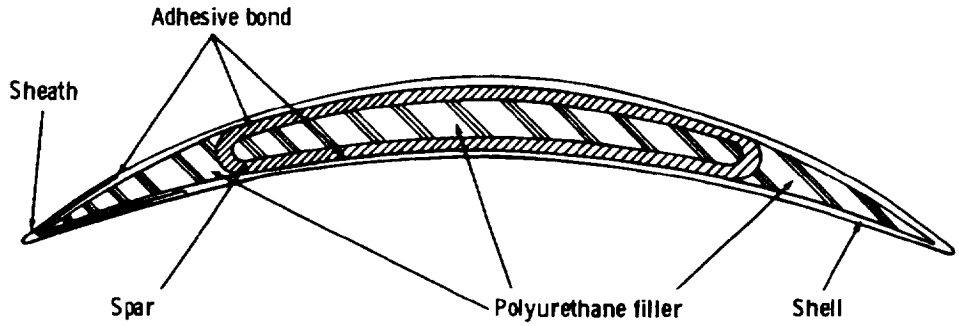

Figure 3d3-4. Typical fan blade spar shell cross section.

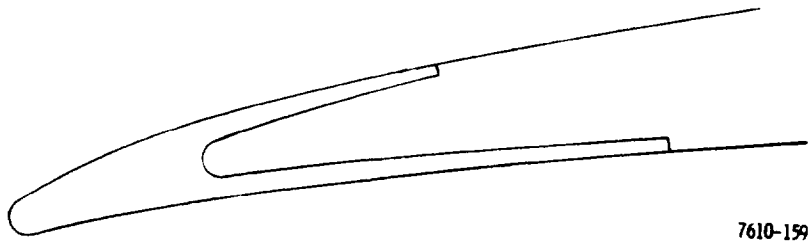

Figure 3d3-5. Q-Fan blade leading edge at 0.8 radius.

Blade Retention

The requirement of variable pitch necessitates the use of a round blade retention method and the inclusion of an antifriction bearing. The 1.25 R_F fan blade retention is a configuration that has been in service on the OV-10 aircraft for six years and has successfully accumulated 36 Gs (1,000,000 flight hours). Blade retention is achieved by an angular contact ball bearing with an integral outer race in the disk and a split inner steel race on the titanium spar. The outer race is induction hardened to Rc-56 minimum in the region of ball contact. The inner race is through-hardened to Rc-56 minimum. The 1.325 R_F fan blade retention shown on the fan assembly drawing has a two-row bearing to support the blade loading in the smaller pitch dimension resulting from the higher number of blades (23) being inserted in the same hub diameter.

A comparison of the loading and Hertz stress in the blade retentions is given in Table 3d3-XV. The Q-Fan blade retentions are well within the operating envelope of the service-proven configurations.

Table 3d3-XV.
Variable pitch retention comparison.

	1.25 R_F	33LF
Pitch diameter, cm (in.)	10.3 (4.040)	12.3 (4.860)
Ball diameter, cm (in.)	1.3 (0.500)	1.4 (0.563)
Number of balls	25	25
Centrifugal load/ball, N (lbf)	5338 (1200)	11,032 (2480)
Steady bending load/ball, m·N (in.-lbf)	81 (720)	86 (760)
Cyclic bending load/ball, m·N (in.-lbf)	29 (260)	43 (380)
Relative Hertz stress	0.92	1.00

Rotor Disk Assembly

The disk is a fully machined component made from D6AC vacuum-melted steel. It is heat treated to a hardness of Rc 40-44. The one exception to this hardness is in the integral retention race which is induction hardened locally in the blade retention race areas. The stresses in the barrel are determined by well-developed and proven ring, beam, and shell analysis methods—all of which are computerized. The influence of the static disk stiffness on the fundamental blade bending frequencies is calculated and included in the prediction of blade response.

Blade Concept

The spar/shell fan blade concept has evolved from V/STOL turboprop technology where—since the early 1960's—some 20 different lightweight blade designs have been manufactured with fiberglass/epoxy airfoil shells bonded to a metallic (steel, Al, Ti) and usually hollow spar. The in-service experience with this blade concept has been outstanding.

In recent years, HSD has been applying this concept to advanced fan blades and this effort has evolved both boron/epoxy and Borsic aluminum shells with titanium, steel, and aluminum spars. The technology base for this fan blade concept is being significantly broadened by current activities which include—in addition to a continuing in-house research and development program—an Air Force-sponsored development program, NASA-sponsored programs on foreign object damage testing, a 1.8-m (6-ft) diameter Q-Fan/fan stage test, and a Q-Fan demonstrator engine test.

Gear Reduction

Gear Train Configuration

The gear train design selected for both Q-fan designs is a star-type planetary gear train located forward of the fan rotor. The gear trains are designed for a useful life of 1.08 Gs (30,000 hr), are based on the typical STOL mission profile specified by NASA. The design point maximum continuous sizing for the gear trains are shown in Table 3d3-XVI.

The star-type planetary gear train has a floating input gear, stationary planet gear support carrier, and a rotating ring gear output. A four planet system was configured for the PD287-5 engine as the maximum number of planets which can be accommodated in a star arrangement at the defined reduction ratio. The required reduction ratio could be obtained, using a five-planet epicyclic arrangement (rotating carrier output/stationary ring gear). However, the carrier rotational speed results in excessively high centrifugal loads on the planet bearings.

Table 3d3-XVI.
Gear train sizing.

Parameters	1.25 R_F	1.325 R_F
Power, MW (shp)	13.5 (18,140)	14.3 (19,200)
Output speed, s^{-1} (rpm)	31 (1860)	42 (2520)
Input speed, s^{-1} (rpm)	121 (7250)	124 (7460)
Output torque, kN·m (lbf·ft)	69.3 (51,200)	54.2 (40,000)
Gear ratio	3.89	2.96
Number of planet gears	4	5
Type of gears	Spur	Spur

The gear reduction stage is mounted forward on the fan disk for the following reasons.

- Envelope restrictions are minimal, thus allowing gearing and bearings to be selected on a basis of performance and weight.
- The reduction assembly is readily available for maintenance requirements and can be constructed in a modular-type configuration for rapid removal and replacement.

Over the past 15 years HSD has developed a series of power reduction stages based on a system of controlled flexibility of the gear support. This flexibility allows the meshing teeth to better conform to each other and produces a more uniform pressure ellipse over the full tooth length. This results in a lightweight gear reduction without the detrimental effects of rigid construction which result in gear tooth end loading and adverse planet load sharing. This controlled flexibility is obtained by supporting the star-type planet gears in a deflection-compensated carrier assembly.

Torque on the fixed star-type assembly is reacted through deflection-balanced titanium planet carrier beams located between the planet gears. Titanium straps, in turn, connect these beams with the planet bearings. This construction not only minimizes face misalignment, but allows the design of the deflection balanced beams to have a relatively low spring rate. This, in turn, results in a more uniform load sharing between the planet gears.

Power is transmitted from the low-pressure turbine to a floating sun gear which is driven through a central flexible spline. The sun gear is centered by the planet teeth and is capable of aligning with the planet gear tooth profile.

Power is extracted from the ring gear central flange web through shear bolts and transferred to the rotor disk through the rotating gear case. This central extraction prevents ring gear torsional deflection, and the flexible large diameter gear case member isolates disk deflections from the ring gear.

A front cover is provided which has been designed to produce equal stiffness to that of the gear case member. This is done to ensure that the ring gear will deflect uniformly across the full tooth profile when deflected by gear mesh separation forces.

The ring gear section has been sized to limit radial deflections that are the result of tooth separation, bending loads, and centrifugal loading of the rotating ring. This deflection—when combined with thermal growth and dimensional tolerances—is sufficient to prevent the ring gear from exceeding permissible tooth meshing limits.

The spur gearing used has a tooth form with a 0.44-rad (25-deg) pressure angle, a 5.3 pitch for the PD287-5 engine, and a 6.0 pitch for the PD287-6 engines. These designs have pitch-line velocities at the rated conditions of 73 m/sec (14,353 ft/min) and 88 m/sec (17,265 ft/min),

respectively. Gear tooth geometry for the four-planet PD287-5 engine has been selected to provide simultaneous meshing of the planets with the ring gear and simultaneous meshing of the planets with the sun gear. These two meshing actions are phased so as to prevent simultaneous meshing of the ring gear and sun gear on the planet gear. Analyses of gear train traveling wave vibration modes indicate that the meshing in sequence or opposite phases provide the only other possibilities in a four-planet system. However, these options may promote undesirable vibration mode shapes. The gear tooth geometry for the five-planet (2.96 ratio) PD287-6 engine has been selected to provide for a star-shaped meshing firing order (i.e., 1-3-5-2-4) for both the planet/ring gear and planet/sun gear meshes. These two meshes have also been phased to preclude simultaneous planet meshing with the ring and sun gear. Preliminary vibration analysis indicates that gear vibration responses are acceptable for both gear trains.

The gear design configuration data is shown in Tables 3d3-XVII and 3d3-XVIII; these designs are for stress levels consistent with current AGMA allowable limits, surface durability, and unidirectional or reverse bending stresses. Scoring limits are within AGMA ratings and HSD experience.

Table 3d3-XVII.
PD287-5 gear configuration data.

	Sun gear	Planet gear	Ring gear
Number of teeth	40	58	156
Pitch diameter	19.17 cm (7.5472 in.)	27.80 cm (10.9434 in.)	74.76 cm (29.4340 in.)
Face width	9.90 cm (3.90 in.)	9.53 cm (3.75 in.)	8.26 cm (3.25 in.)
Speed at rating	121 s^{-1} (7264 rpm)	84 s^{-1} (5010 rpm)	31 s^{-1} (1868 rpm)

Gear Design Comparison

HSD has been active in aircraft power reductions and has accumulated design data backed by operating experience for varied turboprop reductions that covers a broad range of requirements and design executions. Table 3d3-XIX relates the critical design parameters for the QCSEE gear reduction to other aircraft power reductions that have been developed by HSD. This table has been unitized so that the ratio of the specific design criterion of the proposed QCSEE reduction to that of the comparable gearbox can be readily distinguished.

All ratios represent $\frac{\text{reference gearbox}}{\text{proposed QCSEE reduction}}$

Table 3d3-XVIII.
PD287-6 gear configuration data.

	Sun gear	Planet gear	Ring gear
Number of teeth	53	52	157
Pitch diameter	22.44 cm (8.833 in.)	22.01 cm (8.667 in.)	66.46 cm (26.1667 in.)
Face width	6.86 cm (2.70 in.)	6.86 cm (2.70 in.)	5.59 cm (2.20 in.)
Speed at rating	125 s^{-1} (7465 rpm)	127 s^{-1} (7609 rpm)	42 s^{-1} (2520 rpm)

Table 3d3-XIX shows that all of the basic design criteria for power gear reductions are within experience levels. The basic concept of gear support is taken directly from developed power reductions.

Comments On Table 3d3-XIX.

Output Torque

Output torque represents the strongest factor in determining the physical size of a reduction. Gear reduction weight varies directly with this parameter. Table 3d3-XIX shows that HSD experience includes planetary reducers that have operated up to 80% of the QCSEE requirements; other experience in the Sikorsky Division greatly exceeds the QCSEE requirements.

Dynamic Loading

Dynamic loading varies as a function of pitch-line velocity, gear manufacturing quality, and load and gear size. HSD uses a modified Buckingham analysis to establish this factor. Gear quality is controlled by HSD gear specifications and is equivalent to AGMA quality 12 for lead, runout, spacing, and profile tolerances. Appropriate involute modifications to preclude scoring risk are incorporated.

Bending Stress

Bending stress limits are established through the use of a modification of the classical Lewis equation. Dynamic loading and root concentration factors are employed, using the high point of single tooth contact.

Table 3d3-XIX.
Spur-type power gear comparison.

Parameters	PD285-5	PD285-6	First-stage 73EGB1 gearbox	Second-stage 73EGB1 gearbox	First-stage XC-142 gearbox	Second-stage XC-142 gearbox	First-stage VC400 gearbox	Second-stage VC400 gearbox
Output torque, kN·m (in-lb)	69 (614,000)	54.2 (480,190)	4.46 (39,500)	19.7 (174,000)	5.6 (49,800)	24.6 (218,000)	9.8 (86,640)	43 (382,000)
Dynamic loading	1.00	1.00	1.15	1.17	1.10	1.05	1.20	0.95
Bending stress	Base-point reference	1.00	0.85	0.77	0.91	1.00	0.86	0.86
Hertz stress		1.00	0.94	0.94	0.96	1.01	1.00	1.01
Meshing velocity		1.21	1.24	0.51	1.24	0.38	0.83	0.26
Scoring flash temperature		1.00	1.09	1.02	1.09	1.05	1.00	0.85
Face width/pitch dia ratio		1.00	1.00	0.80	1.30	0.66	1.76	1.00
Gear efficiency evaluation		1.00	1.02	1.00	1.02	1.00	1.02	1.00
Load share		1.00	N/A	1.04	N/A	1.04	0.87	1.04
Quill spline misalignment		1.00	1.00	1.00	1.00	1.00	1.00	1.00
Quill contact stress	1.0	1.00	1.00	1.00	1.00	1.00	1.00	1.00

Gear stress limits are consistent with AGMA allowables associated with AMS-6256 vacuum melt materials. However, HSD has run higher stress levels than these for various conditions. Proper relationship between required and allowable cycles for these conditions are maintained to keep the design within established limits.

Hertz Stress

Hertz stress calculations conform to standard Hertzian theory with dynamic effects included in the applied tooth loading. Operational gear reductions when designed to conform to this method of evaluation have never scored, worn, or failed when operating within the design schedule requirements.

Meshing Velocity

Industry has established generally accepted limiting pitch-line velocities for various types of gearing.

Scoring

The scoring index is based on Kelly Flash temperature predictions. This criterion empirically calculates the tooth surface temperature by evaluating the parameters of tooth sliding velocities, tooth load, tooth surface finish, and lubricating oil temperatures. The method used in all cases is based on the high and low points of single-tooth contact.

Face Width/Pitch Diameter Ratio

This factor is affected by the ability of the gearing to maintain a uniform contact pressure pattern across the full-tooth profile.

The major cause of tooth end loading in high quality gearing (where machined tooth lead errors have been minimized) results from gear mounting and case deflections. Increased stiffness or controlled flexibility can be used to reduce this effect in gear reductions. In all power reductions that have been built by HSD the controlled flexibility approach has been selected.

Gear Efficiency

Gear efficiency calculations are made on all power gearing produced at HSD. These values are used in determining scoring and efficiency factors. (Gear reduction efficiency also is considered in the following discussion of the lubrication system. Table 3d3-XIX shows that expected gear tooth efficiency calculations for the QCSEE reduction is consistent with previous power reductions.

Load Share

Load share is the factor used in defining the relative load distribution within the planet gearing. This value is established by determining carrier flexibilities, machining quality, and reduction size effects.

Quill Spline Misalignment and Contact Stressing

The quill shaft drive for the floating sun gear uses a floating spline torque coupling. This type coupling has been used on all HSD power gear reductions. The gear reduction forward concept for the QCSEE reducer allows ample length for this feature.

Lubrication and Cooling System

Lubrication System

The Q-Fan lubrication system is independent from that of the core engine. Oil which has been cooled and filtered is fed into the rotor support case at conventional lubrication pressures and distributed to the gear meshes, bearings, and pitch change system via pressure jets. The retention, having a very low duty cycle, is lubricated by a small residual head of oil. The retention seal is a service-proven design employed on propellers for several years. Blade seal pressure is established by controlling the oil head over the blade retention through the drain-off holes located in the hub-to-gear case interface. Oil is removed from the rotating assembly through the use of a pump located at the maximum radial point in the gear support housing. This oil is transferred to the rotor support housing where it is scavenged by the engine-mounted pump shown in Figure 3d3-6.

The fan rotor shaft seal uses a pressure-balanced carbon face seal operating on a steel runner. This approach is consistent with current engine technology in that running velocities are under 35.6 m/sec (7000 ft/min).

The power transmission efficiency has been calculated for the rotor assembly and the gear reduction. Power loss values for power dependent loss, speed dependent loss, and churning have been made, using analytical methods that are supported by gear train experimental test data. The following typical design features have been incorporated into the assembly and will contribute to high overall efficiency.

- The rotating gear case of the forward-mounted reduction assembly will centrifugally hold oils released from the gear meshes and bearings. This concept will eliminate oil fall back and re-impacting by the gearing.

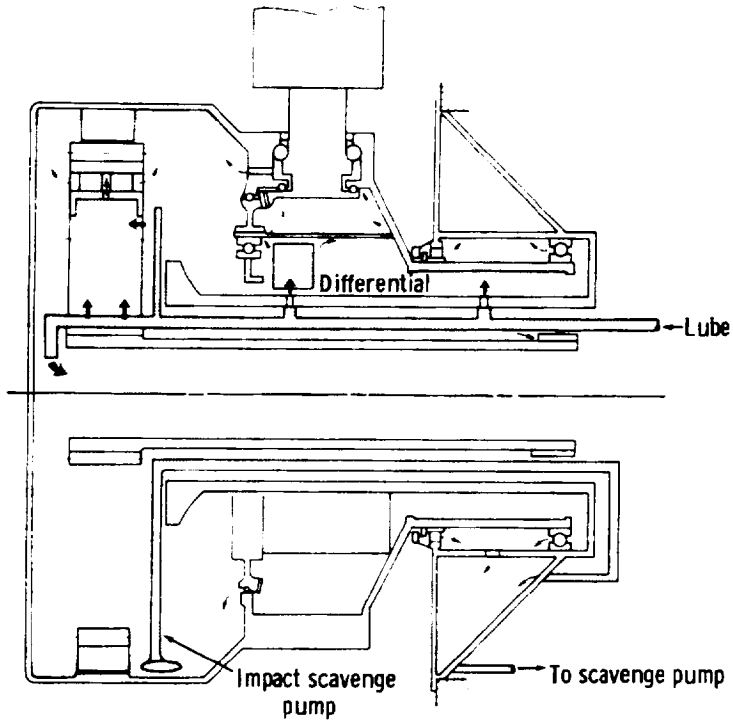

Figure 3d3-6. Lubrication system schematic.

- Lubrication oil cooling is provided by air-to-oil heat exchangers which by proper sizing can maintain low oil inlet temperatures with reduced cooling oil flow rates. Power gear reduction test data have demonstrated that within the flow rates and temperature limits associated with the QCSEE reduction, improved power transmission efficiency (Table 3d3-XX) will be realized and maximum oil out temperature limits will be consistent with present practices for conventional lubricants and materials.

Cooling System

The total cooling requirement of the lubrication system for the PD287-5 engine has exceeded the capacity of oil-to-fuel heat removal. This is a result of the compounding effects of the higher temperatures of advanced engines, the additional cooling requirement of the gear drive, and the use of oil-cooled electrical generators. Heat removal through the use of fan-blown air-to-oil heat exchangers necessitate the addition of a pressure recovery scoop behind the fan which could introduce detrimental effects on fan noise as well as thrust losses. Air-to-oil surface cooling in the fan duct results in weight penalties and increased vulnerability. To alleviate these problems, a different cooling concept has been investigated. This approach uses a compact engine-driven blower which draws air from the outer surface of the fan duct through plate-fin-type air/oil heat exchangers. This arrangement accommodates the three separate lubrication systems: core engine, Q-Fan, and alternator actuator/constant speed drive. The best exchangers are in parallel and located upstream of the blower unit. The blower is an axial type driven by the engine accessory drive. The units are all sized to fit within a 38.1-cm (15-in.) thick duct.

Table 3d3-XX.
PD287-5 and -6 power transmission efficiency.

	PD287-5 propulsion system	
	Takeoff, kW (hp)	Cruise, kW (hp)
Power dependent loss	56.7 (76.03)	29.6 (39.73)
Speed dependent loss	27.0 (36.18)	26.1 (34.99)
Total loss	83.7 (112.21)	55.7 (74.72)
Loss, %	0.62	0.88
Efficiency, %	99.38	99.12
	PD287-6 propulsion system	
	Takeoff, kW (hp)	Cruise, kW (hp)
Power dependent loss	63.0 (84.46)	36.1 (48.44)
Speed dependent loss	35.8 (48.01)	34.8 (46.63)
Total loss	98.8 (132.47)	70.9 (95.07)
Loss, %	0.69	0.93
Efficiency, %	99.31	99.07

Air is brought into the heat exchanger face through ducting from a flush NACA inlet. The heated air is axially discharged from the blower on the outer surface of the fan duct. Proper design of this exit will allow thrust recovery as well as accessory compartment ventilation through ejector extraction of compartment air.

Sizing Criteria

The Q-Fan and gas generator heat exchangers are sized at the maximum load condition, sea level takeoff (Table 3d3-XXI). The maximum load coincides with maximum blower speed, hence cooling airflow is a maximum. The alternator heat exchanger is sized for the sea level idle condition where the heat load is a maximum. The blower speed and cooling airflow is a minimum. The cooling air blower is sized at the maximum speed condition. Excess air is supplied to the alternator heat exchanger.

Hot day ground idle and taxi conditions were checked for the Q-Fan and gas generator cooling and were found not to be sizing conditions. Additional conditions must be investigated to cover the total flight envelope. However, experience indicates that the assumed sizing conditions will control the system configuration.

Refer to the Supplement to this report for the discussion of power transmission bearings and rotor support bearings.

Table 3d3-XXI.
Cooling system sizing.

	Design point		Pressure
			Sea level takeoff condition
Q-Fan heat exchanger			5.5 kN/m^2 (8 lbf/in.^{2})
Oil flow, kg/s (lbm/min)	0.85	(112)	
Oil-in temperature, °K (°F)	408	(275)	
Oil-out temperature, °K (°F)	352	(175)	
Airflow, kg/s (lbm/min)	1.28	(169)	
Air-in temperature, °K (°F)	322	(120)	
Heat transfer rate, kJ/s (Btu/min)	102	(5774)	
Gas generator heat exchanger			4.8 kN/m^2 (7 lbf/in.^{2})
Oil flow, kg/s (lbm/min)	0.22	(29)	
Oil-in temperature, °K (°F)	408	(275)	
Oil-out temperature, °K (°F)	352	(175)	
Airflow, kg/s (lbm/min)	0.33	(44)	
Air-in temperature, °K (°F)	322	(120)	
Heat transfer rate, kJ/s (Btu/min)	26.4	(1500)	
			Sea level idle condition
Alternator heat exchanger			4.1 kN/m^2 (6 lbf/in.^{2})
Oil flow, kg/s (lbm/min)	0.28	(37.4)	
Oil-in temperature, °K (°F)	394	(250)	
Oil-out temperature, °K (°F)	366	(200)	
Airflow, kg/s (lbm/min)	0.27	(36)	
Air-in temperature, °K (°F)	322	(120)	
Heat transfer rate, kJ/s (Btu/min)	16.9	(960)	
			Sea level takeoff static condition
Blower			0.51 m (20 in.) H_2O
Airflow, kg/s (lbm/min)	0.28	(278)	
Pressure in, kN/m^2 (psi)	9.6	(14.02)	
Temperature in, °K (°F)	301	(262)	
Shaft horsepower at 200 s^{-1} (12,000 rpm) input, kW (shp)	18.6	(25)	
Component weight estimate			
Blower, 13.2 kg (29 lbm)			
Engine heat exchanger, 12.7 kg (28 lbm)			
Q-Fan heat exchanger, 43.1 kg (95 lbm)			
Alternator heat exchanger, 6.8 kg (15 lbm)			

Table 3d3-XXII.
Interface loads for PD287-5

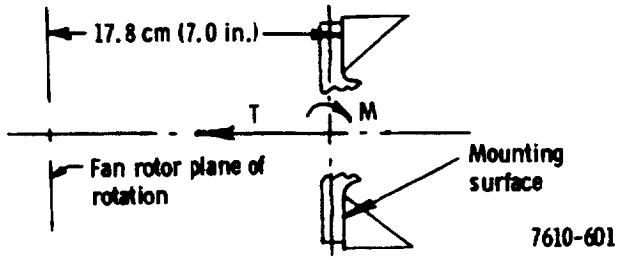

Ultimate		
Centrifugal from one bald shell out × 2 1/2 magnification factor		
Radial load	173.0 kN	(39,000 lbf)
Moment load	29.7 kN·m	(263,000 in.-lbf)
Limit		
Gyro moment at 1.5 rad/s	17.8 kN·m	(157,500 in.-lbf)
Weight at 4g	3.8 kN·m	(33,500 in.-lbf)
$1 \times N_F$ for static takeoff	0.9 kN·m	(8,300 in.-lbf)
Limit moment	21.5 kN·m	(199,300 in.-lbf)
Mean load condition		
Gyro moment at 0.1 rad/s	1.18 kN·m	(10,500 in.-lbf)
Weight at 1g	0.94 kN·m	(8,400 in.-lbf)
$1 \times N_F$ mean	1.32 kN·m	(11,700 in.-lbf)
Mean moment	3.44 kN·m	(30,600 in.-lbf)
Static takeoff		
Thrust	46.3 kN	(10,400 lbf)
Moment	1240 k·m	(11,400 in.-lbf)
Torque	86.8 kN·m	(769,000 in.-lbf)

Fan Rotor Assembly Interface

The interface between the fan rotor and the engine assembly has been evaluated for dynamic and static requirements. Tables 3d3-XXII and 3d3-XXIII show the results of this study.

Table 3d3-XXIII.
Interface loads for PD287-6

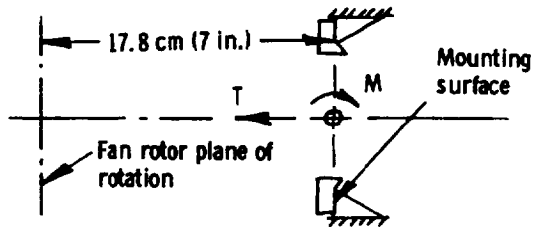

7610-600

Ultimate		
Centrifugal from one blade shell out × 2-1/2 magnification factor		
Radial load	178.0 kN	(40,000 lbf)
Moment load	31.6 kN·m	(280,000 in.-lbf)
Limit		
Gyro moment at 1.5 rad/s	17.8 kN·m	(158,000 in.-lbf)
Weight at 4g	3.2 kN·m	(28,000 in.-lbf)
$1 \times N_F$ for static takeoff	0.9 kN·m	(8,300 in.-lbf)
Limit moment	21.9 kN·m	(194,300 in.-lbf)
Mean load condition		
Gyro moment at 0.1 rad/s	1.18 kN·m	(10,500 in.-lbf)
Weight at 1g	0.79 kN·m	(7,000 in.-lbf)
$1 \times N_F$ mean	1.19 kN·m	(10,600 in.-lbf)
Mean moment	3.16 kN·m	(28,100 in.-lbf)
Static takeoff		
Thrust	51.2 kN	(11,500 lbf)
Moment	900.0 N·m	(8,280 in.-lbf)
Torque	72.5 kN·m	(643,000 in.-lbf)

Whirl Modes

The synchronous (forward) and nonsynchronous (backward) whirl critical speeds were calculated for the fan on its shaft, bearings, bearing support, and Q-Fan support structure. The analysis showed that the fan tailshaft is extremely rigid compared with the bearings, bearing support, and engine cone. The bearing stiffnesses were determined, using the A. B. Jones bearing program and assuming an applied bearing load of 4448N (1000 lb). For unbalance loads smaller than this, the synchronous whirl critical speed is 64 s^{-1} (3940 rpm), which is 2.1 times the maximum normal operating speed for the 1.25 R_F fan and 1.5 times the maximum normal operating speed for the 1.325 R_F fan. Thus, the magnification and the unbalance loading should be low.

The nonsynchronous whirl critical speed was calculated to be 34.7 s^{-1} (2082 rpm), which is sufficiently high to ensure whirl flutter-free operation. This equivalent torsional spring constant for the bearing, bearing support, and fan support structure is 5.8×10^6 N·m/rad (52×10^6 in. lbf/rad), which conservatively ensures stability.

Because of the clearances in the bearings, the effective secant stiffness used for determining the whirl critical speeds is dependent on the relative magnitudes of the applied load and the unbalance load. The aforementioned analysis assumed the applied load was greater than the unbalance load. However, if the applied load is small relative to the unbalance load, then the effective spring rate becomes low and the synchronous and nonsynchronous whirl critical speeds will be much less than those given herein.

Torsional Modes

A torsional dynamic analysis was made of the fan-gearbox-engine system to be sure it would be free of any dynamic problems resulting from normal fan, gear, and engine excitations. The analysis, which included the flexible planet support system, gave the three fundamental torsional critical speeds. Of these three critical speeds—25.5, 102.8, 500 s^{-1} (1530, 6170 and 30,000 rpm)—only the highest excited by 1P (1 × fan rotational speed) excitation is likely to have direct torsional excitations. This excitation should be relatively low because of the duct effect on minimizing the 1P excitations. All such critical speeds are at least 5% away from the normal operating speeds to minimize magnification of any torsional or coupled whirl excitations. Because the lowest significant mode involves the impressed torsional vibration of the fan and engine on the planet support, the planet support will be evaluated for structural integrity under transients and for low-cycle fatigue.

Variable Pitch Actuator

The variable pitch fan uses a mechanical actuator mounted within the rotor hub assembly. The power supply and control system for this unit are located in the fan duct. The mechanical blade actuation consists of the following units: blade segment gears, rotary harmonic torque multiplier, differential gear train, and mechanical one-way drive (no-back).

One-Way Drive

The rotary output signal from the hydraulic motor is transmitted through shafting to a one-way drive (no-back) and then to the fan rotor variable pitch actuator as shown in Figures 3d3-7 and 3d3-8. The no-back allows forward feed signals to the rotor variable pitch actuator but prohibits backward signals to input shafting in the case of loss of control power or a fail open of the signal shafting.

Figure 3d3-7 shows the spring with a single coil, the output (load) shaft, the input drive, and the grounded outer case. There is a press fit between the spring OD and the case. Rotation of the load shaft in either direction drives the spring into a force fit with the ground housing and friction locks these two members (at this time the input drive does not engage the spring). The input drive drags the spring out of engagement with the housing, rotating the load shaft through a direct mechanical path. The input drive then unlocks the spring from the loose end, permitting the load shaft to rotate within the housing.

Differential

A planetary differential gear mesh is used to transmit blade angle positions from the no-back across to the rotor assembly. The differential is composed of a grounded sun gear, an input sun gear, two planet gears on a common carrier, and a reference speed ring gear and a second

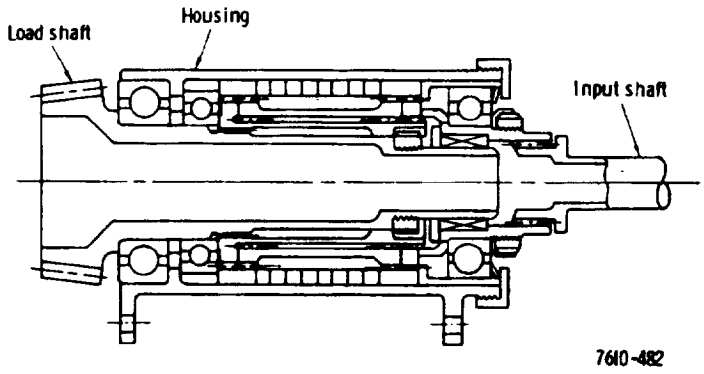

Figure 3d3-7. One-way drive clutch/clutch.

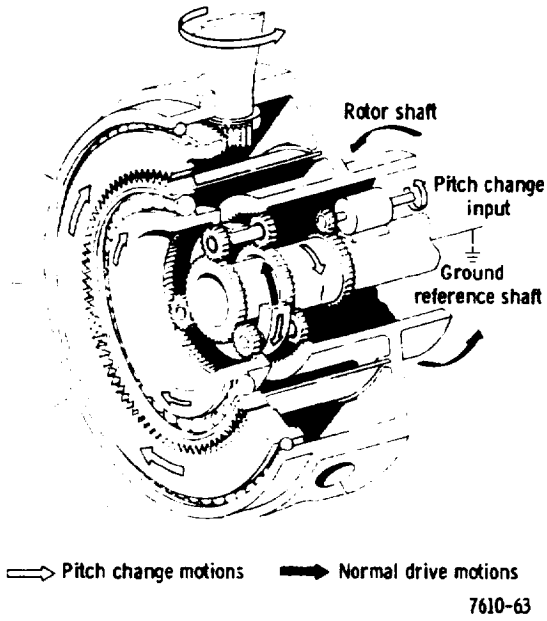

Figure 3d3-8. Q-Fan mechanical actuator.

ring gear connected to the harmonic drive input. With no-pitch-change input signal, the speed of the carrier is established by the reference speed ring gear and the grounded sun gear. The addition of a signal (rotation) of the input sun gear will cause the planet carrier to rotate in advance of or behind the established speed. This additional rotation of the carrier produces a relative rotation between the reference and output ring gears, which is the input rotation to the harmonic drive.

Harmonic Drive

The harmonic drive when on the rotating side of the fan rotor assembly is a high-ratio speed reduction device consisting of three basic components. The first of these is a three-lobed wave generator. It is composed of a thin-race ball bearing which is deflected into an ellipsoidal shape by the rigid-contoured disk within the bearing. A flexing element (called the flexspline) is in the form of a thin-walled cylinder with one end deflected into an ellipsoidal cross section by the wave generator and the other end held in a circular shape and grounded to the disk. The third element is a rigid circular ring gear (called the circular spline) which forms the high torque output of the harmonic drive and is integral with a blade phasing bevel ring gear. The harmonic drive motion is shown in Figure 3d3-9.

Blade Segment Gear

The blade segment gear is a bevel of an arc of approximately 1.9 rad (110 deg). This gear is splined to the blade and supported in the disk by its own shielded bearing which permits removal of individual blades without exposing the barrel and gearbox cavity or affecting the shimming required for proper gear tooth engagement. The mating bevel gear with its integral bearing (to react gear-separating loads) is part of the harmonic drive.

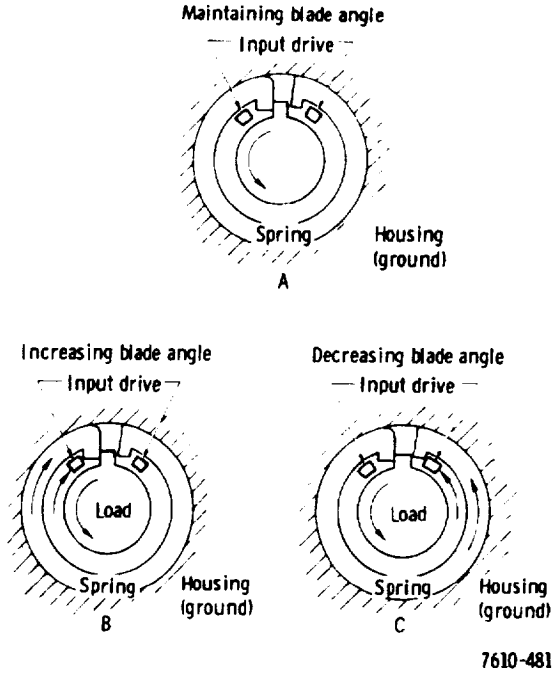

Figure 3d3-9. Schematic of harmonic drive motion.

The bevel gear blade actuation is similar to numerous HSD high-time applications. Allowable tooth stress levels for variable-pitch operating-load spectrums have been developed over the years. The QCSEE bevel mesh sizing is consistent with this experience.

Component Selection

The harmonic-type rotary actuator has been selected for the following reasons.

- This type of actuator eliminates all high-pressure hydraulic oil systems in the rotor assembly.
- The rotor disk envelope affords ample radial space for proper stiffening of the harmonic wave generator disk and the circular spline ring. Because of the web and flange sections used in these members, an effective weight and stiffness design is obtained.

HSD has worked very closely with United Shoe Machinery on several aircraft applications for harmonic drives. The latest of these was a development program to determine the maximum-operating, maximum-holding, and life characteristics as related to circular spline stiffness for the SST leading edge flap system. This, along with extensive vendor development testing, has determined the critical design requirements for harmonic drives. United Shoe has built and developed a harmonic drive for the Bell X-22A duct rotation which is similar in size, load, and application to the proposed design for the QCSEE pitch change actuator.

The sizing of the QCSEE harmonic is consistent with criterion that have been established by combined development programs with United Shoe. The ample diametral envelope has afforded space for a conservative design.

The no-back unit operates on the principle of a self-energized brake. Blade twisting torques when not supported by the hydraulic motor are grounded to the no-back case; this locks the blades in the last set position. The self-energizing principle allows the compact unit to hold maximum overspeed loadings at 126% rated speed.

The spring-type, one-way drive has been selected for the following reasons.

- Spring-brake devices similar to the type selected for the QCSEE have been widely used in general industry. Typical aerospace applications are:
  - AH-56 compound helicopter (engine-to-transmission overrunning clutch)
  - CL-84 VTOL aircraft
  - F-111 flap system (torque-limiting clutch)
  - F-111 weapons bay door system (hold brake)
  - F-14 wing sweep
- The self-energizing feature eliminates weight and complexity and ensures holding maximum loading conditions.
- The multicoil device is designed to tolerate a large range of friction coefficients with minor weight and complexity effects.
- Brake release is affected with relatively low input torque values. This ensures unlocking from maximum brake loads without increasing the size of the hydraulic power source.
- The spring is loaded in compression for structural reliability.
- The spring is sized for maximum loading conditions and, therefore, provides a conservative on-condition design.

HSD has built spring-type, one-way drives for aircraft control surface actuation locks. The function and size requirements of the QCSEE variable pitch actuator are similar to developed systems. Because of the location of this actuator, blade angle hysteresis associated with input triggering results in blade angle error from scheduled to actual angle of less than 0.00087 rad (0.05 deg).

3d4. Combustion

Because this subsection contains classified data, it is presented in the Supplement to this final report.